PROCEEDINGS

International

EEITE-2023

Conference

eeite2023.hmu.gr

Hybrid format

4th International Conference in Electronic Engineering, Information Technology & Education

**15-18 May 2023
Hellenic Mediterranean University
Dept. of Electronic Engineering
Chania, Crete, Greece**

~ i ~

Proceedings of the 4th International Conference in
Electronic **E**ngineering, **I**nformation **T**echnology & **E**ducation
EEITE-2023, 15-18 May 2023, Chania, Crete, Greece
(Hybrid format)

eeite2023.hmu.gr

Hosted by the
Department of Electronic Engineering
of the Hellenic Mediterranean University

ISSN 2654-2099

TOPICS

.

- ➢ The University of the Future
- ➢ Internet of Things (IoT) and Applications
- ➢ Artificial Intelligence (AI) and Applications
- ➢ Microwave, Millimeter wave and Terahertz Communications
- ➢ 5G and 6G Wireless Networks
- ➢ Textile, Wearable and Smart Antennas
- ➢ New Technologies in Electronics
- ➢ Photonics & Optical Communications
- ➢ Quantum Computing
- ➢ Cybersecurity
- ➢ Cybersecurity
- ➢ Virtual and Augmented Reality
- ➢ Functional Materials and Applications
- ➢ STEM & Education
- ➢ 3D Printing and Applications
- ➢ Robotics and Applications
- ➢ Remote Sensing and Applications
- ➢ Power Electronics
- ➢ Plasma Technology
- ➢ Environmental Applications

COMMITTEES

Organizing Committee

– Dr. Antonios Konstantaras, Professor – *chair*

– Dr. Ioannis Fitilis, Assistant Professor – *co-chair*

– Dr. Ioannis Vardiambasis, Professor

– Dr. Ioannis Chatzakis, Professor

– Dr. Konstantinos Petridis, Associate Professor

– Dr. Ioannis Kaliakatsos, Emeritus Professor

TABLE OF CONTENTS

~ iv ~

THE ROLE OF LEADERSHIP IN SHAPING EMPLOYEES` COMMITMENT

Zielińska, A.,
[1]University of Bielsko-Biala, Poland
E-mail: azielinska@ath.bielsko.pl

1. INTRODUCTION

Nowadays the employee is a key stakeholder of the company, and building engagement especially among professionals who work remotely is a significant challenge for organizations. Therefore, the purpose of the presentation was to examine the role of leadership in the relation to employees` commitment.

2. THEORETICAL BACKGROUND OF COMMITMENT

The issue of the commitment in virtual teams attracted the attention of researchers many years ago. This is evidenced by materials from the *Fifth American Conference on Information Systems*, where papers were prepared on the topic of engagement in virtual teams (Powell, 1999a) and research recommended in this area (Powell, 1999b). However, interest in the issue was initially quite scant. Some of the first research on commitment in virtual teams was conducted by Workman, Kahnweiler and Bommer. They stressed that although virtual teams and a form of telecommuting are a strategic organizational innovation, there is little research being conducted in this area, especially empirical research. As the researchers wrote, "practitioners can only speculate on why things succeed or fail for them." For this reason, they conducted a study of virtual teams relate to commitment, information abundance and cognitive style theory. The results of their research showed, among other things, that certain combinations of cognitive styles contribute significantly to commitment in virtual teams (Workman, Kahnweiler, Bommer, 2003).

The knowledge gap on commitment in virtual teams was also recognized by Crossman and Lee-Kelley (2004), who examined the role of trust and commitment based on a case study. They indicated that perceived low levels of organizational commitment do not engender the high levels of trust and real commitment is required among virtual team members to maximize performance. However, over time and with increased information sharing, the level and form of commitment may change, requiring adjustments to existing psychological understanding and trust between virtual team members. The conclusion of the research was that compatibility in reformulating short-term to long-term commitment is beneficial in many dimensions, and then the virtual way of working can be very effective (Crossman, Lee-Kelley, 2004).

Interest in virtual teams, as well as interest in the topic of virtual team member commitment, increased after 2010. For example, researchers Verreault and Fortier (2010), indicated that the formation of virtual groups is dynamic and difficult. They prepared a model related to creating and sustaining commitment in virtual teams. They focused on virtual teams with a high level of multiculturalism and operating on a global scale, and the model they created is based on empirical research on the key behaviors that lead to engagement and trust building in a virtual environment (Verreault, Fortier, 2011).

3. RELATION BETWEEN COMMITMENT AND LEADERSHIP

In research, it has been observed relation between commitment and leadership. For example, the results of study conducted by Lee, Jo, and Lee (2011) indicated that task-oriented leadership has a strong direct effect on performance, while relationship-oriented leadership attitudes had a strong indirect effect on team performance. Commitment has the mediating variable of the relationship between leadership and performance. Based on this research, the following conclusions can be drawn. Leadership should be analyzed in light of different styles.

Moreover, in the article prepared by Pazos, (2012) about the commitment, it is possible to find results of a study focused on the relationship between commitment to team goals, conflict management and team performance. For all those aspects leaders can have influence. In a publication authored by Snyder (2012), recommendations were made on virtual leadership problems, areas of leadership, team cohesion and commitment. Also, in the article titled "Engagement 2.0" (Goga-Cooke, Arico, Mockett, 2013), the authors point out that it is necessary to find new qualitative ways to engage employees. A strongly emphasized assumption is that team members have knowledge and wisdom that should be "mined" by leaders to build networks and take advantage of synergies. In addition, the academic literature also emphasizes the role of leaders in shaping cross-cultural engagement and team members' sensitivity to each other's behavior.

4. SIGNIFICANTLY OF COMMITMENT AND LEADERSHIP IN CONTEXT TO TEAM COLLABORATION

The commitment as well as leadership were analyzed by researchers in different dimensions. For example, results of empirical study (Cao, Xu, Liang, Chaudhry, 2012) showed that team tasks and work engagement have a significant positive impact on knowledge transfer. In addition, team tasks and commitment have an indirect effect on the knowledge transfer process. Based on these studies, it can be indicated that a high level of commitment positively influences knowledge sharing which, consequently, can result in more effective collaboration. There have been studies also by Zwikael, Elias and Ahn (2012) that recommended including various stakeholders in collaboration. This can be a factor influencing the relationship with project team members and, consequently, can determine their greater involvement and success of the virtual project.

Moreover, researchers described, it is necessary to support employees in improving their skills and increasing engagement, since the engagement of virtual team members is the most significant factor affecting their performance and determining the success of the organization (Moradi, Mohamed, Yahya, 2017). Researchers point out that the issue of work engagement can be associated with job burnout or the intention to leave. They significantly affect motivation. For this reason, there is the discussion about intervention leadership. In virtual teams, communication strategies are recommended to improve work results and motivation levels, while reducing burnout (Sang-Woo, 2017). In addition, trustworthiness, interpersonal communication, cross-cultural communication style and commitment were found to be the dominant factors in research on high-performing virtual teams (Lippert, Dulewicz, 2018). One approach to team building is to consider accountability, cohesion and commitment. Another approach is to use organizational factors and social networks to help leaders build high levels of commitment in virtual teams (Ben Sedrine Doghri, Bouderbala, Melliti, 2019).

Aspects of engagement such as feedback, participation in decision-making, employee support and supervision in virtual teams may proceed differently than in traditional teams. Therefore, it is recommended that research be conducted in search of answers to the question "what drives employee engagement in virtual teams?" Research in this area was conducted for example by Shaik and Makhecha (2019) by inviting 26 members of virtual teams occupying different positions and working in different locations for a qualitative study. The study identified cultural intelligence, communication, technology, trust and individual maturity as antecedents of engagement in virtual teams.

5. CONCLUSIONS

Work engagement is not constant, but dynamic and changing. Hence, engagement should be supported, especially if the work is carried out in a virtual way. Virtual leaders can actively promote and boost commitment through the appropriate use of strategies and tactics to foster development, especially that maintaining engagement may require different strategies at different phases of a project.

In addition to a regular and efficient communication process, leading the team using empathy and engaging in the learning process is recommended (Bradley, 2020). The literature indicates that great

difficulties in maintaining engagement arise in global teams. They are characterized by a high degree of multiculturalism, so in cases of global teams. Therefore researchers (Shaik, Makhecha, Gouda, 2020) recommend taking into account the cultural intelligence of team members as well. Thus, it is apparent that many aspects related to the involvement of virtual team members are taken into account.

Summarizing, based on the literature review, the existing relationships between leadership and commitment in the context to team collaboration was presented. Research indicates that leadership has significant role in shaping commitment of members in virtual teams. It is especially important, because based on the literature they affect team performance, and therefore those relations are recommended to future empirical research.

6. REFERENCES (headlines: TNR Bold, 12pt)

Ben Sedrine Doghri, S., Bouderbala, A., Melliti, S. (2019). Etude de l'impact des réseaux sociaux sur l'engagement des cadres au sein des pmes. *Study of the impact of social networks on the engagement of managers in SMEs*., 38(4), 117-141

Bradley, A. (2020). Maintaining engagement in a world of remote work. Public Finance. No 5, pp. 44-45.

Cao, W. L., Xu, L., Liang, L., Chaudhry, S. S. (2012). The impact of team task and job engagement on the transfer of tacit knowledge in e-business virtual teams. Information Technology & Management, 13(4), 333-340. doi:10.1007/s10799-012-0129-6.

Crossman, A., Lee-Kelley, L. (2004). Trust, commitment and team working: the paradox of virtual organizations. Global Networks-a Journal of Transnational Affairs. Nr 4(4),

375-390. doi:10.1111/j.1471-0374.2004.00099.

Goga-Cooke, J., Arico, M., Mockett, M. (2013). Engagement 2.0: Co-creating connection. e-Organisations & People, 20(1), 30-39.

Lippert, H., Dulewicz, V. (2018). A profile of high-performing global virtual teams. Team Performance Management, 24(3-4), 169-185.

Lee, D. S., Jo, N. Y., Lee, K. C. (2011). Leadership styles, web-based commitment and their subsequent impacts on e-learning performance in virtual community. Ubiquitous Computing and Multimedia Applications, PT II, 151, 447-456

Moradi, L., Mohamed, I., Yahya, Y., (2017). Relationship between e-training in virtual team and it project performance with the mediation role of organizational commitment in e-tourism. In Proceedings of the 2017 6th international conference on electrical engineering and informatics. Society for Internet Information, 18(5), 103-112. doi:10.1108/tpm-09-2016-0040

Pazos, P. (2012). Conflict management and effectiveness in virtual teams. Team Performance Management, 18(7/8), 401-417. doi:10.1108/13527591211281138.

Powell, A. L. (1999a). Commitment in a virtual team. Association for Information Systems - Proceedings of the Fifth Americas Conference on Information Systems. Series Editors: Haseman, W. D., Nazareth, D. L., Pages: 355-357. Accession Number: WOS:000086012100124.

Powell, A. L. (1999b). A proposed study on commitment in virtual teams. Association for Information Systems - Proceedings of the Fifth Americas Conference on Information Systems. Series Editors: Haseman, W. D., Nazareth, D. L.1014-1016. Accession Number: WOS:000086012100353.

Sang-Woo, H. (2017). Communication strategies of online-based leadership and members' work engagement and job burnout. Journal of Internet Computing and Services. doi:10.7472/jksii.2017.18.5.103.

Shaik, F. F., Makhecha, U. P., Gouda, S. K. (2020). Work and non-work identities in global virtual teams role of cultural intelligence in employee engagement. International Journal of Manpower, 28. doi:10.1108/ijm-03-2019-0118.

Shaik, F. F., Makhecha, U. P. (2019). Drivers of employee engagement in global virtual teams. Australasian Journal of Information Systems, 23, 44.

Verreault, E., Fortier, D. (2011). Conceptual model for creating and sustaining commitment to norms in multicultural global virtual teams (mgvts). In L. G. Chova, D. M. Belenguer, A. L. Martinez (Eds.), Edulearn11: 3rd international conference on education and new learning technologies (pp. 63-70). Valenica: Iated-Int Assoc Technology Education & Development.

Workman, M., Kahnweiler, W., Bommer, W. (2003). The effects of cognitive style and media richness on commitment to telework and virtual teams. Journal of Vocational Behavior, 63(2), 199-219. doi:10.1016/s0001-8791(03)00041-1.

Zwikael, O., Elias, A. A., Ahn, M. J. (2012). Stakeholder collaboration and engagement in virtual projects. International Journal of Networking & Virtual Organisations, 10(2), 117-136. doi:10.1504/IJNVO.2012.045730.

THE IMPACT DIMENSIONS OF INFORMATION SYSTEMS ON WORK PROCESSES: SUMMARY OF THE MAIN MODELS

Bailoa, Sandra[1] and Bailoa, Sónia[2]

[1]Polytechnic Institute of Beja, Portugal
[2]Sintra City Council, Portugal
sandra.bailoa@ipbeja.pt

1. INTRODUCTION

Even though the management of information systems involve and covers an increasingly wide range of dimensions and aspects, in the literature there is still a reduced number of studies on the impact of technologies on work processes Furthermore, the circumstances surrounding the introduction of technology into work processes have revealed that the dimensions of impact have not always received the same perception over time and that different dimensions have been highlighted as relevant as the diffusion of technology in work processes progresses and deepens Thus, this work intends to identify a set of impact dimensions of information systems on work processes through a review of the main contributions of the literature.

2. THE IMPACT OF INFORMATION SYSTEMS ON ORGANIZATIONS

Technological development, throughout the 20th century and in particular the dissemination of Information Systems (IS), brought significant impacts to societies. IS are now a constant part of the daily life of organizations, where they are used as a working tool to carrying out everyday tasks.

The evolution of IS and their diffusion in organizations has led to diverse and multifaceted impacts on work processes. The management of IS has also faced the challenges of these transformations and has adapted to new contexts and contingencies, in order to achieve a set of advantages and benefits associated with the use of technologies. In the literature some advantages and benefits of IS to organizations are identified:

- Increase of productivity (Doll & Torkzadeh, 1999), (Laudon & Laudon, 2014), (Mendonça et al., 2009) (Lunardi et al., 2010);
- Increase in the number of customers and their satisfaction (Doll & Torkzadeh, 1999), (Mendonça et al., 2009), (Lunardi et al., 2010) (Souza et al., 2010);
- Increased efficiency and organizational performance (Dewett & Jones, 2001), (Mendonça et al., 2009), (Beltrame & Maçada, 2009), (Lunardi et al., 2010) (Souza et al., 2010);
- Improvements in decision making (Dewett & Jones, 2001) (Lunardi et al., 2010);
- Increased ability to innovate (Doll & Torkzadeh, 1999) (Mendonça et al., 2009);
- Reduction of operating costs (Mendonça et al., 2009) (Lunardi et al., 2010);
- Increased revenues (Doll & Torkzadeh, 1999), (Laudon & Laudon, 2014) (Lunardi et al., 2010);
- Increased quality of products/services (Doll & Torkzadeh, 1999) (Mendonça et al., 2009);
- Increased profits (Doll & Torkzadeh, 1999) (Laudon & Laudon, 2014);
- Improvements in employee skills (Beltrame & Maçada, 2009) (Mendonça et al., 2009);
- Improvements of employee satisfaction (Čizmić et al., 2023) (Doll et al., 2004) (Maçada & Borenstein, 2000) (Neto & Riccio, 2003).

3. THE IMPACT OF INFORMATION SYSTEMS ON WORK PROCESSES

The evaluation of different aspects and impacts of IS on work processes allows to analyse the adequacy of technologies to the services necessities, to contribute to monitoring organizational performance and to evaluate the success of investments in IS in any organization, public or private.

Since the impact of IS on individual work can have different dimensions, it is first necessary to

understand how this impact is evaluated. Doll and Torkzadeh (1999) describe the impact of IS on organizations as a result of a chain of factors. Based on behavioral theory, the authors describe a value-added creation chain (figure 1), in which the success of systems is built based on beliefs, attitudes, behaviors and social and economic impacts of IS. Impact at an individual level occupies a fundamental position in the value chain because it is a direct consequence of the application of IS, which in turn is a determining factor for organizational impact.
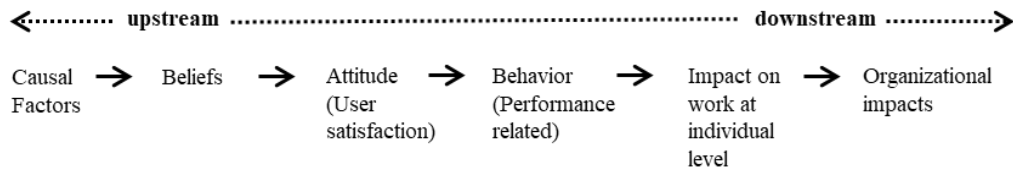
Figure 1. System to value chain
Source: Doll and Torkzadeh (1999, p. 328)

The impact of IS has been different over the different eras and has varied according to the evolution of the IS. In the industrial model, technology was used to replace capital with labor, with impacts on labor productivity and making management control more visible. The post-industrial model continues to focus on productivity and management control but including other impacts of technology such as innovation and user satisfaction (Doll & Torkzadeh, 1999).

The impacts of IS on individual work processes are nowadays multifaceted and complex. Over the past few decades, some studies have emerged that analyze the impacts of IS on work processes. Table 1 presents a summary of the main studies.

Table 1. Synthesis of models and studies on impact dimensions of IS on work processes

AUTHORS	IMPACT DIMENSIONS OF INFORMATION SYSTEMS	STUDIES
DOLL AND TORKZADEH (1999)	Productivity, Innovation, User satisfaction, Management control	89 users of 30 companies, U.S.A. 409 of 18 companies, U.S.A.
PEREIRA (2003)	Productivity, Innovation, User satisfaction, Management control, Phases of the decision-making process	411 users of 10 branches of a bank in different cities, Brazil 408 users of 10 branches of a bank in different cities, Brazil
MAÇADA ET AL. (2007)	Productivity, User satisfaction, Management control, Decision making, Information security, Information quality	334 users of a public company, Brazil
BACHÉGA AND ALMEIDA (2009)	Productivity, Innovation, User satisfaction, Management control	49 users of Botucatu city council, Brazil
RODRIGUES (2009)	Productivity, Innovation, User satisfaction, Management control, Decision making, Information security, Information quality	75 users of University Hospital of Brasilia, Brazil
BAILOA (2011)	Productivity, User satisfaction, Management control, Innovation, Phases of the decision-making process, Decision-making, Information quality, Information security	810 users of IS and different applications of various departments from Sintra city council, Portugal
ANTONELLI ET AL. (2012)	Productivity, Management control, Innovation, Client satisfaction	362 users/accounting professionals from the state of Paraná, Brazil
RIBEIRO (2012)	Productivity, Innovation, Management control, Decision-making, Information quality, Information security, Client satisfaction, User satisfaction	108 users/teachers from Instituto Universitário de Lisboa (ISCTE-IUL), Portugal
CHIMUCO (2017)	Productivity, Innovation, Management control, Decision-making, Information quality, Information security, User satisfaction, Client satisfaction	75 users/teachers from public schools in the province of Namibe, Angola

GALVÃO (2022)	User satisfaction, Productivity, Management control, Innovation, Decision making, Information security, Information quality	121 users of accounting firms in Baixo Alentejo and Central Alentejo, Portugal

These studies generally identify and apply a relevant set of dimensions to assess the impact of IS on individual work processes. The most studied dimensions are the four categories of Doll and Torkzadeh (1999) model: productivity, innovation, user satisfaction and management control. These dimensions have been tested and validated in several studies.

Pioneering work by Doll and Torkzadeh (1999) has been inspiring through the years to others who have followed it adding other dimensions of impact to original model that allowed to complement the analysis to other relevant aspects of work processes. Maçada et al. (2007) extended the original model by adding the dimensions: information quality, information security and decision-making. These dimensions were also tested in several studies.

4. IMPACT DIMENSIONS OF INFORMATION SYSTEMS ON WORK PROCESSES

This work intends to identify a set of impact dimensions of IS on work processes through a review of the main contributions of the literature. The analysis allowed systematizing and synthesizing a set of dimensions based on models and empirical studies developed by different authors such as the following: productivity, user satisfaction, innovation, management control, information quality, decision-making and information security. Table 2 presents some of the most studied and referenced dimensions.

Table 2. Impact dimensions of information systems on work processes

IMPACT DIMENSIONS OF IS ON WORK PROCESSES		REFERENCES
PRODUCTIVITY	Productivity is an indicator that explains the relationship between production factors and production results. In the IS area, productivity relates production with the time spent on tasks, that is, whether the applications improve the users output per unit of time. Productivity increases are evaluated in terms of producing more, in a shorter period of time and with a smaller number of human resources and, therefore, with lower costs.	Doll and Torkzadeh (1999), Mendonça et al. (2009), Pereira et al. (2007), Santos et al. (2007), Laudon and Laudon (2014), Lunardi et al. (2010), Haberkamp et al. (2010)
USER SATISFACTION	A higher degree of user satisfaction with the technological resources and quality of IT services is essential to increase their motivation, autonomy, responsibility and, consequently, their performance. In some studies it can also appear as customer satisfaction meaning the extent to which an application helps the user to create value for the company's internal or external customers.	Doll et al. (2004), Doll and Torkzadeh (1999), Doll and Torkzadeh (1989), Maçada and Borenstein (2000), Neto and Riccio (2003), Lunardi et al. (2010), Souza et al. (2010), Čizmić et al. (2022), Čizmić et al. (2023), Mariano et al. (2020)
MANAGEMENT CONTROL	The use of information systems allows for increased management control, helps to centralize control and facilitates its distribution to other organizational areas.	Doll and Torkzadeh (1999), Pereira et al. (2007), Dewett and Jones (2001), Pereira (2003), Schwarz (2002), Pinsonneault and Kraemer (1993)
INNOVATION	Innovation is a process through which ideas are transformed into new work procedures, products/services and management methods, so IS act as a facilitator of this process promoting the ability to creatively apply knowledge to create competitive advantages and new ideas to solve problems, also enable exploring new forms of communication in organizations therefore, allowing workers to enrich, develop and innovate their work and their capacity to learn.	Dewett and Jones (2001), Sarkar (2005), Pereira et al. (2007), Doll and Torkzadeh (1999), Souza et al. (2010), Augusto et al. (2008), Bianchi et al. (2015), Yoshikuni et al. (2018)
DECISION-MAKING	IS allow obtaining and analyzing information necessary for decision-making, supporting this process more efficiently, therefore, have an important role on the decision-making process, as they support the sequence of steps necessary for this process.	Simon (1960), Maçada et al. (2007), Pereira (2003), Pereira et al. (2007), Armesh (2010), Mafra Pereira et al. (2018), Espírito Santo and Correia (2022), Bastos and Sobral (2023)

INFORMATION QUALITY	The quality of information is a somewhat subjective and multidimensional concept, whose more operational character is related to the usefulness of the information itself and with characteristics associated with it, such as, for example, being credible, clear, accessible, timely, up-to-date, accurate and valid.	Rodrigues (2009), Nehmy and Paim (1998), Paim et al. (1996), Maçada et al. (2007), Marchand (1990), Pipino et al. (2002), Olaisen (1990)
INFORMATION SECURITY	Information security has become a fundamental aspect in IS management, relating to the protection, confidentiality and integrity of information and the systems themselves.	Maçada et al. (2007), Ezingeard et al. (2005), Laureano and Moraes (2005), Marciano (2006), Cox (2002), Araújo and Araújo (2015), Silveira et al. (2019)

Most studies suggest that IS impacts are varied and multifaceted. Furthermore empirical studies carried out at different times have shown that the studied dimensions had a different emphasis over time. Table 3 presents a comparison of the ranking of impact dimensions in different studies.

Table 3. Comparison of the ranking of impact dimensions in different studies

STUDIES	RANKING OF IMPACT DIMENSIONS (MAIN RESULTS)
DOLL AND TORKZADEH (1999)	1st Productivity 2nd User satisfaction 3rd Management control
PEREIRA (2003)	1st Productivity 2nd User satisfaction 3rd Management control
BACHÉGA AND ALMEIDA (2009)	1st Productivity 2nd Innovation 3rd User satisfaction
RODRIGUES (2009)	1st Information security 2nd Management control 3rd Information quality
BAILOA (2011)	1st Information security 1st Productivity 3rd Information quality
BAILOA (2011) (RESULTS FOR THE MAIN APPLICATION USED)	1st Productivity 2nd Information quality 3rd User satisfaction
ANTONELLI ET AL. (2012)	1st Productivity 2nd Management control 3rd Client satisfaction
RIBEIRO (2012)	1st Management control 2nd Information security 3rd Client satisfaction
CHIMUCO (2017)	1st Productivity 2nd Management control 3rd Information security
GALVÃO (2022)	1st Decision-making 2nd Productivity 3rd Information quality

In most studies, the dimension with higher impact was productivity, as well as user satisfaction and management control. In addition to these, more recent studies also highlight information security, information quality and decision-making, showing that the impacts can be diverse and the technologies affect different aspects of the individual work. Thus, other dimensions have been highlighted as relevant in work processes over time.

5. CONCLUSION

Technological development has influenced the way IS are viewed in organizations, the investments made and the way these systems are managed. These same challenges have been verified at the level of work processes in which the impacts have been visible with different intensities over time. If in the industrial era the use of technology was intended to replace human work and to increase productivity and reinforce management control, in the post-industrial model other aspects became equally relevant in the good use of IS, such as security and quality of information, innovation and user satisfaction. The focus continued to be based on productivity and management control, but technologies began to be seen as driving and generating of user and customer satisfaction, innovation, information quality and support in decision making. Therefore, different aspects derive from the use of technology in work processes, making it necessary to study and evaluate all impacts as a way of enhancing the advantages inherent to the use of IS.

In literature the studies on technological impacts on individual work processes present multifaceted analyses of the dimensions in which technology can have an impact. The most studied dimensions have been productivity and management control, which have justified many of the investments made in IS. Despite this, the impacts of technology are not limited to these dimensions and other relevant impacts to the success and survival of organizations in current times cannot be ignored or neglected.

This work allowed to identify, systematizing and synthesizing a set of impact dimensions of information systems on work processes through a review of the main contributions of the literature namely empirical studies and models developed by different authors. The dimensions identified were the following: productivity, user satisfaction, innovation, management control, information quality, decision-making and information security.

Different dimensions have been tested in several empirical studies showing that management of IS seems to increasingly encompass the analysis of the impact of these systems in different aspects of work. So it is suggested that in future empirical studies be applied a model with the different dimensions identified for a better and more complete perception of the impact of IS on the work process.

6. REFERENCES

Antonelli, R., Almeida, L., Colauto, R. and Silova, W. (2012). Percepções dos profissionais de contabilidade quanto à influência da tecnologia da informação no seu processo de trabalho individual. 12º Congresso USP de Controladoria e Contabilidade, São Paulo/SP.

Araújo, S. and Araújo, W. (2015). A dimensão humana no processo de gestão da segurança da informação: um estudo aplicado à Pró-Reitoria de Gestão de Pessoas da Universidade Federal da Paraíba. Pesquisa Brasileira em Ciência da Informação e Biblioteconomia, João Pessoa, 10(2): 237-250.

Armesh, H. (2010). Decision Making. In Proceedings of 12th International Business Research, Dubai, 1-23.

Augusto, C., Takahashi, L. and Sachuk, M. (2008). Impactos da inovação tecnológica na competitividade e nas relações de trabalho. Caderno de Administração, 16 (2): 57-66.

Bachéga, C. and Almeida, P. (2009). Benefícios proporcionados pela TI na prefeitura municipal de Botucatu: Uma análise da percepção dos usuários e dos gerentes de informática. Actas da ETIC - Encontro de Iniciação Científica, 5(5): 1-12.

Bailoa, S. (2011). Impacto dos sistemas de informação nos processos de trabalho: O caso da câmara municipal de Sintra (Dissertação de Mestrado). Instituto Universitário de Lisboa.

Bastos, E. and Sobral, R. (2023). The use of information systems as a decision-making instrument in financial institutions in the municipality of Medianeira-PR: the managers' perception. Revista Interdisciplinar Científica Aplicada, Blumenau, 17(2): 47-67.

Beltrame, M. and Maçada, A. (2009). Validação de um Instrumento para medir o Valor da Tecnologia da Informação (TI) para as organizações. Organizações em contexto, 5 (9): 1-23.

Bianchi, I., Bigolin, F. and Jacobsen, A. (2015). Technology and System Information as Support Tools in Open Innovation Processs. Prisma.com, 29: 157-172.

Chimuco, Y. (2017). O impacto do Hipermanager nos processos de trabalho: aplicação aos docentes dos colégios Saidy Mingas e Nossa Senhora de Fátima em Moçâmedes (Dissertação de mestrado). Lisboa: ISCTE-IUL.

Čizmić, E., Rahimić, Z., Šestić, M. and Ahmić, A. (2022). The Impact of Job Design Parameters on Employee Satisfaction and Effectiveness in Developing Countries Within Digitization Context. In: Karabegović, I., Kovačević, A., Mandžuka, S. (eds) New Technologies, Development and Application V. NT 2022, Lecture Notes in Networks and Systems, Springer, Cham. 472: 1076-1082.

Čizmić, E., Rahimić, Z. and Šestić, M. (2023). Impact of the main workplace components on employee satisfaction and performance in the context of digitalization. Zbornik Veleučilišta u Rijeci, 11 (1): 49-68.

Cox, W. (2002). The Most Critical Security Issue. GIAC - Global Information Assurance Certification, GSEC Practical Assignment, 1.2: 1-9.

Dewett, T. and Jones, G. (2001). The role of information technology in the organization: a review, model and assessment. Journal of Management, 27: 313-346.

Doll, W. and Torkzadeh, G. (1989). A Discrepancy Model of End-User Computing Involvement. Management Science, 35(10): 1151–1171.

Doll, W. and Torkzadeh, G. (1999). The development of a tool for measuring the perceived impact of information technology on work. Omega, 27(3): 327-339.

Doll, W., Deng, X., Raghunathan, T., Torkzadeh, G. and Xia, W. (2004). The Meaning and Measurement of User Satisfaction: A Multigroup Invariance Analysis of the End-User Computing Satisfaction Instrument. Journal of Management Information Systems, 21(1): 227-262.

Espírito Santo, P. and Correia, L. (2022). Multi-criteria model for prioritizing information technologies in a public security department. Revista CIATEC – UPF, 14 (2): 57-81.

Ezingeard, J., Mcfadzean, E. and Birchall, D. (2005). A Model of Information Assurance Benefits. Information Systems Management. ABI/INFORM Global: 20-29.

Galvão, J. (2022). O Impacto dos Sistemas de Informação nos Processos de Trabalho dos Contabilistas do Baixo Alentejo e Alentejo Central (Dissertação de Mestrado). Instituto Politécnico de Beja.

Haberkamp, A., Maçada, A., Raimundini, S. and Bianchi, M. (2010). The impact of investments in information technology (it) on the strategic variables of Accounting services firms. BASE – Revista de Administração e Contabilidade da Unisinos, 7(2):149-161.

Laureano, M. and Moraes, P. (2005). Segurança como estratégia de gestão da Informação. Revista Economia & Tecnologia, 8(3): 38-44.

Laudon, K. and Laudon, J. (2014). Management Information Systems: Managing the Digital Firm. New Jersey: Pearson (13rd edition).

Lunardi, G., Dolci, P. and Maçada, A. (2010). Adopção de Tecnologia de Informação e seu Impacto no Desempenho Organizacional: Um Estudo realizado com Micro e Pequenas Empresas. RAUSP-Revista de Administração, 45(1): 5-17.

Maçada, A. and Borenstein, D. (2000). Medindo a satisfação dos usuários de um sistema de apoio à decisão. Actas do 24 Actas do Encontro Nacional da ANPAD (ENANPAD), Florianópolis. Administração da Informação: 1-11.

Maçada, A., Lucht, R. and Hoppen, N. (2007). Ampliação do Modelo de Impacto de TI de Torkzadeh e Doll à luz do Processo Decisório e da Segurança da Informação. Actas do XXXI Encontro da ANPAD, Rio de Janeiro: 1-16.

Mafra Pereira, F., Sobrinho, W. and Alves, R. (2018). Decision-making model of a multinational company based on information systems and flows. Revista de Administração FACES. Journal Belo Horizonte, 17 (2): 30-54.

Marchand, D. (1990). Managing information quality. In: Wormell, I. (Ed.) Information quality:

definitions and dimensions. London: Taylor Graham, 7-17.

Marciano, J. (2006). Segurança da informação: uma abordagem social. (Tese de Doutoramento). Universidade de Brasília.

Mariano, A., Monteiro, S., Ramírez-Correa, P., Moysés, D. and Santos, M. (2020). Information Systems User Satisfaction: Application of a model for e-Government. 15th Iberian Conference on Information Systems and Technologies (CISTI) 24 – 27 June 2020, Seville, Spain.

Mendonça, M., Freitas, F. and Souza, J. (2009). Tecnologia da informação e produtividade na indústria brasileira. ERA, São Paulo, 49(1): 74-85.

Nehmy, R. and Paim, I. (1998). A desconstrução do conceito de qualidade da informação. Ciência da Informação, 27(1): 36-45.

Neto, J. and Riccio, E. (2003). Desenvolvimento de um instrumento para mensurar a satisfação dos usuários de sistemas de informações. Revista de Administração, 38(3): 230-241.

Olaisen, J. (1990). Information quality factors and the cognitive authority of eletronic information. In: Wormell, I. (Ed.) Information quality: definitions and dimensions. London: Taylor Graham, 84-91.

Paim, I., Nehmy, R. and Guimarães, C. (1996). Problematização do conceito "Qualidade" da Informação. Perspectivas em Ciência da Informação, Belo Horizonte, 1(1): 111-119.

Pereira, M. (2003). O impacto da tecnologia da Informação sobre o processo de trabalho bancário (Dissertação de Mestrado). Escola de Administração, Universidade Federal do Rio Grande do Sul, Porto Alegre, Brasil.

Pereira, M., Becker, J. and Lunardi, G. (2007). Relação entre Processo de Trabalho e Processo Decisório Individuais: uma análise a partir do Impacto da Tecnologia da Informação. RCA – Electrónica, ANPAD, 1 (1): 151-166.

Pinsonneault, A. and Kraemer, K. (1993). The impact of information technology on middle managers. Mis Quarterly, 17(3): 271-292.

Pipino, L., Lee, Y. and Wang, R. (2002). Data quality assessment. Communications of the ACM, 45(4).

Ribeiro, R. (2012). Impacto do Fénix nos Processos de Trabalho: Aplicação dos Docentes do ISCTE-IUL (Dissertação de Mestrado). Lisboa: ISCTE-IUL.

Rodrigues, J. (2009). Avaliação do impacto de uma Tecnologia de Informação para gerenciamento de serviços de saúde na percepção dos clientes internos do Hospital Universitário de Brasília (Dissertação de Mestrado). Universidade de Brasília.

Santos, F., Morikane, C., Oliveira, E. e Chamon, M. (2007). O Paradoxo da Produtividade e a Gestão da Tecnologia da Informação. Actas do XI Encontro Latino Americano de Iniciação Científica e do VII Encontro Latino Americano de Pós-Graduação – Universidade do Vale do Paraíba, Brasil, 1-4.

Sarkar, S. (2005). Innovation, entrepreneurship and development. Int. J. Entrepreneurship and Innovation Management, 5(5/6): 359-365.

Schwarz, G. (2002). Organizational hierarchy adaptation and information technology. Information and Organization, 12: 153–182.

Silveira, J., Dolci, D., Cerqueira, L., Wendland, J. and Silva, B. (2019).Information Security: an analysis of the perception of threats that affect the Intention to Comply with Information Security Policies for users of organizations in the State of Rio Grande do Sul. Revista de tecnologia aplicada, 8(1): 3-19.

Simon, H. (1960). The new science of management decision. Harper & Row, New York and Evanston, 1-50.

Souza, B., Schdmit, V. and Araújo, M. (2010). Tecnologia da informação nas organizações. Actas do VII SEGET – Simpósio de Excelência em Gestão e Tecnologia: 1-13.

Yoshikuni, A., Favaretto, J., Albertin, A. and Meirelles, F. (2018). As influências dos Sistemas de Informação Estratégicos na relação da Inovação e Desempenho Organizacional. Brazilian Business Review (Portuguese Edition), 15(5): 444-459.

REMOTE MEASUREMENTS AND DISTANCE LEARNING ON ELECTRONIC LABORATORIES

Hatzopoulos A. T.[1], Tsiakmakis K.[1], Delimaras V.[1], Vassios V.[1], Tokatlidis C. G.[1] and Papadopoulou M. S.[1]

[1]Department of Information and Electronic Engineering, International Hellenic University, Sindos, Thessaloniki, 57400, Greece
ahatz@ihu.gr

1. INTRODUCTION (headlines: TNR Bold, 12pt)

During the last decades, the term "remote laboratory" was rarely heard and more rarely implemented because it was immature and the technology was not able to offer the necessary connectivity. Before the pandemic of covid-19, many universities have already used the remote or virtual laboratories to offer the distance learning. Nowadays, after the pandemic, it is necessary to change the education procedure. The academic staff has to adopt distance learning practices that have beed urgently developed. While several steps have been made for the theory lectures, the adapting of the laboratory lessons to the new requirements has been delayed. In the present work, we study and design a hybrid system, for on-the-spot and distance-learning students, for electronic measurements in a laboratory. The implementation of the circuit is done locally by student or teacher. The measurements are taken by electronic equipment and displayed locally, as well as remotely, to distance learning students. The students are able to monitor, record and configure the measurements on the selected circuit points.

2. OBJECTIVES

Due to covid-19 pandemic, many studies and researches on the different ways to implement a remote or a virtual laboratory have taken place. Almost all the universities tried to change their way of teaching. The theory lectures adapted distant meetings applications, like zoom and webex, and achieved good results. The laboratory lessons can be categorized in three groups. The first group is by using a personal computer (PC) with specific software and can be more easily carried out by the students in their home, like software teaching laboratories. The second group is using measuring instruments connected to a PC or a network and executes remotely the needed measurements, like electronic circuits laboratories. The third group is using measuring instruments and devices that cannot be connected to any PC or network.

The traditional electronic laboratory courses are carried out with the corresponding theory lectures, so that students can combine both theoretical design knowledge and laboratory skills. Before the laboratory exercise, the students must carry out a preliminary assignment with theoretical calculations. Next, comes the software simulation stage of the electronic circuit by the students, even at their home, so students can understand the way the circuit works and have the best preparation and understanding of the circuit's theory. Finally, the students team up in groups, make the circuit work properly and measure the preselected circuit points to confirm their calculations and understand the differences between theory, simulation and experiment. Usually, in this last part, the students can obtain the laboratory skills but they work in groups and they usually have maximum up to 1,5 hour. This time period is too small, especially if the group is consisted by three or more students or, even worse, if the circuit is not configured to work properly, according to the theoretical calculations.

At the first stage of the pandemic lockdown, the universities were not prepared. In order to minimize this loss of the laboratory skills, many steps were made, but not enough. The laboratory measurements were difficult to be taken, so the try was focused on increasing the laboratory skills

obtaining, by simulating the instruments operation with software, wherever it was possible. This work is aiming to combine instrument handling and measuring for students in the laboratory room and for remote students connected to the instruments through internet, while the teacher can show the instrument's configuration and operation to both local and remote students.

3. TEACHING LOCAL STUDENTS

Probably, the most difficult electronic circuit laboratory exercises are those which use oscilloscope and function generator. The difficulty is due to the oscilloscope's complexity and the students poor understanding of alternating and sinusoidal signals. This work, was applied on an AC signal amplifier laboratory exercise, in which both oscilloscope and function generator must be used.

Usually, the teacher in the electronics circuits laboratory has to deal with the following steps.

Step 1.   Preliminary preparation of students on theory and on circuit simulation results.
Step 2.   Instrument operation explanation that is usually achieved by teacher's oral instructions to all students.
Step 3.   Instrument hands-on configuration, individually to every team, showing the operation's key points that are not already covered by step 2.
Step 4.   During the measurements, necessary corrections and adjustments on the circuit.
Step 5.   During the measurements, instrument configuration changes and understanding of the readings.

Step 1 can be easily done locally or by previous document preparation by students, according to the teacher's instructions. This work has not any innovative to propose for this step.

Step 2, possibly can be enriched with a PC, a projector and a video file showing the instrument's functions and operations. If the instruments can be connected to the PC and controlled by a software application, like NI LabVIEW instrument drivers, the teacher can use a simple web camera to show live on the projector the necessary settings and the response of the instruments, showing their display (fig. 1). NI LabVIEW software is used as software application for this work. (National Instruments, 2023), (Siglent Technologies, 2012), (Siglent Technologies, 2014).
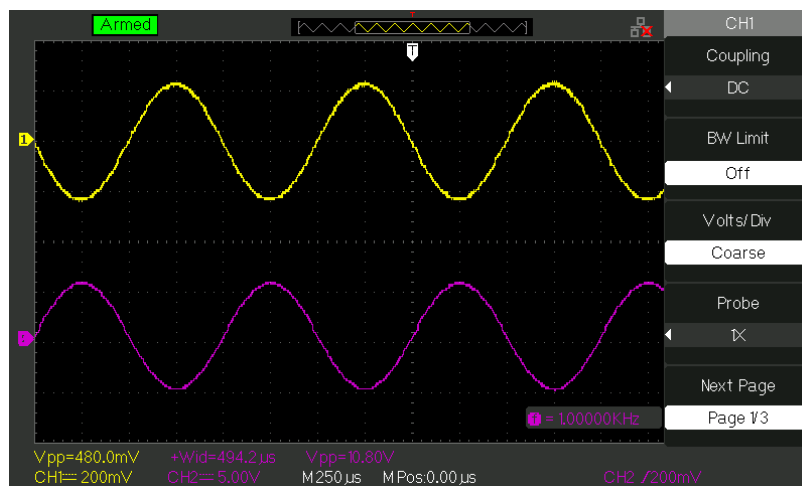
Figure 1. The display of the oscilloscope shown to students, while explaining the two channel operation.

Step 3 includes the initial instrument configuration. At least at the first exercises, the teacher has to check every team's ability to control the instruments, especially the complicated, like the oscilloscope with triggering handling. The experience and knowledge of the teacher is very important. For the first exercises, this repeated demonstration and configuration to all student teams probably can be faster if the teacher can acquire in his display the oscillator's and generator's display and settings and apply the necessary corrections with a single button pressed.
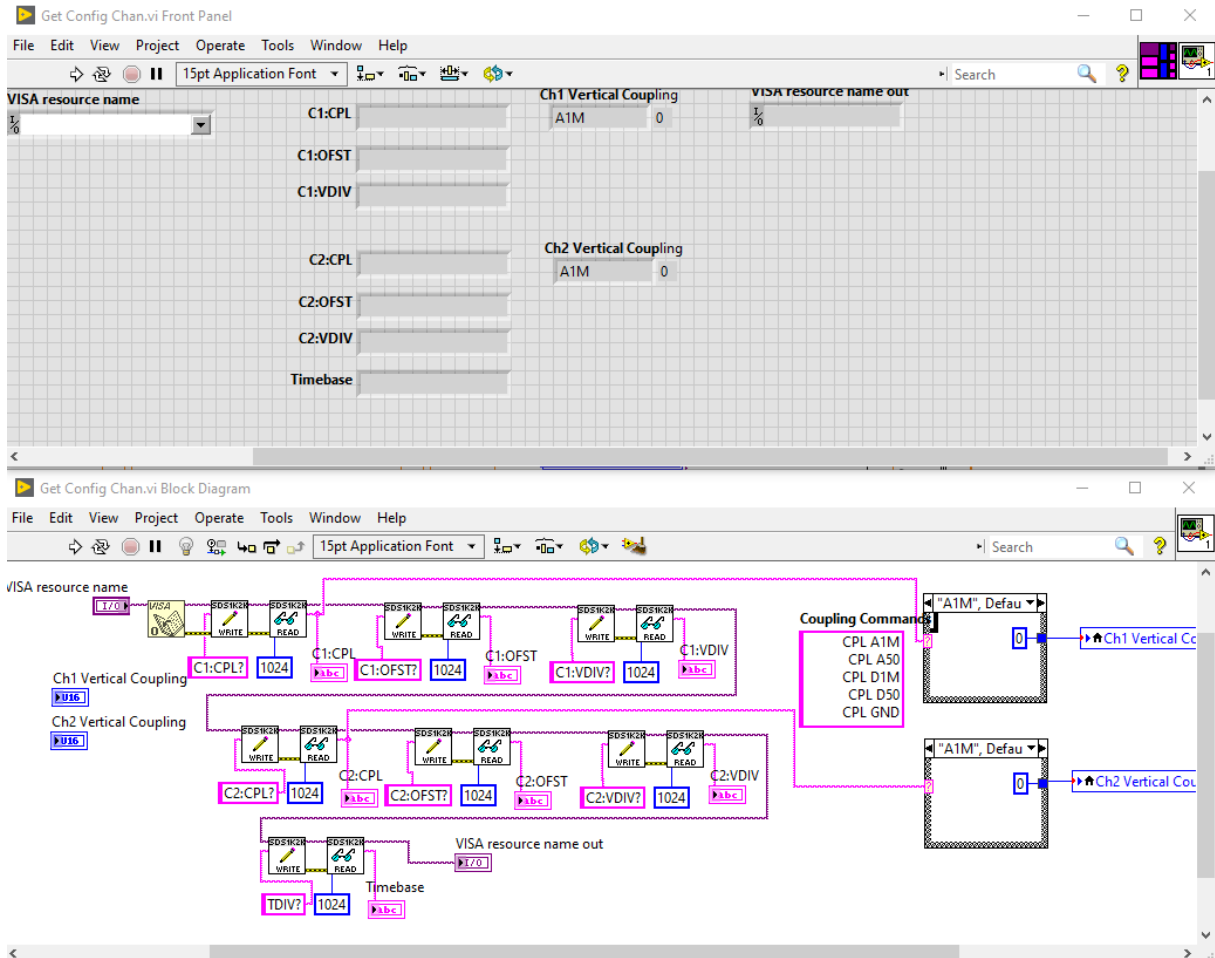
Figure 2. LabVIEW application to acquire the oscilloscope's settings.

Step 4 includes the faults on the circuit's breadboard and cables and can be done only by hand inside the laboratory room.

Step 5 is the most demanding for the students because if there is a measurement that is not similar with the calculations, the source of this problem is unknown. The student probably will try to change the settings of the oscilloscope, which keeps the circuit unchanged, or will try to change the function generator and the circuit elements, which will provoke significant changes. The teacher, using the application, can see exactly what the oscilloscope screen shows and then make the proper questions to the students to guide them to find the source of the fault or make the necessary settings. Obviously, the best way to show to students the fault is achieved inside the laboratory room, next to them.
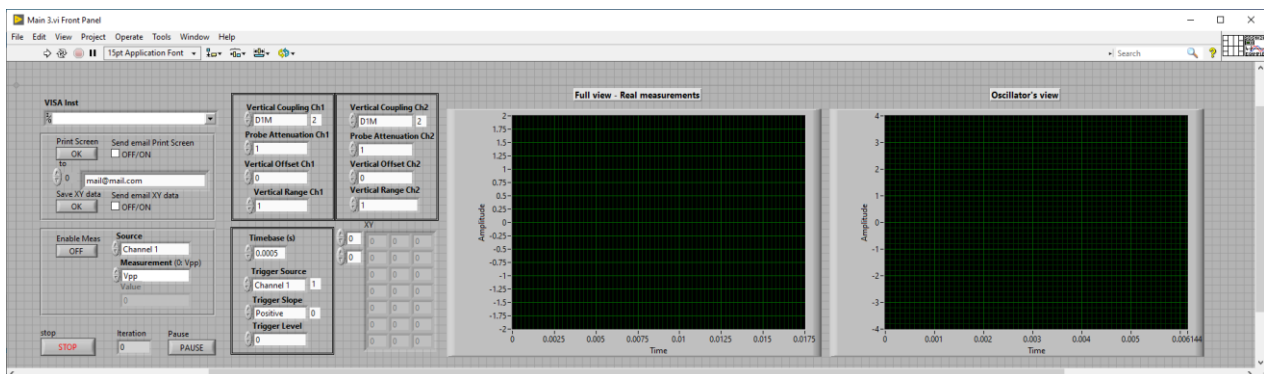
Figure 3. Application for teacher with full oscilloscope control.

4. TEACHING REMOTE STUDENTS

Due to the covid-19 pandemic, new methods of implementing remote laboratories were developed. This work focuses on the remote laboratory students and the way to increase the educational results of distance-learning. The proposed methods will be categorized according to the five steps presented in part 3.

Step 1 is already individual of the laboratory room. The theoretical preparation is done in home and the circuit simulation must follow the preparation to give students the ability to confirm their calculations.

Step 2 for remote students is more difficult than for local, because they cannot see the front panel of the instrument. The proposed way to help them minimize this problem is the following. While teacher is explaining to all local students simultaneously, if the instruments are connected to PC, he can show the buttons and their function on an image shown on the projector. The same image and explanation can be shown to the remote students with the software application designed for the specific instrument. Depending on teacher's decision, the application can show only the necessary buttons. This work's application can be used by the teacher and all students, local or remote and both will be able to see it (fig 4). Additionally, the teacher can get an image of the display of the instrument he is controlling. For this work, as mentioned above, the application is controlling a function generator and an oscilloscope. Teacher, local students and remote students can see the same image (fig. 5) and the teacher can easily give the proper advices.
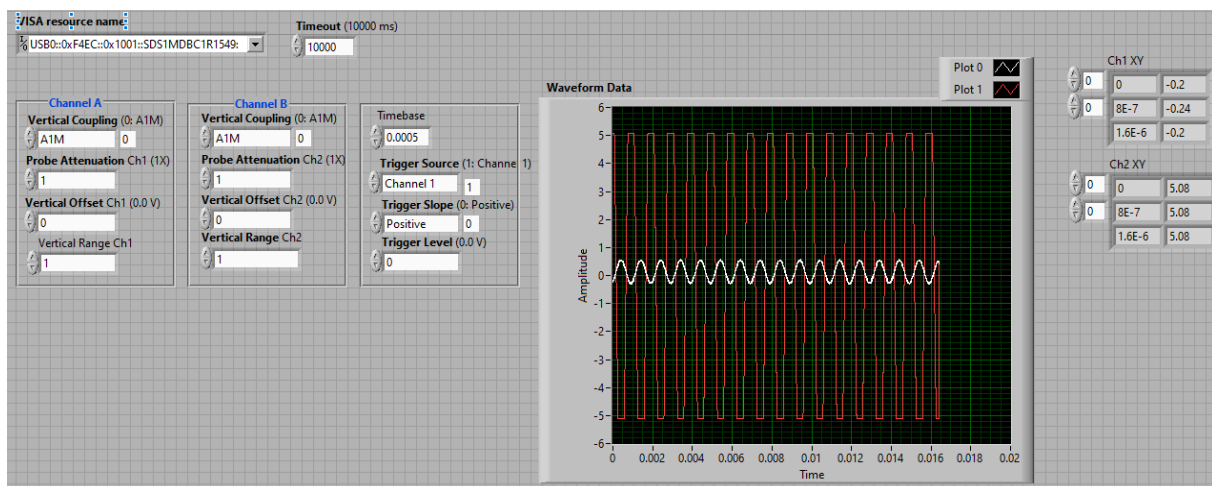
Figure 4. Application used by the local students
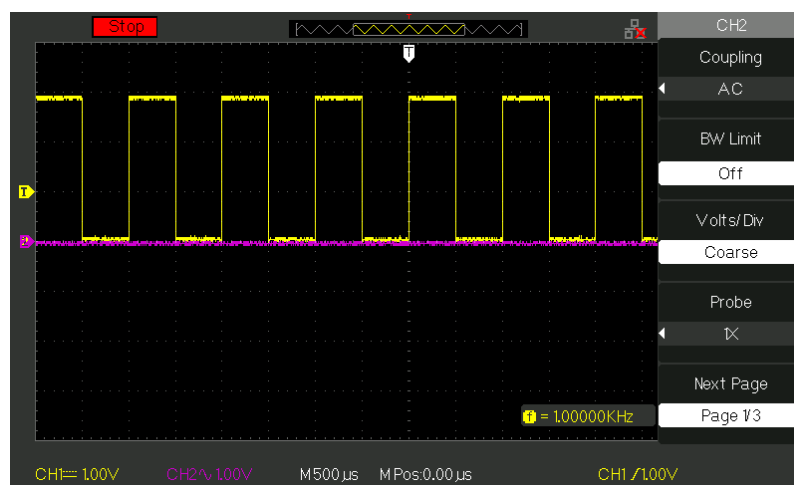
Figure 5. Oscilloscope's display shown to students

Step 3 can be implemented for both students with the same application that is described again for the step 3 in the previous part (fig 2). The teacher can see every oscillator's settings with a button

pushed. The same capability can be given to the remote students and run simultaneously for both users, if the oscilloscope is connected to a network.

Step 4, as described above, is related with the faults on the circuit's breadboard and cables and can be done only by hand inside the laboratory room.

Step 5 is more demanding for remote students and needs the cooperation of a local and a remote student. If the fault is in the oscilloscope's settings, both students can find and change it. If the fault is in the circuit, only the local student can correct it. The measurements can be taken by both students using the application (fig. 3). Also, they can record and exchange the measurement values or a signal's set of points, acquired easily in a file in the PC (fig 6).
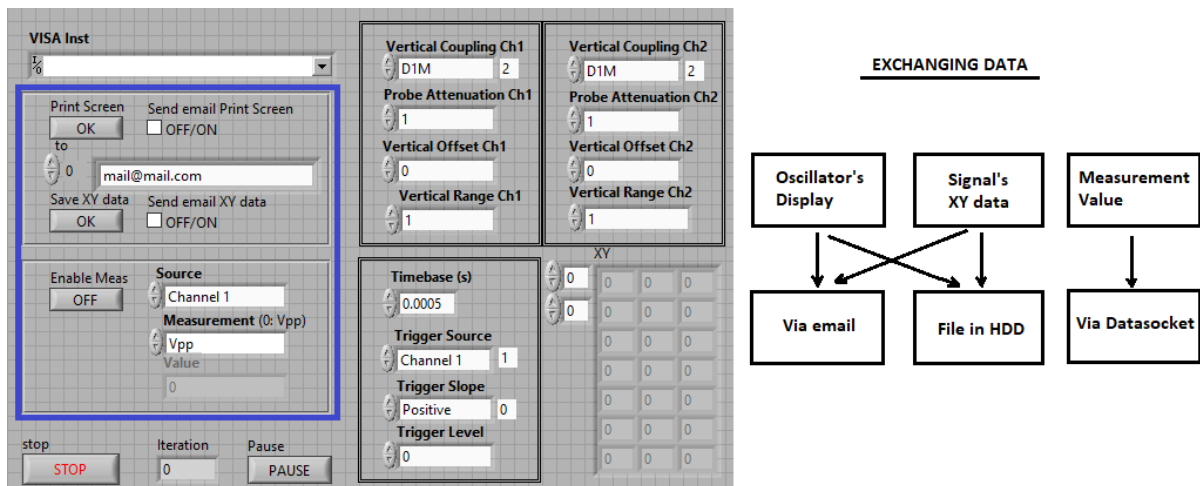
Figure 6. Sending data through different ways

5. PRACTICING WITH INSTRUMENTS FOR REMOTE STUDENTS

All students have little time available to spend in the laboratory and get familiar with the instruments. Some departments have scheduled some time slots in the laboratory rooms, when the students can practice on the instruments to learn their operation.

For remote students, some oscilloscopes and function generators, or even some circuits, can be enabled and connected to a PC or a network. Then, by using the proper remote control application, the students can extend the laboratory duration for much more time, by practicing in their home, even together with the electronic circuit simulation application. For each set of instruments connected, many students can benefit, even 24/7 (fig. 7).
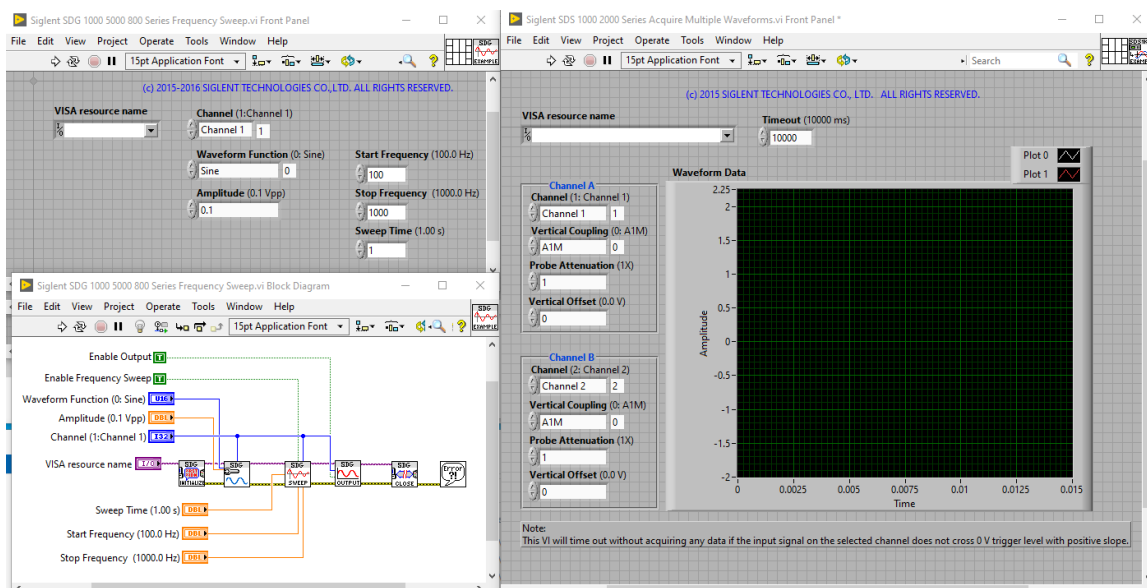
Figure 7. Remote students can practice on instrument usage

6. CONCLUSION

With new technological advances, the laboratory exercises can be implemented in a satisfying level, even for remote students. The technology provides connectivity and remote operation to many new instruments, which can be controlled through a PC or a network. The universities must use these new capabilities and focus on the ways to give to local and remote students increased knowledge and laboratory skills acquisition.

7. REFERENCES

National Instruments (2023) LabVIEW, Viewing and Controlling Front Panels Remotely with the Web Server, www.ni.com.

Siglent Technologies CO., LTD (2012), Remote Control Manual SDS1000 Series Oscilloscopes, "Siglent.eu".

Siglent Technologies CO., LTD (2014), Remote Control Manual SDG1000 Series Function/Arbitrary Waveform Generator, "Siglent.eu".

ASSESSING THE IMPACT OF STUDENT SYNDROME ON MEETING SINGLE-PROJECT DEADLINES: A QUANTITATIVE ANALYSIS

Tomaž Aljaž[1], Nikolaos S. Petrakis[2]

[1]FINI Novo mesto, Slovenia
[2]HMU, Greece
E-mail: tomaz.aljaz@fini-unm.si (corresponding author)

1. INTRODUCTION

To stay competitive, organizations use their information systems and technology to quickly adapt to global market changes through projects (Xiaodong et.al., 2009) to meet customer requirements and increase Business Value. Measuring Business Value includes productivity gain, product quality, customer satisfaction, and profit and market measures (Anavi-Isakow et.al., 2003). However, in the ever-changing information technology landscape with fluctuating demand, variable task duration, and technological uncertainty, meeting project goals is challenging, as indicated by the Standish Group Chaos Study report evaluating over 50,000 software development projects over 25 years (Standish Group, 2021).

Table 1: Standish Group Chaos Study revealing success rate of IT projects from 1994 to 2020.

	1994	1995 -1999	2000 - 2004	2005 - 2009	2010 - 2014	2015 - 2020
Successful	16%	27%	30%	33%	38%	35%
Challenged	53%	43%	51%	46%	43%	46%
Failed	31%	30%	19%	21%	19%	19%

The Standish Group Chaos Study found that project success depends on meeting the triple constraint of time, budget, and scope. Successful projects meet all three constraints, while challenging projects meet only two. According to the study, as shown in Table 1, around 35 percent of projects are successful, and 46 percent are challenging, thus leaving room for improvement in managing projects management.

A traditional approach (Bhardwaj et.al., 2010), (Aljaž, 2021) to these issues is to estimate the workload and to set completion time for the individual tasks or groups of tasks (e.g., new software release), based on the customer needs or priority. However, this approach often results in inflated estimates to accommodate last-minute changes and uncertainties. In addition, setting due dates for tasks can lead to procrastination and ultimately delays, reduced quality, and increased stress for the project team), as shown in Figure 1. This phenomenon is known as the Student Syndrome. (Goldratt, 1997.

Figure 1 Student Syndrome example (Holt et.al, 2014).

Figure 2: Student Syndrome domino effect (Holt et.al, 2014).
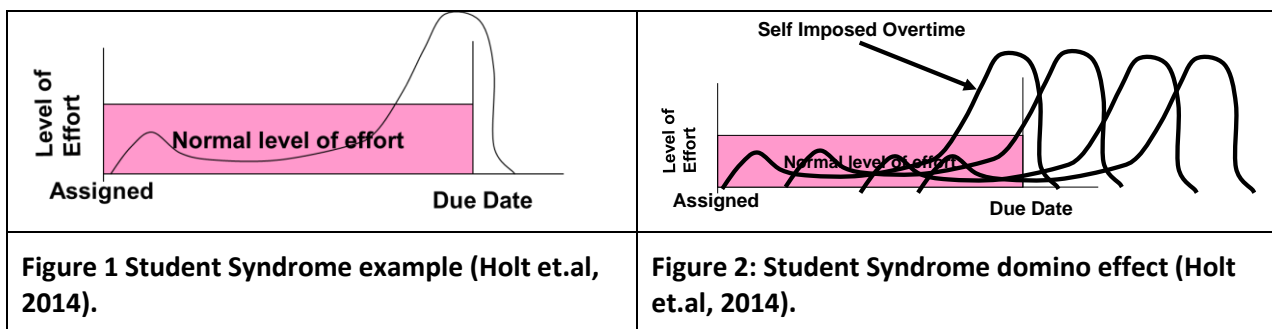
The Figure 1 displays an employee's effort and time spent on a task, with the task length shown by vertical lines representing the assigned and due dates. Initial effort is put into evaluating real effort at task assignment, but significant effort is put in towards the due date to finish on time. However, lost time cannot be compensated for, resulting in delay or reduced quality. This delay has a domino effect on remaining tasks, as shown in Figure 2.

The focus of the study presented in the paper is to show devastating effect of project task deadline approach and human behavior in a form of Student syndrome at different project examples. The paper contributes to the research and practice of managing information technology Projects by (i) giving a comprehensive overview of human behavior in a form of Student Syndrome on project due date and (ii) validating the findings by a using discrete-event simulation model built with PmSim (Elyakim 2.03).

In Section 2 the problem definition is given and the research methodology in Section 3. In Section 4 are presented the results and the findings are summarized and discussed. Section 5 draws conclusions and gives implications for further practice.

2. PROBLEM DEFINITION

According to (Standish Group, 2021) the project success rate is low. One of the reasons of this poor performance is also influenced by Student Syndrome, as we have discussed in Section 1. This results in failure to deliver project on defined project due date.

The task of the simulation is to get answer on the following questions:

- What is the average probability of project due date in single project environment (to be used as a baseline)?
- What is the impact of the Student Syndrome on the same process for the single project due dates?
- What is the impact of the Student Syndrome on the same process for the single project due dates with 90% probability?

3. SIMULATION SETUP

In our study, we use a quantitative approach that includes a Simulator, observations, and personal experience. The Simulator allows us to examine different project parameters one at a time, avoiding the effects of interacting variables. This approach helps us manage project tasks and address Student Syndrome systematically.

We use PmSim simulation tool (Elyakim 2.03) as in (Aljaž, 2020) to analyze and compare results. The simulated environment includes example projects with sequential and parallel tasks, interdependencies, and limited resources, mimicking real-life scenarios.

The planned completion time is 98 days, where each resource has planned 14 days to finish his/her tasks as shown in Figure 3.

Figure 3. Project simulation environment
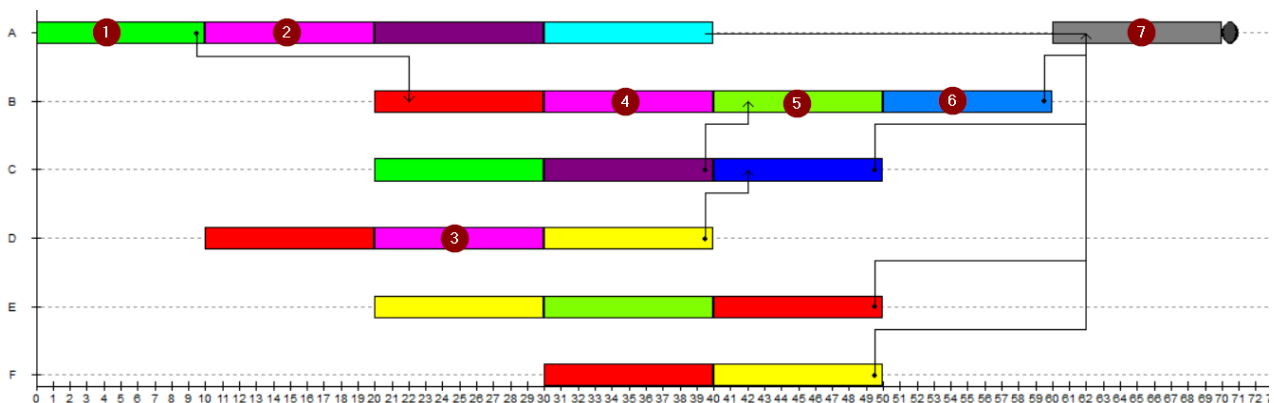
The Critical Path - CP (PMI, 2021) of the project is shown with numbered tasks, from 1 to 7. The CP is the longest sequence of tasks that must be completed to finish a project. Delaying tasks on the critical path will delay the entire project.

Additionally, scheduling project tasks can be done in two well-known general approaches: starting non-critical tasks that don't have any time restrictions associated with them (1) As Soon As Possible – ASAP or (2) As Late As Possible - ALAP relative to the start and the end of the project (PMI, 2021).
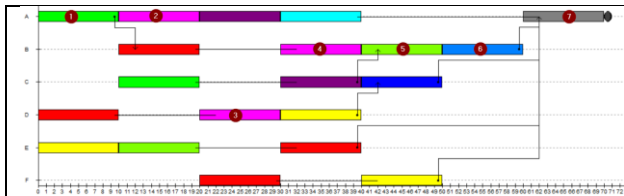
Figure 4. Project simulation environment with tasks started "as soon as possible".	Figure 5. Project simulation environment with tasks started "as late as possible".
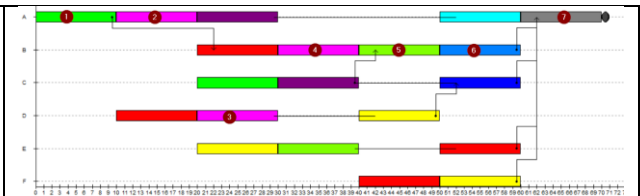
Starting a task ASAP, as shown in Figure 4, is often preferred, but may result in starting without all necessary information, potentially impacting success. ALAP scheduling, as shown in Figure 5, can be used to avoid this, but unexpected delays can cause missed completion times and delays to CP tasks.

4. RESULTS AND DISCUSSION

The project due date is important parameter for success of the project. A shorter due date is preferable to maximize Business Value (Bhardwaj, 2010).

Figure 6 shows average task completion times for different scenarios, with the highest probability of meeting the due date in scenarios without Student Syndrome (94%-99% on average) and low dispersion. In contrast, scenarios with Student Syndrome have significantly lower and more dispersed results (50%-83% on average). The probability of finishing a project on time is 97% on average without Student Syndrome and 71% with it.

The project due date is 38% longer with tasks affected by Student Syndrome due to variability in task execution, resource contention, and converging points of parallel tasks. Student Syndrome magnifies these negative effects and contributes to missed project deadlines.
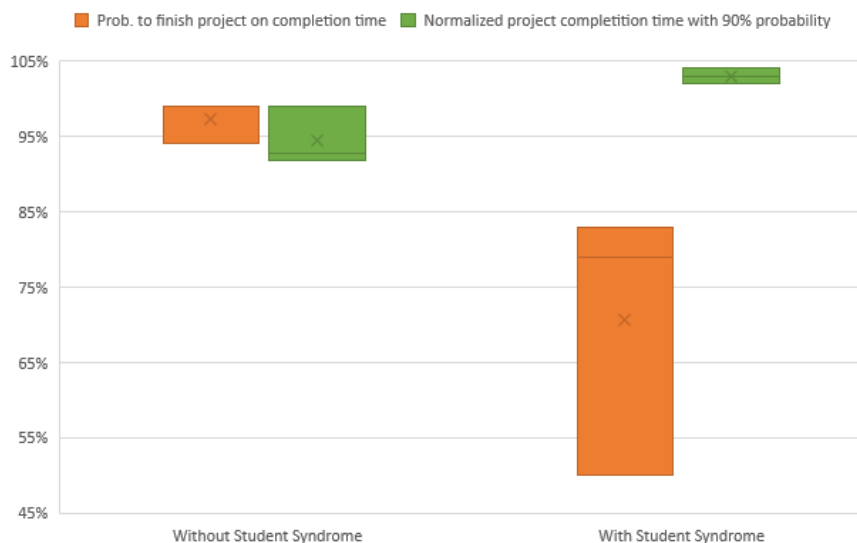
Figure 6. Quartile chart of results at the end of a simulation run for different simulation scenarios.

The Figure 6 shows the normalized project due date with 90 percent probability for each simulation run. For project management community, the due date time with 90 percent probability is considered acceptable (Holt et.al., 2014). Without Student Syndrome, the project's due date is always met, with completion times ahead of schedule, ranging from 92 percent to 99 percent on average. However, with Student Syndrome, completion times are delayed in most simulation runs, ranging from 102 percent to 104 percent on average.

Results of simulation runs can be summarized:

- Project completion probability improves by 38% without Student Syndrome compared to with it. Completion times are always above 94% without it, while with it, they are below.
- Without Student Syndrome, project due dates are always met with defined completion times with a 10% improvement in the due date with 90% probability.

5. CONCLUSION

This study examines how the Student Syndrome affects project due dates. We analyze various project scenarios, task performance metrics, and human behavior, and find that the Student Syndrome prolongs individual task completion time, leading to a delay in the project due date. The study uses the PmSim simulator to formalize the results.

The first important conclusion of the study is that project convergence points, thus tasks which cannot start before preceding parallel ones are not completed, are in most cases missed. The execution delay is noticeable in slack project tasks with scheduled late start (ALAP), which does not take advantage to start based on the actual finish of the preceding activity when variability in tasks execution exists. Second, Student Syndrome combined with resource contention and their task execution variability additionally worse overall situation on project due dates. Finally, eliminating the Student Syndrome ensures a considerable and immediate improvement in project due date, ranging up to 38 percent better compared to situations with Student Syndrome.

The overall objective of this study is not to propose solutions to reduce the impact of human behavior in form of Student Syndrome, but to identify and surface this issue to project failure. Organizations must fully understand the core issues of project management, where human behavior is only one of them that needs to be addressed in its environment before proposing a comprehensive solution to identified problems. Without this systems perspective, a proposed solution may create more problems than it solves.

6. ACKNOWLEDGMENT

7. REFERENCES

Aljaž T. (2021). Improving throughput and due date performance of IT DevOps teams, Elektrotehniški vestnik 88(3): 121-128

Aljaž T. (2020). From Efficient to Effective Project Teams, Izzivi prihodnosti. 2020, leto 5, št. 1, str. 1-16. ISSN 2463-9281

Anavi-Isakow, S., & Golany, B. (2003). Managing multi-project environments through constant work-in-process. International Journal of Project Management, 21(1)

Bhardwaj, Gupta. (2010). Drum-Buffer-Rope: The Technique to Plan and Control the Production Using Theory of Constraints. World Academy of Science, Engineering and Technology, Article 19, page 103

Elyakim Management System. PmSim Version 2.03 (student version)

Goldratt E. (1997). Critical Chain, Gower Publishing Ltd

A Guide to the Project Management Body of Knowledge and the Standard for Project Management and the Standard for Project Management - 7th Edition, Project Management Institute, 2021

Holt, J., Aljaž, T., Johnson, R., Holt, S., Furback, R., Button, S. (2014). EM 530 Lecture materials, Washington State University 2014

Review Standish Group – CHAOS 2020. (2023). Beyond Infinity, https://hennyportman.wordpress.com/2021/01/06/review-standish-group-chaos-2020-beyond-infinity/, accessed 15th of March 2023

Xiaodong Zhang, Le Luo, Yu Yang, Yingzi Li, Christopher M. Schlick & Morten Grandt (2009). A simulation approach for evaluation and improvement of organisational planning in collaborative product development projects, International Journal of Production Research, 47:13, 3471-3501

DETECTION OF BRAIN TUMORS IN T2 MRIS BASED ON VARIOUS AI ALGORITHMS: ANN, ANFIS, CNN FED BY DWT MRIS ANALYSIS

Afentakis, N.[1], Polydorou, A.[2], Sergaki, E.[2], Krasoudakis, A.[3], Tsalikis, G.[3], Stavrakakis, G.[2], Zervakis, M.[2], Polydorou, A.A.[4], and Vardiambasis, I.O.[1*]

[1] Laboratory of Telecommunications and Electromagnetic Applications, Department of Electronic Engineering, Hellenic Mediterranean University, Chania, Greece

[2] School of Electrical and Computer Engineering, Technical University of Crete, Chania, Greece

[3] Clinic of Neurosurgeon, General Hospital Agios Georgios, Chania, Greece

[4] Medical School, National and Kapodistrian University of Athens, Athens, Greece

* ivardia@hmu.gr

1. INTRODUCTION

Magnetic resonance imaging (MRI) remains one of the most tested and trusted indispensable tool to scan and detect a possible brain tumor, to further enhance a clinical patient's data, up to the point that his or hers symptoms, as well as their macroscopic examination, tune towards a well-defined treatment protocol. As MRI, a by far superior technique than CT (computed tomography) or ultrasound, delivers highly accurate data, painless and by high volumes, it's their huge amount and their fully investigate nature that introduce the main factor enabling errors and miscalculations concerning the positive detection of depicted anomalies. The MR method generates images showing tissue surface contrast as greyscale pixels (2-dimensional, for each slice), their value based on differences of the magnetic properties of the atomic nuclei of Hydrogen (H_2).

Benign and malignant pathologies could be very tricky to distinguish (Buetow et al., 1991). Lower grade Gliomas can be developed and grow slowly in any part of the brain or the central spinal cord (Bigos et al., 2015) and are quite hard to detect even by the trained eye. Gliomas are mainly heterogeneous in appearance and manifest variable degrees of typology and activity. Given their variable nature and presence, we must assume that the current state of the art MRIs on glioma is more challenging (Zinn et al., 2011). There are also rare cases of angiomatous and microcystic meningiomas that are showing as multiple tiny intralesional cysts or as entrapped peritumoral cyst formations (Choi et al., 2022).

Therefore, the process of manually inspecting one MR image after another, for long periods of time, multiplied by long lists of patients, is a time-consuming routine and a hugely error-prone procedure. This tedious work is accomplished by the radiologists at first and by the assigned doctor on a second level. It is easy to understand that each type of tumor reveals itself differently as an atypical congregation of pixels among other healthy pixels. Another common problem is that sometimes, even multiple complex tumors, manifest themselves on only a small number of images, in a sense that very few brain slices are affected.

Recently, Computer Aided Diagnosis (CAD) tools based on Machine Learning (ML) and AI, provided promising forms of automated classification and grading of malignant or cancerous brain tumors, by analyzing MR images and suggesting specific areas of interest (potential tumor manifestations) for the radiologists/doctors to focus on, in their earlier diagnosis stages. A combined intelligence scheme, that of using both AI and human expertise, is the ultimate task, during the near future of this kind of semi-automated diagnosis, taking in account both intricacies and limitations (Bakas et al., 2017).

There are three common types of MRIs that can be easily obtainable now-days. The examined brain specifics are depicted with consistent image variation, depending on the type of MR parameters used to aggregate their areas and boundaries. Table 1 is summarizing this distinction per these three types of MRI.

As different modalities of MRI scans (T1, T2, T2-FLAIR and moreover: Gradient Imaging, Diffusion Weighted Image or DWI, Functional Image and Diffusion Tensor Imaging) respond to the various biological information in the brain differently, we have to test which one is the most promising, combined with our rest of methodologies, so to reach in an accurate diagnosis, through valuable suggestions. T1-weighted MRIs provide a clear view of the brain's anatomical features and can reveal extensive injuries. T2- weighted MRIs are able to provide good visual results of diffuse injuries (less concentrated) and they can clearly highlight fat and water within the mass of the brain. In contrast, T1-weighted images highlight fat tissue within the brain but tent to eliminate the water. In the example of high grade gliomas, they would manifest themselves in a T2-weighted MRI as clearly heterogeneous or ring-shaped contrasting areas, or patterns.

Table 1. Comparative gray scale tones of various brain areas as seen by selected MRI modalities.

Type of MRI	T1-weighted	T2-weighted	T2-FLAIR (Fluid Attenuated Inversion Recovery)
How to obtain (TE and TR times)	Short	Long	Very long
Best for	Observing anatomical details	Observing pathological details	Obtaining fast possible pathological traces
CSF (Cerebrospinal Fluid)	Very Dark Grey	White	Dark Grey
Grey matter / White matter	Grey / Light Grey	Light Grey / Medium Grey	Dark Grey / Light Grey
Fat / Water	White / Dark Grey	Dark Grey / White	Grey / White
General abnormalities	Dark Grey	White	White

Classification methods using Artificial Neural Networks (ANN) (pattern recognition methods) are able to perform this kind of recognition and to separate tumor regions from the healthy brain tissues, by utilizing a great number of datasets (Watts et al., 2014). To compensate, we must perform an extraction of specific features on the slices or regions of interest (ROI), therefore to reduce the dimensionality of the initial feature dimensional space, in a way that conserves its initial structure intact. Feature extraction methods can be (i) statistical, (ii) model-based or (iii) transform methods. Various neural network architectures, such as CNNs (Alis et al., 2022), (Jeong et al., 2022), joint CNNs and recurrent NNs (CNN-RNNs) (Kuang, 2022), and generative adversarial networks (GANs) (Cinar et al., 2022b) have been used for classification of specific symptoms, promoting significant performance gains in medical CAD.

Generally speaking, the CNN's job is to compress the pictures into a format that is easier to manage while retaining key components for generating a good forecast. The most productive use for CNNs is image classification. The limitations of CNNs are that: (i) CNNs do not encode the position and orientation of objects, therefore if the pictures have a degree of tilt or rotation, (ii) CNNs have a hard time categorizing them, (iii) CNNs have inability to be spatially invariant with respect to the supplied data. (iv) Coordinate frames, which constitute an essential component of human vision, are not present in CNNs. (iv) A ConvNet requires a large dataset to process and train the neural network. Their advantages are: (i) CNNs have very high accuracy in image recognition problems. (ii) CNNs can automatically detect the important features without any human supervision. (iii) CNNs are enabling weight sharing.

CNN disadvantages are: (i) that they do not encode the position and orientation of the object, (ii) the lack of ability to be spatially invariant to the input data, and (iii) that lots of training data is required.

As bibliography (Fayaz et al., 2021), (Savareh et al., 2019), (Kumar & Mahajan, 2020), (Liu et al., 2019) proves, all deep learning models are improved when they are based on a combination of CNNs and Discrete Wavelet Transform (DWT).

In our study we compared the CNN versus ANN and ANFIS. The ANFIS is a machine learning

technique that integrates the adaptive neural network (ANN) rules and fuzzy logic (FL) theories inside an adaptive network framework to form a logical relationship between inputs and outputs. The toolbox feature of the ANFIS forms a fuzzy inference system (FIS) whose membership structure or parameters can be calibrated either by using a back-propagation method alone or combining with the least-squares-type method. Our work is mainly focused on the assessment of the possible higher performance of a CNN binary classifier, by using DWT data analysis to control the loss of information of the simple CNN model. Moreover, a comparison between SVMs, with and without DWT analysis, is presented.

The following developments and comparisons are performed: (1) A robust CNN architecture is for binary classification of the glioma brain tumors against other tumor types, (2) a satisfying reduction of information loss in the pooling layers of our CNN, by using T2-SWI MRI sequences (parallel to the axial plane of the brain, one slice), compressed into DWT form, thus achieving higher performance binary classification, as opposed to a CNN that is based only on pixel intensities and (3), as a result of (2), a less intensive performance of the machine learning SVM and in general, compared to a traditional simple CNN, ANFIS and ANN.

2.   MATERIALS AND METHODS

The data protocol used in this study approved by the ethics committee of the Greek Universities, in accordance with national and international law. Table 2 summarizes our training and testing data. Moreover, we applied to our data augmentation technique.

2.1.   MRI protocol, training and testing subsets

The initial dataset we used are MRIs of 226 images of T2-Weighted sequences (T2W) of the axial plane, one for each patient, 24 healthy cases and 202 non-healthy cases, male and female adults. The non-healthy MRIs are from "MICCAI BraTS 2015" database, and "The Whole Brain Atlas" from the Harvard database. The healthy cases are from the Greek General Hospital "St. George" of Chania. The T2W characteristics are: fast spin eco TR/TE 4800-4900/ 78 milliseconds FOV: 24cm thickness 5mm. The non–healthy dataset used are 202 cases diagnosed with brain tumors, Are neurosurgeon visually are inspected and selected by an expert neurosurgeon, including 5% high grade, 82% low grade glioma, 3% unhealthy but not recognizable. The 10.6% of the dataset are healthy cases. There are not included full enlarged tumors or clear-cut types of tumors. In our MRIs we did not mention unwanted intensity variation due to non- uniformity in RF coils and noise due to thermal vibrations of electrons and ions.

For the development of an Artificial Intelligence (AI) algorithm there is need for unbiased and statistically random data input, and different datasets for the training and testing procedures. We proceed on splitting our 226 cases original dataset in a 61% to 39% ratio, to one training and one testing dataset, respectively - but always ensuring that each one of them is inclusive of a 30% of healthy cases.

Moreover, we formulated a scenario of each one of the above datasets having 10% of healthy cases each time.

Table 2. Training and testing data used.

Data groups	Data cases
Testing Dataset (39% of the original Dataset)	34 cases, containing a ratio of 70%/30% non-healthy/healthy cases and 89 cases, containing a ratio of 90%/10% non-healthy/healthy cases
Training Dataset (61% of the original Dataset)	96 cases, containing a ratio of 70%/30% non-healthy/healthy cases and 124 cases, containing a ratio of 90%/10% non-healthy/healthy cases

2.2. Texture analysis and image processing

Due to the different sources of data, the format was not the same, we modified them in two dimensional images in "jpeg" file format. The data from the BraTS database are in "mha" file format, which refers to three dimensional images, while images from the Harvard database and from the hospital are in "gif" file format. The modified images are of 240x240 pixels of grayscale type, with 8-bit grey level depth. In next step, our skull stripping process was implemented by an algorithm based on thresholding segmentation and other morphological operations.
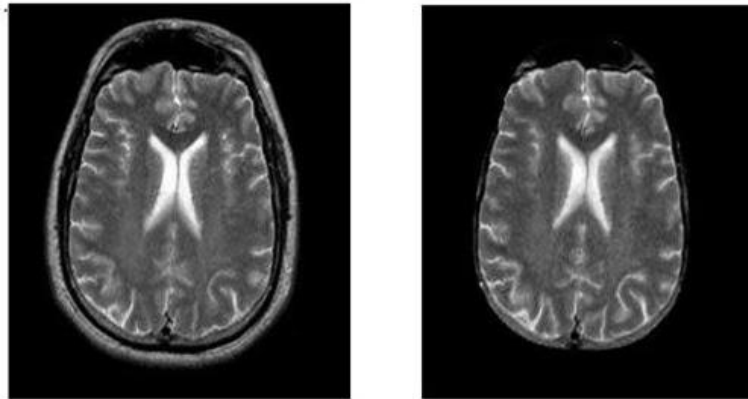
Figure 1. An example of the application of the skull stripping algorithm. Left, initial MRI image. Right, MRI image after the application of the algorithm.

2.3. GLCM texture analysis

Grey Level Co-occurrence Matrix (GLCM) analysis calculate the texture and contrast information using 1st order derived from Histogram , 2nd order statistics from gray level matrix, regarding the distribution of pixel pairs. GLCM quantifies higher-level information of an image such as texture and contrast, the GLCM is one of the most widely used image analysis applications introduced by (Haralick et al., 1973). The co-occurrence matrix allows extraction of statistical information regarding the distribution of the pixels pairs.

On the present study, no filters applied to sharpen the original MRI image. For the texture analysis, we acquired first order statistics from the original images: average and standard deviation (SD) of grey-level intensities. The intensity values were mapped in the range of 0 to 255.

Our study includes different versions of feeding our data into our AI algorithms. One idea was to feed the pixels in the form of GLCM features. We applied was image texture analysis of the Gray Level Co-Occurrence Matrix (GLCM) (Haralick et al., 1973). In total, we calculated 13 GLCM texture features for each MRI contrast. Finally, we used only the four of them: (i) skewness, (ii) homogeneity, (iii) energy and (iv) kurtosis. Kurtosis is introduced as a measure of how flat the top of a symmetric distribution is when compared to a normal distribution of the same variance, is usually of interest only when dealing with approximately symmetric distributions. These features provide variation between malignant and normal tissues, which may not be visible to the human eye. The technique consists of two steps, first it computes the GLCM matrix and then the texture features based on the GLCM are calculated. Pairs of pixels are separated by a predefined distance based on certain directions in the image and the resulting values are allocated in the co-occurrence matrix. The count is based on the number of pairs of pixels that have the same distribution of grey level values. For our 2D images, their co-occurrence matrix is computed by averaging as a function of distance S=1, in the following directions: 0°, 45°, 90°, 135°. Our gray scales x and y, calculate how often a pixel with intensity x, occurs in relation with another pixel y at a certain distance S and orientation.

In our GLCM study, the best combination and minimum number of features that finally proved to us as the most efficient for diagnosis were: (i) skewness, (ii) energy, (iii) homogeneity and (iv) kurtosis.

2.4. DWT texture analysis

Discrete wavelet transform (DWT) has become the method of choice for image analysis and classification problems, because it gives information about the signal, both in frequency and in time domains. DWT decomposes the image into the corresponding sub-bands with their relative DWT coefficients (Haykin, 2009). The inverse DWT can reproduce the original images. Generally the DWT is calculated by applying cascaded filter banks in which a low and the high pass filter satisfy certain criteria. Our idea was to feed our algorithms by the pixels in the form of DWT coefficients. We calculated the discrete wavelet transform (DWT) decomposition to obtain wavelet coefficients at three levels. This decomposition produced four sub-band (LL, LH, HH, HL) images at each scale. For every step of the decomposition only the LL sub-band was used for producing the next level. Our 2D level image decomposition displayed an approximation with detailed three images that represents low and high-level frequency contents in an image, respectively. Next, we reduced the great number of DWT coefficients by applying the principal components analysis (PCA). Our input feature space was transformed into a lower feature space using the largest eigenvectors and forms a new set of ordered variables according to their variances or the importance. This technique orthogonalizes the components of the input vectors so that uncorrelated with each other, then it orders the resulting orthogonal components so that those with the largest variations come first, and finally it eliminates those components which contributes least to the variation in the dataset.

Figure 2. An example of our application of Level 1, DWT decomposition of a healthy MRI type T2.
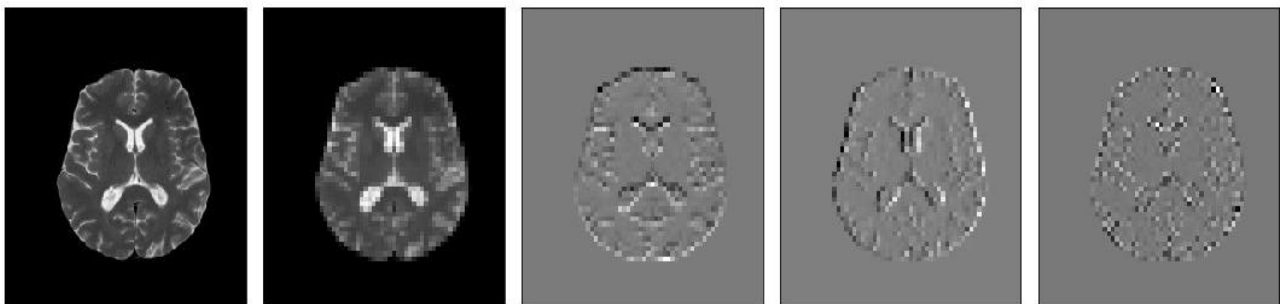
Figure 3. An example of our application of Level 2, DWT decomposition of a healthy MRI type T2.

Figure 4. An example of our application of Level 3, DWT decomposition of a healthy MRI type T2.

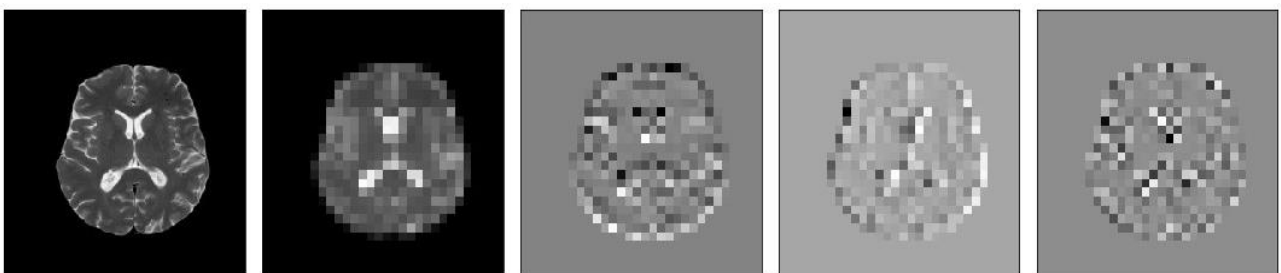### 3. CLASSIFICATION BASED ON CNN, ANN, SVM AND ANFIS

For the classification of brain tumor MRI images into normal and abnormal we developed different AI algorithms: (i) a CNN, (ii) an adaptive neuro fuzzy ANFIS classifier (Shing & Jang, 1993) and

(iii) a neural network (ANN) classifier, and (iv) SVM classifier. All these AI algorithms are trained and tested by feeding them of different scenarios of input data extracted from our original data group, see Table II. The input are in the form of different scenarios: (a) pixels, (b) GLCM features, (c) DWT coefficients. All of our models were developed using Python. In the post-processing step, the decimal values were removed from the output by rounding the values to the integer number. The results of the studied classification algorithms are presented in Table IV.

3.1. Scenario 1.1: ANN fed by GLCM and histogram features

The proposed ANN neural network is fed by 4 inputs fed by (i) skewness, (ii) homogeneity, (iii) energy, and (iv) kurtosis. Our ANN is a binary classifier, with output and is designed with two different back-propagation methods: with the scaled conjugate gradient backpropagation function, using two hidden layers with 10 neurons respectively and with the Levenberg-Marquardt back-propagation function, two hidden layers with 20 and 15 neurons respectively. Our input data are extracted from the data subset of 34.6% images with healthy tissues named whole dataset (with ratio of 10% of healthy tissues). For gradient back-propagation function, the best validation performance was 0.01889 at epoch 24. For the Levenberg-Marquardt back-propagation function the best validation performance was 0.0032662 at epoch 25.

3.2. Scenario 1.2: ANN fed by DWT features

The proposed ANN is fed by 288 features extracted by DWT texture analysis and is designed is designed with two different back-propagation methods: with the scaled conjugate gradient back-propagation function and two hidden layers with 10 and 8 neurons respectively and the Levenberg-Marquardt back-propagation function, two hidden layers with 20 and 15 neurons respectively.

In our case of ANN with gradient back-propagation function, our best validation performance was 4.0239×10^{-6} at epoch 36, while in our case of ANN with Levenberg-Marquardt back-propagation function, our best validation was 0.00021559 at epoch 28. Our evaluation parameters were: True positive 40, False positive 1, True negative 14, False negative 1, with Sensitivity 97.6%, Specificity 93.3%, and Accuracy 96.4%.

3.3. Scenario 2.1: ANFIS fed by GLCM and histogram features

Our ANFIS classifier uses an inference system generated with grid partition and 3 layers with 5 Gaussian membership functions on each layer, 125 rules, is fed by three GLCM features: skewness, homogeneity, energy, and kurtosis. The error tolerance was set equal to 10^{-4} and the number of epochs at 100. The testing results for both datasets are shown in Tables 3 and 4.

In the case of ANFIS with gradient back-propagation function, our evaluation parameters were: True Positive 45, False Positive 2, True Negative 13, False Negative 0, with Sensitivity 100%, Specificity 86.7%, and Accuracy 96.7%.

Table 3. Comparison of classification results from between the different scenarios.

	Sensitivity	Specificity	Accuracy	Precision
ANN, GLCM, 70%/30%	1	0.778	0.943	0.926
ANN, GLCM, 90%/10%	0.963	0.444	0.91	0.939
ANN, DWT, PGA 70%/30%	0.923	0.67	0.857	0.889
ANN, DWT, PGA 90%/10%	0.975	0.337	0.91	0.929
ANFIS GLCM 90%/10%	0.9	0.444	0.854	0.935
CNN DWT	1	0.93	0.97	0.95
CNN DWT, PCA	0.89	0.86	0.88	0.89
CNN, DWT, PCA, Augmentation	0.94	0.93	0.94	0.94

In the case of ANFIS with Levenberg-Marquardt back-propagation function, our validation evaluation parameters were: True Positive 122, False Positive 1, True Negative 14, False Negative 0, with Sensitivity 100%, Specificity 93.3%, and Accuracy 99.3%.

3.4. Scenario 2.2: ANFIS fed by DWT features
The testing results are shown in Table 3.

3.5. Scenario 4.1: CNN fed by whole image pixel values and using augmentation DWT coefficients
The testing results are shown in Table 3.

3.6. Scenario 4.2: CNN fed by DWT coefficients of the whole image pixel values
The testing results are shown in Table 3.

3.7. Scenario 4.3: CNN fed by DWT coefficients of the whole image pixel values using PCA
The testing results are shown in Table 3.

4. RESULTS
Statistical measurements should be used to evaluate the model prediction acceptability, but also the ability of the model to predict the output correctly when the input data is slightly different than the data used in building the model, and has never been seen before.

We are using evaluation metric parameters of sensitivity, specificity and accuracy. Special in medical diagnosis sensitivity is more important than specificity and accuracy, because represents the ability to identify a disease as True Positive rate, whereas specificity is the ability of the test to correctly identify cases without a disease as True Negative rate. The appropriate equations are [1]-[3].

$$\text{Sensitivity} = \frac{TP}{TP + FN} \qquad [1]$$

$$\text{Specificity} = \frac{TN}{TN + FP} \qquad [2]$$

$$\text{Accuracy} = \frac{TP + TN}{TP + FN + TN + FP} \qquad [3]$$

Our testing results are shown in Table 3. In Table 4 there is the comparison of our best scenario (CNN-DWT) with recent published studies.

Table 4. Comparison of our best method (CNN-DWT 2023) with recent published studies.

Research Team	Classification Algorithm	Multiclass	MRI data	Accuracy (%)
(Cinar et al., 2022a)	CNN	Yes	Tl-W	99.64
(Raza et al., 2022)	Deep CNN	Yes	Tl-W	99.67
(Ozyurt et al., 2020)	SR-FCM-CNN	Yes	Tl-W	98.33
(Deepak & Ameer, 2019)	GoogLeNet	Yes	Tl-W	98
(Cinar & Yildirim, 2020)	Hybrid ResNet50	Yes	Tl-W	97.2
(Sajjad et al., 2019)	CNN-TL	Yes	Tl-W	96.14
(Ozyurt et al., 2019)	AlexNet SVM KNN	Yes	Tl-W	95.62
(Kaplan et al., 2020)	LBPSVM KNN	Yes	Tl-W	95.56
(Swati et al., 2019)	Deep CNN VGG-19	Yes	Tl-W	94.84
(Our work, 2023)	CNN-DWT	Binary	T2	97

Comparing the classification results using as input GLCM versus DWT, drives to the conclusion that CLCM is more efficient for the MRIs feature extraction. It is our opinion that this happens because inside the tumor area there is no discontinuity and discontinuities at the edges exist in both healthy and non-healthy tissues. Maybe, the GLCM features are able to successfully recognize a tumor area because of the quantifying of the angular relationships and distances between neighboring image voxels inside tumor areas. In contrast, GLCM the DWT, with their transformed wavelet representation, provide a versatile mathematical tool to analyze transient, time-variant signals that are not statistically predictable, especially in the region of discontinuities.

5. CONCLUSIONS

So far, a lot of research have been done towards the field of the automated diagnosis of head tumors, as shown in MRI images. Most of the proposed algorithms are usually multi-layered, as they apply multiple stages of image pre-processing before extracting the features needed to be fed to the final classifier. All image pre-processing approaches have covered a broad field of image analysis theory, offering notable results of similar diagnosis success. Our indignation differs from existing ones because we use T2WI (all the publications use T1) and we extract the features from raw images (no pre-process like sharpening). We analyzed a total of 202 conventional T2 type MRI images of the axial plane, in BRATS 2015 open access data set, for the un-healthy cases, and 24 healthy cases are from the Greek public hospital Saint George.

In our present study, the adequacies of the CNN, ANN and ANFIS techniques in predicting brain tumors in T2WI MRIs were carefully analyzed and compared. Both techniques displayed excellent abilities in predicting and classifying the tumors in high or low glioma tumors.

Through our thorough tests, we conclude that:

1. The extraction of interesting attributes is more accurate (less prone to information loss) if derived without pre-editing from the original MRI images, as well as if their classification is exercised with a classifier based on machine learning.
2. The data in the form of GLCM texture features proved more efficient than those in the form of 2D DWT features.
3. The CNN using DWT coefficients as input is relatively superior classifier versus the rest scenarios.
4. The comparison of ANN versus ANFIS algorithms indicates that ANN is relatively superior to the ANFIS techniques.

Our plans for feature work are: (i) the implementation of three separate machine learning classifiers, able to process features from T1WI, T2WI and Flair in parallel, in order to considerably accelerate the process, and (ii) the use of relevant patient's history data available such as morning headache with vomiting, which can contribute effectively as additional input data for a classifier.

6. REFERENCES

Alis, D., Alis C., Yergin M., Topel C., Asmakutlu O., Bagcilar O., Senli Y.D., Ustundag A., Salt V., Dogan S.N., et al. (2022). A joint convolutional-recurrent neural network with an attention mechanism for detecting intracranial hemorrhage on non contrast head CT. Sci. Rep. 12: 2084.

Bakas, S., Akbari H., Sotiras A., Bilello M., Rozycki M., Kirby J.S., Freymann J.B., Farahani K., and Davatzikos C. (2017). Advancing the cancer genome Atlas glioma MRI collections with expert segmentation labels and radiomic features. Nat. Sci. Data, 4: 170117.

Bigos, K., Hariri A., and Weinberger D. (2015). Neuroimaging Genetics: Principles and Practices. Oxford University Press.

Buetow, M.P., Buetow P.C., and Smirniotopoulos J.G. (1991). Typical, atypical, and misleading features in meningioma. Radiogr. A Rev. Publ. Radiol. Soc. N. Am. 11: 1087–1106.

Choi, K., Kim D.Y., Kim H.J., Hwang G., Kim M.K., Kim H.G., and Paik S. (2022). Imaging features and pathological correlation in mixed microcystic and angiomatous meningioma: A case report. J. Korean Soc. Radiol. 83: 951–957.

Cinar, N., Kaya B., and Kaya K. (2022a). A novel convolutional neural network-based approach for brain tumor classification using magnetic resonance images. Wiley On Line Library. doi: 10.1002/ima.22839

Cinar, N., Ozcan A., and Kaya M. (2022b). A hybrid DenseNet121-UNet model for brain tumor segmentation from MR images. Biomed. Signal Process. Control 76: 103647.

Cinar, A. and Yildirim M. (2020). Detection of tumors on brain MRI images using the hybrid convolutional neural network architecture. Med. Hypotheses 139: 109684.

Deepak, S. and Ameer P.M. (2019). Brain tumors classification using in-depth CNN features via transfer learning. Comput. Biol. Med. 111: 103345.

Fayaz, M., Torokeldiev N., Turdumamatov S., Qureshi M.S., Qureshi M.B., and Gwak J. (2021). An efficient methodology for brain MRI classification based on DWT and convolutional neural network. Sensors 21: 7480.

Haralick, R.M., Shanmugam K., and Dinstein I. (1973). Textural features for image classification. IEEE Transactions on Systems, Man and Cybernetics 3 (6): 610-621.

Haykin, S. (2009). Neural Networks and Learning Machines, Pearson Prentice Hall, 3rd Edition.

Jeong, J.J., Tariq A., Adejumo T., Trivedi H., Gichoya J.W., and Banerjee I. (2022). Systematic review of generative adversarial networks (GANs) for medical image classification and segmentation. J. Digit Imaging 35: 137–152.

Kaplan, K., Kaya Y., Kuncan M., and Ertunç H.M. (2020). Brain tumors classification using modified local binary patterns (LBP) feature extraction methods. Med. Hypotheses 139: 109696.

Kuang, Z. (2022). Transfer learning in brain tumor detection: From AlexNet to Hyb-DCNN-ResNet. Highlights Sci. Eng. Technol. 4: 313–324.

Kumar, Y. and Mahajan M. (2020). Recent advancement of machine learning and deep learning in the field of healthcare system. In Computational Intelligence for Machine Learning and Healthcare Informatics, De Gruyter, Berlin, Germany: 7–98.

Liu, P., Zhang H., Lian W., and Zuo W. (2019). Multi-level wavelet convolutional neural networks. IEEE Access 7: 74973–74985.

Ozyurt, F., Sert E., and Avci D. (2020). An expert system for brain tumor detection: Fuzzy C-means with super resolution and convolutional neural network with extreme learning machine. Medical Hypotheses 134: 109433. doi: 10.1016/j.mehy.2019.109433

Ozyurt, F., Sert E., Avci D., and Dogantekin E. (2019). Brain tumor detection based on convolutional neural network with neutrosophic expert maximum fuzzy sure entropy. Measurement 147: 106830.

Raza, A., Ayub H., Khan J.A., Ahmad I.S., Salama A., Daradkeh Y.I., Javeed D., Ur Rehman A., and Hamam H. (2022). A hybrid deep learning-based approach for brain tumor classification. Electronics 11: 1146. doi: 10.3390/electronics11071146

Sajjad, M., Khan S., Muhammad K., Wu W., Ullah A., and Baik S.W. (2019). Multi-grade brain tumors classification using deep CNN with extensive data augmentation. J. Comput. Sci. 30: 174–182.

Savareh, B.A., Emami H., Hajiabadi M., Azimi S.M., and Ghafoori M. (2019). Wavelet-enhanced convolutional neural network: A new idea in a deep learning paradigm. Biomed. Eng./Biomed. Tech., 64: 195–205.

Shing, J. and Jang R. (1993). ANFIS: Adaptive network based fuzzy inference system. IEEE Transactions on Systems, Man and Cybernetics 23 (3).

Swati, Z.N.K., Zhao, Q., Kabir M., Ali F., Ali Z., Ahmed S., and Lu J. (2019). Brain tumors classification for MR images using transfer learning and fine-tuning. Comput. Med. Imaging Graph 75: 34–46.

Watts, J., Box G., Galvin A., Brotchie P., Trost N., and Sutherland T. (2014). Magnetic resonance imaging of meningiomas: A pictorial review. Insights Imaging 5: 113–122.

Zinn, P.O., Majadan B., Sathyan P., Singh S.K., Majumder S., Jolesz F.A., and Colen R.R. (2011). Radiogenomic mapping of edema/cellular invasion MRI-phenotypes in glioblastoma multiforme. PLoS ONE 6: e25451.

MACHINE LEARNING IN BIOMEDICAL APPLICATIONS

Athanasiou, S., Baklezos, A.T., Nikolopoulos, C.D., and Vardiambasis, I.O.*

Laboratory of Telecommunications & Electromagnetic Applications,
Department of Electronic Engineering,
Hellenic Mediterranean University,
Romanou 3, Chalepa, GR-73133 Chania, Crete, Greece
* ivardia@hmu.gr

1. INTRODUCTION

Machine learning has emerged as a transformative technology with significant applications in various fields, including biomedical research and healthcare (Strzelecki & Badura, 2022). Combining advanced algorithms, statistical models and computational power, machine learning enables the analysis of large and complex datasets to extract valuable insights and make accurate predictions.

In biomedical applications, machine learning plays a crucial role in improving disease diagnosis and prediction as well as personalise treatment, drug discovery and treatment planning. It enables physicians to uncover hidden patterns and trends within biomedical and clinical data often time consuming and difficult for human experts to discover. With machine learning, we are able to process high amount of data and handle high-dimensional data as such genomic and proteomic data (Swan et al., 2013).

One of the key areas where machine learning has made significant contributions is disease diagnosis (Foster et al., 2014). By training models on vast amount of labelled data, machine learning algorithms can identify patterns and biomarkers associated with specific diseases. Then these models can analyse new patients' data and provide accurate predictions, aiding in early detection and more precise diagnoses. Machine learning algorithms have demonstrated success in diagnosing various conditions, including brain cancer (Papadomanolakis et al., 2023), cardiovascular diseases (Bhatt et al., 2023), neurological disorders as Parkinson's disease (Mahmood et al., 2023), and infectious diseases such as COVID-19 (Montazeri et al., 2021).

Furthermore, machine learning has the potential to revolutionize drug discovery and development. Traditional drug discovery processes are time consuming and costly, but by using machine learning techniques the process can be accelerated and provide the opportunity to identify potential drug candidates faster (Dara et al., 2022). By analysing large datasets of molecular structures, biological interactions and clinical trial data, machine learning models can predict the efficacy and safety of new compounds. This enables researchers to prioritize the most promising candidates for further investigation, ultimately expediting the drug development pipeline.

Moreover, machine learning can facilitate personalized medicine through personalized treatment plans to individual patients. By analysing patient specific data, including genetic information, patient history and treatment outcomes, machine learning algorithms can identify optimal treatment strategies and predict potential side effects and responses to different therapies (Sebastiani et al., 2022). That way treatment is more targeted and effective, reducing the risk of side effects and improving patients' outcomes.

2. CONCLUSION

The introduction of machine learning in biomedical applications holds great promise for revolutionizing healthcare and advancing our understanding in human brain, body and numerous diseases. By harnessing the power of data and algorithms, machine learning can contribute to faster and more accurate diagnosis, personalized treatment, and streamlined drug discovery processes, ultimately improving patient care and treatment outcomes.

However, it is important to state that the integration of machine learning in biomedical

applications comes with challenges. Ensuring data privacy (Murdoch et al., 2021), maintaining ethical standards, and addressing issues of interpretability and transparency are critical considerations in deploying machine learning models in healthcare settings.

To conclude the main areas that machine learning is finding applications in biomedical engineering are the following:

- i. medical imaging and analysis,
- ii. disease diagnosis and prognosis,
- iii. drug discovery and development,
- iv. bioinformatics,
- v. biomechanics and prosthesis design,
- vi. synthetic biology and genetic engineering.

Machine learning is supporting physicians and researchers globally already, always working hand by hand and complementary without one replacing the other, and all the challenges mentioned above should always be taken under consideration.

3. REFERENCES

Bhatt, C.M., Patel P., Ghetia T., and Mazzeo P.L. (2023). Effective heart disease prediction using machine learning techniques. Algorithms 16 (2): 88. doi: 10.3390/a16020088

Dara, S., Dhamercherla S., Jadav S.S., Babu C.M., and Ahsan, M.J. (2022). Machine learning in drug discovery: A review. Artificial Intelligence Review 55 (3): 1947-1999. doi: 10.1007/s10462-021-10058-4

Foster, K.R., Koprowski R., and Skufca J.D. (2014). Machine learning, medical diagnosis, and biomedical engineering research - commentary. BioMed Eng OnLine 13: 94. doi: 10.1186/1475-925X-13-94

Mahmood, A., Mehroz Khan M., Imran M., Alhajlah O., Dhahri H., and Karamat T. (2023). End-to-end deep learning method for detection of invasive Parkinson's disease. Diagnostics 13: 1088. doi: 10.3390/diagnostics13061088

Montazeri, M., Zahedi Nasab R., Farahani A., Mohseni H., and Ghasemian F. (2021). Machine learning models for image-based diagnosis and prognosis of COVID-19: Systematic review. JMIR Medical Informatics 9 (4): e25181. doi: 10.2196/25181

Murdoch, B. (2021). Privacy and artificial intelligence: Challenges for protecting health information in a new era. BMC Med Ethics 22: 122. doi: 10.1186/s12910-021-00687-3

Papadomanolakis, T.N., Sergaki E.S., Polydorou A.A., Krasoudakis A.G., Makris- Tsalikis G.N., Polydorou A.A., Afentakis N.M., Athanasiou S.A., Vardiambasis I.O., and Zervakis, M.E. (2023). Tumor diagnosis against other brain diseases using T2 MRI brain images and CNN binary classifier and DWT. Brain Sciences 13: 348. doi: 10.3390/brainsci13020348

Sebastiani, M., Vacchi C., Manfredi A., and Cassone G. (2022). Personalized medicine and machine learning: A roadmap for the future. J Clin Med 11 (14): 4110. doi: 10.3390/jcm11144110

Strzelecki, M. and Badura P. Machine learning for biomedical application. (2022). Applied Sciences 12 (4): 2022. https://doi.org/10.3390/app12042022

Swan, A.L., Mobasheri A., Allaway D., Liddell S., and Bacardit J. (2013). Application of machine learning to proteomics data: Classification and biomarker identification in postgenomics biology. Omics 17 (12): 595-610. doi: 10.1089/omi.2013.0017

NEURAL NETWORK PREDICTION OF HEART RATE DURING EXERCISE WITH VARIOUS CONSTANT AND EXPONENTIALLY INCREASING SPEEDS

Lampou, A.N., Zakynthinaki, M.S., Baklezos, A.T., Nikolopoulos, C.D., and Vardiambasis, I.O.*

Laboratory of Telecommunications & Electromagnetic Applications,
Department of Electronic Engineering,
Hellenic Mediterranean University,
Romanou 3, Chalepa, GR-73133 Chania, Crete, Greece
* ivardia@hmu.gr

1. INTRODUCTION

The Heart Rate (HR) is defined as the number of heart beats per minute. The prediction and analysis of the *HR* during exercise is very important for the physiology, fitness and sport sectors as it is one of the most informative cardiovascular variables (Whipp, 1972), (Wilmore & Costill, 2007), (Zakynthinaki, 2016), (Zakynthinaki & Stirling, 2007). It can also be a useful tool in cardiovascular health by providing the detection of hidden physiological responses or abnormalities (Astrand et al., 2003), (Davies et al., 1972), (Hill & Lupton, 1923), (Linnarsson, 1974), (Zakynthinaki et al., 2011). In this work, it is presented a way of the heart rate prediction response to exercise for constant and exponentially increasing speeds. This prediction is done by Artificial Neural Networks (ANNs) and for a given initial set of *HR* data (Zakynthinaki, 2015), (Zakynthinaki, 2016).

2. MATERIALS AND METHODS

2.1. Neural network setup

In order to train the neural network 40 data sets for each of the two speed categories (constant and exponentially increasing) were generated. Each data set was including the HR and the corresponding beat-to-beat time intervals (t_b).

The neural network training was done with inputs the speed and the t_b and outputs the HR.

In the case of the constant speed exercises, each of the 40 data sets corresponded to a different constant exercise speed while for the exponentially increasing speed exercises, 40 different scenarios were also generated.

In both exercise speed cases, the number of the input training data was 36,000 and the number of the test data was 4,000. Also, the best results were obtained with a neural network consisting of two hidden layers and 25 and 15 neurons at each layer respectively. The training algorithm which was chosen as the optimal was the Levenberg-Marquardt algorithm (LM). Figure 1 shows the neural network architecture.
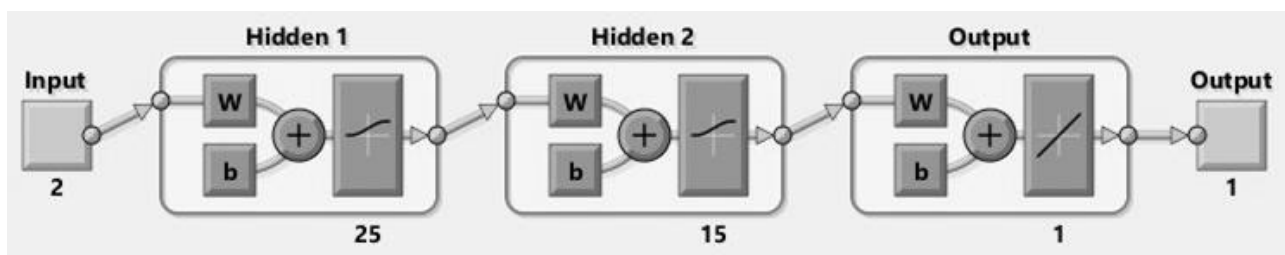

Figure 1. Neural network architecture.

3. RESULTS
3.1. Statistical measures

The performance evaluation of the proposed neural network model was carried out for all the different exercise cases through the calculation of statistical measures, such as the testing mean absolute error MAE_{te}

$$MAE_{te} = \frac{1}{K} \sum_{k=1}^{K} \left| p_k - t_k \right| \quad [1]$$

and the testing relative mean square error $RMSE_{te}$

$$RMSE_{te} = \frac{1}{K} \sum_{k=1}^{K} \left(\frac{p_k - t_k}{t_k} \right)^2 \quad [2]$$

3.2. Results for constant and exponentially increasing speeds

The constant exercise velocity was approximately between 11 – 18 km/h and the velocity in all of the exponentially increasing 40 cases was approximately between 0 – 18.5 km/h.

Table 1 presents the MAE and RMSE results of the test and training data.

Table1. Training and test MAE & RMSE for the 40 constant and exponentially increasing speeds.

Scenario	MAE_{te}	$RMSE_{te}$	MAE_{tr}	$RMSE_{tr}$
Constant Speeds (40 cases)	0.0201	5.2120e-08	0.0195	3.7101e-08
Exponentially Increasing Speeds (40 cases)	0.0201	4.5420e-08	0.0202	4.5347e-08

Figures 2 – 4 show the predicted and measured Heart Rate (beats/min) results of the test output and predicted data for all the 40 constant and exponentially increasing speeds exercise cases respectively.
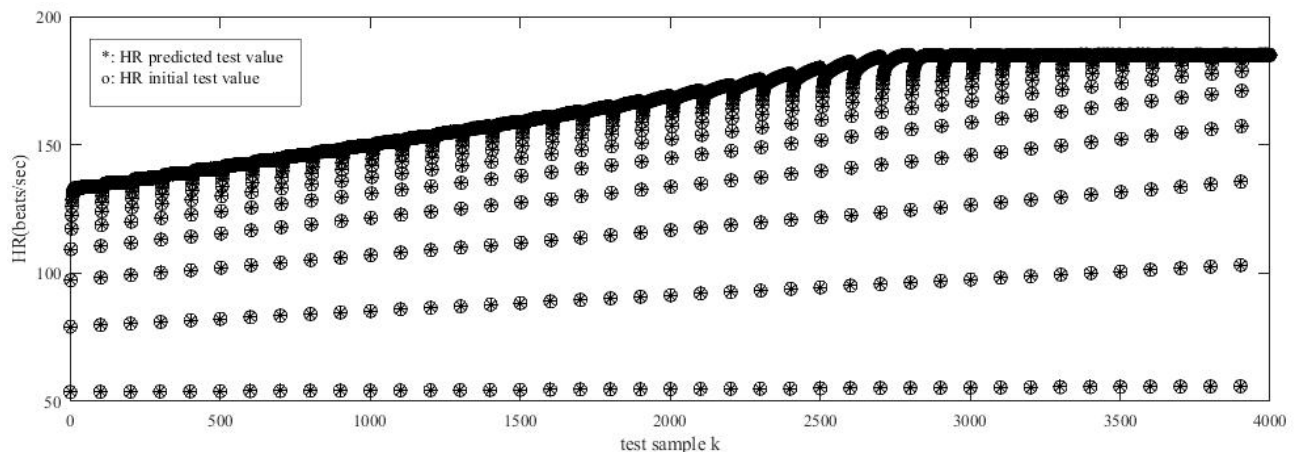
Figure 2. HR predicted test value and HR initial test value for the 40 constant speed scenarios.
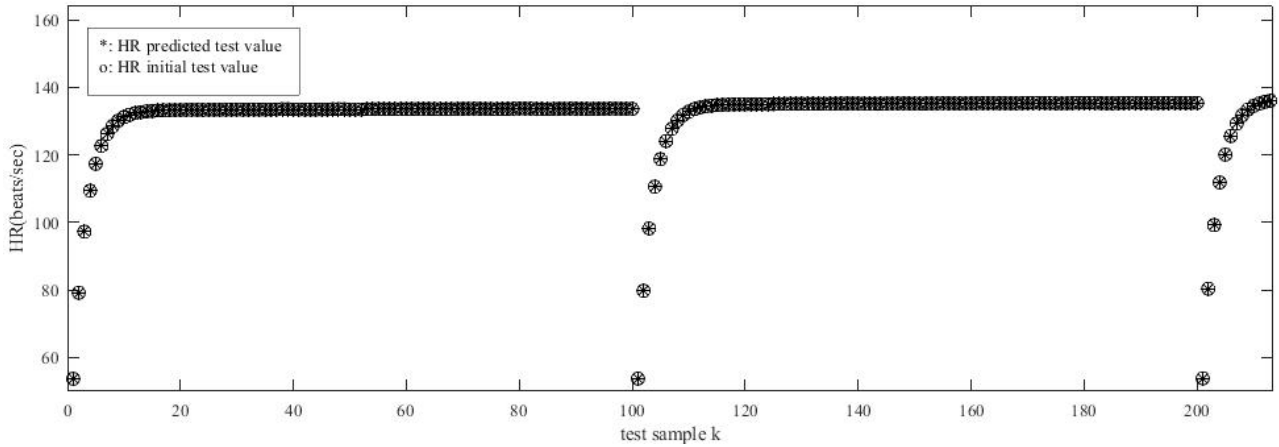
Figure 3. HR predicted test value and HR initial test value for the first 100 samples of constant speed 10km/h.

Figure 3 shows in details the first 100 HR results of Figure 1, which correspond to 10 km/h exercise speed.
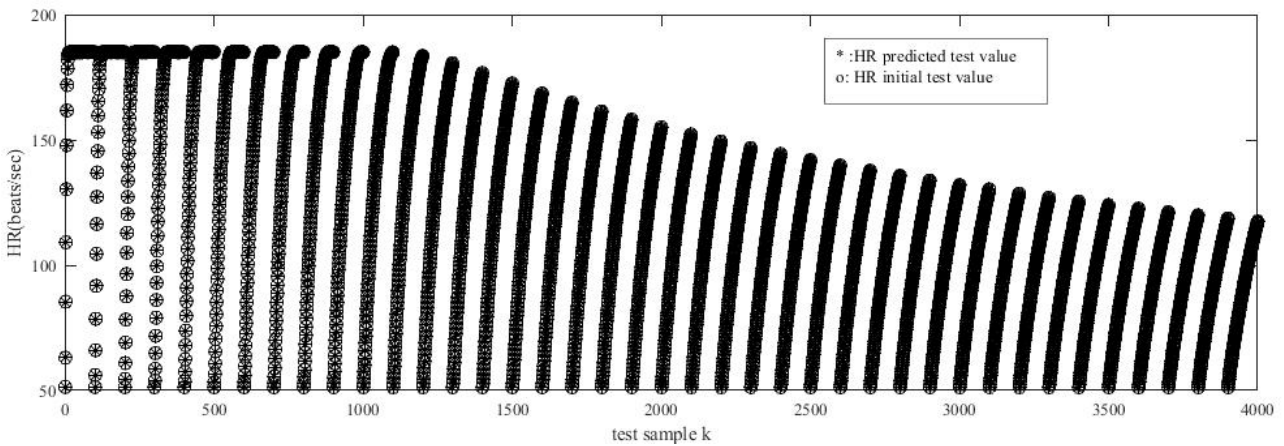
Figure 4. HR predicted test value and HR initial test value for the 40 exponentially increasing speed scenarios.

Figure 5 shows in details the first 100 HR results of Figure 4, which corresponds to the first 2 of the 40 exponentially increasing speed scenarios.
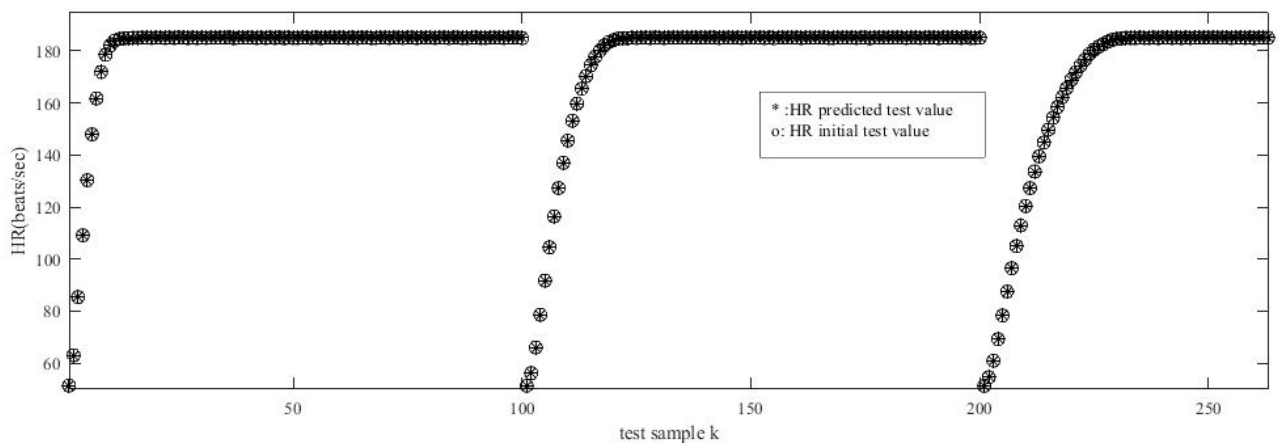
Figure 5. HR predicted test value and HR initial test value for the first two exponentially increasing speed scenarios.

As it can be observed, the measured and the predicted values have a very close agreement.

4.   CONCLUSION

The previous comparison between the measured and the predicted HR values shows that the proposed Neural Networks models can be a very important tool and possible solution for HR prediction. These HR predictions can provide significant information for analysis in population groups for which direct HR recordings would not be possible or allowed for intense exercises, such as pregnant women or elderly people (Zakynthinaki, 2015), (Zakynthinaki, 2016).

4.   REFERENCES

Astrand, P.O., Rodahl K., Dahl H.A., and Stromme S.B. (2003). Textbook of work physiology - Physiological bases of exercise. Human Kinetics, 4th edition.

Bowers, R. and Fox L. (1992). Sports Physiology. Brown Co, 3rd edition.

Burke E.R. (1998). Precision Heart Rate Training. Human Kinetics, 2nd edition.

Davies, C.T., Di Prampero P.E., and Cerretelli, P. (1972). Kinetics of the cardiac output and respiratory gas exchange during exercise and recovery. J Appl Physiol 32: 618–625.

Hairer, E., Norsett S., and Wanner G. (1993). Solving Ordinary Differential Equations I: Nonstiff Problems. Springer-Verlag, 2nd edition.

Hill, A.V. and Lupton L. (1923). Muscular exercise, lactic acid and the supply and utilization of oxygen. Q J Med 16: 135171.

Karvonen, J. and Vuorimaa T. (1988). Heart rate and exercise intensity during sports activities: Practical application. Sports Med 5 (5): 303-311.

Linnarsson, D. (1974). Dynamics of pulmonary gas exchange and heart rate changes at start and end of exercise. Acta Physiol Scand Suppl 415: 1-68.

Maffetone, P. (1996). High Performance Heart: Effective Training with the HRM for Health, Fitness and Competition. Human Kinetics, 2nd edition.

Powers, S.K. and Howley E.T. (1997). Exercise Physiology: Theory and Application to Fitness and Performance. Brown & Benchmark, 3rd edition.

Whipp, B.J. and Wasserman K. (1972). Oxygen uptake kinetics for various intensities of constant load work. J Appl Physiol 33: 351-356.

Wilmore, J. and Costill D. (2007). Physiology of sport and exercise. Human Kinetics, 4th edition.

Zakynthinaki, M.S. (2015). Modelling heart rate kinetics. PLOS ONE 10 (4): e0118263.

Zakynthinaki, M.S. (2016). Simulating heart rate kinetics during incremental and interval training, *Biomed Hum Kinet 8*(1), 144-152.

Zakynthinaki, M.S., Barakat R.O., Cordente C.A. and Sampedro J. (2011). Stochastic optimization for the detection of changes in maternal heart rate kinetics during pregnancy. Comp Phys Commun 182(3): 683-691.

Zakynthinaki, M.S., Kapetanakis T.N., Lampou A., Ioannidou M.P., and Vardiambasis I.O. (2021). A neural network model for estimating the heart rate response to constant intensity exercises. Signals, 2: 852–862. https:// doi.org/10.3390/signals2040049

Zakynthinaki, M.S. and Stirling J.R. (2007). Stochastic optimization for modelling physiological time series: application to the heart rate response to exercise. Comp Phys Commun 176 (2): 98-108.

Zakynthinaki, M.S. and Stirling J.R. (2008). Stochastic optimization for the calculation of the time dependency of the physiological demand during exercise and recovery. Comp Phys Commun 179 (12): 888-894.

PORTFOLIO SELECTION ON HYBRID MODULAR, AND RADIAL BASIS FUNCTIONS NETWORKS

N., Loukeris

University of West Attica
Dept. Business Administration
P. Ralli 56, 111 00 Athens, Greece
nloukeris@uom.edu.gr

Abstract: The evaluation of two distinct groups of neural networks as a competitive classifier for the efficient portfolio optimization to support core issues of the modern portfolio theory: i) the investors behavior, ii) the Entropy characteristics of returns and their Chaotic reactions in the Fractal Market Hypothesis, iii) the selection of the optimal classifier between 40 Modular, and 40 Radial Basis Function Networks of Neural and Neuro-Genetic Hybrids optimizing portfolia.

Keywords: Modular Networks, Radial Basis Functions, Genetic Algorithms, Portfolio Optimization, Entropy, Tsallis Statistics, Chaotic Dynamics, Stochastic Differential Equations

1. INTRODUCTION

The process of optimizing portfolia on the second phase detects detailed elements of risk in advanced higher moments (volatility, hyperkurtosis, ultrakurtosis, hyperultrakurtosis, etc), [1] is discussed in the current research paper. On the first stage, portfolia are ranked hierarchically providing the feasible set and afterwards the efficient frontier [2], [3], [4],[5],[6],[7],[8],[9], [10], [11], [12], [29]. We examine the first step resolving the second step. 40 Modular (MDN) models are evaluated in neural or neuro-genetic hybrids in 10 Modular neural and 30 Modular hybrids, 40 Radial Basis Functions, in 10 neural and 30 hybrid RBFN, different topologies to declare the optimal classifier model of portfolio allocation, and thus:

i) Providing a detailed model we have been working [29] on the preferences and investors behavior in higher moments,
ii) Upgrading Markowitz's portfolio theory, with hidden information of fundamentals, out of bias, researching for healthy assets, in the Fractal Market Hypothesis and Markets Chaos Dynamics
iii) Testing MDNs and the RBFN family in various forms of neural or hybrids to define the optimal classifier in high frequencies trading.

2. INVESTING BEHAVIOR

Investors are usually irrational and affected by emotional biases thus non-linear models of higher complexity can support the computational part. Our high fluctuational times of the series of Global Crises (Financial, Health, War, etc) encourage short-term investments suitable for the Fractal Markets Hypothesis. [13], as returns are not n.i.i.d., and EMH was proven weak in the markets. The investors tend to be more sensitive to their potential losses [14], consequently the investments should be supported by the Entropy Dynamics observed in the markets and relevant groups forming fractals in the chaotic activity of markets. Investors set their utility expecting a logical rate of return, under the consideration of risk-loss. Higher moments describe the investors hidden patterns on the implied utility function of the HARA (Hyperbolic Absolute Risk Aversion), thus advanced moments further than the 5th of hyperskewness are used [1], [8], [9], [10], [29]:

$$U_t(R_{t+1}) = \sum_{\lambda_v=1}^{\omega}(-1)^{\lambda_v+1}\frac{a_{\lambda_v}}{n}\sum_{i=1}^{n}\left(x_i - \sum\frac{x_i}{n}\right)^n \tag{1}$$

where λ_v is the accuracy on investors preferences to risk, depending on the behavior, $a_{\lambda v}$ a constant on investors profile: $a_{\lambda v} = 1$ for rational risk averse individuals, $a_{\lambda v} \neq 1$ for the non-rational, xi the value of return i in time t. The Isoelastic Utility, a unique HARA function of Constant Relative Risk Aversion, is for the risk averse investors:

$$U = \begin{cases} \frac{W^{1-\lambda}-1}{1-\lambda}, & \lambda \in (0,1) \cup (1,+\infty] \\ log(x), & \lambda = 1 \end{cases} \tag{2}$$

where, W the wealth, λ a measure of risk aversion. [6], [7] indicated the Makowitz model can have a broader alternative relaxing its essential assumption on the normaly distributed prices. The initial convex problem of quadratic utility maximization, [15] is non- effective in the markets:

$$min_x f(x) = Var(r_p) \tag{3}$$

[15] incorporated higher order moments:

$$min_x f(x) = \lambda Var(r_p) - (1-\lambda)E(r_p) \tag{4}$$
$$r_p = \sum_i x_i r_i \tag{5}$$
$$x_i \geq 0 \tag{6}$$
$$\sum_i x_i = 1 \tag{7}$$

where r_p the portfolio return, x_i the weight of asset i, r_i the return of ith asset, μ the mean and σ^2 the variance. Regarding the chaotic dynamics, [17] relative entropy (TRE), which is the generalization of Kullback-Leibler relative entropy (KLRE) to non-extensive systems, describes complex systems with nonlinearity, long range interaction and long-term memory effect. The stock markets research on the Tsallis generalization of the KLRE was implemented by [18], [19], [20], [21], [22], [23], [24], [29].

3. THE MODEL

[6], [7], showed that further higher moments are necessary to describe the behavior of investors:

$$min_x f(x) = \lambda v_\gamma [bVar_t(r_p) + dKurt_t(r_p) + fHypKurt_t(r_p) - hUltraKurt_t(r_p)]] - (1-\lambda)v_\gamma [aE_t(r_p) + cSkew_t(r_p) + eHypSkew_t(r_p) + g\,U\,ltraSkew_t(r_p)] \tag{8}$$

$$v_\gamma = 1 - \varepsilon_\tau \tag{9}$$

$$r_p = \sum_i x_i r_i^* \tag{10}$$

where v_γ company's financial health (binary: 0 to bankruptcy, 1 healthy), ε_τ the heuristic output as the evaluation result (binary: 0 healthy, 1distressed), r_i^* the return of stock i from the efficient frontier and is superior than the others, x_i their weights. Hence

$$U_t(r_p) = \sum_i U_t(R_t(i_i^*)) \tag{11}$$

The non-convex problem demands robust heuristics, where I contribute in a more efficient hybrid classifier that considers also hidden accounting among the ordinal data. Thus fraud and manipulation are filtered.

4. THE COMPUTATIONAL INTELLIGENCE

The classifier that consist the core of this paper will be tested in the various forms of the Modular neural and hybrid and hybrid neuro-genetic networks, on various topologies.

5. THE MODULAR NETWORKS AND THEIR HYBRIDS

Modular feedforward networks are a special class of MLP. These networks process their input using several parallel MLPs, and then recombine the results. This tends to create some structure within the topology, which will foster specialization of function in each sub-module. In the models the number of hidden layers, and the network topology can be defined. There are four modular topologies supported, and in all the models is applied the linear feedforward form without bypasses of the signals. In contrast to the MLP, modular networks do not have full interconnectivity between their layers. Therefore, a smaller number of weights are required for the same size network (same number of neurons). This tends to speed up training times and reduce the number of required training examplars. There are many ways to segment a MLP into modules. It is unclear how to best design the modular topology based on the data. There are no guarantees that each
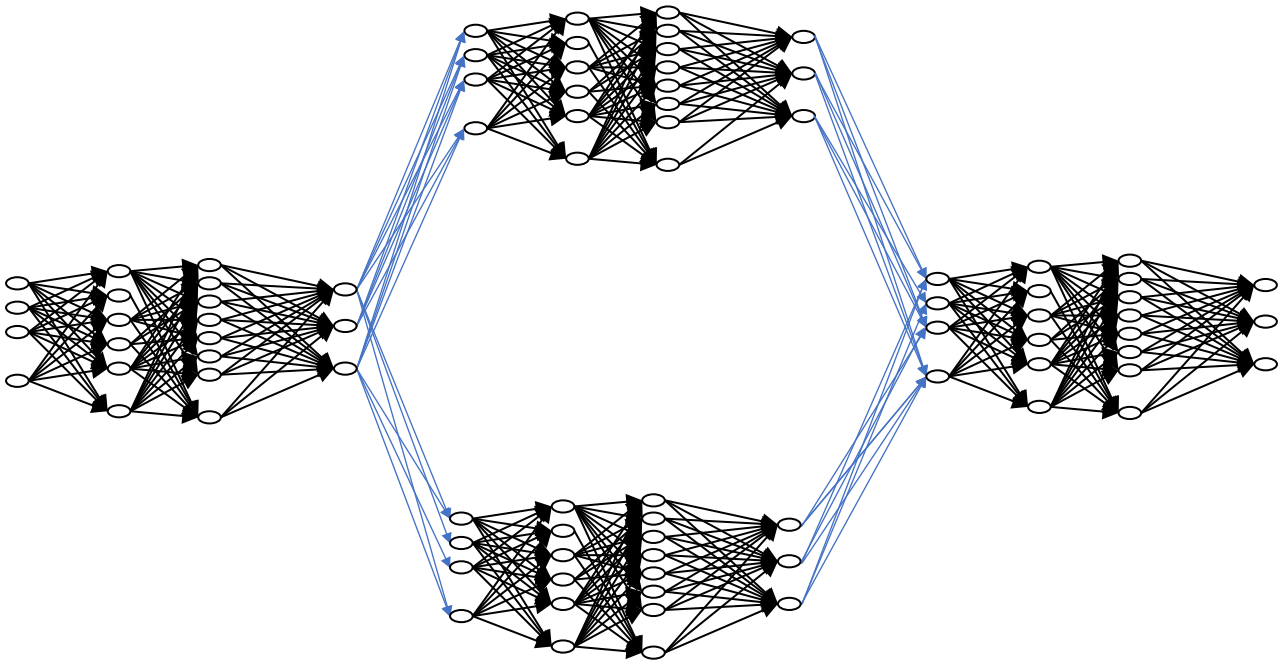
Fig. 1. The Modular Neural Networks

module is specializing its training on a unique portion of the data. The Input neurons were 16, Output 1, Exemplars 706, in the 4Hidden layers the Upper Neurons were 4 with no GA, Upper Transfer TanhAxon, Lower Neurons were in no GA, Lower Transfer TanhAxon, Learning Rule was Momentum, Step size 0.1, Momentums 0.70. Backpropagation is a usual form of learning; the weights are changed according to their previous value and a correction term. The learning rule specifies the correction term, and the Supervised Learning Control was used, Max epochs: 1000, Termination is under minimal MSE, threshold 0.01, Minimum criterion, Load best on test, in Batch learning. The Maximum Epochs specifies how many iterations (over the training set) will be done if no other criterion appears. The Minimum function terminates when the MSE drops below the specified Threshold. The Incremental function terminates when the change in MSE from one iteration to the next is less than the threshold. The default Incremental error is much smaller than the Minimum error. The MSE termination bases the stop criteria on the Cross Validation set, instead of the training set. In case the MSE of the cross-validation set begins to increase, this indicates that the network starts to overtrain, - to simply memorizes the training set and is unable to generalize the problem. Cross validation is highly efficient method to end network training and it is used in 11 similar hybrid models.

It monitors the error on an independent set of data and stops training when this error is starting to increase, offering the best point of generalization to the calculations. The testing set evaluates the network's performance. Once the network is trained the weights are then frozen, the testing set is fed into the network and the network output is compared with the desired output. The models are MDNs neurals and hybrids with GA:

i)   on the inputs layer only,
ii)   on the inputs and outputs layers only,
iii)   into all the layers and cluster centers,

into all the layers and cluster centers with cross validation,
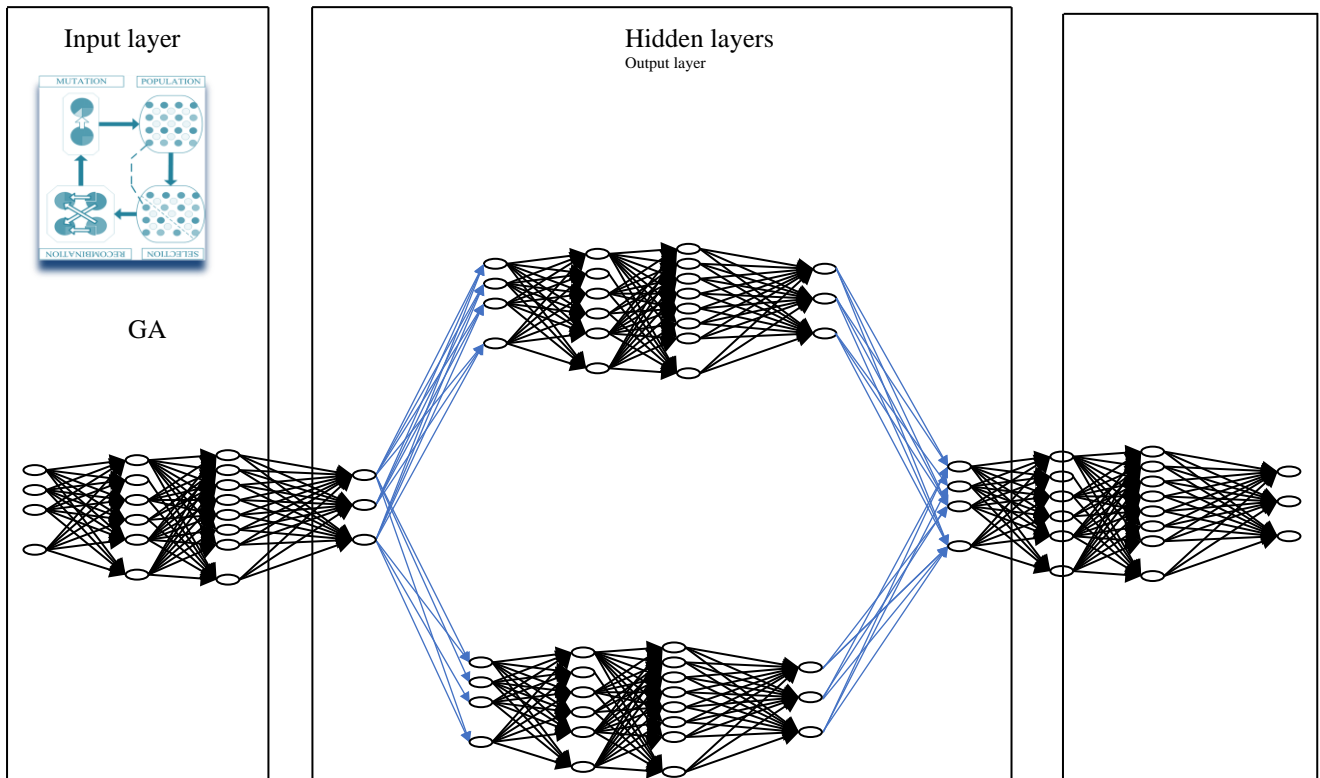
Fig. 2. The Hybrid Modular Net of GA optimization and Cross Validation on the Input layers only

6.   THE RADIAL BASIS FUNCTIONS NETWORKS AND THEIR HYBRIDS

The Radial Basis Function-RBF nets are linear models of supervised learning used in time series predictions, regressions, classifications, their Linear models have the form:

$$f(x) = \Sigma_m w_j \, h_j(x), \tag{12}$$

where $f(x)$ a linear combination on m set of fixed functions-the basis functions, w_j the coefficients of linear combinations, h_j the weights. Figure 3 demonstrates an RBF net, every input component (p) is on a hidden layer, each node is a p multivariate Gaussian function (RBF):

$$G(x, x_i) = e^{[-1/2\sigma^2]\Sigma(x_k - x_{ik})^2} \tag{13}$$

of mean xi and variance, the linear weight on the hidden nodes, produces the output that may create a very large hidden layer:

$$F(x) = \Sigma \, Nwi \, [G(x, x_i)] \tag{14}$$

The significance of each financial indices out of the 16 inputs in hybrid RBF network is unknown to the model hence GAs select them. Each model is trained multiple times to define the inputs of the lowest error. GAs were implemented in different hybrid:

i)   on the inputs layer only,
ii)   on the inputs and outputs layers only,
iii)   into all the layers and cluster centers,

in different topologies. Batch learning was selected to update the weights of hybrid neuro-genetic RBF, after the presentation of the entire training set. The competitive rule was the Conscience Full function in Euclidean metric as the conscience mechanism keeps a count on how often a neuron wins the competition, and enforces a constant wining rate across the neurons. There were 4 neurons per hidden layer, using the TanhAxon transfer function, on the Momentum learning rule. GAs resolved the problem of optimal values in a) Neurons, b) Step Size and c) Momentum Rate, and d) Cluster Centers. RBF nets require multiple training to obtain the lowest error. The output layer elaborated GAs optimizing the Step size and the Momentum.

7. PROBLEM DEFINITION

The significance of further higher moments in the model was revealed by [1], [6], [7], [16], that provide a more realistic representation of preferences and thus the dynamic behavior of investors. [1] introduced the form of the problem as:

$$U_t(R_t(i)) = \sum_{\lambda_v=1}^{\omega} (-1)^{\lambda_v+1} \frac{a_{\lambda_v}}{n} \sum_{i=1}^{n} \left(x_i - \sum \frac{x_i}{n} \right)^n + W_x(u,s) \tag{16}$$

$$\text{as} \quad z = y^2 = \sigma^4 \tag{17}$$

then identical, [1], to

$$min_x f(x) = \lambda v_\gamma \sigma^2 (r_p)[b + dz + ez^2] \tag{18}$$

The non-convex form of the problem demands robust heuristics for the solution. Rumors, manipulation, cooked accounting has higher levels of investment risk. In terms of the Chaotic Dynamics the risky stock prices follow the Stochastic Differential Equation, [24]:

$$dS(t) = S(t)(\mu dt + \sigma \, d(t) + J dN(t) - \lambda u dt) \tag{19}$$

where μ expected return of the stock, σ volatility without jumps, J a random variable of the jump amplitude within the stock (J > −1). As $u = E(J)$ where $E(\cdot)$ an expectation operator, $\{N(t), t \geq 0\}$ a Poisson process with strength λ, $\lambda u dt$ an average growth by the Poisson jump, $\{W(t), t \geq 0\}$ a standard Brownian motion defined on probability (F, $\{Ft\}$ $t \geq 0$, P), $\{N(t), t \geq 0\}$ and $\{W(t), t \geq 0\}$ are independent of each other, [24].

The SDE (17) solution is [24]:

$$S(t) = S(0) \prod_{i=0}^{N(t)} (1 + J_i) e^{\mu t - \frac{\sigma^2}{2}} \int_0^t P^{1-q}(\Omega, s) ds - \lambda u t + \sigma \Omega(t) \tag{21}$$

The random variable Ω(t) satisfies:

$$d\Omega(t) = Pq(\Omega,t)^{(1-q)/2}dW(t) \qquad (22)$$

where $Pq(\Omega,t)$ the maximum Tsallis entropy distribution of Non-extensive statistics. The model can describe the volatility clustering and long-term memory phenomena of asset prices [24]. Given that the return x_i is:

$$x_t = (S_t - S_0)/S_0 \qquad (23)$$

Then (18) is the optimal utility function on this model. This approach was utilized in finance [28].

8. DATA

Data were produced by 1411 companies from the loan department of a Greek commercial bank, with the following 16 financial indices, [27]:
1) EBIT/Total Assets,
2) Net Income/Net Worth,
3) Sales/Total Assets,
4) Gross Profit/Total Assets,
5) Net Income/Working Capital,
6) Net Worth/Total Liabilities,
7) Total Liabilities/Total assets,
8) Long Term Liabilities/(Long Term Liabilities+Net Worth),
9) Quick Assets/Current Liabilities,
10) (Quick Assets-Inventories)/Current Liabilities,
11) Floating Assets/Current Liabilities,
12) Current Liabilities/Net Worth,
13) Cash Flow/Total Assets,
14) Total Liabilities/Working Capital,
15) Working Capital/Total Assets,
16) Inventories/Quick Assets,

and a 17th index with initial classification, done by bank executives. The test set was 50% of the overall data, and the training set 50%. Multiple combinations were chosen to detect the optimal performance of MDN, SOFM, GFF Networks: i) MDN neural nets, ii) Hybrid MDNs with GA only on the inputs layer, iii) Voted Perceptron neural net, iv) Hybrid MLPs with GA only on the inputs layer, v) Hybrid MLP s with GA in All layers, vi) Hybrid MLP s with GA in All layers and Cross Validation, vii) MLP neural nets.

9. RESULTS

The Modular models outperformed all the RBF models (Table I). The best MDN model was the Hybrid MDN with Genetic Algorithms of 2 hidden layers in a fine classification, fine performance and an extended processing time.

The Hybrid RBF had a competitive performance, as the best model is the Hybrid RBF with GA on inputs & outputs only of 3 hidden layer, lower errors, high impartiality, in a medium computing time, [39, 40].

Third was the Hybrid RBF of GAs and no hidden layers in a good classification, medium errors, fine performance, significant partiality, in medium time.

10. CONCLUDING REMARKS

The Hybrid MDN with Genetic Algorithms of 2 hidden layers is the optimal classification model. On the second rank, the RBFN Hybrid model of 3 layers is in a high efficiency, higher partiality, and a medium time. Third is the RBFN Hybrid of GA in all layers net without hidden layers, in an

adequate performance but lower partiality in a medium time. And Fourth was the RBFN hybrid of GA only in the input layer, without hidden layer, in an adequate classification efficiency and shorter medium time. Thus the MDN Hybrid net of 2 layers consists a robust classifier in portfolio optimisation, (Table I).

TABLE I. OPTIMAL MODELS OF MDN, RBFN

Models	Active Confusion Matrix					Performance							Time
	Layers	0→0	0→1	1→0	1→1	MSE	NMSE	r	%error	AIC	MDL		
MDN GA All	2	97.56	2.43	18.8	81.19	0.12	0.29	0.967	7.26	-533.73	71.40		18h 29' 29"
RBF input-out GA	3	97.24	2.76	27.52	72.48	0.166	0.393	0.925	9.039	672.93	1912.74		5h 48'56"
RBF GA	0	98.15	1.85	39.91	60.09	0.188	0.445	0.815	13.009	37.12	820.831		5h 02'28"
RBF inputs GA	0	97.73	2.26	46.32	53.67	0.219	0.519	0.791	12.383	282.78	1154.02		4h 19'42"

11. REFERENCES

[1] Loukeris N., I. Eleftheriadis, (2017), Control of Corporate Ownership in the Evolutional Portfolio Intelligent Complex Optimization (EPICO) model, *Corporate Ownership and Control 14(4-1), 271-285,*

[2] Loukeris, N., and N. Matsatsinis,(2006a), Corporate Financial Evaluation and Bankruptcy Prediction implementing Artificial Intelligence methods, *WSEAS Trans. Business and Economics, 4(3),*

[3] Loukeris N., (2008), Comparative Evaluation of Multi Layer Perceptrons to hybrid MLPs with Multicriteria Hierarchical Discrimination and Logistic Regression in Corporate Financial Analysis, *11th International Conference on Computers CSCC*, Elounda Agios Nikolaos, Crete, Greece 26-28 July

[4] Loukeris, N., D. Donelly, A. Khuman, Y. Peng, (2009), A numerical evaluation of meta-heuristic techniques in Portfolio Optimisation, *Operational Research*, Volume 9 (1), ed. Springer,

[5] Loukeris N., and I.Eleftheriadis, (2012a), Bankruptcy Prediction into Hybrids of Time Lag Recurrent Networks with Genetic optimisation, Multi LayerPerceptrons Neural Nets, and Bayesian Logistic Regression, Proc. *Int.Summer Conference* of the*Int.Academy of Business and Public Administration Disciplines (IABPAD),* Honolulu, Hawaii, USA (August 1- 5)-*Research Paper Award*

[6] Loukeris N., Eleftheriadis I.,& S. Livanis (2014a) Optimal Asset Allocation in Radial Basis Functions Networks, and hybrid neuro-genetic RBFNs to TLRNs, MLPs and Bayesian Logistic Regression, *World Fin. Conf.*, July 2-4, Venice, Italy

[7] Loukeris N., Eleftheriadis I. and E. Livanis (2014b), Portfolio Selection into Radial Basis Functions Networks and neuro-genetic RBFN Hybrids, *IEEE 5th Int.Conference IISA*, July 7-9, Chania Greece,

[8] Loukeris N. and I. Eleftheriadis, (2015b), Further Higher Moments in Portfolio Selection and A-priori Detection of Bankruptcy, under Multi Layer Perceptron Neural Networks, Hybrid Neuro-Genetic MLPs, and the Voted Perceptron, International Journal of Finance and Economics, 20(4), Oct., Wiley

[9] Loukeris N., Bekiros S.,and Eleftheriadis I., (2016), The Intelligent Portfolio Selection Optimization System, (IPSOS), IEEE 6th International Conference on Information, Intelligence, Systems and Applications, IISA2016, 13-15 July, Porto Carras Grand Resort Hotel, Halkidiki, Greece,

[10] Loukeris N., Bekiros S.,and Eleftheriadis I., (2016), The Portfolio Yield Reactive (PYR) model, IEEE 6th International Conference on Information, Intelligence, Systems and Applications, IISA2016, 13-15 July, Halkidiki, Greece,

[11] Loukeris N., Chalamandaris G., Eleftheriadis I. (2019), Self Organized Features Maps SOFM and hybrid neuro-genetic SOFMs in optimal portfolio management, *IEEE 2019 International Conference on Computational Science and Computational Intelligence, CSCI2019*, Symposium on Artificial Intelligence (CSCI-ISAI) 5-7, December, Las Vegas, Nevada,

[12] *Loukeris N., (2021), The Evolutional Returns Optimisation System – EROS, IEEE 2021 International Conference on Data Analytics for Business and Industry (ICDABI), DOI: 10.1109/ICDABI53623.2021.9655962*

[13] Kristoufek, L. (2013), Fractal Markets Hypothesis and the Global Financial Crisis: Wavelet Power Evidence. *Sci Rep* **3,** 2857

[14] Subrahmanyam, A. (2008), Behavioural Finance: A Review and Synthesis. European Financial Management, 14: 12-29.

[15] MarkowitzH.,(1952),Portfolio Selection, The Journal of Finance, 7(1)

[16] Maringer D., and P. Parpas, (2009), Global Optimization of Higher Order Moments in Portfolio Selection, *J. Global Optimization.* (43)2-3,

[17] Tsallis C., (1988), Possible generalization of Boltzmann-Gibbs statistics, *J Stat Phys;52(1–2):479–87*

[18] Tsallis C., Anteneodo C., Borland L., Osorio R., (2003), Non-extensive statistical mechanics and economics, *Phys A; 324(1):89–10 0*

[19] Kaizoji T., (2006), An interacting-agent model of financial markets from the viewpoint of non-extensive statistical mechanics, *Phys A;370(1):109–13*

[20] Rak R., Drozdz S., & J., Kwapien, (2007), Non-extensive statistical features of the polish stock market fluctuations. *Phys A; 374:315–24 .*

[21] Kozaki M., & A., Sato, (2008) Application of the beck model to stock markets: value-at-risk and portfolio risk assessment, *Phys A; 387:1225–46*

[22] Queirós SMD, Moyano LG, Souza JD, Tsallis C, (2007), A non-extensive approach to the dynamics of financial observables, *Eur Phys J B; 55:161–7 .*

[23] Biró T.S., & R., Rosenfeld, (2012), Microscopic origin of non-gaussian distributions of financial returns, *Phys A; 387(7):1603–12*

[24] Zhao P., Pan J., Yue Q. & J., Zhang (2021), Pricing of financial derivatives based on the Tsallis statistical theory,*Chaos, Solitons and Fractals 142, 110463*

[25] Kohonen, T., (1982), Self-Organized Formation of Topologically Correct Feature Maps, Biological Cybernetics, 43 (1): 59–69,

[26] Holland, J. H., (1975/1992), Adaptation in Natural and Artificial Systems. Cambridge, MA, *MIT Press*, Second edition (1992).

[27] Courtis J., (1978), Modelling a Financial Ratios Categoric Framework, Journal of Business Finance & Accounting, 5, 371 – 386,

[28] Wang Y., & P., Shang (2018), Analysis of financial stock markets through the multi- scale cross-distribution entropy based on Tsallis entropy, *Nonlinear Dyn:1–16*

[29] Loukeris N., Eleftheriadis I., & G., Polychronopoulos (2021), Optimal Portfolio Selection in MultiLayer Perceptrons and Self Organized Features Maps hybrids, *World Finance Conference*, Norway, August 3-5

[30] Freund, Y., and R. Schapire, (1996), Experiments with a new boosting algorithm, Machine Learning: *Proceedings of the Thirteenth International Conference*, 148-156

[31] Freund, Y. and R., Schapire, (1999), Large margin classification using heperceptron algorithm, *Machine Learning*, 37(3):277-296

[32] Hornik, K., Stinchcombe M., and H., White (1989), Multilayer feedforward networks are universal approximators, *Neural Networks*, vol. 2, no. 5. pp. 359-366.

[33] Lippman R., An introduction to computing with neural nets, *IEEE Trans, ASSP 4,* (1987)*, 4-22*

[34] Lapedes A., and R. Farber, (1987), Nonlinear signal processing using neural networks: prediction, and system modelling, *LA-VR-87-2662, Los Alamos*.

[35] Makhoul J., (1992), Pattern recognition properties of neural networks*, Proc. 1991 IEEE Workshop on Neural Networks for Signal Processing*, pp 173-187

[36] Rumelhart D., G. Hinton, & R. Williams, (1986), Learning internal representations by error back-propagation, in *Parallel distributed processing: explorations in the microstructure of cognition* (Rumelhart, D. & McClelland, J., eds.), *MIT Press, Cambridge, MA.*

[37] Principe J., deVries B., Kuo J. and Oliveira P., (1992), Modeling applications with the focused gamma network, *Neural Information Processing Systems* 4, (eds. Moody, Hanson, Touretsky), pp121-126, Morgan Kaufmann,

[38] Principe J., Euliano N.R., and W.C., Lefebvre, (1999), Neural and adaptive systems: Fundamentals through simulations, Wiley, New York.

[39] Genkin, A., Lewis, D., and D., Madigan, (2007), Large-scale Bayesian logistic regression for text categorization, *Technometrics*, 49, 291-304.

[40] Loukeris N., Eleftheriadis I., and S. Livanis (2014a) Optimal Asset Allocation in Radial Basis Functions Networks, and hybrid neuro-genetic RBFNs to TLRNs, MLPs and Bayesian Logistic Regression, *World Finance Conference*, July 2-4, Venice, Italy

[41] Loukeris N., Eleftheriadis I. and E. Livanis (2014b), Portfolio Selection into Radial Basis Functions Networks and neuro-genetic RBFN Hybrids, *IEEE 5th Int.Conference IISA*, July 7-9, Chania Greece.

TOWARDS A SUSTAINABLE FUTURE DATA MANAGEMENT: A CITIZEN-CENTRIC, SECURE AND TRUSTWORTHY CROSS-SECTOR DATA SHARING FRAMEWORK

Veroni, E[1,2], Evangelatos, S[1,2], Konidi, M[1], and Nikolopoulos, C[1]

[1]Hellenic Mediterranean University, Dept. of Electronic Engineering, Crete, Greece
[2]Netcompany-Intrasoft SA, Dept. of Research and Innovation Development, Luxembourg, Luxembourg
E-mail (ddk187@edu.hmu.gr)

1. INTRODUCTION

In recent years, Europe has led the way towards an open, fair, inclusive and people-centric Internet with its standard-setting General Data Protection Regulation (GDPR) and its rules for platform-to-business cooperation[1]. Digital services are increasingly becoming an essential part of our daily lives as numerous ongoing digital transformations are taking place across most industrial sectors. According to Gartner, 91% of businesses are engaged in some form of digital initiative[2]. The focus has been mainly on improving the efficiency of processes and potentially the customer satisfaction having as goal to enhance productivity, increase revenue and reduce costs. Yet, for this digital transformation to be fully successful, the right frameworks need to be created that ensure trustworthy technology and give businesses the confidence, competences and means to digitalise.

In the meantime, data is growing faster than ever. Forbes has identified that more than 1.7 megabytes of new data is created every second[3]. Historically, organisations have been collecting a plethora of data for developing products and services for their customers. For the development of these services, data are required to be widely and easily available, easily accessible, and simple to use and process. However, in many cases this is happening at the expense of the citizens' privacy.

Organizations must keep up with protecting not only their customer's personal information but also other sensitive data information. Risk Based Security identified 1,767 publicly reported breaches between January 1, 2021 and June 30, 2021 during which 18.8 billion records were exposed[4]. The associated costs related to citizens privacy both from the users' side and the organisations side are huge, creating an imperative need for digital solutions that will ensure users' privacy. An indicative example is the data breach that took place on Marriott Hotels in 2018[5] and affected 339 million guests resulting in the enormous fine of € 21.7 M. Privacy and confidentiality are also important in the context of administrations and public organisations. An administrator has the duty not to disclose or relate confidential information to public or any third-party without receiving explicit consent from the information issuer or the organisation itself. Office, health, business or public administration are few of the examples where highly confidential data are managed, stored and shared. In most of these cases, at some point during the data cycle, paper is still used to input/record data or transfer data among entities, which induces risks in terms of privacy, confidentiality, integrity, transparency, and raises environmental issues.

At the same time, with climate change being the defining issue of our time, operators are now quickly realising that there is an urgent need to increase the energy efficiency of data centres and reduce their environmental impact. According to the International Energy Agency, data centres consume approximately 200 TWh of electricity, or nearly 1% of global electricity demand,

---

[1] https://ec.europa.eu/info/sites/default/files/communication-shaping-europes-digital-future-feb2020_en_4.pdf

[2] https://www.gartner.com/en/information-technology/insights/digitalization

[3] https://www.forbes.com/sites/bernardmarr/2015/09/30/big-data-20-mind-boggling-facts-everyone-must-read/#2de24ce417b1

[4] https://www.securitymagazine.com/articles/95793-data-breaches-in-the-first-half-of-2021-exposed-188-billion-records

[5] https://www.bbc.com/news/technology-54748843

contributing to 0.3% of all global CO_2 emissions[6]. However, as the need to develop and train even larger and more accurate Artificial Intelligence (AI) models increases, the need for stronger data centres continues to grow. In a recent publication, the estimated carbon footprint of training a single big language model was found equal to around 300,000kg of CO_2 emissions[7]. With big data exploding and computing needs swiftly growing, these figures are only expected to rise without proactive steps to reduce data centres' energy consumption. The European Commission, in a recent publication for Europe's digital future[8] highlighted that new decentralised digital technologies offer a further possibility for both citizens and companies to manage data flows and usage, based on individual free choice and self-determination. Such technologies will enable dynamic data portability for individuals and companies in real time, disrupting the market with new business models.

To tackle the above challenges, we propose the TANGO framework which aims to establish a stronger cross-sector data sharing, in a citizen-centric, secure and trustworthy manner, by developing innovative solutions while addressing environmental degradation and climate change challenges. The overall outcome is a novel platform exhibiting the following capabilities: userfriendly, secure, trustworthy, compliant, fair, transparent, accountable and environmentally sustainable data management, having at its core technology components for distributed, privacy preserving and environmentally sustainable data collection, processing, analysis, sharing and storage. This platform will promote trustworthy and digitally enabled interactions across society, for people as well as for businesses. TANGO will leverage the power of emerging digital technologies to strengthen the privacy for citizens and private/public organisations, reduce costs and improve productivity. It will unlock the innovation potential of digital technologies for decentralised, privacy-preserving applications, while making accessible and demonstrating this potential within the Gaia-X and European Open Science Cloud (EOSC) ecosystem.

2. CONCEPT & METHDOLOGY

TANGO's unique value proposition is the one-of-its-kind platform, which provides a trustworthy data management and sharing platform deployed in federated, distributed, multi-cloud environments ensuring data sovereignty, governance and provenance for public/private organizations while empowering citizens to get control of their data. Through the provision of TANGO technologies, a trustworthy environment will be designed acting as a gatekeeper to information and data flows. Citizens and public/private organisations will be empowered to act and interact providing data both online and offline. TANGO will focus on the following 4 main pillars:

i. the deployment of trustworthy, accountable and privacy-preserving data-sharing technologies and platforms;
ii. the creation of data governance models and frameworks;
iii. the improvement of data availability, quality and interoperability – both in domain-specific settings and across sectors;
iv. energy consumption optimization at infrastructure, application and inference (AI) level.

In-line with the strategic agenda of the Gaia-X initiative, TANGO will boost data sovereignty and enable cloud/edge and AI applications that adhere to European values. Moreover, aligned with the EOSC, it will provide seamless access and reliable re-use of research and industrial data to European researchers, innovators, companies and citizens through a trusted and open distributed data environment.

TANGO has translated the above challenges into the following tangible goals:

• Design and develop a holistic, flexible and open framework for fair, responsible and green data management, sharing and storage while maintaining data ownership based on

---

6 https://www.forbes.com/sites/forbestechcouncil/2021/05/03/renewable-energy-alone-cant-address-data-centers-adverse-environmentalimpact/?sh=448950e65ddc

7 https://www.nature.com/articles/s42256-020-0219-9?proof=t

8 https://ec.europa.eu/info/sites/default/files/communication-european-strategy-data-19feb2020_en.pdf

energyefficient Smart Contracts, Artificial Intelligence, Self-Sovereign Identity, Self-Encryption and Continuous Behavioural Authentication.

TANGO will design, develop and integrate a coherent and holistic framework based on state-ofthe-art technologies such as Blockchain and Smart Contracts, Artificial Intelligence, Self-Sovereign Identity, Self-Encryption, Data Analytics, and Continuous Behavioural Authentication. Through a technological gap analysis, the shortcoming of current approaches in data management, storage and sharing approaches including current privacy and energy concerns will be identified. The findings of the gap analysis will be combined with the reported user needs and requirements, leading to the elicitation of user and system requirements. The analysis of the system requirements will shape the TANGO architecture as the basis for the integration of the individual modules into an interoperable, high-scalable and cost-efficient platform.

- Provide a secure, trusted and audible data management, storage and sharing environment by developing advanced, energy-efficient Blockchain services and specifying novel security and privacy-preserving protocols for guaranteeing the ownership of the data throughout the whole data lifecycle.

Distributed data management, storage and sharing solutions are at the core of the TANGO platform, interconnecting various tools that enhance untampered and secure data handling, sharing and re-use in various application areas such as public administration, smart hospitality, autonomous vehicles, smart manufacturing, banking and retail. The distributed data management and sharing will be based on energy-efficient blockchain technology ensuring the traceability, integrity and ownership of the data whilst maintaining GDPR compliance. A distributed data tokenisation solution combined with privacy and confidentiality by design will be developed, providing access control to the data. Distributed self-encryption/decryption combined with recovery solutions based on trust, will provide high security for data storing and sharing.

- Design and implement distributed trust management mechanisms that leverage SelfSovereign Identity for identity management, innovative user and device onboarding approaches, user and device continuous behavioural authentication mechanisms, and hardening of side-channel attacks, providing highly secure and user-friendly access control.

TANGO targets the development and incorporation of several security tools within its platform that will empower, secure and facilitate data management and enhance trust and privacy-preservation. These tools will provide a privacy-preserving identity management with inherent sovereignty through Self-Sovereign Identity as well as security for the IoT devices, the users themselves and to the integrated platform. The security elements comprise the identity verification of users and devices during the onboarding process as well as the continuous reassurance regarding the identity of users and devices. Furthermore, it will expose strong mechanisms for preventing side-channel attacks, hardening and defending against potential tampering of the end-user devices, ensuring the security of the platform at the device level.

- Exploit the power of Artificial Intelligence in order to produce accurate decision making targeting the data, security and infrastructure management towards "green" data operations.

TANGO's value proposition is tied with the design, development and deployment of novel Artificial Intelligence (AI) and Machine Learning (ML) techniques for environmentally sustainable data operations. The proposed solutions have been designed to optimise not only the trade-off among energy consumption, privacy, data transfer and security but also the energy and cost efficiency in code level within a single node of a system. TANGO's impact and adoption will be accelerated by the energy efficient training of AI models considering the constraints of edge computing devices. Moreover, AI and ML methods will be employed to generate alerts and recommendations aiming to mitigate privacy and security risks. Explainable AI (X-AI) mechanisms will reveal to end users the logic followed by the AI algorithms to reach certain conclusions supporting decisions about green and responsible operations.

- To validate and demonstrate the effectiveness of the proposed solution in six diverse use cases with the active engagement and training of several different stakeholders' groups accomplishing a TRL-6 level for the entire TANGO platform.

TANGO's developments will be extensively evaluated in real-life settings, in six different use cases, considering different operational procedures and diverse environments. The targeted use cases have been selected for their high societal, environmental, and financial impact on the EU citizens and the data ecosystem. The foreseen scenarios include data management in (a) Smart Hospitality, (b) Autonomous Vehicles, (c) Smart Manufacturing, (d) Financial Institutes, (e) Public Administration and (f) Retail. The activities will include TANGO's technical verification, assessing, improving and validating the platform's technology readiness, which is expected to reach TRL-6, as well as end-user validation, showcasing the key value proposition of the TANGO platform at different levels.

3. MAIN BUILDING BLOCKS & REFERENCE ARCHITECTURE

TANGO aims to improve the efficiency and the use of trustworthy digital technologies safeguarding citizens, private companies and public organisations from risks that may compromise their privacy or result in commercial and administrative confidentiality breach. The proposed technology solutions involve environmentally sustainable data operations for data collection, access, processing and storage honouring compliance with prevailing and emerging legislation.

TANGO consists of 15 innovative technological components that provide fair, accountable, trustworthy and green ways for end-users and organisations to share, store and manage data. The core of the TANGO platform lies in the data management layer where data coming from heterogeneous sources such as mobile phones, IoT devices, wearables, autonomous vehicles, etc. along with information stored in local level dataspaces including legacy systems and IT operational systems, is processed, stored and shared among relevant stakeholders. Dedicated user-friendly interfaces connect the processed data and the extracted knowledge with the operators from private and public organisations as well as with users such as organisations' employees and citizens. All the above will be combined under an agile, highly scalable, and flexible architecture. The envisaged conceptual architecture is depicted in layers in Figure 1.
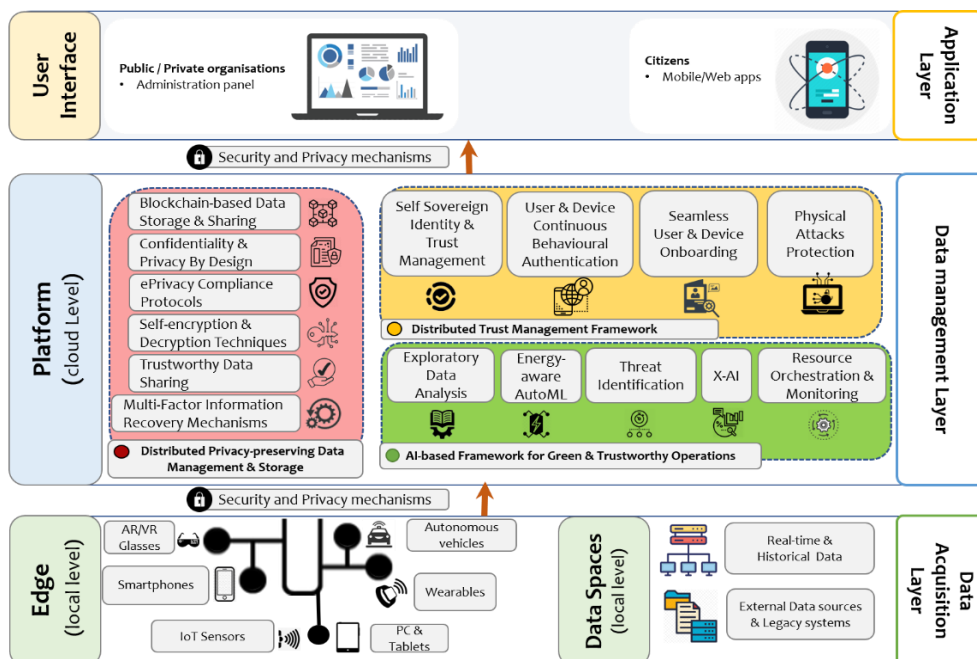

Figure 1: TANGO High-Level Architecture

The core TANGO platform is based on the *Blockchain-based Data Storage and Sharing* module that allows data sharing, storage and management (Alexopoulos, et al. 2017) in a privacypreserving, accountable, fair and green way, leveraging state-of-the-art distributed and interoperable (Gaia-X

compliant) data sharing mechanisms, including energy efficient blockchain (Dorri, Kanhere and Jurdak 2017). External data sources are connected through the Gaia-X gateway while IDS Connectors are utilised to interconnect with distributed data storage, ensuring data and system interoperability.

On top of the later module, the *Trustworthy Data Sharing* module provides another layer of privacy allowing users to share data in a sovereign manner through the concept of trustworthiness and an innovative distributed data tokenisation technique for sensitive data sharing (Putzer and Wozniak 2020). When data are generated, they are watermarked and stored in the platform through the *Confidentiality and Privacy by Design* that enables data producers to maintain the data ownership throughout the data lifecycle (D'Acquisto, et al. 2015). In parallel, *ePrivacy Mechanisms* ensure that all personal and non-personal data containing business-sensitive information are treated in the same manner. From the data source level and throughout their lifecycle, data are protected by the *Distributed Self-encryption module with Recovery Abilities*.

The **Distributed** Trust Management framework handles the data access control for users and devices through various innovative security and privacy mechanisms. Once new users access the TANGO platform, they are forwarded to the *AI-powered seamless onboarding for users and devices* to create a profile. These profiles constitute the digital identity of the users and the associated IoT devices, which are stored and managed at the *Self-Sovereign Identity & Trust Management*. The data access control both at the device and platform level is ensured by the complimentary *User and Device continuous behavioural authentication* through learning the behavioural patterns of both the users and devices, while monitoring for any abnormalities (Palaghias, et al. 2016). The IoT devices connected to the TANGO platform are protected from exploitations by the *Hardening against Sidechannel Attacks* module (Belleville, et al. 2018)**.**

Energy efficiency is an essential part of the TANGO platform. Optimisations with respect to the energy consumption for both the TANGO platform itself and additional services, materialise at various levels including a) the infrastructure level where *Infrastructure Management based on AI* (Notaro, Cardoso and Gerndt 2021) balances the trade-off among energy, privacy, security and data transfer**,** b) the application execution level through *Dynamic Intelligent Execution on Heterogeneous Systems* (Khalid, et al. 2019) that reduces energy consumption on a single node, c) the AI model training and execution level through *Energy efficient AI model training* (Bisong 2019), which introduces environmentally sustainable deep learning models and achieves optimal performance in the trade-off between the resulting models and energy consumption.

Considering the vast amount of data TANGO will handle, intelligent data analytics will generate knowledge and recommendations to stakeholders, through the *Exploratory Data Analysis Engine* (Dhaenens and Jourdan 2016). Both at the *Exploratory Data Analysis Engine* and across the TANGO platform, AI-based decision-making occurs. *X-AI for Privacy and Trust Enhancement* (Ribeiro, Singh and Guestrin 2016) provides a better understanding to end-users and stakeholders for the type of information used, the process internally and inference result. To further strengthen the trust towards TANGO platform *Privacy Threat Modelling and Identification for Trustworthy AI* (Song, Shokri and Mittal 2019) module a-priori identifies AI related privacy risks in mechanisms.

4. FUTURE WORK

TANGO represents a significant step forward in establishing a citizen-centric, secure, and trustworthy cross-sector data sharing framework. While the presented concept already encompasses the combination of cutting-edge innovative solutions, there are several areas where further work is required to ensure its long-term sustainability and impact. More specifically, additional functionalities will be considered to support data sharing across diverse sectors and domains, which would require further research and development efforts, particularly in the areas of data management, security, and privacy. To amplify its impact, TANGO will seek to collaborate with other initiatives and organizations working in the area of cross-sector data sharing and environmental sustainability, in order to build synergies and leverage complementary efforts. Moreover, TANGO will be evaluated on the ground, by monitoring and assessing the uptake and effectiveness of the platform in promoting

cross-sector data sharing and addressing environmental challenges. In summary, TANGO represents an important contribution to the emerging field of cross-sector data sharing and environmental sustainability. By developing and expanding the above framework, engaging with key stakeholders, collaborating with other initiatives, and evaluating its impact in real life scenarios, TANGO has the potential to become a key tool for promoting sustainable development and addressing the pressing environmental challenges of our time.

5. ACKNOWLEDGMENT

6. REFERENCES

Alexopoulos, Nikolaos, Jörg Daubert, Max Mühlhäuser, and Sheikh Mahbub Habib. 2017. "Beyond the Hype: On Using Blockchains in Trust Management for Authentication." *2017 IEEE Trustcom/BigDataSE/ICESS.* Sydney, Australia: IEEE. doi:10.1109/Trustcom/BigDataSE/ICESS.2017.283.

Belleville, Nicolas, Damien Couroussé, Karine Heydemann, and Henri-Pierre Charles. 2018. "Automated Software Protection for the Masses Against Side-Channel Attacks." *ACM Trans. Archit. Code Optim.* (ACM) 15 (4). doi:10.1145/3281662.

Bisong, Ekaba. 2019. *Building Machine Learning and Deep Learning Models on Google Cloud Platform.* CA: Apress.

D'Acquisto, Giuseppe , Josep Domingo-Ferrer, Panayiotis Kikiras, Vicenç Torra, Yves-Alexandre De Montjoye, and Athena Bourka. 2015. "Privacy by design in big data: An overview of privacy enhancing technologies in the era of big data analytics." arXiv. doi:10.48550/arXiv.1512.06000.

Dhaenens, Clarisse, and Laetitia Jourdan. 2016. *Metaheuristics for big data.* John Wiley & Sons.

Dorri, Ali, Salil Subhash Kanhere, and Raja Jurdak. 2017. "Towards an Optimized BlockChain for IoT." *IoTDI '17: Proceedings of the Second International Conference on Internet-of-Things Design and Implementation.* Pittsburgh, Pennsylvania, USA: ACM. 173–178. doi:10.1145/3054977.3055003.

Khalid, Yasir Noman, Muhammad Aleem, Usman Ahmed, Muhammad Arshad Islam, and Muhammad Azhar Iqbal. 2019. "Troodon: A machine-learning based load-balancing application scheduler for CPU–GPU system." *Journal of Parallel and Distributed Computing* (Elsevier) 132: 79-94. doi:10.1016/j.jpdc.2019.05.015.

Notaro, Paolo, Jorge Cardoso, and Michael Gerndt. 2021. "A Systematic Mapping Study in AIOps." *Service-Oriented Computing – ICSOC 2020 Workshops.* Springer. doi:10.1007/978-3-03076352-7_15.

Palaghias, Niklas, Nikos Loumis, Stylianos Georgoulas, and Klaus Moessner. 2016. "Quantifying trust relationships based on real-world social interactions." *2016 IEEE International Conference on Communications (ICC).* Kuala Lumpur, Malaysia: IEEE. 1-7. doi:10.1109/ICC.2016.7510835.

Putzer, Henrik J, and Ernest Wozniak. 2020. "A Structured Approach to Trustworthy Autonomous/Cognitive Systems." arXiv. doi:10.48550/arXiv.2002.08210.

Ribeiro, Marco Tulio, Sameer Singh, and Carlos Ernesto Guestrin. 2016. ""Why Should I Trust You?": Explaining the Predictions of Any Classifier." *KDD '16: Proceedings of the 22nd ACM SIGKDD International Conference on Knowledge Discovery and Data Mining.* ACM. 1135–1144. doi:10.1145/2939672.2939778.

Song, Liwei, Reza Shokri, and Prateek Mittal. 2019. "Privacy Risks of Securing Machine Learning Models against Adversarial Examples." *CCS '19: Proceedings of the 2019 ACM SIGSAC Conference on Computer and Communications Security.* London, United Kingdom: ACM. 241–257. doi:10.1145/3319535.3354211.

INNOVATIVE STRATEGIES FOR COMBATTING CORRUPTION: THE ROLE OF CUTTING EDGE TECHNOLOGIES IN STRENGTHENING ANTI-CORRUPTION MEASURES

Konidi, M[1,2], Evangelatos, S[1,3], Veroni, E[1,3] and Nikolopoulos, C[1]

[1]Hellenic Mediterranean University, Department of Electronic Engineering
[2]Ubitech Ltd.
[3]Netcompany-Intrasoft S.A., Luxembourg
ddk184@edu.hmu.gr

1. INTRODUCTION

Corruption is a complex social, political and economic phenomenon that affects all countries and hinders the rule of law. In general, there is no internationally agreed definition of corruption[a] but there are many actions which are recognised worldwide as forms of corruption, such as the abuse of power, bribery, embezzlement of public funds, maliciously interfering with the justice system or hiding the financial gains of illicit activities. Several cases of corruption have been reported in national media almost on a daily basis highlighting the harm caused not only to public and private organisations, but also to society. Corruption is a feature of almost all criminal activities in the EU, whether it involves petty bribery or complex multi-million-euro corruption schemes[b]. It has strong ties with criminal networks weakening institutions of states and hampering economic development and the respect for human rights. Studies have also indicated corruption as one of the root causes of poverty, since it increases income inequality by reducing the progressivity of the tax system and the effectiveness of social spending, also perpetuating unequal access to education[c]. On top of that, corruption became more damaging during the COVID-19 pandemic crisis when all countries around the world faced unprecedented corruption-related challenges. The response to the pandemics created new opportunities to exploit weak oversight and inadequate transparency, diverting funds away from people in great need. Governments acted in haste without verifying suppliers or determining fair prices for the goods needed including pharmaceuticals. Faulty products such as defective ventilators, poorly manufactured rapid tests or counterfeit medicines were reported along with lower accessibility and quality of healthcare services. In a recent report in 2022 published by EC through the Eurobarometer survey conducted in 27 EU member states[d], 68% of European citizens believe that corruption is widespread in their country but only a minority of them think that the fight against corruption is effective. Despite their view that the main reason for not reporting corruption incidents is the difficulty in providing solid evidence and proofs, the majority of EU citizens trust by far the Police Authorities (or the specialised anti-corruption agencies within the Police structure) to deal with cases of corruption, ranking Police well above Justice.

Despite the fact that corruption is met in all countries, there are some notable examples of best practices in place such as the access to information for everyone[e], in many countries in the OSCE region, transparency in the financing data of political parties – especially regarding donations by foreign donors – to avoid the so-called "Trading in Influence" also featured in early drafts of the UN Convention Against Corruption[f], Conflict of Interest and Post-employment Code for public officials in an attempt to tackle favouritism or anti-nepotism laws[g], specific legislations for political and

55

---

[a] Corruption and integrity: https://www.unodc.org/e4j/en/secondary/corruption-integrity-ethics.html
[b] Serious and Organised Crime Threat Assessment:
https://www.europol.europa.eu/cms/sites/default/files/documents/socta2021_1.pdf
[c] IMF - Does Corruption Affect Income Inequality and Poverty? https://www.imf.org/external/pubs/ft/wp/wp9876.pdf
[d] Special Eurobarometer 523, March-April 2022, Corruption, https://europa.eu/eurobarometer/surveys/detail/2658
[e] https://rm.coe.int/access-to-official-documents-recommendation-rec-2002-2-of-the-committe/1680483b2b
[f] https://www.unodc.org/documents/brussels/UN_Convention_Against_Corruption.pdf
[g] https://rm.coe.int/fighting-nepotism-within-local-and-regional-authorities-governance-com/16809312c3

judicial immunity where specific procedures for waiving parliamentary immunity are described in several countries (and in the EU parliament[h]), ethical standards for public servants as described within the International Code of Conduct for Public Officials, employees complaint mechanisms for whistleblowers to report their suspicions or offer evidence on corruption[i] and expose wrongdoing and many more listed in various compendia.

Several emerging technologies are currently used in the fight against corruption: (a) Big Data, which allows the processing of massive amounts of data with sophisticated analysis tools in cloud environments, (b) Machine Learning and Artificial Intelligence, targeting the reduction of false negatives in investigations, detection of illicit activities and identification of abnormal behaviour, (c) Distributed Ledger Technologies and Blockchain that facilitates the replacement of the physical record by a digital and auditable record, ensuring immutability, i.e., remain a permanent, indelible, and unalterable history of transactions, just to name a few.

To tackle the above-mentioned challenges, a holistic platform for the Law Enforcement Agencies (LEAs) is needed that will build upon already identified anti-corruption best practices from different domains, providing a unifying framework coupled with emerging technologies that will help LEAs to quickly identify, detect and prevent corruption. The foundations of this platform should be built on the following undisputable facts: (1) Corruption is a global phenomenon that affects all countries in the world both developed and not. It does not concern only certain countries of the EU (e.g., east or southern Europe) but also several other central and west European countries, which are facing large-scale corruption scandals (e.g., the SIEMENS case[j]). (2) Corruption is met not only in the public domain but also in the private sector which is generally under-represented. In corruption practices, two actors are involved, the corrupted and the corrupter. In some cases, the private sector is often a victim of some types of corruption but at other times it is primarily a beneficiary and drives corruption through links with bureaucrats and politicians. (3) Most anti-corruption measures currently target petty corruption. While this activity is not insignificant, a greater focus needs to be shifted to grand corruption which has the most devastating impact on sustainable development and human right. Grand corruption involves major executive actors whose illegal activities subvert the legal, political, and economic aims of entire countries or corporations, and often have a transnational dimension that hinders investigation and prosecution.

The solution that should be developed must try to fight corruption in both public and private organisations, assisting LEAs from EU countries in rapidly identifying, detecting and effectively preventing cross-border, large-scale corruption practices and incidents. A holistic risk assessment framework must accompany the platform based on thorough interdisciplinary research in current corruption processes and existing best practices enhanced with emerging technologies, such as robust Machine Learning, Artificial Intelligence and (Big) Data Analytics. The developed solutions should provide security practitioners with insightful knowledge on the impact of corruption practices (namely during the COVID-19 pandemics), the root causes of the phenomenon and the modus operandi of criminal networks using corruption practices. In addition, there is a need of training curricula to be co-designed in order to familiarise with technology tools and best anti-corruption practices and facilitate international cooperation in the fight against corruption through capacitybuilding training sessions for security practitioners and policy recommendations.

2. PROPOSED SOLUTION

The foreseen solution will be based upon the identification of the operational challenges that security practitioners face in the context of identifying, detecting and preventing corruption practices while at the same time gathering lawful evidence acceptable to the court of justice. It will investigate "Crime-as-a-Service" (CaaS)[k] where several advanced methods related to corruption practices can be

56

[h] https://www.europarl.europa.eu/news/en/faq/5/parliamentary-immunity
[i] https://edps.europa.eu/data-protection/data-protection/reference-library/whistleblowing_en
[j] https://www.dw.com/en/siemens-bribery-fines-top-1-billion-euros/a-3877528
[k] https://www.europol.europa.eu/cms/sites/default/files/documents/internet_organised_crime_threat_assessment_iocta_2021.pdf

offered by different criminal groups to criminals or criminal networks who have limited knowledge and expertise. In its core, the foreseen solution will equip LEAs with intelligence extraction tools based on Artificial Intelligence, (Big) Data Analytics and Risk Management that will assist them in identifying, detecting and preventing corruption. In detail, anti-money laundering techniques for cryptocurrencies will be explored based on heuristics, AI and blockchain analysis, in order for LEAs to detect laundering of corruption proceeds through cryptocurrencies and other virtual assets. Opensource intelligence through clean, dark and surface web crawling techniques will be provided uncovering corruption or wrongdoing while public sentiment processing and entity recognition from online sources (and social media) will be performed, assisting anti-corruption agencies and fraud investigators to identify cases of corruption patterns faster and with more discretion. The eminent role of Big Data will be highlighted through highly scalable searching capabilities and data mining techniques applied in governmental digital records, judicial documents, open data on contract amounts, awards and the number of bidders, citizens' complaints, etc., revealing patterns that indicate corruption. Knowledge Graphs and Artificial Intelligence methods will be deployed in order to identify the links between corruption and transnational organised crime, analyse the structural properties and re-construct high-risk criminal networks that use different forms of corruption involved in other crimes such as firearms and drugs trafficking, trafficking in human beings, environmental crimes, etc. Last, an innovative real-time analytics service will be developed that detects risk factors and anomalies in the ownership structure along with other characteristics of registered companies that can raise an alert for corruption practices and other criminal activities. All these innovative technology tools will be integrated into a unique platform tailored to the needs of the security practitioners. The platform will fuse and analyse the input of all the above-mentioned tools, providing insightful recommendations based in Explainable AI (XAI) through its user-friendly interfaces coupled with reporting mechanisms.
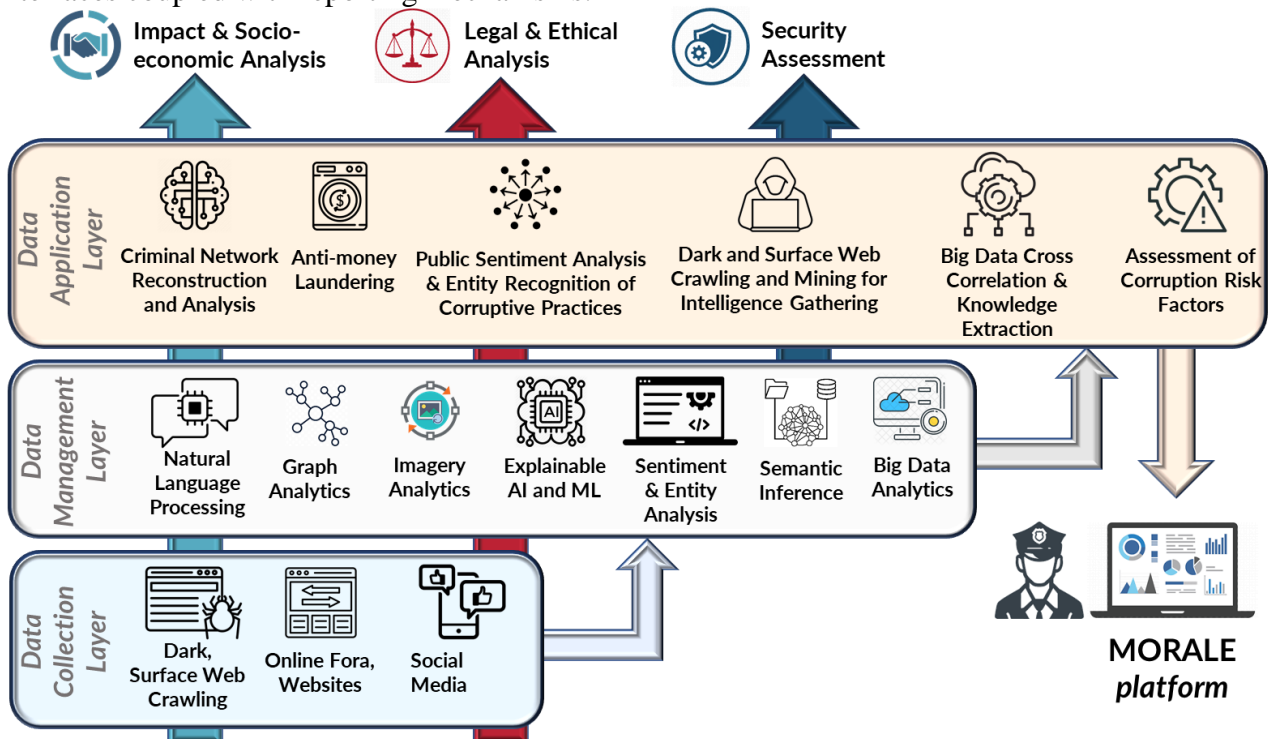

Figure 1. Proposed solution's high-level architecture

The proposed technology follows a layered and modular approach organized into three tiers: a) trustworthy data sources in the data collection layer, b) processing and analysis in the data management layer and c) intelligence and application layer. State-of the-art technologies such as AI, Big Data and NLP will be at the core of the platform leveraging data coming from the various data sources in the data collection layer such as social media and fora, websites and microblogs, etc. The

platform user interface will consist of several ground-breaking technology modules appearing at the data application layer coupled with Explainable recommendations to end users and innovative reporting techniques that will facilitate their daily operational activities. The overall platform will be equipped with privacy and security mechanisms for data sharing between layers ensuring compliance with national and EU legal and ethical regulations. The user-friendly interface will be tailored made to the specific needs of LEAs, facilitating the dynamic collaboration between multiple security practitioners throughout EU. The individual components of the platform are described in the following sub-sections below.

2.1. Anti-money Laundering Techniques Based on Cryptocurrencies

The cryptocurrencies analysis will harvest the collected data and gathered intelligence to correlate them with transactions related with financial cybercrime (i.e., fraud, money laundering, pyramid schemes, gambling). The core mechanism will build the transactions graph attributed with time, space and contextual criteria and will implement graph-based algorithms for community and cluster detection of illegal transactions (Silfversten et al., 2020). The true positives from the newly detected money laundering techniques and transactions and their metadata will be used as keywords by the Web Crawler to optimise the search space to more relevant URLs. Graph analytics will be deployed to deliver a holistic view of the various entities involved in financial crimes and corruption targeting the exposure of the relationships between these entities, and their hidden connections and uncovering previously invisible patterns in an explainable manner. On top of the proposed technology, powerful visualizations will be developed allowing anti-corruption agents and police officers to intuitively explore relationships among key stakeholders in near real-time and create thorough and accurate reports of corruption practices identified in several impactful domains. The proposed service will complement conventional AML technologies enhancing the fight against money laundering from corruption.

2.2. Dark and Surface Web Crawling and Mining for Intelligence Gathering

The Web Crawler module will gather, harmonise and generate analytics for corruption activities, networks, clusters and communities related with money laundering activities identified over the surface and dark web forums, social media and marketplaces. Strong time, space and context correlations will help to efficiently identify such activities in cross-border settings. The data collection and intelligence gathering will be based on a user-assisted approach, involving automated form-filling techniques, predefined list of keywords which can be enriched, and manual ad hoc queries constructed incrementally using relevant temporal, spatial, keywords or multimedia (i.e., images, etc.) criteria.

The crawler's core mechanisms will implement a genetic algorithm (Katoch et al., 2021) to improve the corresponding keywords, semantic, spatiotemporal and keywords / content captured during crawling and provide new optimized keywords (Yan et al., 2018). At the same time, a graph-based community detection algorithm will take into consideration these keywords to re-feed the crawler and drive the search to more relevant URLs by using some well-known dark websites indices (Desai et al., 2013). The descriptive analytics targeting anti-money-laundering will focus on correlating time, space and context in text mining tasks and on collecting timestamped evidence and document differentiation methods for lawful court-proof collection of crime evidence. A storage component
(for data persistence) and REST APIs will be exposed for smooth integration with the core
platform.

2.3. Public Sentiment Analysis of Corruptive Practices from Online Sources

The public sentiment analysis module will analyse citizens' complaints in social media and public fora, identifying the main entity that it referred within the comments/posts/blogs which might be using corruption practices. Thus, it will act as an alert raising mechanism for security practitioners for further investigation. The module will exploit NLP capabilities and leverages the BERT model

for feature extraction. The module assesses the emotional polarity of a corruption-related keyword and extracts the entity that is referred to, e.g., public administration office in a specific area. It will aggregate all the collected data and pre-process it to increase the accuracy of the output maximizing the classification performance. During the pre-processing phase, anonymization of the user accounts will be performed along with the elimination of any information that can trace back the online users, removal of links and replacing emoji characters with corresponding text/keyword. Following the preprocessing phase, the system will proceed with feature extraction using a BERT model, to learn the contextual relations between words in a text/post. The proposed model will be specifically trained to extract the entity referred within the post and an indication of the referred area. Data from the Twitter public API for keywords associated with corruption will be used to detect user-generated messages reporting or discussing experiences with corruption capitalising on the increased digital engagement of citizens in the social media and the anonymity provided by online platforms and fora to enable reporting of corruption-related activities (Giachanou et al., 2016). This module will be customisable to the end-users needs, producing specific KPIs that can be linked with the events fuelling corruption.

2.4. Big Data Cross Correlation and Data Mining for Knowledge Extraction

Effective identification of corruption processes and corruption related activities requires the rapid search, processing and analysis of vast amounts of data stemming from heterogeneous sources (Ali et al., 2022). The proposed solution will develop ground-breaking and sophisticated AI-enabled deep graph neural network architectures, particularly tailored to the needs of security practitioners towards their combating of corruption-related incidents (Zhang et al., 2019). In particular, a suitable (to the domain of concern) graph architecture will be initially defined, accounting for the particularities of the corruption incidents data landscape. Then, a set of advanced robust AI-enabled analytics will be applied to the formed graph analysing, fusing and detecting patterns in the vast amounts of collected information. More specifically, the generated data-driven graph-based infrastructure will be capable of estimating accurate insights, detecting complex events in the examined data, identifying (inter)relations among the various data sources and instances and the identification of global-level trends. The ultimate goal of the developed solution will be to detect efficiently and accurately the occurrence of corruption events, patterns of suspicious/illegal behaviour and outliers (in relation to the expected norms). Moreover, through the deployment of dynamic graphical models, trends in corruption will also be revealed through cross-correlations and clusters of similar information (Zhichun et al., 2018). Combined with state-of-the-art searching algorithms, deep hashing mechanisms will allow LEAs, Border Authorities and Anti-corruption Agencies to rapidly search in a large pool of data and identify evidence of corruption.

2.5. Criminal Network Reconstruction and Analysis

Cutting-edge methodologies will be used to address the challenges imposed by tracing and reconstructing a criminal network using corruption practices (Xiaomin et al., 2020). Towards this direction, a thorough analysis of the criminal networks will be performed in order to deeply understand the anonymous network structures and the key actors involved, identify methods used (online and offline), algorithms for key actor identification, tools and strategies capable of locating corruption crimes and criminals not only in the web but also in the Dark/Deep Web. The whole process will follow a step-by-step methodology by identifying one reaction at a time and then employ Knowledge Graph Theory compiling the criminal network structure layer by layer. The proposed service will create conceptual networks consisting of actors (nodes) and relationships (ties), by correlating pieces of evidence data based on the details of their inter-relationships revealing criminal entities (and their roles) involved in corruption acts.

2.6. Assessment of Corruption Risk Factors in Organizational Structure

A tool will be developed as an real-time analytics platform able to (a) trace the ownership structure and the beneficial owners of registered companies across borders; (b) identify adverse events (i.e., sanctions, enforcement, adverse media news) potentially linked to companies, company owners, directors and other related entities; (c) detect risk factors and anomalies in the ownership structure and other characteristics of registered companies which could alert about risks of corruption practices and other criminal or suspicious activities (Europol Enterprising criminals, 2018). The technology will make use of Machine Learning algorithms that process the anomaly indicators suggested by relevant guidelines (ex., Anti-fraud and anticorruption) worldwide. It will exploit state-of-the-art real time data on worldwide registered companies, combining them with proprietary information (Bosisio et al., 2020). The risk indicators that will be produced, will be used by private and public organisations for third-party risk assessment, Anti-money laundering customer due diligence, procurement integrity checks and antifraud activities.

3. CONCLUSION

This paper presents a high-level overview for a holistic solution that will assist LEAs, Border Authorities and Anti-corruption Agencies in identifying, detecting and finally preventing corruption activities, through emerging technologies, such as robust Machine Learning, Artificial Intelligence, Big Data Analytics and Risk Management. The innovation of the proposed solution lies in the integration of the above technologies into a unique platform, tailored to the needs of the security practitioners.

4. REFERENCES

Ali A. et al., (2022). Financial Fraud Detection Based on Machine Learning: A Systematic Literature Review. Applied Sciences.

Bosisio, A. et al., (2020). Opacity and complexity of European firms' ownership structure. Preliminary results of Project DATACROS.

Desai, K. et al., (2013). Web Crawler: Review of Different Types of Web Crawler, Its Issues, Applications and Research Opportunities. International Journal of Advanced Research in Computer Science, 8(3).

Europol Enterprising criminals, (2018). The Hague: Europol, https://www.europol.europa.eu/cms/sites/default/files/documents/efecc_-_enterprising_criminals__europes_fight_against_the_global_networks_of_financial_and_economic_crime_.pdf.

Giachanou A. et al., (2016). Like It or Not: A Survey of Twitter Sentiment Analysis Methods", ACM Computing Survey, Vol.49(2), pp. 41.

Katoch, S. et al., (2021). A review on genetic algorithm: past, present, and future. Multimedia Tools and Applications, 80(5), 8091-8126.

Silfversten, E.et al., (2020). Exploring the use of Zcash crypto currency for illicit or criminal purposes. RAND Corporation, UK.

Xiaomin Wu et al., (2020). Analyses and applications of optimization methods for complex network reconstruction, KBS, Vol.193.

Yan, W., et al., (2018). Designing focused crawler based on improved genetic algorithm. IEEE 10th International Conference on Advanced Computational Intelligence (ICACI) (pp. 319-323).

Zhang, F. et al., (2019). OAG: toward linking large-scale heterogeneous entity graphs. Proceedings of Knowledge Discovery and Data Mining Conference, 2585–2595.

Zhichun W., et al., (2018). Cross-lingual knowledge graph alignment via graph convolutional networks. Conference on Empirical Methods in Natural Language Processing.

Withdrawn paper

Withdrawn paper

Withdrawn paper

Withdrawn paper

Withdrawn paper

3D MODELLING OF SEISMICALLY ACTIVE PARTS OF UNDERGROUND FAULTS VIA RECURRENT DEEP LEARNING NEURAL NETWORKS

Frantzeskakis, T[1], Moshou, A[1], Maravelakis, E[1] and Konstantaras, A[1]

[1]Department of Electronic Engineering, Hellenic Mediterranean University, Chania, Greece
akonstantaras@hmu.gr

1. INTRODUCTION

Underground faults are strain energy storage elements, the partial release of which is being depicted as a series of earthquakes, in the form of foreshocks-main seismic event-aftershocks, ones it reaches the surface of the Earth's outer crust (Moshou, et al., 2021). Several underground faults, mostly bellow mainland, have been well mapped in terms of their three-dimensional extent. This is hardly the case though for underground faults beneath the sea (Konstantaras, 2016, 2020). In the case of the latter, expensive efforts have produced two-dimensional mappings mostly in areas of hydrocarbon interest, such as the area of the Southern Hellenic Seismic Arc in the Eastern Mediterranean Sea.

The challenge lies in deriving the in-depth extent of the latter when the surface of the Earth is covered by up to 3-4km of sea water as is the case in parts of the Eastern Mediterranean Sea. To that respect, known earthquakes' hypocentres can provide valuable information regarding the in-depth extent of the seismically active part of the particular underground fault that caused the aforementioned earthquakes.

For this to be achieved it is of impeccable importance to correctly associate a seismic sequence not just to a particular underground fault, but to the certain part of it that gave rise to the observed earthquakes. This task falls well within the learning capabilities of neural networks (Konstantaras, et al., 2002), which can be trained with known pairs of earthquakes and associated underground faults to map one to another. Several difficulties arise in terms of overtraining due to the small training data set available, especially in training recurrent deep learning neural networks , and also due to the fact that most of the training data comprise of mainland underground faults rather than underground faults in the crust beneath the sea. Still, in the cases were results from the deep learning neural network are deemed to be successful, the assertion of the vertical component to the initial two-dimensional mapping of underground faults becomes possible, producing three dimensional models of the latter.

Further work shall deploy CUDA heterogeneous parallel processing to enable 3D modelling (Axaridou et al., 2014) and imaging and navigation amongst the spatial dataset of the seismically active parts of underground faults situated within the Earth's crust.

2. ACKNOWLEDGMENT

3. REFERENCES

Axaridou A., I. Chrysakis, C. Georgis, M. Theodoridou, M. Doerr, A. Konstantaras, E. Maravelakis. 3DSYSTEK: Recording and exploiting the production workflow of 3D-models in cultural heritage. IISA2014 - 5th International Conference on Information, Intelligence, Systemsand Applications, 51-56, 2014.

Konstantaras A. Deep learning and parallel processing spatio-temporal clustering unveil new Ionian distinct seismic zone. Informatics. 7 (4), 39, 2020.

Konstantaras A.J. Expert knowledge-based algorithm for the dynamic discrimination of interactive natural clusters. Earth Science Informatics. 9 (1), 95-100, 2016.

Konstantaras A., M.R. Varley, F. Vallianatos, G. Collins, P. Holifield. Recognition of electric earthquake precursors using neuro-fuzzy methods: methodology and simulation results. Proc. IASTED Int. Conf. Signal Processing, Pattern Recognition and Applications (SPPRA 2002), Crete, Greece, 303-308, 2002.

Moshou A., P. Argyrakis, A. Konstantaras, A.C. Daverona, N.C. Sagias. Characteristics of Recent Aftershocks Sequences (2014, 2015, 2018) Derived from New Seismological and Geodetic Data on the Ionian Islands, Greece. Data. 6 (2), 2021.

MODELING OF RADIOWAVE PROPAGATION THROUGH RAIN

Boumpouras, Nikolaos-Panagiotis[1], and Ioannidou, Melina[1]

[1]Department of Information and Electronic Engineering, International Hellenic University,
GR-57400 Thessaloniki, Greece
E-mail: melina@ihu.gr (corresponding author)

1. INTRODUCTION

Path loss during terrestrial links design is a key concern of engineers and scientists. It is well known that, apart from free space path loss, one of the most decisive factors causing attenuation of radiowaves in such links is precipitation and especially rainfall (Seybold, 2005). The attenuation caused by the latter is significant for frequencies above 10 GHz and is mainly due to absorption and scattering.

Modeling of rain attenuation has drawn strong interest over the years; a lot of studies and models have been proposed in an attempt to predict this attenuation (Huang et al., 2019; Livieratos & Cottis, 2019; Tataria et al., 2021). Four existing prediction models for rain attenuation in terrestrial links are considered and compared in this paper: ITU-R.P 530-18 (2021), Moupfouma (2009), Silva Melo & Pontes (2012) and Singh et al. (2020). We develop an application in Matlab environment in order to calculate and plot path loss due to rainfall; free space loss is also considered. The input data include parameters such as the frequency and the rainfall rate, whereas the output comprises plots of the path loss versus distance.

2. PREDICTION MODELS FOR RAIN ATTENUATION

2.1 Recommendation ITU-R P.530-18

According to ITU-R P.530-18 (2021), the path attenuation exceeded for 0.01% of the time may be calculated by:

$$A_{0.01} = \gamma_R d_{eff} \quad \text{(dB)} \tag{1}$$

In Eq. [1] γ_R stands for the specific attenuation and $\boldsymbol{d_{eff}}$ is the effective path length. The former may be computed for the frequency, polarization and rain rate of interest from the following power law relationship (ITU-R P.838-3, 2005):

$$\gamma_R = kR^a \quad \text{(dB/km)} \tag{2}$$

where R (mm/hr) is the rain rate of interest and k, a are coefficients determined as functions of frequency in the range from 1 to 1000 GHz. Explicit expressions for k, a may be found in (ITU-R P.838-3, 2005). The effective path length that appears in Eq. [1] is given by $\boldsymbol{d_{eff} = dr}$, where d represents the actual path length and r is a distance factor defined in (ITU-R P.530-18, 2021); r depends on the frequency, the exponent a (Eq. [2]) and $\boldsymbol{R_{0.01}}$ which is the rain rate exceeded for 0.01% of time.

2.2 Moupfouma model

The model proposed by Moupfouma (2009) introduces the equivalent propagation path $L_{eq} = \delta L$, where L is the actual path length and δ is a coefficient that depends on L and $R_{0.01}$, i.e., the rain rate value exceeded for 0.01% of time in the locality of interest. Once L_{eq} is calculated, the attenuation exceeded for 0.01% of time is given by Eq. [1] provided that d_{eff} is replaced by L_{eq} and γ_R is the

specific attenuation given by a power law relationship similar to Eq. [2]. Explicit expressions for the coefficients, as well as a detailed description of the model may be found in (Moupfouma, 2009).

2.3 Silva Melo & Pontes model

This model retains the general expression for the path attenuation and d_{eff}, given in Eq. [1], but modifies the ITU-R method by replacing the rain rate in Eq. [2] by the effective rain rate, R_{eff} (mm/hr):

$$R_{eff} = 1.763 R^{0.753+0.197/d} \qquad [3]$$

where R stands for the point rainfall rate measured in the link region and d is the actual path length. The model is also extended in order to include slant paths; detailed expressions and description may be found in (Silva Melo & Pontes, 2012).

2.4 Singh et al. model

The model proposed by Singh et al. (2020) is based on approximation curves plotted from calculations of the specific attenuation versus frequency at different rain rates, by using the ITU-R model. Finally, the following equation is obtained for the specific attenuation:

$$A\ (dB/km) = af^3 + bf^2 + cf + d \qquad [4]$$

The coefficients a, b, c, d are polarization dependent and involve the rain rate. Their explicit expressions may be found in (Singh et al., 2020).

3. APPLICATION DEVELOPMENT FOR RAIN ATTENUATION

The four aforementioned models have been used in order to develop an application, in matlab environment, for the calculation of path loss in the presence of rain. Moreover, free space loss has been taken into account by using Friis equation, which, when expressed in dB, is given by (Seybold, 2005):

$$L_{FS} = 32.4 + 20 log_{10} d_{km} + 20 log_{10} f_{MHz} \qquad [5]$$

where d_{km} is the path length in km and f_{MHz} represents the frequency in MHz. The gains G_T and G_R (in dB) of the transmitting and the receiving antenna, respectively, are subtracted from L_{FS} (if any).

The user of the application has the option to choose between plotting the free-space path loss alone, rainfall attenuation alone, or the combination of both. All plots depict losses in dB versus distance in km. For the calculation of free-space loss, the input data given by the user are: the frequency (GHz), the maximum distance (km) used for the plot and the antenna gains (if any). Additionally, the polarization, the elevation angle and the rain rate (mm/hr) are required as input data in order to take into account attenuation due to rainfall. Furthermore, the user has the option to choose one of the four rainfall pathloss prediction models, i.e., ITU-R.P 530-18, Moupfouma, Silva Melo & Pontes or Singh et al..

A typical picture obtained from the application is shown in Fig. 1. The plots depicted therein include losses due to rainfall and free space. Another option given to the user is to enter up to four additional rain rates (see "Graph details" in Fig. 1) in order to include more curves in the graph and compare the losses for different rain rates. Moreover, the application offers the possibility of calculating the losses at a specific distance given by the user.
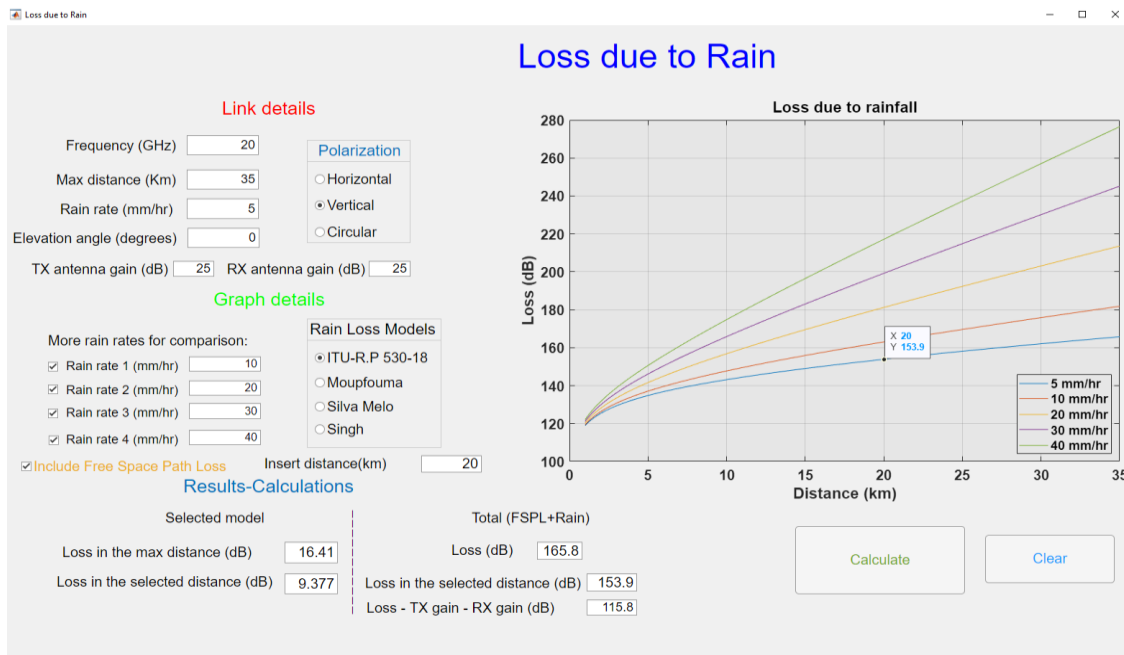
Figure 1. Example of a screenshot obtained from the application.

4. RESULTS AND COMPARISONS

Figure 2, resulted from the computer code developed for the calculation of path loss in the presence of rain, offers a comparison among the four models reported in Section 2. Both free space and rainfall have been considered. The frequency has been set equal to 20GHz and horizontal polarization has been assumed; the rain rate is either 5mm/hr (Fig. 2a) or 30mm/hr (Fig.2b).
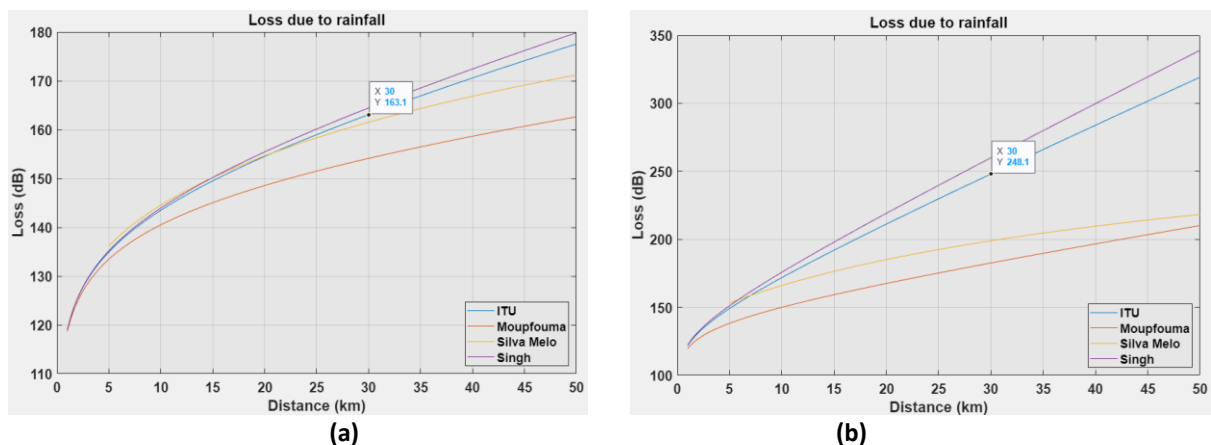

(a)   (b)

Figure 2. Losses (dB) versus distance (km) predicted by the four models reported in the inset. Horizontal polarization is assumed. *f*=20 GHz and (a) *R*=5mm/hr, (b) *R*=30mm/hr.

A first remark about Fig. 2 is that, despite the rain rate, the Moupfouma model predicts the lower attenuation among all models, while the losses computed by applying the Singh et al. model are the highest, albeit the corresponding curve is closely followed by that of the ITU-R model. Moreover, Fig. 2a suggests that for small rain rates the ITU-R, the Silva-Melo & Pontes and the Singh et al. models predict, more or less, similar losses for distances up to 20km. As the distance increases, the three aforementioned models tend to diverge from each other. The difference among the models is more pronounced for great rain rates (Fig. 2b). For example, for *R*=30mm/hr and *d*=30km the Moupfouma model predicts about 70dB lower attenuation than the ITU-R model; the prediction of the Silva-Melo & Pontes model is somewhere between them, whereas the losses computed by the Singh et al. model are slightly higher than those of the ITU-R. A similar behavior of the four models has been observed for vertical polarization, but the losses predicted are generally lower and the

difference among the models is less pronounced. Pertinent results are not shown herein for the sake of brevity.

5. CONCLUSIONS

An application in Matlab environment has been developed in this paper, in order to calculate and plot the attenuation of radiowaves through rain. Four existing prediction models for rain attenuation in terrestrial links were considered. The application takes as input data the frequency, the rainfall rate, the polarization and the elevation angle as well as the maximum distance and the gain of the antennas (if any). The end result of the calculations is a plot of the path loss versus distance; free space and rainfall are both taken into account.

Our study and application showed that the ITU-R, the Silva-Melo & Pontes and the Singh et al. models predict similar losses for small rain rates and distances. As the distance increases, the Singh et al. model tends to calculate higher attenuation of the radiowaves, though it is closely followed by the ITU-R model. Moreover, we found that in the whole frequency spectrum, as well as for all rainfall rates, the Moupfouma model predicts the lower attenuation out of all models examined.

6. REFERENCES

Huang, J., Cao, Y., Raimundo, X., Cheema, A., and Salous, S. (2019). Rain statistics investigation and rain attenuation modeling for millimeter wave short-range fixed links. IEEE Access, 7:138745-138756.

Livieratos, S.N. and Cottis, P.G. (2019). Rain attenuation along terrestrial millimeter wave links: A new prediction method based on supervised machine learning. IEEE Access, 7:156110-156120.

Moupfouma, F. (2009). Electromagnetic waves attenuation due to rain: A prediction model for terrestrial or L.O.S SHF and EHF radio communication links. J. Infrared Milli Terahz Waves, 30:622-632.

Recommendation ITU-R P.838-3 (2005): *Specific attenuation model for rain for use in prediction methods.* ITU, Geneva, Switzerland.

Recommendation ITU-R P.530-18 (09/2021). *Propagation data and prediction methods required for the design of terrestrial line-of-sight systems.* ITU, Geneva, Switzerland.

Seybold, J.S. (2005). *Introduction to RF propagation.* John Wiley & Sons, Hoboken, New Jersey, USA.

Silva Mello, L.A.R. and Pontes, M.S. (2012). Unified method for the prediction of rain attenuation in satellite and terrestrial links. J. Microw. Optoelectron. Electromagn. Appl., 11(1):1-14.

Singh, H., Kumar, V., Saxena, K., Boncho, B., and Prasad, R (2020). Proposed model for radio wave attenuation due to rain (RWAR). Wireless Personal Communications, 115:791-807.

Tataria, H., Haneda, K., Molisch, A.F., Shafi, M., and Tufvesson, F. (2021). Standardization of propagation models for terrestrial cellular systems: A historical perspective. Int. J. Wireless Informat. Networks, 28:20-44.

DATA TRAFFIC PREDICTION IN CELLULAR NETWORKS

Evangelos Lykakis[1], Evangelos Kokkinos[1]

[1]Hellenic Mediterranean University Department of Electronic Engineering
lykakisev@hmu.gr, ekokkinos@hmu.gr

1. INTRODUCTION

The fifth generation (5G) wireless network is expected to transform the way we live and work by enabling new and innovative applications, devices and services that require high speed, low latency and reliable connectivity. With the proliferation of mobile devices, Internet of Things (IoT) devices and emerging technologies such as virtual reality, autonomous vehicles and smart cities, there is a growing demand for wireless data traffic. Accurate prediction of data traffic is essential to ensure a high-quality user experience and efficient network use. In this article, we will explore the challenges and opportunities of data traffic prediction in 5G networks, focusing on the different types of data traffic and the techniques used for prediction.

5G networks are designed to handle a wide range of data traffic, including voice, video, gaming, IoT and machine-to-machine communication. Each type of data traffic has unique traffic characteristics, such as traffic patterns, traffic volumes, and quality of service (QoS) requirements. For example, voice traffic is highly delay-sensitive and requires low latency, while video traffic has high bandwidth requirements and can tolerate some latency. IoT traffic, on the other hand, typically involves a large number of devices with sporadic traffic patterns and low data rates.

Data traffic prediction accuracy is critical for network operators to efficiently plan and allocate resources. Traditional data traffic forecasting methods, such as statistical models and time series analysis, may not be sufficient to deal with the complex and dynamic nature of 5G networks. Therefore, new techniques such as machine learning (ML) are being developed to handle the Big Data requirements and heterogeneous nature of network traffic.

Machine learning (ML) techniques, such as supervised learning, deep learning (DL), and neural networks, can analyze vast amounts of data from different sources to accurately predict future data traffic patterns. For example, deep learning models can learn from historical data to predict future data traffic patterns, while supervised learning can optimize network resource allocation based on data traffic prediction. These techniques can also take into account external factors that may affect data traffic, such as weather conditions, public events and holidays. In addition, hybrid methods that combine traditional forecasting methods with machine learning techniques can predict with higher accuracy the data traffic for 5G networks.

However, there are several challenges associated with data traffic prediction in 5G networks. One of the main challenges is the heterogeneity of network traffic, which includes different types of data traffic, as well as different architectures, technologies and network protocols. Another challenge is the dynamic nature of network conditions, which can vary significantly based on location, time of day, and user behavior. In addition, the Big Data requirements for training and validating machine learning (ML) models are a significant challenge.

In this article, we will consider the following key questions:
What are the different types of data traffic in 5G networks and what are the characteristics and volume of data traffic of each type? What are the different data traffic patterns in 5G networks and what prediction techniques are recommended for each pattern? What are the existing traffic prediction techniques for mobile networks? What are the key challenges associated with predicting data traffic in 5G networks? What are the emerging trends in predicting data traffic in 5G networks?
How can accurate data traffic prediction contribute to improving the performance of 5G networks?
By addressing these questions, we aim to provide a thorough overview of data traffic forecasting in 5G and next-generation wireless networks.

2. METHODOLOGY

This article provides a thorough literature review on data traffic prediction in cellular networks. Initially, the types and patterns of data traffic will be analyzed. Then the types of existing techniques, key challenges and emerging trends for data traffic prediction in cellular networks will be analyzed.

2.1 Types Of Data Traffic And Data Traffic Patterns In 5G Networks

5G technology is the next generation of mobile communication and is designed to handle massive amounts of data traffic with greater efficiency and speed than previous generations. The three types of data traffic in 5G networks include enhanced Mobile Broadband (eMBB), Ultra-Reliable and Low-Latency Communications (URLLC), and massive Machine Type Communications (mMTC) (Navarro-Ortiz et al., 2020). Each type of data traffic has its own unique characteristics and traffic volume. Table 1 shows the types of data traffic in 5G with the type of data, requirements and volumes of each type.

Table 1: Types of Data Traffic in 5G Based On Data Traffic Volume

Type	Applications	Requirements	Data Traffic Volume
eMBB	(HD) Video Streaming, Virtual Reality (VR), Online Gaming	High Bandwidth	High
URLLC	Industrial Automation, Autonomous Vehicles, Remote Healthcare	Low Latency and High Reliability	Low to Moderate
mMTC	Industrial IoT, Smart Homes, Smart Cities	Low Bandwidth	Low

Data traffic patterns in 5G networks are becoming increasingly diverse and complex, as 5G is expected to support a wide range of applications with different requirements. Different types of data traffic patterns include burst traffic (characterized by short, intermittent bursts of data), streaming traffic (involves a continuous stream of data), and interactive traffic (requires real-time interaction and is highly sensitive to network delay). Additionally, IoT traffic is associated with low data rates, infrequent transmissions, and sporadic traffic patterns. Finally, background traffic is running processes that affect data traffic even if the device is not actively being used. Anticipating these data traffic patterns in 5G networks is essential to efficiently allocate and optimize network resources. Machine learning and deep learning techniques are being developed and deployed to improve the accuracy of data traffic prediction, allowing network operators to better allocate resources and improve the overall performance of 5G networks. Table 2 shows the data traffic patterns in 5G network.

Table 2: Data Traffic Patterns In 5G

Pattern	Applications	Requirements	Proposed Method of Data Traffic Prediction
Burst Data Traffic	Web Browsing, Video streaming, Online Gaming	High Data Speeds, Short Duration, Irregular Patterns, Variable Packet Sizes	ML, DL, Hybrid
Streaming Data Traffic	Video and Audio Streaming	High Bandwidth, Consistent Data Rates, Long Duration, Sensitive To Delays	ML, DL, Hybrid
Interactive Data Traffic	Online Games, Virtual Reality, Remote Healthcare	Low Latency, High Bandwidth, Explosive Data Transfer, Variable Data Rates	ML, DL, Hybrid
IoT Data Traffic	Smart Home, Industrial Sensors	Low Data Rates, High Connection Density, Usually Predictable Patterns	Statistical, Time Series, ML, DL, Hybrid
Background Data Traffic	Software Updates, Email Synchronization	Low Priority, Data Explosion, Large Data Volumes, Long Duration, Variable Patterns	ML, DL, Hybrid

2.2 Existing Data Traffic Prediction Methods For Cellular Networks

According to Li et al. (2017) internet data traffic will increase tenfold by 2027 and this will influence the architecture of the new generation of cellular networks. Data traffic prediction is very important for the optimization and management of communication networks, such as optimal routing, energy saving, and network anomaly detection (Li et al., 2017). According to Sun et al. (2000) data traffic demand exhibits spatial and temporal patterns, which help predict traffic load. The traffic at the base stations shows a repeating daily pattern in different weeks, namely low demand at night and high demand during the day (Sun et al.,2000), (Paul et al., 2011). Data traffic peaks depend on regions. More specifically, a rural area will have a different daily data traffic peak and a city will have a different peak during the day (Paul et al., 2011), (Wang et al., 2013), (Zhang et al., 2012). It can also be observed that the traffic load on weekends is lower than that on weekdays (Paul et al., 2011), (Wang et al., 2013). Other studies have shown that nearby areas have similar average cell phone demands on weekdays, but a huge variability on weekends. Summarizing all of the above, effective congestion control is considered one of the key elements of 5G/6G technology that allows users to perform various processes using a single infrastructure with better quality of service.

Data traffic prediction methods are separated into three categories. The first category is statistical data traffic prediction methods (e.g. Hidden Markov, Markov Chain and Naive Bayes) (Chen et al., 2021). As cellular network technology became complex, statistical methods became ineffective due to the complexity of the data and the network.

The second category is time series models for data traffic prediction. Time series methods are separated into linear (e.g. ARIMA, HOLT-WINTERS, SARIMA, FARIMA) (Chen et al., 2021), (Tikunov et al.,2007), (Medhn et al.,2017), (AsSadhan et al.,2017), non-linear (e.g. GARCH) (Chen et al., 2021), probabilistic (Choi et al.,2002), hybrid (e.g. GARCH+ARIMA) (Zhou et al. ,2007) and in clustering methods (Levine et al.,1997). Time series methods were more efficient than statistical methods as they introduced concepts of space and time to predict the data traffic. The hybrid time

series methods that have been proposed are more accurate than the simple time series methods. With the introduction of the 5G network and the increase of data traffic, traditional traffic prediction methods such as time series methods and statistical methods have been found to be insufficient due to the complexity of the 5G network architecture, heterogeneous traffic data, and the introduction of the concept of big data.

To overcome the weakness of time series models, machine learning methods are used which provide higher prediction accuracy. The third category of methods concerns the use of machine learning to predict the data traffic. This category is separated into two subcategories: supervised machine learning (e.g. LSTM, ESN, CNN, Random Forest, MLP, MLPWD, ILP, Back Propagation) (Chen et al., 2018), (Zhou et al., 2018), (Cui et al., 2014), (Nikravesh et al., 2016), (Yue et al., 2017), (Zhang et al., 2018), (Liang et al., 2019), (Bouzidi et al.,2018) and (Zhao et al.,2022) where the model is trained from historical traffic data, and the hybrid methods (e.g. LSTM+CNN, ILP+LSTM+MLP, ARIMA+LSTM, EEMD+GAN) (Pelekanou et al.,2018), (Li et al., 2020), (Yadav et al., 2021), and (Li et al.,2022) which combine statistical methods, time series methods, and supervised machine learning. Supervised machine learning methods have better prediction accuracy than time series methods and statistical methods. However, hybrid methods using supervised machine learning have even better accuracy than all methods.

The accuracy of the prediction method calculated with several statistical measures like True Positive Ratio (TPR) Eq. [1], Mean Square Error (MSE) Eq. [2], Normalized Mean Square Error (NMSE) Eq. [3] , Root Mean Square Error (RMSE) Eq. [4], Normalized Root Mean Square Error (NRMSE) Eq. [5] , Mean Absolute Error (MAE) Eq. [6], Mean Absolute Percentage Error (MAPE) Eq. [7], and Squared Correlation ($\mathbf{R^2}$) Eq.[8].

$$TPR = \frac{Number\ of\ Correctly\ predicted}{n} *100 \quad (1),$$

$$MSE = \frac{1}{n}\sum_{t=1}^{n}(x_t - \overline{x_t})^2 \quad (2),$$

$$NMSE = \frac{\frac{1}{n}\sum_{t=1}^{n}(x_t - \overline{x_t})^2}{\frac{1}{n}\sum_{t=1}^{n}(x_t - \frac{1}{n}\sum_{t=1}^{n}x_t)^2} \quad (3),$$

$$RMSE = \sqrt{\frac{1}{n}\sum_{t=1}^{n}(x_t - \overline{x_t})^2} \quad (4),$$

$$NRMSE = \frac{\sqrt{\frac{1}{n}\sum_{t=1}^{n}(x_t - \overline{x_t})^2}}{\frac{1}{n}\sum_{t=1}^{n}x_t} \quad (5),$$

$$MAE = \frac{1}{n}\sum_{t=1}^{n}|x_t - \overline{x_t}| \quad (6),$$

$$MAPE = \frac{1}{n}\sum_{t=1}^{n}(\frac{|x_t - \overline{x_t}|}{x_t}) \quad (7),$$

$$R^2 = 1 - \frac{\sum_{t=1}^{n}(x_t - \overline{x_t})^2}{\sum_{t=1}^{n}(x_t - \frac{1}{n}\sum_{t=1}^{n}x_t)^2} *100 \quad (8),$$

where, x_t is historical data series $\overline{x_t}$ is predicted data series and n is the total number of the data.

For each data traffic prediction method there is a specific model for the prediction process. Figure 1 shows the data traffic prediction model for the statistical methods while, Figure 2 for time series methods and Figure 3 for the machine learning methods. For the hybrid methods of time series and machine learning there are several ways of calculations. There are three basic ways of modeling. The first hybrid method (time series - machine learning) makes a prediction with the first time series method and the predictions of the first method are the input data of the second method. The second hybrid method makes predictions with the first method and its predictions train the data for the second method and for the test data is used the historical data. The third hybrid method, both methods calculate their predictions and the final prediction of the data traffic comes out of a mathematical formula (e.g. with the percentage of participation of each method Eq. [9].

$$z = w1x1 + w2x2 \ (9),$$

where z is the new predicted data, w1 the percentage of method 1 participation, x1 is the predicted data of method 1, w2 the percentage of method 2 participation and x2 is the predicted data of method 2.
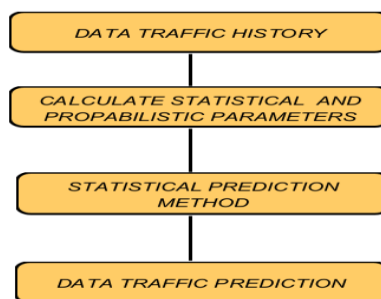
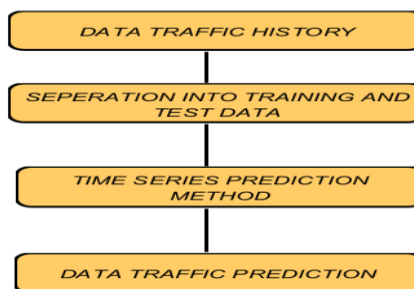Figure 1: Data Traffic Prediction Model of Statistical Methods.

Figure 2: Data Traffic Prediction Model of Time Series Methods.
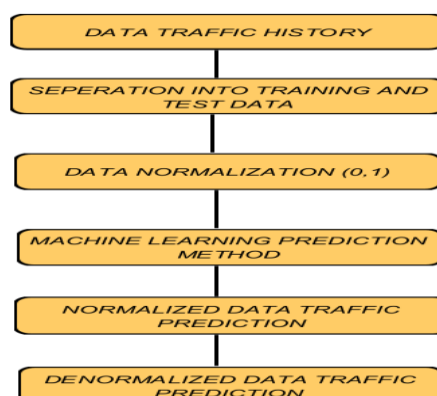

Figure 3: Data Traffic Prediction Model of Machine Learning Methods.

2.3 Challenges For Data Traffic Prediction In 5G Networks

The deployment of 5G networks has increased the demand for higher data rates, lower latency and better network capacity in wireless networks. Data traffic Prediction in 5G networks is critical to achieving these goals, optimizing network resource allocation, improving user experience, and reducing costs. However, many challenges are associated with predicting data traffic in 5G networks, including network complexity, network traffic heterogeneity, dynamic nature of network conditions, Big Data requirements, etc.

The complex topology of the 5G network can be a significant challenge for traffic prediction because it involves multiple layers of virtualization, which makes it difficult to accurately predict the behavior of different network elements. To achieve accurate traffic prediction in 5G networks, operators must use a combination of techniques such as network modeling, traffic engineering, network performance monitoring, and applying machine learning algorithms to network topology data. Network modeling is a mathematical model that can be used to identify bottlenecks and predict network performance. Traffic engineering is a routing optimization method ensures that data traffic flows smoothly by determining certain parameters such as transmitted packets, lost packets, and delay. Network monitoring is a technique used to observe network behavior and collect data about network performance. By applying machine learning algorithms to network topology data, operators can identify patterns of network behavior and predict how the network will behave under different conditions.

Network traffic heterogeneity is one of the key challenges in predicting data traffic in 5G networks. 5G networks support a wide range of applications with different traffic characteristics, such as video streaming, online gaming, social media and IoT devices. Each of these applications generates different types of data traffic, including voice, video, data, and control traffic. The heterogeneity of network traffic makes it difficult to accurately predict data traffic in 5G networks. Different types of data traffic require different approaches to data traffic prediction. The heterogeneity of network data traffic poses significant challenges in predicting data traffic in 5G networks. Addressing these challenges requires developing traffic models that can capture the different traffic patterns generated by various applications, developing real-time prediction algorithms that can adapt to dynamic traffic changes, and collecting big datasets for training and testing prediction models. By addressing these challenges, using hybrid methods based on machine learning and especially deep learning, 5G networks can achieve efficient use of resources and provide high-quality services to a wide range of applications and users.

The dynamic nature of network conditions is another major challenge for predicting data traffic in 5G networks. 5G networks are subject to various dynamic network conditions, such as changes in user mobility, in network topology & capacity, and changes in user behavior. These changes can cause significant fluctuations in data traffic, making accurate forecasting difficult. To address this challenge, supervised machine learning algorithms or hybrid methods based on supervised learning techniques, can be used to learn data traffic patterns under different network conditions. However, machine learning algorithms require big datasets to learn patterns accurately.

Big Data requirements are one of the most significant challenges in predicting data traffic in 5G networks. Machine learning algorithms require big datasets to accurately learn data traffic patterns. However, collecting big datasets in 5G networks is challenging due to many factors, such as user privacy concerns, diversity of network conditions, and high variability of network traffic. To address this challenge, synthetic datasets can be used to train machine learning algorithms. Synthetic datasets (data generated using machine learning that is trained with some initial data to learn all the features, relationships and statistical patterns without including personal information) can be created using models that simulate the behavior of applications and real world users. One technique that can be used to construct synthetic data is the Generative Adversarial Network (GAN). However, synthetic datasets may not accurately reflect real-world data traffic variability.

The lack of historical data related to predicting data traffic in 5G networks is a challenge that arises due to the fact that 5G networks are still in the early stages of development and adoption. Since 5G is a relatively new technology, there is not enough historical data available to make accurate predictions about network traffic patterns and behavior. To overcome this challenge we will need to analyze data from other sources (e.g. from the 4G network), perform simulations of various scenarios and variables, with the cooperation of network operators to exchange historical data and create patterns and using machine learning techniques on real-time data.

Security concerns are also a major challenge for predicting data traffic in 5G networks. 5G networks are vulnerable to cyber-attacks and data traffic patterns can change due to security breaches. This makes it difficult to accurately predict data traffic and requires new techniques to detect and mitigate security threats in real time. To mitigate these security concerns, data anonymization and encryption techniques should be used, with datacenter access control, with continuous network monitoring, and with machine learning techniques that the outliers will not be calculated.

Scarcity of tagged data, or delays in accessing tagged data, is one of the main challenges for moving data across the network. Principal Component Analysis (PCA) techniques (is a dimensionality reduction method often used to reduce the dimensionality of big datasets), manual or synthetic labeling, or Active-Learning techniques (a special case of machine learning in which a learning algorithm can interactively query a user or some other source of information to label new data points with the desired outputs. In this particular case to label the data is density-based sampling), are measures that could be taken to overcome the problem (Lohrasbinasab et al., 2022).

Prediction accuracy versus speed. Because the increasing accuracy of the techniques used for prediction can lead to higher computational load and time, any improvement in accuracy will come at the cost of slowing down their training and vice versa. To mitigate the risk of increasing computational load and time there should be a balance between accuracy and speed and use hybrid prediction methods based on machine learning and data retraining (Ayoubi et al., 2018).

Retraining models that are dynamic like 5G networks, where resource allocation is constantly changing, is difficult due to the high computational cost. A common solution to deal with the problem is to use some stepwise methods for retraining in which the model is updated only with new observations (Lohrasbinasab et al., 2022). Stepwise methods for data traffic prediction combine old historical traffic data with the new by selecting from the new data the data which does not exist in the old.

Issues of **developing data traffic prediction frameworks** for 5G networks are a significant challenge as there may be deviation from test data to real-time data. Auto-Adaptive Machine Learning (AAML) is a technique proposed to solve this problem. Auto-Adaptive Machine Learning (AAML) is a machine learning technique that automatically adapts to changes in the data and environment and contributes to the improvement of data traffic prediction (Diethe et al., 2019). To predict data traffic using this technique, the best method will be automatically selected by parameterizing, the hyper-parameters of the machine learning method will be optimized using optimization algorithms, and the data will be retrained in real time.

The challenges associated with predicting data traffic in 5G networks vary depending on the type (eMBB, URLLC, mMTC) and pattern (Burst Traffic, Streaming Traffic, Interactive Traffic, Internet of Things Traffic, Background Traffic) of the data traffic. Addressing these challenges requires hybrid methods based on machine learning and especially deep learning methods that can capture the unique characteristics of each type of data traffic. Table 3 presents in detail the challenges for predicting data traffic in 5G networks.

Table 3: Challenges of Data Traffic Prediction in 5G Networks

Challenge	Confrontation
Complex Network Topology	Network Modeling, Traffic Engineering, Network Performance Monitoring, Machine Learning Algorithms on Network Topology Data.
Network Traffic Heterogeneity	Hybrid Methods Based On Machine Learning And Especially Deep Learning.
Dynamic Nature of Network Conditions	Supervised Machine Learning Algorithms, Hybrid Methods Based On Supervised Machine Learning Algorithms.
Anonymization of Big Data	Use Of Synthetic Data.
Lack of Historical Data	Simulations Of Various Scenarios And Variables, Cooperation Of Network Operators, Use Of Machine Learning Techniques On Real-Time Data.
Safety Concerns	Data Anonymization And Encryption Techniques, By Controlling Access To Datacenters, With Continuous Monitoring Of The Network, By Using Machine Learning Techniques That Outliers Will Not Be Calculated.
Prediction Accuracy VS Prediction Speed	Balance Between Accuracy And Speed, Using Hybrid Prediction Methods Based On Machine Learning, Retraining The Data.
Sparsity Of Labeled Data	Principal Component Analysis (PCA) Techniques, Labeling Manually or Synthetically, Active-Learning Techniques.
Retraining the Models	Use of Stepwise Methods.
Framework Development	Auto-Adaptive Machine Learning (AAML).

3. RESULTS AND DISCUSSION

As we observe from existing research, the increasing complexity, diversity of data traffic, use of real-time data, deficiencies in data histories, and user privacy concerns pose a significant challenge to accurately predict data traffic patterns. There are two major trends in data traffic prediction.

The first trend is the development of machine learning-based models that leverage advanced algorithms and data analysis techniques to accurately predict data traffic patterns. Machine learning methods such as neural networks, decision trees, and support vector machines have proven efficient in predicting data traffic in 5G networks. In addition, machine learning-based models have been applied to deal with different types of data traffic, including video, voice, and data. For example, convolutional neural networks (CNN) have been used to predict video traffic patterns, while recurrent neural networks (RNN) have been used to predict patterns of voice traffic data.

In particular, machine learning-based hybrid methods, which combine multiple algorithms to improve prediction accuracy, have gained increasing attention in recent years. These hybrid methods leverage the strengths of different algorithms to overcome their respective limitations, resulting in more accurate and reliable predictions than basic machine learning methods.

The machine learning techniques that have been used to improve the accuracy of the data traffic predictions of cellular networks. Their accurate prediction contributes to the better management of network resources, the creation of new techniques for network slicing, optimal routing and the detection of network anomalies. All this contributes to increasing the user experience (QoE), increasing the quality of services (QoS), saving energy (using the sleep technique for unused resources) and reducing latency. However, due to the rapid increase in traffic data complexity and the even more complex structure of next-generation cellular networks (6G and above), the prediction of accurate data traffic is a challenge for researchers and an open field of research to find new prediction methods for the data traffic. In particular, frameworks must be created that have high prediction accuracy with adequate prediction speed.

4. CONCLUSION

In this paper firstly were analyzed the types of data traffic (eMBB, URLLC, mMTC) for 5G networks. Then the data traffic patterns were analyzed, which are divided into five categories according to the special characteristics of each pattern. These are Burst Data Traffic, Streaming Data Traffic, Interactive Data Traffic, Internet of Things Data Traffic and Background Data Traffic. Then the existing data traffic prediction methods can be separated into three categories: statistical, time series prediction and machine learning. From the existing methods, we notice that the prediction of data traffic is very important for 5G networks, because it contributes to the better management of network resources. Moreover, data traffic prediction helps to optimize network slicing, routing and the detection of anomalies of the network. Better resource management contributes to better quality of service (QoS), user experience (QoE), energy savings and latency reduction. However, increasing complexity, diversity of data traffic, use of real-time big data, lack of historical data, and user privacy concerns are some of the challenges. All of the above, in combination with the fact that methods must be created that combine accuracy and speed of the prediction, constitute an open research topic.

5. REFERENCES

Navarro-Ortiz, J., Romero-Diaz, P., Sendra, S., Ameigeiras, P., Ramos-Munoz, J. J., & Lopez-Soler, J. M., 2020, "A survey on 5G usage scenarios and traffic models.", IEEE Communications Surveys & Tutorials, 22(2),pp. 905-929.

Li, R., Zhao, Z., Zheng, J., Mei, C., Cai, Y., & Zhang, H., 2017, "The learning and prediction of application-level traffic data in cellular networks., IEEE Transactions on Wireless Communications, 16(6), pp. 3899-3912.

Sun, H., Halepovitc, E., Williamson, C., & Wu, Y., 2000, Characterization of CDMA2000 Cellular Data Network Traffic. networks, 7(8), 10.

Paul, U., Subramanian, A. P., Buddhikot, M. M., & Das, S. R. , 2011, "Understanding traffic dynamics in cellular data networks." In 2011 Proceedings IEEE INFOCOM,IEEE, pp. 882-890 .

Wang, Y., Faloutsos, M., & Zang, H., 2013, "On the usage patterns of multimodal communication: Countries and evolution.", In 2013 Proceedings IEEE INFOCOM ,IEEE, pp. 3135-3140.

Zhang, Y., & Årvidsson, A., 2012, "Understanding the characteristics of cellular data traffic.", In Proceedings of the 2012 ACM SIGCOMM workshop on Cellular networks: operations, challenges, and future design ,pp. 13-18.

Chen A, Law J, Aibin M., 2021, "A Survey on Traffic Prediction Techniques Using Artificial Intelligence for Communication Networks." Telecom, 2(4), pp. 518-535.

Tikunov, D., & Nishimura, T. ,2007, " Traffic prediction for mobile network using Holt-Winter's

exponential smoothing." In 2007 15th international conference on software, telecommunications and computer networks, IEEE , pp. 1-5.

Medhn S., Seifu B., Salem A.,Hailemariam D.,2017, "Mobile data traffic forecasting in UMTS networks based on SARIMA model: the case of Addis Ababa.", Ethiopia. 2017 IEEE AFRICON: Science, Technology and Innovation for Africa, AFRICON 2017, pp. 285-290.

AsSadhan, B., Zeb ,K., Al-Muhtadi, J., Alshebeili S. ,2017, "Anomaly detection based on LRD behavior analysis of decomposed control and data planes network traffic using SOSS and FARIMA models." IEEE Access. 2017, pp.13501-13519.

Choi, S. and Shin, K.G.,2002, "Adaptive bandwidth reservation and admission control in QoS-sensitive networks," In IEEE Transactions on Parallel and Distributed Systems, vol. 13, issue 9, pp. 882 – 897.

Zhou, B., He, D. and Sun Z., 2006, "Traffic Modeling and Prediction Using ARIMA/GARCH Model", Boston, MA, USA: Springer US, pp. 101-121.

Levine, D.A. , Akyildiz, I.F. ,and Naghshineh , M. ,1997, "A resource estimation and call admission algorithm for wireless multimedia networks using the shadow cluster concept," In IEEE/ACM Transactions on Networking, vol. 5, issue 1, pp. 1–12.

Chen, L., Yang, D., Zhang, D., Wang, C., & Li, J., 2018, "Deep mobile traffic forecast and complementary base station clustering for C-RAN optimization., Journal of Network and Computer Applications, 121,pp. 59-69.

Zhou, Y., Fadlullah, Z. M., Mao, B., & Kato, N., 2018, "A deep-learning-based radio resource assignment technique for 5G ultra dense networks." IEEE Network, 32(6),pp. 28-34.

Cui, H., Yao, Y., Zhang, K., Sun, F. and Liu, Y., 2014, "Network traffic prediction based on Hadoop". In 2014 International Symposium on Wireless Personal Multimedia Communications (WPMC),IEEE , pp. 29-33.

Nikravesh, A.Y., Ajila, S.A., Lung, C.H. and Ding, W., 2016, "Mobile network traffic prediction using MLP, MLPWD, and SVM.", In 2016 IEEE International Congress on Big Data (Big Data Congress),IEEE , pp. 402-409.

Yue, C., Jin, R., Suh, K., Qin, Y., Wang, B., & Wei, W., 2017, "LinkForecast: Cellular link bandwidth prediction in LTE networks.", IEEE Transactions on Mobile Computing, 17(7),pp. 1582-1594.

Zhang, C., Zhang, H., Yuan, D., & Zhang, M., 2018, "Citywide cellular traffic prediction based on densely connected convolutional neural networks.", IEEE Communications Letters, 22(8),pp. 1656-1659.

Liang, D., Zhang, J., Jiang, S., Zhang, X., Wu, J. and Sun, Q., 2019, "Mobile traffic prediction based on densely connected CNN for cellular networks in highway scenarios.", In 2019 11th International Conference on Wireless Communications and Signal Processing (WCSP), IEEE , pp. 1-5.

Bouzidi, E. H., Luong, D. H., Outtagarts, A., Hebbar, A., & Langar, R., 2018, "Online-based learning for predictive network latency in software-defined networks." , In 2018 IEEE Global Communications Conference (GLOBECOM), IEEE, pp. 1-6.

Pelekanou, A., Anastasopoulos, M., Tzanakaki, A., & Simeonidou, D., 2018, "Provisioning of 5G services employing machine learning techniques." In 2018 International Conference on Optical Network Design and Modeling (ONDM), IEEE, pp. 200-205.

Li, M., Wang, Y., Wang, Z., & Zheng, H., 2020, "A deep learning method based on an attention mechanism for wireless network traffic prediction.", Ad Hoc Networks, 107, pp. 102258.

Yadav, A., Singh, H., Mala, S. and Shankar, A., 2021, "Recognizing Massive Mobile Traffic Patterns to Understand Urban Dynamics.", In 2021 11th International Conference on Cloud Computing, Data Science & Engineering (Confluence), IEEE, pp. 894-898.

Ayoubi, S., Limam, N., Salahuddin, M. A., Shahriar, N., Boutaba, R., Estrada-Solano, F., & Caicedo, O. M., 2018, "Machine learning for cognitive network management." IEEE Communications Magazine, 56(1), 158-165.

Lohrasbinasab, I., Shahraki, A., Taherkordi, A., & Delia Jurcut, A., 2022, "From statistical-to machine learning-based network traffic prediction.", Transactions on Emerging Telecommunications Technologies, 33(4), e4394.

Diethe, T., Borchert, T., Thereska, E., Balle, B., & Lawrence, N., 2019, "Continual learning in practice." arXiv preprint arXiv:1903.05202.

Zhao, B., Wu, T., Fang, F., Wang, L., Ren, W., Yang, X., Ruan, Z., & Kou, X., 2022, "Prediction method of 5G high-load cellular based on BP neural network." 2022 8th International Conference on Mechatronics and Robotics Engineering, ICMRE 2022, pp. 148–151.

Li, J., & Li, X.,2022 ,"5G Network Traffic Prediction based on EEMD-GAN.", ACM International Conference Proceeding Series, pp. 408–412.

A LOW-COST BUTLER MATRIX FOR 2.4GHz APPLICATIONS

Adamidis, G.A.[1], Ioannidou, M.P.[2], Baklezos, A.T.[1], Kapetanakis, T.N.[1], Nikolopoulos, C.D.[1], and Vardiambasis, I.O.[1*]

[1]Laboratory of Telecommunications and Electromagnetic Applications, Department of Electronic Engineering, Hellenic Mediterranean University, Romanou 3, Chalepa, 73133 Chania Crete, Greece

[2]Department of Information and Electronic Engineering, International Hellenic University, GR-57400 Thessaloniki, Greece

* ivardia@hmu.gr

1. INTRODUCTION

Beamforming networks (BFNs) are at the cutting edge of modern wireless communications mainly because of their use in feeding multibeam antennas by changing the radiating elements' phase and amplitude in order to steer the main beam (Vallappil et al., 2021). Butler matrix (BM) is one of the most common BFNs and a lot of pertinent studies have been presented in the literature (Shallah et al., 2022). A compact structure based on Lange couplers has been proposed by Trail et al. (2008), a glass-based thin film integrated passive device technology has been reported in (Lin et al., 2013), a miniaturized BM network has been constructed by using stub-loaded transmission lines (Nie et al., 2015), while Ausordin et al. (2014) have employed a multilayer topology in order to eliminate crossovers. Recently, various BM networks have been implemented for 5G applications (Vallappil et al., 2020), (Babale at al., 2022), (Rahayu et al., 2022).

In this paper, a 4×4 BM is designed and fabricated by using a common FR4 laminate. The scattering parameters of the BM are measured in order to assess the structure's performance, while the predicted beam directions of a multibeam antenna are tested by measuring the radiation characteristics of a 4-element array fed by the proposed BM.

2. MATERIALS AND METHODS

The schematic diagram of the 4×4 BM implemented in this paper is depicted in Figure 1. It comprises four 90° hybrids, fixed phase shifters (boxes with the notation -45°) and transmission lines. Ports 1-4 are the inputs of the BM, whereas ports 5-8 serve as outputs; the latter may be connected to the 4 elements of an antenna array in order to produce 4 independent, orthogonal beams provided that one input port of the BM is excited at a time. The phase progression, i.e., the phase by which the current in each array element leads the current of the preceding element, is given by $\beta_i = \pm(1 + 2n)(180°/4)$, $i = 1, ..., 4$ and $n = 0,1$ (Adamidis et al., 2019). Then, the beam directions are calculated from $\theta_i = cos^{-1}(\beta_i/kd)$, where $k = 2\pi/\lambda$ is the propagation constant in free space and λ stands for the wavelength.
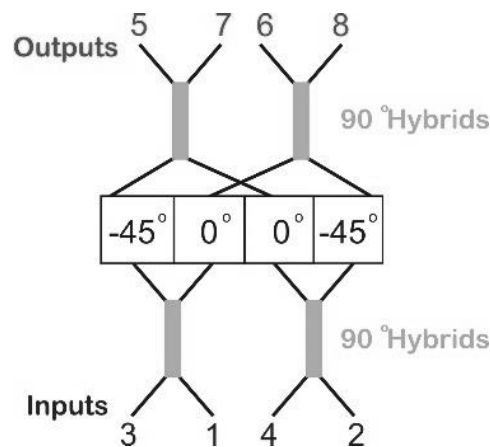

Figure 1. Schematic diagram of the BM.

The layout topology applied in order to fabricate the 4×4 BM is depicted in Figure 2(a). The phase shifters are actually microstrip lines with fixed length, whereas the 90° hybrids have the form of a ring. The size of the whole layout is $8 \times 8 cm^2$. All ports are isolated from each other and they are matched to the fixed impedance $50\,\Omega$. The ADS software package has been used to optimize the design of the BM; the operation frequency of the latter is 2.44GHz. The advantage of this specific layout is that it can be realized in a single layer, without any crossover section. A very low-cost laminate has been adopted to construct the BM: an FR4 substrate was used, with 1.5mm thickness and relative dielectric permittivity and loss tangent $\varepsilon_r = 4.35$ and $tan\delta = 0.01$, respectively. A picture of the fabricated prototype is shown in Figure 2(b).
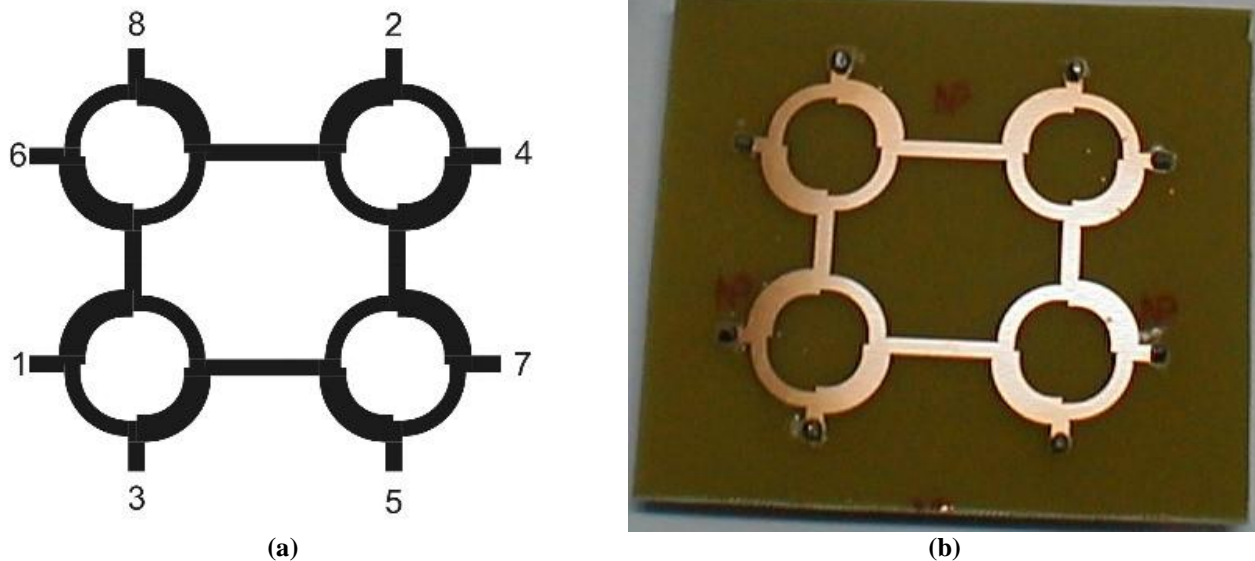
Figure 2. (a) Layout and (b) picture of the fabricated prototype.

3. RESULTS AND DISCUSSION

The proposed BM has been tested experimentally. Firstly, the S-parameters of the structure have been measured; indicative results are presented in Figure 3. The measured return losses, i.e., $|S_{ii}|, i = 1, ..., 4$, are plotted in Figure 3(a), while the measured magnitude response, when port 3 is fed, is plotted in Figure 3(b).

Figure 3(a) suggests that $|S_{ii}|$ for all ports are below -15dB in the range 2.3-2.6 GHz. Regarding the magnitude of the isolation coefficients between the input ports, they were also found to be less than -15dB over the aforementioned bandwidth; the corresponding plots are omitted for the sake of brevity. The measured $|S_{i3}|, i = 5, ..., 8$ (Figure 3b) approach the ideal value of -6dB in the frequency range of interest. Specifically, they take values between -6dB and -7dB over the range 2.32-2.52GHz. Other results (not reported herein for brevity) have shown that the amplitude imbalance of all the output signals, when different input ports are excited, does not exceed 1dB in the aforementioned band. Similar results have also been reported by other researchers: the transmission coefficients are about -6.5dB for a 4×4 BM operating in 2.4-2.5 GHz (Trail et al. 2008), whereas they vary in the range [-8.1, -6.5] dB for a BM that operates at 2.4GHz (Nie et al., 2015). The amplitude imbalance is within 1.1dB for a 4×4 BM operating in the range 2.4-2.6 GHz (Lin et al., 2013).

Furthermore, the phase differences between ports have been measured and compared to the ideal ones. A reasonable agreement between the measurements and the theoretical values was achieved over the aforementioned bandwidth; the common phase difference deviation was $\pm 3^o$, whereas the maximum deviation measured was $\pm 7^o$. Similar phase difference deviations may be found in the literature (Ausordin et al., 2014).

Consequently, the BM presented herein was used to feed a 4-element antenna array consisting of 4 printed dipoles of length $\lambda/2$, placed in front of a plane reflector at a distance 0.3λ; their spacing

has been set equal to $\lambda/2$. The operating frequency of the antenna was 2.44GHz. The generated four beams of the 4-element antenna array, fed by the 4×4 BM of Figure 2, are normalized and plotted in Figure 4, together with the theoretical radiation patterns. It may be verified that the measured radiation patterns coincide, more or less, with the theoretical ones especially as regards the main lobes; the beams are successfully steered towards the directions predicted by theory. Moreover, the measured side lobe levels (SLLs) do not exceed -10dB, albeit certain discrepancies may occur between the theoretical and the measured results in the side lobes of the patterns.

(a)
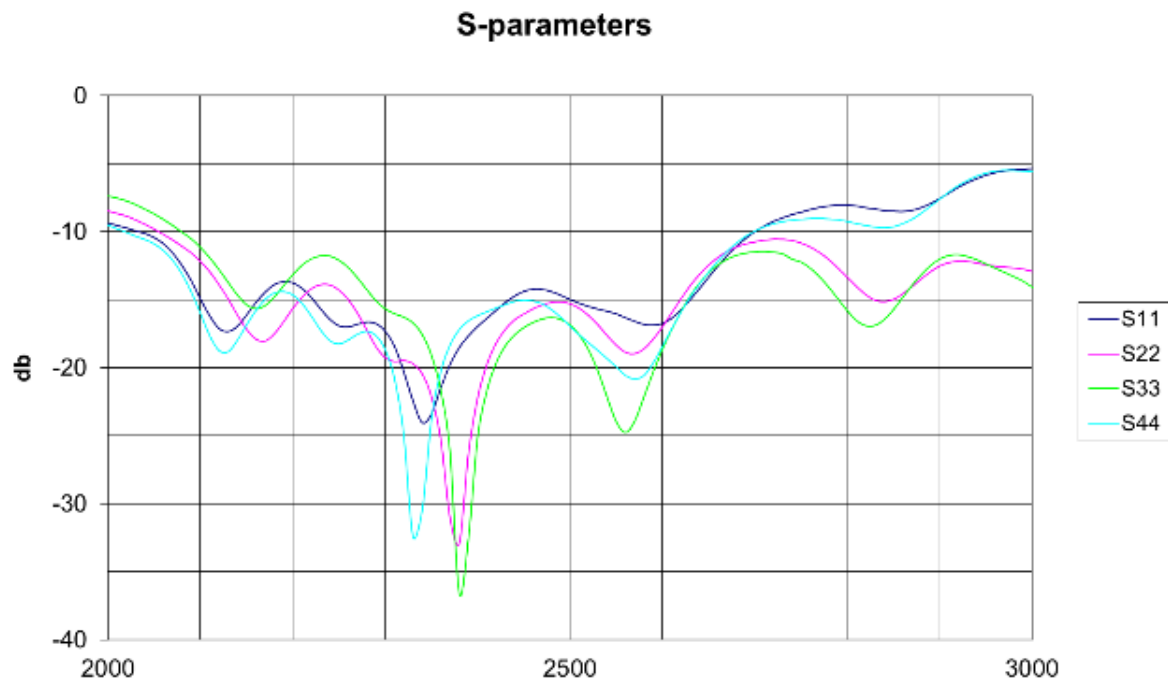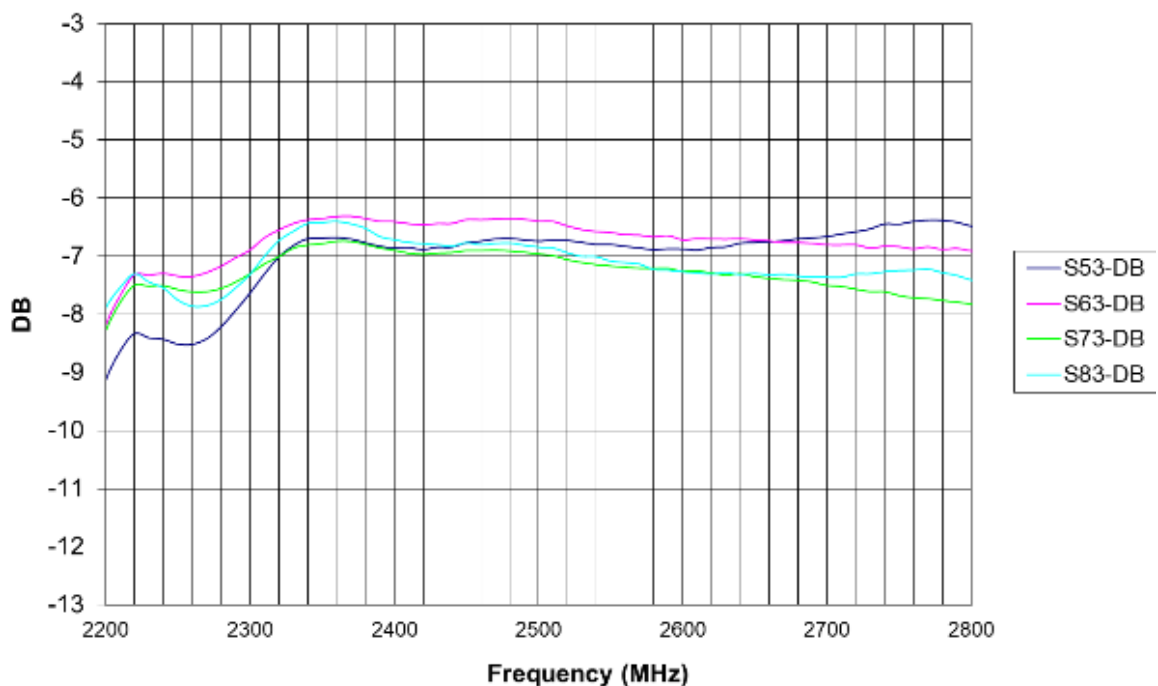
(b)

Figure 3. Measured magnitude of (a) the return losses and (b) the S-parameters when port 3 is excited.
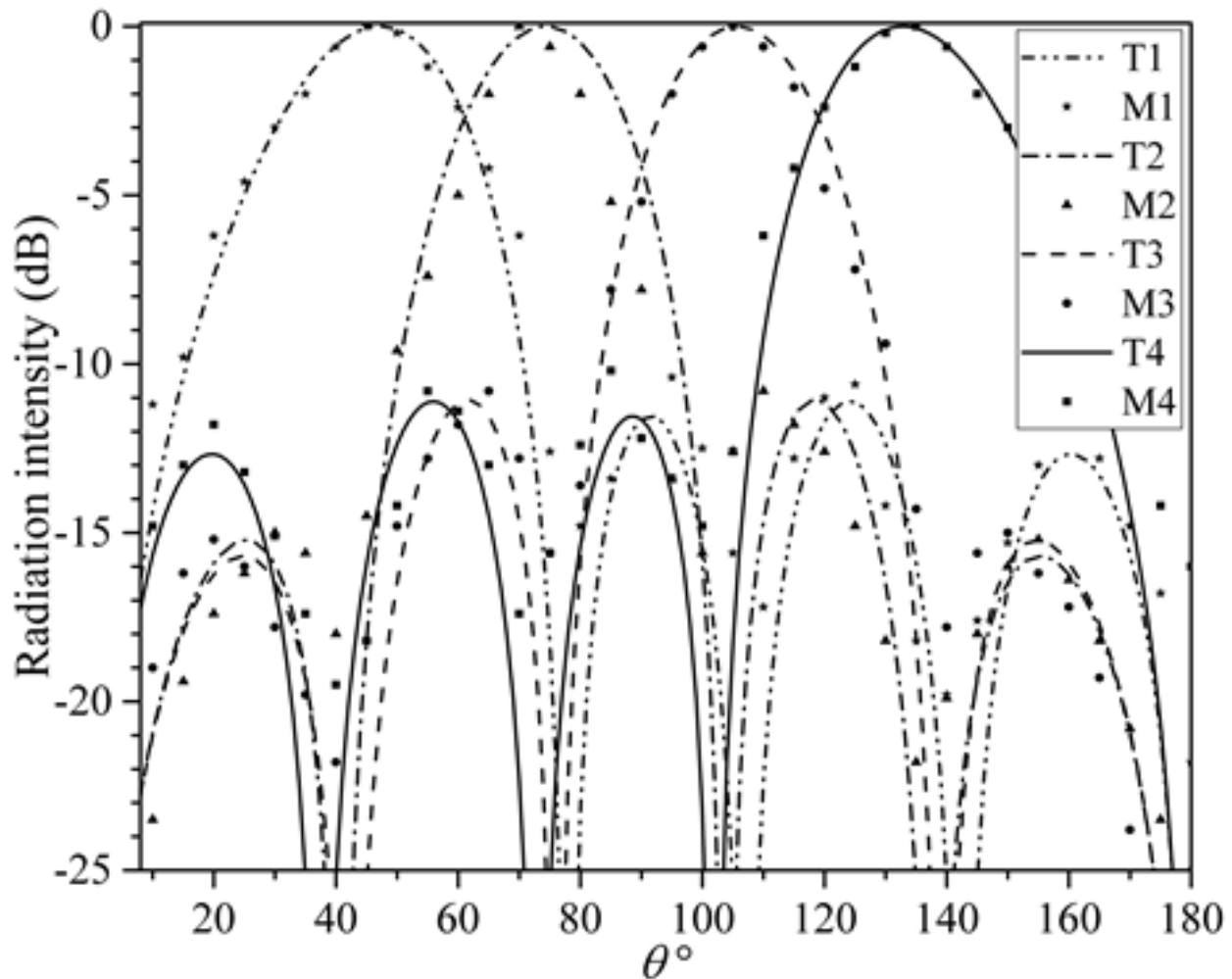
Figure 4. Normalized radiation patterns at 2.44GHz of a 4-element antenna array fed by the BM. The curves T1-T4 depict the theoretical results that correspond to beams 1-4. The markers M1-M4 stand for the measurements.

4. CONCLUSION

A single-layer and inexpensive 4×4 BM, operating at 2.44GHz, was designed and implemented in this paper. An easy-to-fabricate microstrip layout topology was employed and the final arrangement of the BM allows realization without any crossovers.

The performance of the network was evaluated by measuring its frequency response. The return loss and the isolation were found below -15dB, whereas the transmission coefficients were all better than -7dB with an amplitude imbalance less than 1dB over the range 2.32-2.52GHz. A 4-element antenna array was connected to the output of the BM in order to test the radiation characteristics of the resulting multibeam antenna. The radiation patterns were measured and compared with theoretical data; a good agreement was achieved. Moreover, the side lobes were sufficiently low, compared to the corresponding theoretical predictions.

5. REFERENCES

Adamidis, G.A., Vardiambasis I.O., Ioannidou, M.P., and Kapetanakis T.N. (2019). Design and implementation of single-layer 4×4 and 8×8 Butler Matrices for multibeam antenna arrays. Int. J. Antennas Propagat., volume 2019, Article ID 1645281:1-12.

Assorting, S.F., Rahim, S.K.A., Seman, N., Dewan, R., and Sa'ad, B.M. (2014) A compact 4×4 Butler matrix on double-layer substrate. Microw. Optical Technol. Lett., 56(1):223-229.

Babale, S.A., Ishfaq, M.K., Raza, A., Nasir, J., Fayyaz, A., and Ijaz, U. (2022). Compact Multibeam Array with Miniaturized Butler Matrix for 5G Applications. Computers, Materials & Continua, 72(1):925-937.

Lin, Y.S. and Lee, J.H. (2013). Miniature Butler matrix design using glass-based thin-film integrated passive device technology for 2.5-GHz applications. IEEE Trans. Microw. Theory Tech., 61(7):2594-2602.

Nie, W., Fan, Y., Luo, S., and Guo, Y. (2015). A switched-beam microstrip antenna array with miniaturized Butler matrix network. Microw. Optical Technol. Lett., 57(4):841-845.

Rahayu, Y., Simanihuruk, J.R.M., and Wahyu, Y. (2022). A compact design of 4×4 Butler matrix with four linear array antenna at 38GHz. Int. J. Electrical, Energy and Power System Engin. (IJEEPSE), 5(3):80-85.

Shallah, A.B., Zubir, F., Rahim, M.K.A., Majid, H.A., Sheikh, U.U., Murad, N.A., and Yusoff, Z. (2022). Recent developments of Butler matrix from components design evolution to system integration for 5G beamforming applications: A survey. IEEE Access, 10:88434-88456.

Trail, M., Nedil, M., Gharsallah, A., and Denidni, T.A (2008). A new design of compact 4×4 Butler matrix for ISM applications. Int. J. Microw. Science Technol., vol. 2008, Article ID 784526, 7 pages.

Vallappil, A.K., Rahim, M.K.A., Khawaja, B.A., and Iqbal, M.N. (2020). Compact metamaterial based 4×4 Butler matrix with improved bandwidth for 5G applications. IEEE Access, 8:13573-13583.

Vallappil, A.K., Rahim, M.K.A., Khawaja, B.A., Murad, N.A., and Mustapha, M.G. (2021). Butler matrix based beamforming networks for phased array antenna systems: A comprehensive review and future directions for 5G applications. IEEE Access, 9:3970-3987.

NOVEL EMBROIDERED TEXTILE THERMOCOUPLES FOR USE IN PERSONAL PROTECTIVE EQUIPMENT

Soukup, Radek[1], Kalcik, Jan[1], and Reboun, Jan[1]

[1]University of West Bohemia, Faculty of Electrical Engineering,
Department of Materials and Technology / RICE
rsoukup@fel.zcu.cz

1. INTRODUCTION

This paper discusses the issues of fabrication and testing of textile thermocouples with a focus on the methods of creating thermocouple hot joints. The paper follows the development of a textile thermocouple that has already been published (Kalcik et al., 2021). The development of textile thermocouples is also being pursued by other research teams around the world, but nowhere is it being implemented using hybrid conductive threads (Root et al., 2020), (Gidik et al., 2015).

Embroidered textile thermocouples are developed at the level of interdisciplinary development and are applicable in a large number of applications in various fields. One possible use of this E-textile applications are smart firefighting suits.

Figure 1. Possible applications a) smart protective glove SensPRO with contact and contactless temperature measurement b) smart protective firefighter suit smartPRO

2. SENSORS

The textile thermocouples made of hybrid conductive threads were embroidered with a Bernina 770QE semi-professional embroidery machine. The principle of the textile thermocouples designed in this work is based on two different hybrid conductive threads. These are the so-called hybrid constantan and copper threads. The constantan thread is composed of polyester multifilaments with a diameter of 14 µm and four constantan (Cu/Ni) microwires with a diameter of 28 µm. Electron microscope images of the constantan and copper threads are shown in Fig. 2. The copper thread is composed of polyester multifilament fibers with a diameter of 14 µm and four silver-coated copper microwires with a diameter of 30 µm. Due to the materials used for the microwires, they are T-type textile thermocouples.
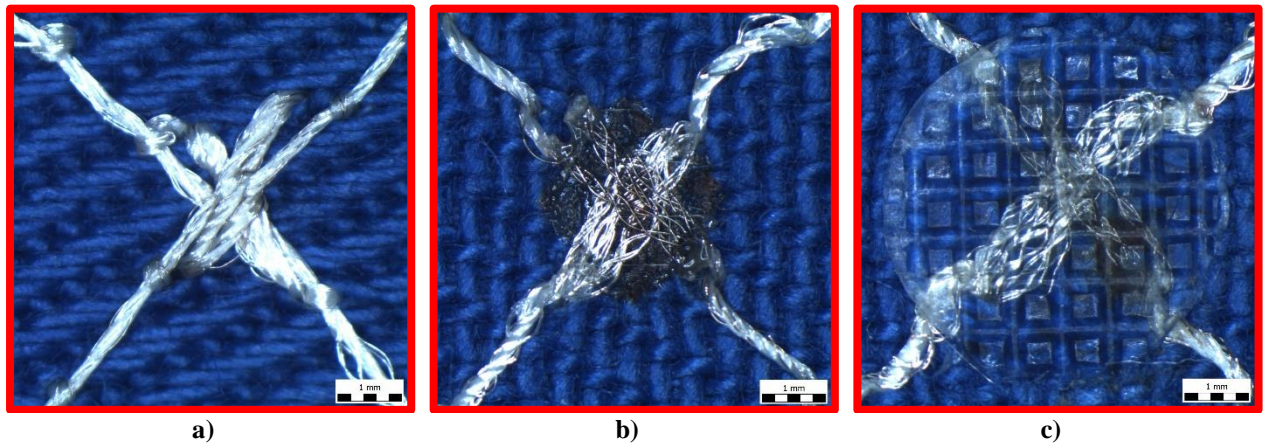
The thermocouple hot joint contacts were realized using the thermocompression welding method by resistance welding machine and ultrasonic welding method. Sunstone resistance welding machine

and Herrmann ultrasonic welding machine were used. The thermocouple hot joint contacts were realized by sewing the threads in a Z-shape to form 3-point and 9-point contacts. The contact structures can be seen in Fig. 3. In the case of ultrasonic welding, a foil of TPU material was added on the top and bottom side, which was previously prepared on a 3D printer. The material was added due to the lack of fusible material in ultrasonic welding. Such material is present in the filament in the form of polyester fibers, but the amount is too low for sufficient fixation of the metal microwires forming the thermocouple contact of the hot joint. Embroidered textile thermocouples are shown in Fig. 4.

a)
b)
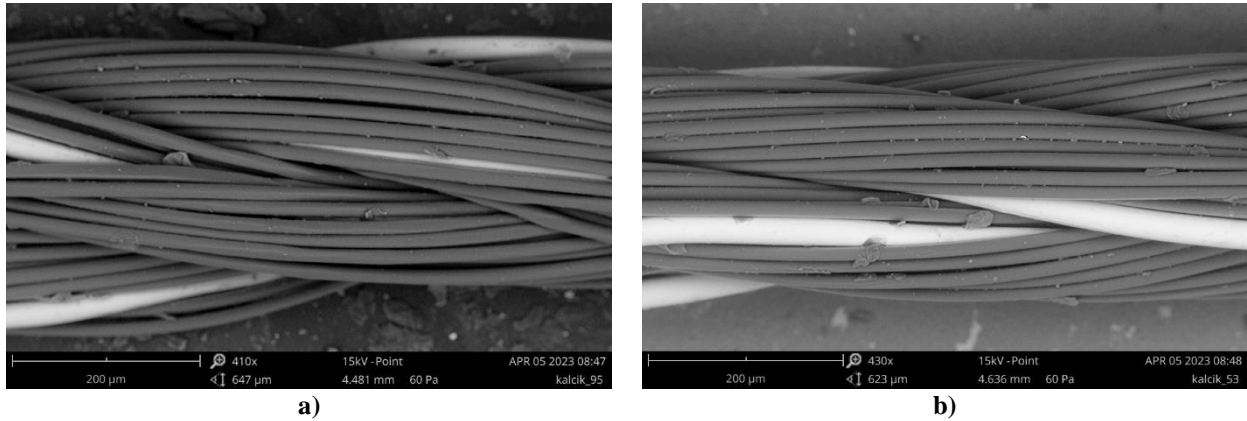
Figure 2. Structures of the hybrid conductive threads: a) constantan thread   b) copper thread.

a)
b)
c)

Figure 3. The contact structures: a) embroidered   b) realized using the thermocompression welding method by resistance welding machine   c) realized using the ultrasonic welding method
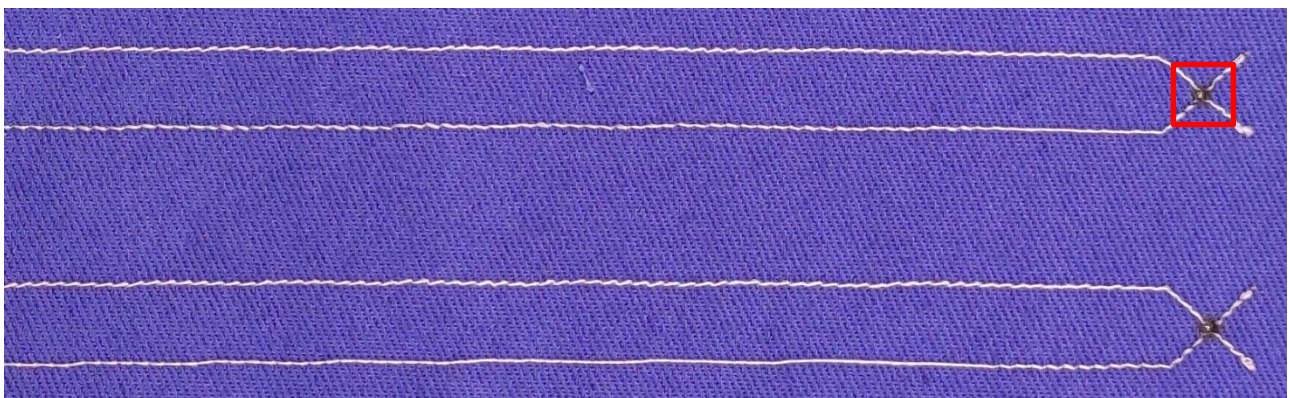
Figure 4. Embroidered textile thermocouples.

3. EXPERIMENT

Samples of textile thermocouples realized in this way were tested in a SalvisLab TC-40 laboratory furnace using a stepped temperature profile. The test was performed to measure the temperature dependence of the generated thermoelectric voltage of the textile thermocouples. The temperature profile consisted of twelve steps at increasing temperatures in the range from 40 °C to 140 °C. The laboratory furnace temperature profile used in the sensor testing is shown in Fig. 5 a). The laboratory furnace contained samples of textile thermocouples based on hybrid conductive threads, 2 commercial T-type thermocouples and 2 commercial Pt1000 class A platinum temperature sensors from Tesla Blatná a.s. The commercial thermocouples were used to compare the values with the sensors under development and the Pt1000 temperature sensors were used as a reference meter. The electrical voltage of the thermocouples and the electrical resistance of the Pt1000 temperature sensors were measured using a Keithley K2700 multimeter with a Keithley 7702 multiplexing card. The cold ends of the thermocouples were taken out of the laboratory furnace during the test. The temperature of the cold ends of the thermocouples was also measured using the Pt1000 temperature sensor locations. The positioning of samples in the furnace is shown in Fig. 5 b).
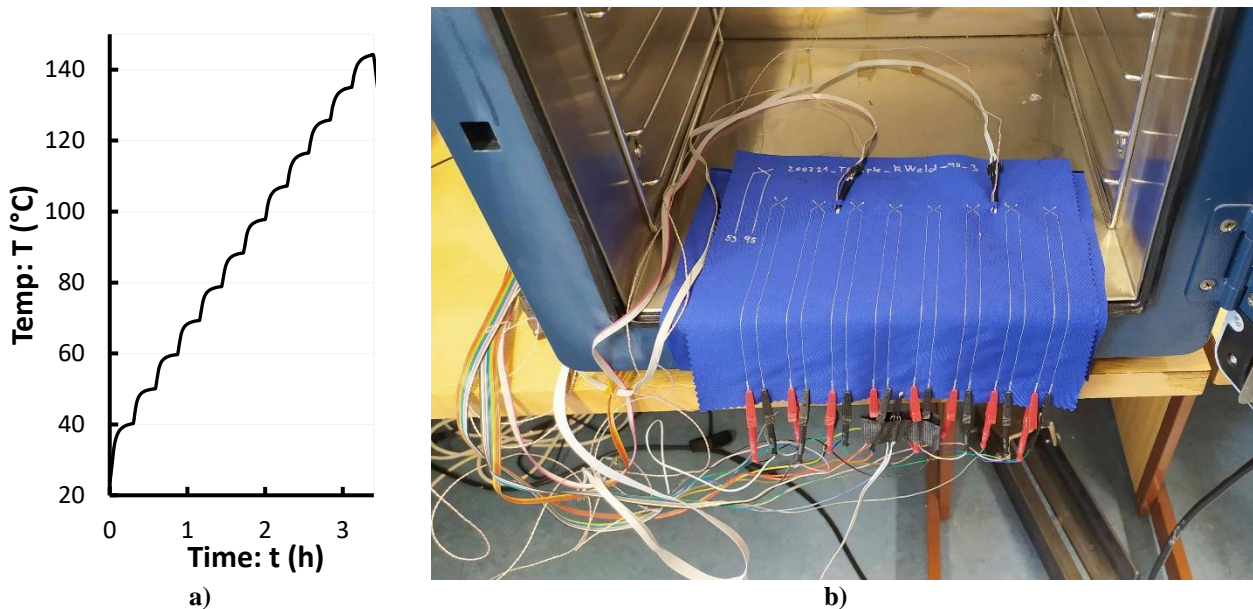

a)   b)

Figure 5.   a) Stepped temperature profile   b) positioning of samples in the furnace.

4. RESULTS AND DISCUSSION

Samples were produced in sets of eight and tested in sets of eight. The best results of textile thermocouples realized using the ultrasonic welding method were 3-point contact samples. The best results of textile thermocouples realized using the thermocompression welding method by resistance welding machine were 9-point contact samples. These two results are shown in Fig. 6. The samples with 3-point contact were labelled TC3_1-8 and the samples with 9-point contact were labelled TC9_1-8. A commercial thermocouple also placed in the furnace during the test of the textile thermocouples was labelled TCc_1. The cold ends of the thermocouples were placed at 25 °C. The curves of the temperature dependence of the generated thermoelectric voltage were generated from the measured data after the test.

The next tests were realized ageing tests, cyclic bending resistance test and domestic washing resistance test. Ageing test by dry heat was carried out for 1000 h at 125 °C according to the standard (EN 60068-2-2). Ageing test by temperature shocks was performed by rapid sample passes between -40 °C and 125 °C with a settling time of 10 minutes according to the standard (EN 60068-2-14), the test was repeated in 100 cycles. A cyclic bending resistance test was performed with 1000 bending

cycles with a radius of 10 mm at the weld area. The domestic washing resistance test was carried out with 5 wash cycles at 40 °C/400 rpm according to the standard (EN 6330).

The results of these stress tests were recorded as box plots of the standard deviations of the sample sets compared to the reference Pt1000 sensor. This is a comparison of 3 sets of 3 samples in each box. UZS_3b and UZS_9b are 3-point and 9-point samples realized using the ultrasonic welding method. And OdS_3b and OdS_9b are 3-point and 9-point samples realized using the thermocompression welding method by resistance welding machine.

a)   b)
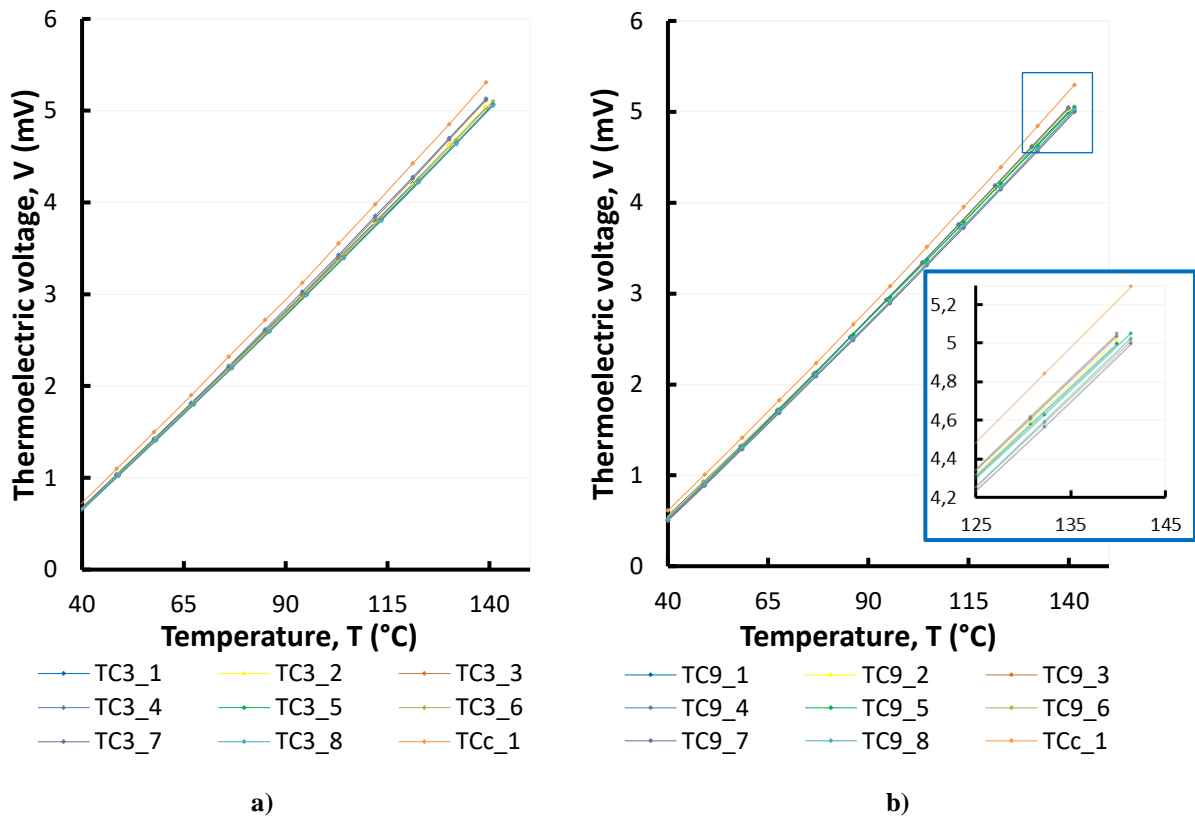
Figure 6. The curves of the temperature dependence of the generated thermoelectric voltage textile thermocouples realized using   a) the 3-point ultrasonic welding   b) the 9-point thermocompression welding by resistance welding machine
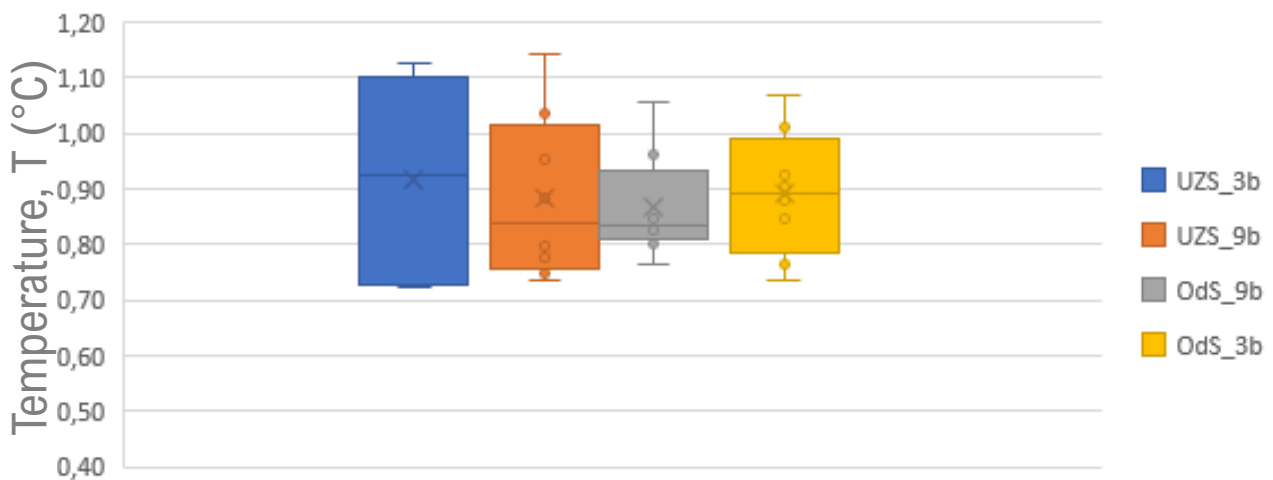
Figure 7. Comparison of standard deviations to reference sensor depending on welding method after accelerated ageing test.
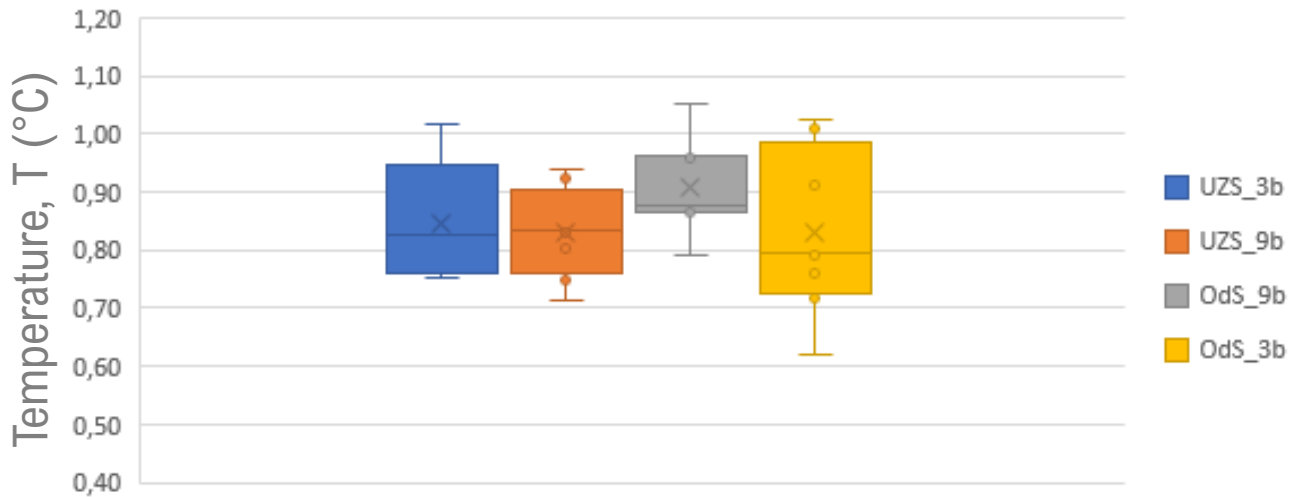
Figure 8. Comparison of standard deviations to reference sensor depending on welding method after bending test.
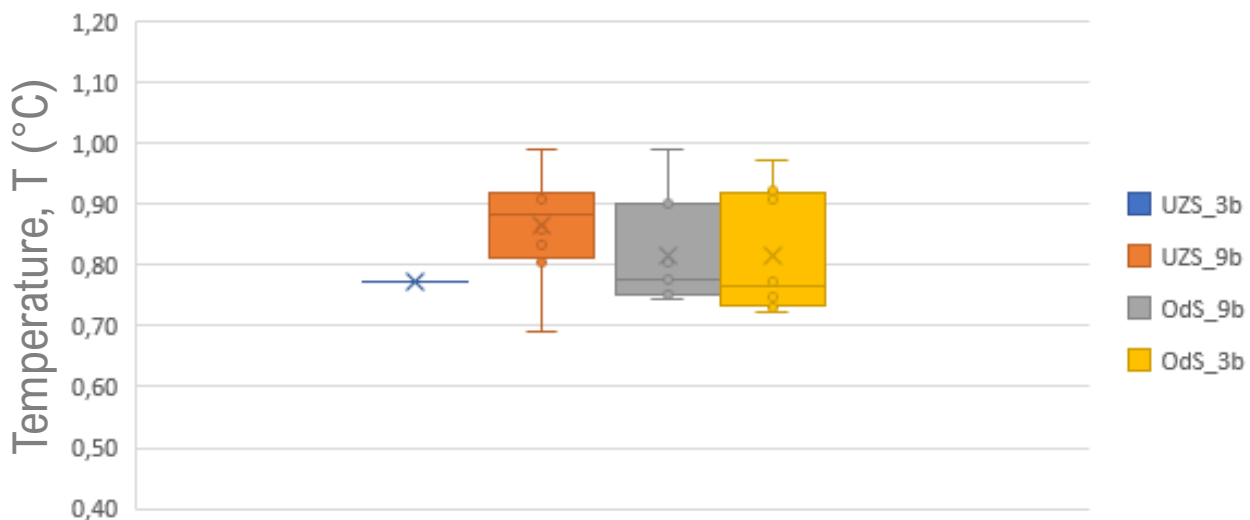

Figure 9. Comparison of standard deviations to reference sensor depending on welding method after washing test.

5. CONCLUSION

Embroidered textile thermocouples were successfully produced and tested. 2 methods were used to realize the thermocouple hot joints (thermocompression welding method by resistance welding machine and ultrasonic welding method). The sensitivity of the textile thermocouples is between 44,1 µV/°C and 44,5 µV/°C by the IEC 584. The standard deviation of test sets after fabrication is <±0,8 °C it corresponds with Class 2 IEC 584. The standard deviation of test sets after stress tests is <±1,2 °C.

6. ACKNOWLEDGMENT

7. REFERENCES

Gidik, H., Bedek, G., Dupont, D., & Codau, C. (2015). Impact of the textile substrate on the heat transfer of a textile heat flux sensor. In *Sensors and Actuators, A: Physical* (Vol. 230, pp. 25–32). Elsevier B.V. https://doi.org/10.1016/j.sna.2015.04.001

Kalcik, J., Sima, K., & Soukup, R. (2021). Textile Hybrid Thread Thermocouples. *Proceedings of the International Spring Seminar on Electronics Technology*, 2021-May. https://doi.org/10.1109/ISSE51996.2021.9467514

Root, W., Bechtold, T., & Pham, T. (2020). Textile-Integrated thermocouples for temperature measurement. In *Materials* (Vol. 13, Issue 3). MDPI AG. https://doi.org/10.3390/ma13030626

CHAOTIC HYSTERESIS IN ELECTRONIC CIRCUIT

Korneta, W

University of Lomza, Akademicka 1, 18-400 Łomża, Poland
wkorneta@ansl.edu.pl

1. INTRODUCTION

The hysteretic behavior of a system is its state dependence on the direction of the input change (Bertotti & Mayergoyz, 2005). The phenomenon of hysteresis most often appears as a loop in the input-output dependence, where two different system states correspond to a given input value depending on system history. The best-known cases of hysteresis occur in ferromagnetic materials (Bertotti, 1998), while the first examined type of hysteresis was elastic hysteresis (Hopkinson & Williams, 1912). The hysteresis is observed in many physical, biological and economic processes and it is intentionally added e.g. to electronic control systems to prevent unwanted rapid switching.

In recent years the hysteretic behavior was observed in systems with chaotic dynamical behavior (Storace & Bizzarri, 1999, Berglund & Kunz, 1997, Vadasz, 2006). The phenomenon of simultaneous occurrence of chaotic dynamics and hysteresis is called chaotic hysteresis. The aim of this paper is to show the phenomenon of chaotic hysteresis in electronic Chua's circuit (Chua, 1992, Ayrom & Zhong, 1986) induced by very slow triangular input voltage, by presenting experimental phase portraits taken from oscilloscope. Full description of experimental observation of chaotic hysteresis in Chua's electronic circuit driven by DC and slow triangular voltage source inserted into its inductor branch is given by Silva et al. (2023).

2. MATERIALS AND METHODS

Chua's electronic circuit consists of a resistor, an inductor, two capacitors and nonlinear element called Chua diode made in our case of two operational amplifiers and six resistors, as it was described by Kennedy (1992). Chua diode has piecewise-linear characteristic $I = f(V) = m_1 V + 0.5(m_0 - m_1)(|V + V_0| - |V - V_0|)$ with $m_0 = -0.758$ mA/V , $m_1 = -0.409$ mA/V and $V_0 = 1.08$ V. The power supply was $18.9\ V$. The experimental setup is shown in Figure 1a. Possible system states are usually represented in the phase space in which each axis corresponds to one of physical variables required to specify the state of a system (Nolte, 2010). In this space, successive states of the system form its dynamical trajectory. The subset of the phase space of the dynamical system toward which it tends to evolve for a wide variety of starting conditions is called an attractor (Milnor, 1985). Attractors in Chua's electronic circuit can be in the form of fixed point, limit circles, single and double scroll (Ayrom, 1986). For the selected values of electronic components given in Figure 1 and E(t)=0 the circuit is in the chaotic single scroll regime. In this regime dynamic trajectory has the form of a scroll produced by irregular oscillations around a fix point with frequencies around a certain dominant value. There are two possible single scroll attractors and one is chosen depending on the uncontrollable initial conditions. Experimental phase portraits of these two attractors in the phase space (V_1, V_2), where V_1 and V_2 are voltages on capacitors C_1 and C_2, are shown in Figure 1b. In the scroll having the fix point with positive V_1 value dynamic trajectory oscillates clockwise, whereas in the scroll having the fix point with negative V_1 value it oscillates counterclockwise.

The chaotic hysteresis is produced by very slow triangular forcing E(t) applied in series with the inductor. The observation of chaotic hysteresis described in this paper is for the triangular voltage with the amplitude 1 V and the period 100 s.
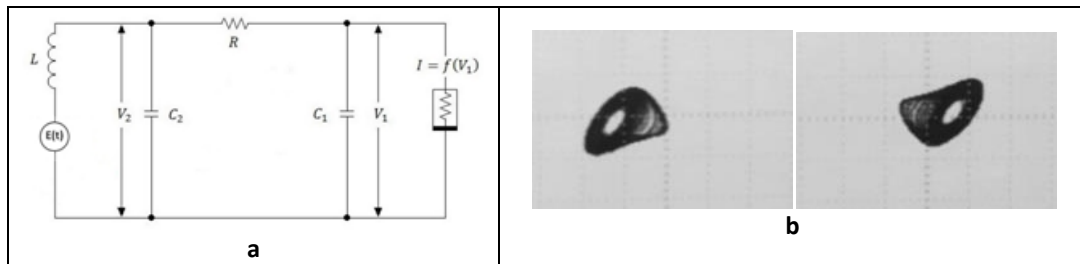
Figure 1. The experimental setup to observe chaotic hysteresis (a) consisting of the inductor $L = 18$ mH, the resistor R=1725 Ω, two capacitors $C_1 = 10$ nF and $C_2 = 100$ nF, the nonlinear Chua diode with piecewise-linear characteristic $I = f(V_1)$ and the triangular voltage source E(t). Experimental phase portraits (b) taken from oscilloscope in the phase space (V_1, V_2) of two possible single scroll chaotic attractors observed for E(t)=0. Horizontal axis: V_1 5 V/div, vertical axis: V_2 2 V/div.

3. RESULTS AND DISCUSSION

In this section we present experimental phase portraits of dynamic trajectory taken from oscilloscope observed in the phase space (V1,V2) obtained from Chua's electronic circuit for different triangular voltage E(t) values. The inset 1 is for E(t)=0. Insets 1-9 present attractors for the voltage E(t) increasing linearly up to 1 V. First the single scroll decreases (insets 1-3) and becomes very small. Around E(t)≈0.55 V there is sudden change from the attractor 3 to 4. The size of the attractor increases greatly and the direction of dynamic trajectory oscillation changes from counterclockwise to clockwise. A further increase in E(t) causes a sequence of bifurcations and attractor changes (insets 4-9). Then reducing the voltage E(t) one can observe similar sequence of bifurcations and attractor changes. For E(t)=0 the attractor is shown in the inset 10. For negative voltages E(t) (insets 11-16) attractor changes are symmetrical to changes for positive voltages.
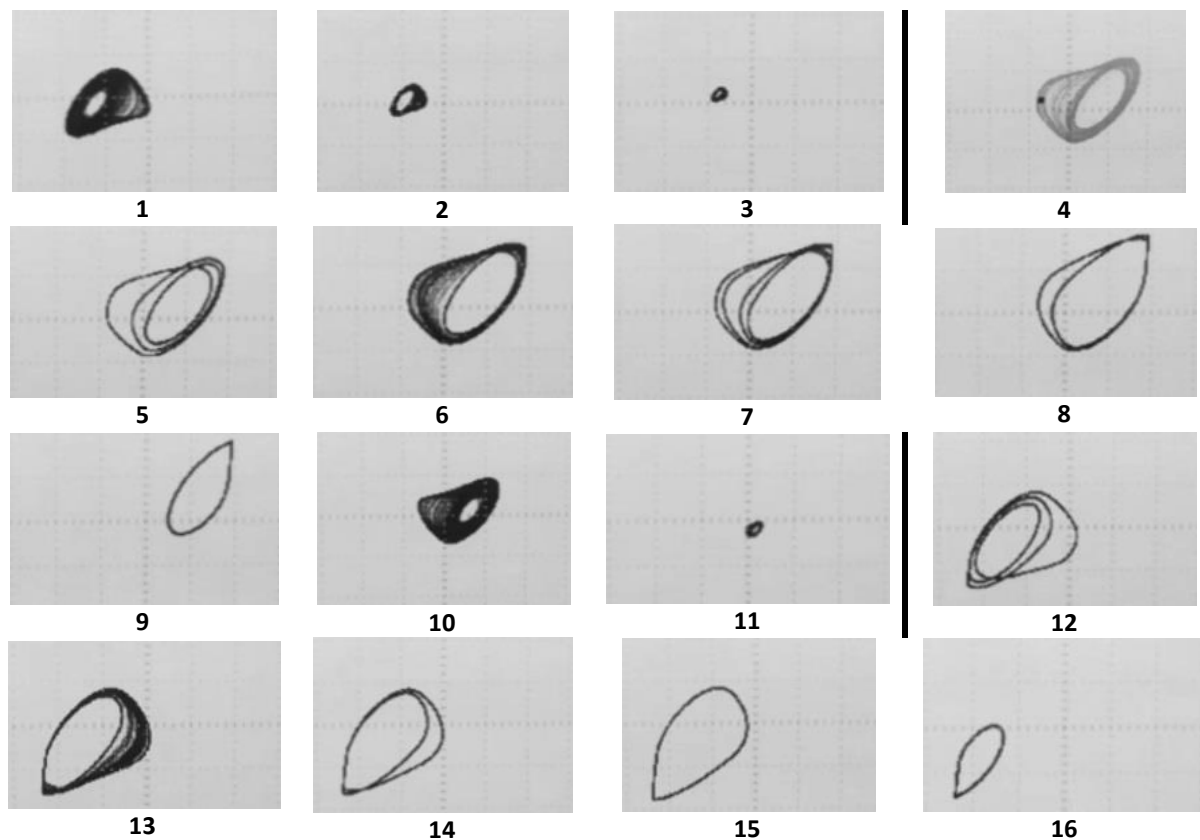
Figure 2. Experimental phase portraits taken from oscilloscope observed in the phase space (V_1, V_2) of dynamic trajectory for E(t) lineary increasing from 0 V to 1 V (1-9) and lineary decreasing from 1V to -1 V (9-16). The period of E(t) is 100s. Horizontal axis: V_1 5 V/div, vertical axis: V_2 2 V/div. The dark blsck lines indicate sudden change of the attractor.

4. REFERENCES

Ayrom F. and Zhong G.-Q. (1986). Chaos in Chua's circuit. IEE Proceedings D - Control Theory and Applications. 133(6): 307-312.

Berglund N. and Kunz H. (1997). Chaotic Hysteresis in an Adiabatically Oscillating Double Well. Phys.Rev.Lett. 78 (9): 1691-1694.

Bertotti G. (1998). Hysteresis in Magnetism: For Physicists, Materials Scientists, and Engineers. Academic Press

Bertotti G. and Mayergoyz I.D. (2005). The Science of Hysteresis. Academic Press

Chua L.O. (1992). The genesis of Chua's circuit. Archiv Elektronik Übertragungstechnik 46(4): 250–257.

Hopkinson B. and Williams G. T. (1912). The Elastic Hysteresis of Steel. Proceedings of the Royal Society. 87 (598): 502-511.

Kennedy P. (1992). Robust op amp realization of Chua's circuit. Frequenz 46(3-4): 66-80.

Milnor J. (1985). On the concept of attractor. Communications in Mathematical Physics 99: 177–195

Nolte D.D. (2010). The tangled tale of phase space. Physics Today. 63 (4): 33–38.

Silva I.G., Korneta W., Stavros Stavrinides G., Picos R. and Chua L.O. (2023). Chaos, Solitons and Fractals 166: 112927

Storace M. and Bizzarri F. (1999). Dynamic behaviour of hysteresis chaotic circuit. Electronics Letters 35 (22): 1896-1897.

Vadasz P. (2006). Chaotic Dynamics and Hysteresis in Thermal Convection. Journal of Mechanical Engineering Science 220 (3): 309-323.

AUTOMATED PLANT IRRIGATION SYSTEM USING ARDUINO MICROCONTROLLER

George Xenofontos[1], Maria S. Papadopoulou[1,2]

[1]Interantional Hellenic University, Department of Information & Electronic Engineering, 57400 Sindos, Greece
[2]ELEDIA Research Center (ELEDIA @AUTH-Aristotle University of Thessaloniki)
xenofontosgiorgos@gmail.com, mspapa@ihu.gr

1. INTRODUCTION

Watering plants is a crucial task in agriculture, while at the same time, its manual management can be laborious and time-consuming [Aher, et. al, 2020]. To address this challenge, the present project focuses on the development of an automated plant irrigation system using an Arduino microcontroller [Badamasi et al., 2014] and a humidity sensor. The device aims to optimize the irrigation process by monitoring and adjusting the water supply based on the soil moisture level. By automating the irrigation process, farmers can save time and resources while ensuring that plants receive the appropriate amount of water for healthy growth [Shiraz Pasha et al., 2014].

To evaluate the effectiveness of the auto-irrigation system, a mint plant was chosen as the test subject. The system's performance was assessed by monitoring the soil moisture level throughout the plant's growth cycle. The results demonstrated that the auto-irrigation system successfully maintained the soil moisture within the desired range, leading to improved plant growth and enhanced yield. The system proved to be highly efficient in optimizing water usage, ensuring that plants received adequate hydration while minimizing water waste.

This project highlights the potential of integrating electronics and automation to enhance the efficiency and efficacy of agricultural processes. By utilizing an Arduino microcontroller and a humidity sensor, the developed auto-irrigation system offers a practical solution to the challenges faced in plant irrigation.

2. MATERIALS AND METHODS

Components Used

The auto-irrigation system developed in this project utilizes several key components to automate the plant irrigation process effectively. These components include a submersible pump [FIT0200], a humidity sensor [YL-69], and an Arduino Uno [Arduino Uno R3]. Each component plays a specific role in measuring soil moisture and controlling the water supply to the plants.

Arduino Uno

The Arduino microcontroller serves as the brain of the auto-irrigation system. It receives data from the humidity sensor, compares it with a predefined threshold, and controls the submersible pump accordingly. The microcontroller is programmed with appropriate algorithms to interpret the sensor data and make informed decisions regarding irrigation. It is also responsible for regulating the timing and duration of watering cycles to ensure optimal plant hydration.

Submersible Pump

The submersible pump is responsible for transferring water from the water reservoir to the plant. It is designed to be submerged in water, allowing it to efficiently draw and deliver water to the plant's

root zone. The pump is connected to the water reservoir through appropriate tubing, ensuring a continuous supply of water for irrigation.

Relay

The relay [2 Channel 5V Relay Module] serves as a vital component in the auto-irrigation system by acting as a switch to control the submersible pump. Its integration with the Arduino microcontroller allows for precise and reliable control of the irrigation process based on the soil moisture levels. By effectively managing the power supply to the pump, the relay contributes to the overall automation and efficiency of the system, ensuring optimal watering of the plant.

Humidity Sensor

The humidity sensor is a crucial component that measures the moisture content in the soil. It provides real-time data on the soil's moisture level, enabling the system to determine when irrigation is required. The humidity sensor is typically placed near the plant's root zone, ensuring accurate measurements. It is connected to the Arduino microcontroller for data transmission and analysis.

System Configuration and Connectivity

The auto-irrigation system comprises several key components, including the humidity sensor, Arduino microcontroller, relay, and submersible pump. These components are carefully connected and configured to automate the plant irrigation process effectively presented to the figure 1. The flowchart is presented in Figure 2.
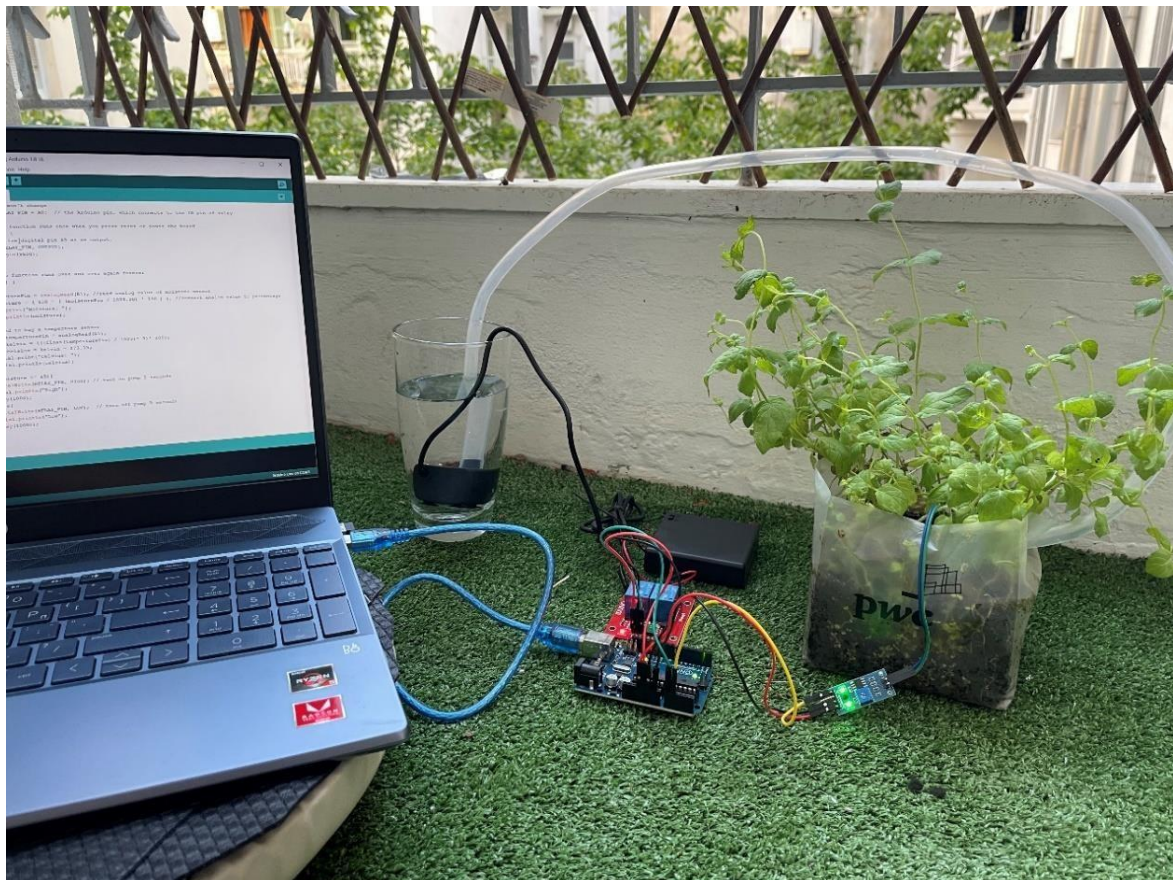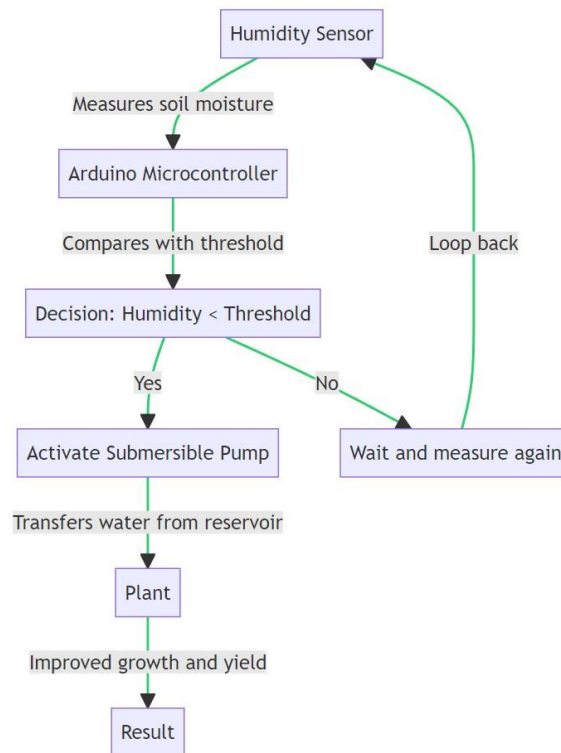

Figure 1:Device for the auto-irrigation

Figure 2: Flowchart of the code in the Arduino

The flowchart in Figure 1 illustrates the code structure and the control flow of the auto-irrigation system. It outlines the decision-making process based on the soil moisture readings obtained from the humidity sensor. The flowchart provides a visual representation of how the Arduino microcontroller interacts with the various components to automate the irrigation process.

By following the flowchart, the system determines the soil moisture level, compares it with the predefined threshold, and activates the relay to control the submersible pump accordingly. This ensures that the plants receive the appropriate amount of water based on their moisture needs.

3. RESULTS AND DISCUSSION

During the two-week testing period, we observed notable differences between manual and autoirrigation methods. When watering the plant manually, the leaves started to darken in color, indicating a potential issue with the water amount. Additionally, the timing of watering was inconsistent, which affected the plant's overall health. The plant required watering every two days to maintain optimal conditions.

However, after implementing the auto-irrigation system, we observed significant improvements. The plant regained its natural color, indicating a healthier state. The auto-irrigation device ensured that the soil moisture level remained within the recommended range of 70-75% (Boopathy et al., 2020). The auto-irrigation device effectively maintained the moisture level within this range, ensuring the plant received the appropriate amount of water for its growth and development. The data are shown in figure 3.

The auto-irrigation system proved to be a successful solution for maintaining optimal soil moisture levels and ensuring the plant's well-being. It eliminated issues related to inconsistent watering and provided the plant with the necessary water at regular intervals, resulting in improved plant health and overall growth.
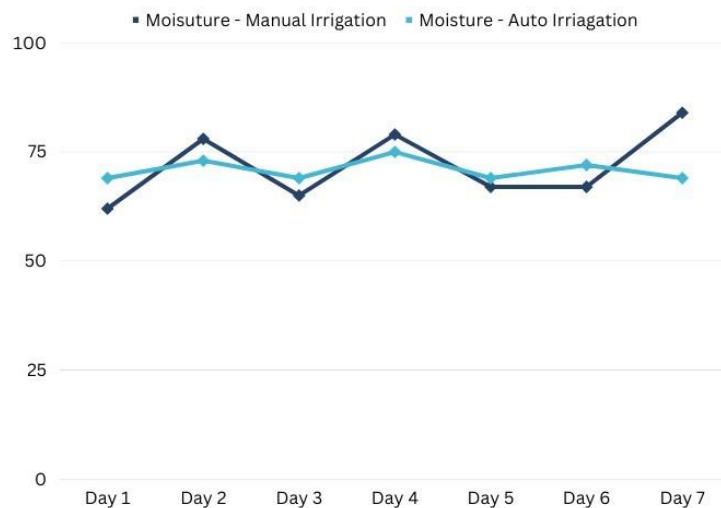
Figure 3: Manual irrigation compared to auto-irrigation moisture level

4. CONCLUSION

The automated plant irrigation device developed using an Arduino microcontroller and a humidity sensor has proven to be highly effective in maintaining optimal soil moisture levels for plant growth [Yasin et al., 2019]. The principles and generalizations inferred from the results highlight the significance of real-time monitoring and control in ensuring that plants receive adequate water. By automating the irrigation process, the device addresses the challenges associated with manual watering, such as inconsistent watering schedules and incorrect water amounts.   In conclusion, the automated plant irrigation system using an Arduino microcontroller and a humidity sensor offers a practical and reliable solution for efficient plant irrigation. Future improvements, such as incorporating IoT technology for distance monitoring, solar panel for sustainable power supply, and additional sensors for comprehensive environmental monitoring, will further enhance the device's capabilities. It is recommended to continue exploring advancements in sensor technology and automation to maximize the benefits of such systems in agriculture and contribute to sustainable farming practices [Shekhar et al., 2017].

5. REFERENCES

Aher, S., Mahakalkar, V. S., Masand, M., & Deshmukh, P. (2020). Automated Irrigation System for Efficient Water Management in Agriculture using Arduino. International Journal of Scientific Research and Management, 8(12), 101-105.

Badamasi, Y. A. (2014). The working principle of an Arduino. In 2014 11th International Conference on Electronics, Computer and Computation (ICECCO) (pp. 1-4). Abuja, Nigeria. DOI: 10.1109/ICECCO.2014.6997578.

Boopathy, S., Anand, G., & Rajalakshmi, N. R. (2020). Smart Irrigation System for Mint Cultivation through Hydroponics Using IoT. Test Engineering and Management, 83, 13706-13714.

Shekhar, Y., Dagur, E., Mishra, S., & Sankaranarayanan, S. (2017). Intelligent IoT based automated irrigation system. International Journal of Applied Engineering Research, 12(18), 7306-7320.

Shiraz Pasha, B. R., & Yogesha, D. B. (2014). Microcontroller based automated irrigation system. The International Journal Of Engineering And Science (IJES), Volume3, (7), 06-09.

Yasin, H. M., Zeebaree, S. R. M., & Zebari, I. M. I. (2019). Arduino Based Automatic Irrigation System: Monitoring and SMS Controlling. In 2019 4th Scientific International Conference Najaf (SICN) (pp. 109-114). Al-Najef, Iraq. DOI: 10.1109/SICN47020.2019.9019370.

PERFORMANCE EVALUATION OF COMBO PONS

Bibas, C., Liodakis, G.*, Baklezos, A., Nikolopoulos, C., Petrakis, N., and Vardiambasis, I.O.

Laboratory of Telecommunications & Electromagnetic Applications,
Department of Electronic Engineering,
Hellenic Mediterranean University,
Romanou 3, Chalepa, GR-73133 Chania, Crete, Greece
* gsl@hmu.gr

1. INTRODUCTION

Passive Optical Networks (PONs) are already playing an important role for various broadband access use cases, mostly for connecting households and businesses. Along with the ever increasing gigabit connectivity which is at the centre of digital strategies worldwide, each generational upgrade in PON technology comes with new features as dictated by new use cases (e.g., lower latency, increased availability of network, increased reliability of applications). However, from an infrastructure point of view, the optical distribution network (ODN) of a PON should accommodate both current and future generations of PONs due to the high cost associated with the implementation of the Fiber-to-the-Home (FTTH) and Fiber-to-the-Building (FTTB) architectures.

As of September 2022, the evolution of coverage rate (i.e., the homes passed as a proportion to total households) and of take up rate (i.e., the subscribers as a proportion of homes passed) in Europe are depicted in Figures 1 and 2, respectively (FTTH Council Europe, 2023). More specifically, according to the FTTH/B Market Panorama study data of the FTTH Council Europe released in April 2023, there exists a positive trend of fiber rollouts across Europe with full-fiber connectivity being a clear priority for EU authorities, national governments, and market players across Europe. However, such a fiber infrastructure needs to ensure a high Quality of Service/Experience (QoS/QoE), due to the coexistence of legacy and forthcoming PON technologies in the ODN.
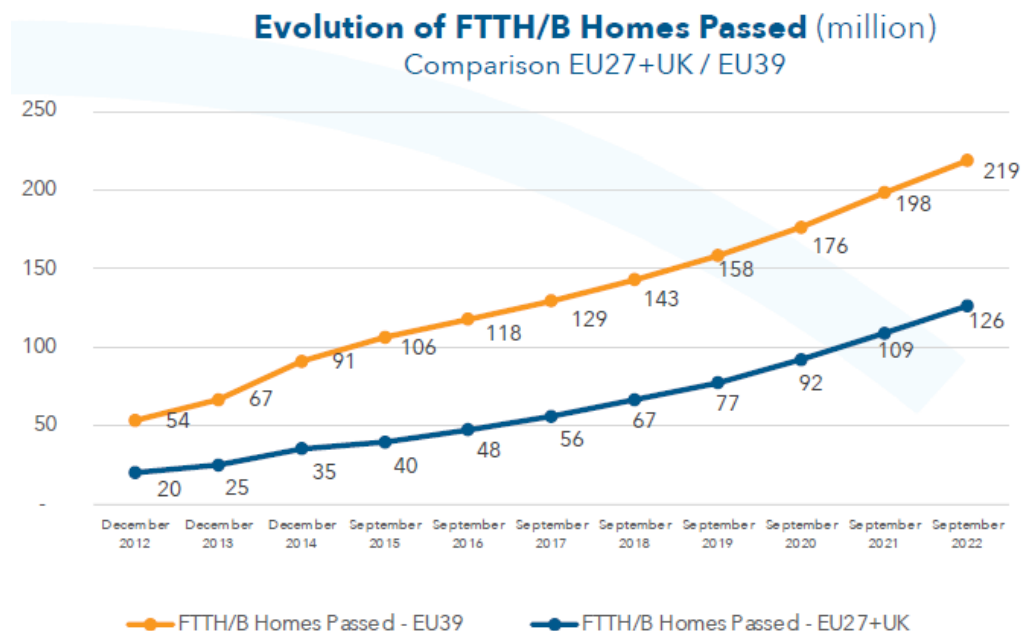

Figure 1. Evolution of coverage rate.

In light of the aforementioned issues, the objective of this article is to carry out a downstream stress test in case of two PON technologies coexisting on the same ODN. The two PON network technologies examined here are based on two ITU-T standards, namely the XG-PON and the 50G

PON standards. It should be mentioned that XG-PON is one of the most commercially deployed PONs, whereas the commercial deployment of 50G PONs is envisaged around 2025. The resultant performance evaluation in terms of Q factor and BER values is of great importance for all parties involved in the design and deployment of PON networks (standardization bodies, optical communication equipment manufacturers, communication service providers, regulatory authorities). In the remainder of this article, we first provide main technical points related to the ITU-T PON standards and the so called combo PON concept (Section 2). Then, in Section 3, the simulation model and the performance evaluation results for the downstream scenario under consideration are presented. Finally, in Section 4, conclusions and further directions for the study of combo PONs are included.
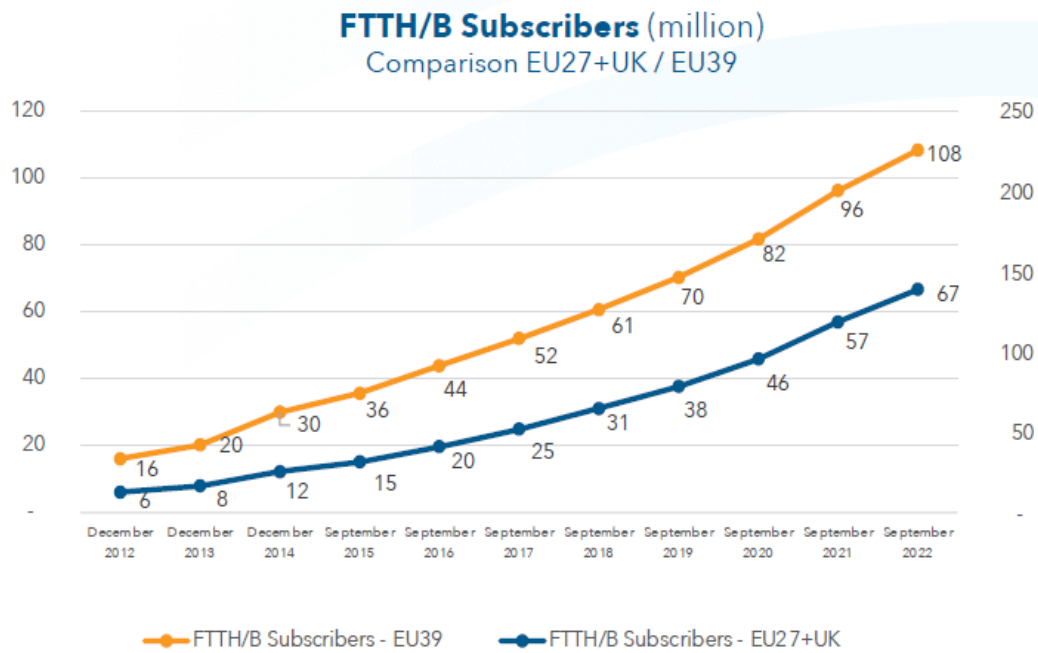
Figure 2. Evolution of take up rate.

2. COMPO PONS

The "combo concept" has been introduced in the past for the coexistence and evolution of POTS services and DSL services. The same concept is, also, used for the coexistence and evolution for two ITU-T standards, such as GPONs and XG-PONs (ZTE, 2020). In other words, the term coexistence refers to the ability of two or more PON generations to operate simultaneously on a common fiber section (i.e., ODN). It becomes evident that various coexistence scenarios may be realized according to an operator's need. Among these scenarios, the combo PON scenario of XG-PON and 50G PON technologies which represents an important evolution direction in the post 10G PON era, is examined in this article. More specifically, a specifications recap for major ITU-T PON standards are shown in Table 1 and should be accordingly used for performance evaluation purposes.

Table 1. Specifications recap for major ITU-T PON standards.

STANDARD	DOWNSTREAM RATE (GBPS)	UPSTREAM RATE (GBPS)	DOWNSTREAM WAVELENGTH (NM)	UPSTREAM WAVELENGTH (NM)
GPON	2.488	1.244	1480-1500	1290-1330
XG(S)-PON	9.952	9.952 or 2.448	1575-1580	1260-1280
50G-PON (ITU-T G.9804.x)	49.7664	49.7664 24.8832 12.4416	1340-1344	1260-1280 (US1) or 1290-1310 (US2-wideband: 1300+/-10nm or US2 narrowband: 1300+/-2nm)

When a PON system is migrated from a legacy PON to a 50G-PON, there can be several approaches (ITU-T G.9804 Series of Recommendations, 2019). Among these approaches, the OLT (Optical Line Terminal) multi-PON module (MPM) method, described in Appendix IV of ITU-T G.984.5 and shown in Figure 3, is adopted in this article.

From a performance evaluation perspective, to the best of our knowledge there exist only a few works for combo PONs in the public literature. Furthermore, most of them are experimental in nature and were carried out by communication service providers (Li et al., 2015), (Mat Sharif et al., 2018), (Saliou et al., 2022).
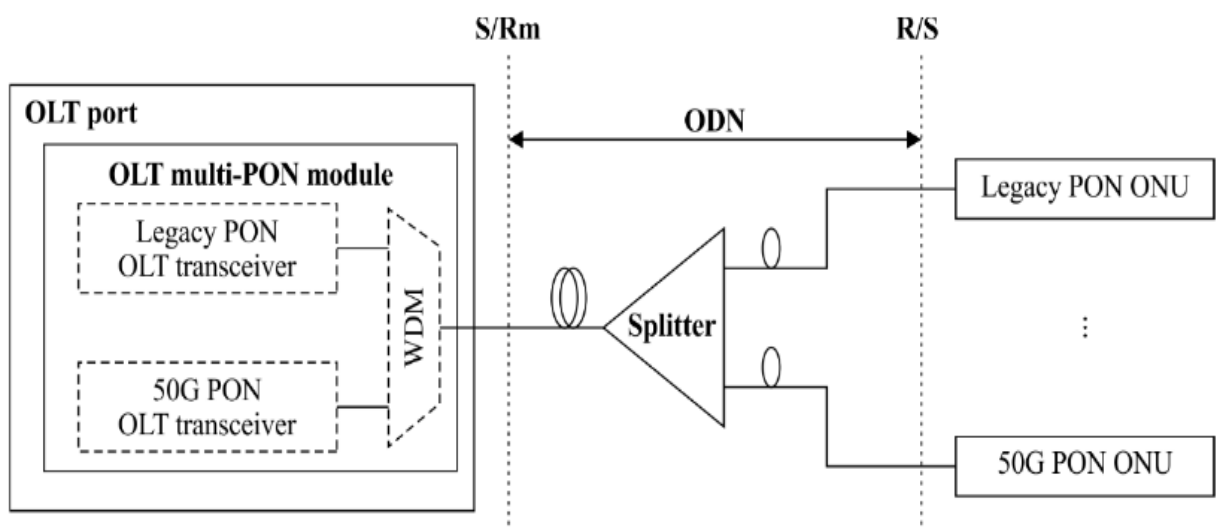

Figure 3. General architectural diagram of 50G-PON coexisting with legacy PON using the OLT MPM method.

3.   SIMULATION MODEL AND RESULTS

A schematic of the simulated transmission system used in this article is illustrated in Figure 4. Simulations were carried out by the use of the OptiSystem 14.2.0 simulation software. At first, the effect of transmission distance at the maximum differential distance of 40km envisaged for the 50G PON, was examined. More specifically, as shown in Table 2, the maximum Q factor and the minimum BER values at the receiver (i.e., at users' Optical Network Units (ONU)) are obtained. Basic input system parameters, such as wavelengths used, launch powers and type of detectors used (PIN or APD), are also included in Table 2. As it can be observed, the performance of the 50G PON in the combo PON scenario under consideration is highly affected. This, in turn, imposes some ODN fiber length restrictions as it relates to the 50G PON operation.

Table 2. Performance evaluation for the maximum differential distance.

| TRANSMITTER @ OLT	LAUNCH POWER (dBm)	RECEIVER MAX Q FACTOR	RECEIVER MIN. BER
XGPON (PIN) (1577 NM)	5	10.2358	5.9593e-15
50G PON (APD) (1340 NM)	7	3.74383	7.59161e-05
50G PON (PIN) (1340 NM)	7	3.72608	8.0457e-05

Furthermore, in Table 3, the effect of the line coding used for the data bits to be transmitted through the 50G PON, is examined. As can easily be seen, the NRZ coding results in a much better communications performance in comparison to RZ coding in terms of the minimum BER achieved, either by using a PIN or APD at the ONU. This is in line with what is proposed by the (ITU-T G.9804 Series of Recommendations, 2019).

In Table 4, the effect of the transmission distance for the combo downstream scenario is demonstrated. More specifically, the maximum Q factor and minimum BER values for the 50G PON

users who may be distributed in the 20-50km range, are presented. Although the fiber distances examined are not the typical ones, typical values for the responsivity of PIN and APD detectors, gain of APD, etc. were used for the simulation.

Table 3. Performance evaluation according to line coding.

LINE CODING	Max Q Factor (APD)	Min BER (APD)	Max Q Factor (PIN)	Min BER (PIN)
NRZ	3.69341	9.04215e-05	3.74428	7.5767e-05
RZ	3.10389	0.000713574	3.14291	0.000642101
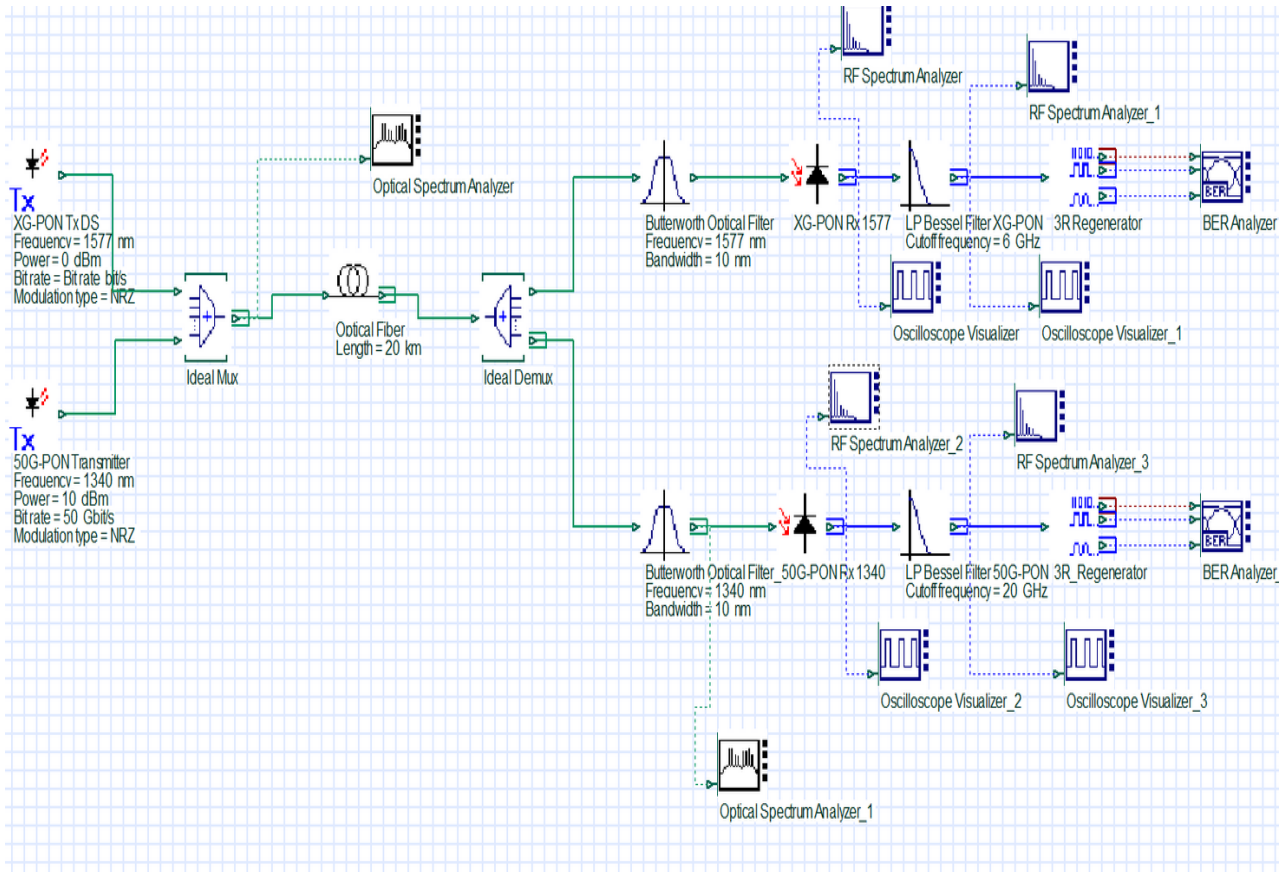
Figure 4. Snapshot of the combo PON simulation model.

Table 4. Performance evaluation of 50G PON for various fiber distances (combo PON scenario).

FIBER DISTANCE (KM)	MAX Q FACTOR (APD)	MIN BER (APD)	MAX Q FACTOR (PIN)	MIN BER (PIN)
20	2.4287	0.00506179	2.43021	0.00504793
25	3.6036	0.000147088	3.58323	0.000158451
30	3.583	0.000156311	3.60786	0.000143995
35	4.07412	1.81072e-05	4.08831	1.73585e-05
40	3.69341	9.04215e-05	3.74428	7.5767e-05
45	3.67626	0.000103736	3.59282	0.000136261
50	3.54888	0.000145057	3.55643	0.000140993

4. CONCLUSIONS AND FURTHER DIRECTIONS

An intensity modulation/direct detection (IM/DD) simulation model was adopted in this article for the performance evaluation of combo PONs under stress test conditions. Simulation results were highly affected by the presence of nonlinear effects in optical fibers, namely stimulated Raman scattering (SRS) and four-wave mixing (FWM). These effects provide gains to some channels while depleting power from others, thereby producing crosstalk between the PON wavelengths used in our simulation model. As an extension of the work presented here, a more realistic simulation model (including DSP processing and FEC coding at the 50G ONU receiver) should be devised, thus resulting in a holistic performance evaluation analysis of ITU-T G.9804.x PONs. Furthermore, by the incorporation of the variant of the TDEC (Transmitter and Dispersion Eye Closure) parameter which was firstly introduced for assessing the transmitter performance of 50G(S) PONs, the overall Quality of Transmission (QoT) for the combo PON under consideration could be evaluated.

The approach followed in this article may be used for the performance evaluation of other combo PON scenarios with other legacy PONs. These may include ITU-T (such as GPON and NG-PON2), IEEE Ethernet (such as 10G-EPON and 50G-EPON) and MSA (25GS-PON) PON standards. In addition, other PON technologies under research, experimentation or standardization (coherent PONs and SuperPONs), may be examined. In any case, the combo PON concept is expected to not only facilitate the smooth evolution of PON technologies, but also to guarantee that the most valuable part of the access network (i.e., the ODN) will be fully exploited for the delivery of FTTH services.

5. REFERENCES

Bonk, R., Geng D., Khotimsky D., Liu D., Liu X., Luo Y., Nesset D., Oksman V., Strobel R., Van Hoof W., and Wey J.S. (2022). 50G-PON: The First ITU-T Higher-Speed PON System. IEEE Communications Magazine 60 (3): 48-54.

FTTH Council Europe (2023). FTTH/B Market Panorama.

ITU-T G.9804 Series of Recommendations for Higher Speed Passive Optical Networks, G.9804.1 (Requirements), approved in Nov. 2019; G.9804.2 (ComTC), consented in Apr. 2021; G.9804.3 (50G-PON PMD), consented in Apr. 2021.

Li, J., He H., and Hu W. (2015). Theoretical and experimental analysis of Inter-channel crosstalk between TWDM and fronthaul wavelengths due to stimulated Raman scattering. Opt. Express 23 (7): 8809-8817.

Mat Sharif, K.A., Ngah N.A., Ahmad A., Manaf Z.A., and Tarsono D. (2018). Demonstration of XGS-PON and GPON co-existing in the same passive optical network. 7th International IEEE Conference on Photonics (ICP), Langkawi, Malaysia, 2018, pp. 1-3, doi: 10.1109/ICP.2018.8533167.

Saliou, F., Gaillard G., Simon G., Le Huerou S., Potet J., and Chanclou P. (2022). Triple coexistence of PON technologies: Experimentation of G-PON, XGS-PON and 50G(S)-PON over a Class C+ ODN. 2022 European Conference on Optical Communication (ECOC), Basel, Switzerland, 2022, pp. 1-4.

ZTE (2020). Combo PON Technical White Paper.

REVOLUTIONIZING CRIME AND TERRORISM PREVENTION: CUTTING-EDGE BIOMETRIC TECHNOLOGIES FOR PRECISE CRIMINAL IDENTIFICATION AND PARTIAL EVIDENCE ANALYSIS

Evangelatos, S[1,2], Veroni, E[1,2], Konidi, M[1], Baklezos, A[1], and Nikolopoulos, C[1]

[1]Hellenic Mediterranean University, Department of Electronic Engineering
[2]Netcompany Intrasoft S.A., Luxembourg
ddk186@edu.hmu.gr (corresponding author)

1. INTRODUCTION

Biometrics addresses a longstanding concern to prove one's identity, irrefutably, by using what makes a person unique. During the prehistoric times, humans already had a feeling that individual characteristics such as the trace of their fingers were enough to identify them, and they used to sign any official document or contract with their fingers. Nowadays, biometrics have moved from a novel technology to a part of everyday life as a means of people to authenticate themselves and gain access in devices (mobile phones) and services (e-banking). In 2019, the global biometric technology market was forecasted to be over $16.6 billion and it is expected to expand fast, reaching a whopping $55.42 billion by 2027[l]. Biometric identification together with behavioural detection, emotion recognition, brain-computer-interfaces and similar techniques are being used to an increasing extent by public and private bodies. They serve a broad variety of purposes, ranging from healthcare to law enforcement and border control and are deployed in public as well as in private spaces[m]. The undisputable power of biometrics became evident within the last century especially regarding criminal identification. Police Authorities and Forensic Investigators rely on Automated Fingerprint Identification Systems (AFIS) to tackle global terrorism, criminality and illegal migration. In the real-world forensics, matching latent, or unintentionally deposited, fingerprints to a specific person, is way more complicated. Identifying the owner requires matching the evidence - often smudged, incomplete, or deposited on top of other markings - with complete prints on file in AFIS databases[n]. Nevertheless, a single biometric technology is not always accurate and robust[o]. To overcome this obstacle, forensic investigators rely more and more on the combination of multiple biometric modalities such as fingerprint and voice biometrics.

2. BACKGROUND

The field of behavioural biometrics that includes cognitive behaviour such as gait analysis, voice recognition and keystroke dynamics, despite being at its early stages, constitutes a well-promising technology for multi-factor identification. It necessitates the use of another biometric modality for initial authentication despite the fact that its reliability is inferior to that of other biometrics. However, behavioural biometrics can provide additional intelligence and contextual information including even the mental state of the person through the inference of the stress and anxiety levels and once fused with other biometric technologies, compensate the error of the biometric itself.

Nowadays there are 6.3 billion smartphone users which accounts to nearly 81% of the world's population[p] and inevitably some of them are involved in criminal activities. Smartphone devices

[l] https://www.statista.com/statistics/1048705/worldwide-biometrics-market-revenue/
[m] https://www.europarl.europa.eu/RegData/etudes/STUD/2021/696968/IPOL_STU(2021)696968_EN.pdf
[n] https://www.mitre.org/publications/project-stories/gaining-advantage-in-a-forensic-match-game
[o] https://www.nist.gov/system/files/documents/oles/7-Phillips_P-Jonathon-Challenges-in-Forensic-Face-Recognition.pdf
[p] https://www.radicati.com/wp/wp-content/uploads/2019/01/Mobile_Statistics_Report,_2019-2023_Executive_Summary.pdf

contain a wealth of data such as images, videos, locations of interest, etc., that in case of criminal acts, can constitute a lawful proof evidence. Even though there is not an official report on how often investigators are blocked by inaccessible mobile phones, in 2018, the Federal Bureau of Investigation (FBI) estimated that they recovered from crime scenes around 8000 locked smartphones for analysis[q]. Nearly 2,500 of these devices were inaccessible to security practitioners, hindering investigations e.g., into child sexual exploitation, financial crimes, theft, violence, terrorism and other crimes. During 2019, INTERPOL managed to achieve more than 1600 identifications, due to the increased exchange and matching of fingerprint biometrics provided by the member countries[r]. Searching and identifying a criminal across databases in a timely manner is crucial; when a child has been abducted, every minute is of paramount importance. The current state-of-the-art identification process requires (a) *several minutes* when the person is unknown through the automated process, (b) *an hour* through the semi-automated process when the person is registered in the database, and (c) *an hour* through the manual procedure when latent prints are retrieved from the crime scene. INTERPOL has clearly identified the need for a faster and more accurate matching of fingerprint and other biometric technologies. Furthermore, like any data, biometric data can fall into the wrong hands if not protected, and the potential for nefarious use is high. In the meantime, the upcoming Artificial Intelligence (AI) Act[s] will fundamentally change the way high-risk AI systems are being developed and placed in the market. Biometrics are strongly coupled with AI, while even the Act is not final, the draft contains multiple and specific clauses regarding the biometric data and technologies. The requirements for transparency under the AI Act also raise some thorny practical questions. How are the operators of a system in a public space, which could be any one of many law enforcement groups, supposed to notify all potential data subjects of the use of facial recognition or another remote biometric identification technology? According to the European Biometric Association, the impact of Europe's new artificial intelligence regulation on vendors and users of biometrics could be quite severe, and even determine the success or failure of some biometric technology providers in the years ahead.

To tackle the above-mentioned challenges, a holistic platform for the Law Enforcement Agencies (LEAs) is needed that facilitates the biometric evidence extraction, sharing and storage in cross border environments allowing them to share best practices in an automated, robust, secure, privacy-preserving and scalable manner. The full potential of biometric technologies can be then exploited along with their fusion in order to strengthen their acceptance in court, especially when partial evidence is gathered from the crime scenes. More particularly, novel tools for security practitioners should focus on (a) **Extraction of biometrics** and other **more or less distinctive features** that will assist LEAs in identification, identity verification, intelligence and investigation processes and can be leveraged to unlock criminals' mobile devices; (b) **Sharing of biometrics** through secure, scalable exchange of biometric intelligence and court-proof evidence among LEAs in a cross-border manner, enhancing the interoperability among legacy systems owned by security practitioners and Forensic Institutes; and (c) **Storage of biometrics** in a privacy-preserving way through a biometric data protection mechanism enabling revocability of biometric templates. In addition, there is also an imperative need to introduce a European Biometric Data Space creating a common ground among LEAs, Forensic Institutes and Security Researchers assisting in the faster adoption of modern biometric solutions. Biometrics technologies can derive lawful evidence from CCTVs (face, gait, voice), mobile devices (behavioural) and fingerprints combined with more or less distinctive features targeting accurate and multimodal identification along with criminal identity verification. Through novel blockchain mechanisms and smart contracts, a trusted environment can be created, equipped with self-learning capabilities, checking the integrity and identifying the mismatches and biometric anomalies of forensic evidence once shared among LEAs.

---

[q] https://www.pressreader.com/usa/usa-today-international-edition/20200213/281496458290144
[r] https://www.interpol.int/en/How-we-work/Forensics/Fingerprints
[s] https://eur-lex.europa.eu/legal-content/EN/TXT/?uri=CELEX%3A52021PC0206

3. PROPOSED SOLUTION

In this paper, a novel approach is proposed, aiming to unlock the potential of biometrics technologies towards combating crime and terrorism and safeguarding EU citizens. The developed trustworthy and legally compliant digital technologies will strengthen forensic intelligence and evidence collection through fusing multiple physiological and behavioural biometrics as well as facilitating the biometric data sharing among LEAs in a secure and scalable manner. The proposed technology solutions involve biometric data operations for data collection, access, processing and
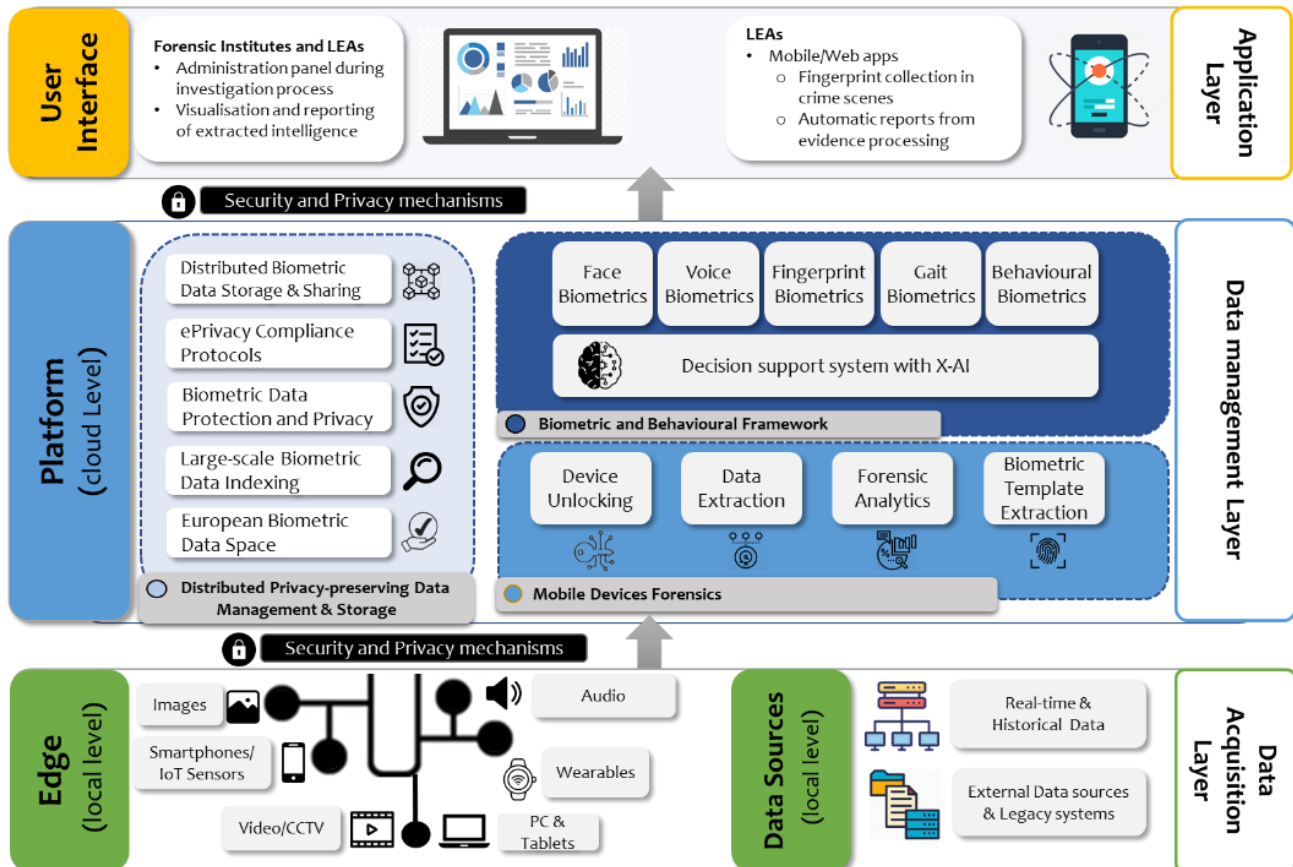
storage honouring compliance with prevailing and emerging legislation. The foreseen solution consists of several innovative technological components that provide biometric data extraction, analysis and sharing following with the derivation more or less distinctive features to empower the identification, identity verification, intelligence and investigation process for Forensic Institutes and LEAs. The core of the platform lies in the data acquisition, management and application layers, where biometric data can be extracted from multiple heterogeneous sources such as smartphones, IoT devices, wearables, audio, video, image etc. along with information stored in local level data spaces including legacy systems and IT operational systems, is processed, stored and shared among relevant security practitioners. Dedicated user-friendly interfaces connect the security practitioners with the data acquisition process and with the analysed biometric data and knowledge. The core of the platform is also based on the **Distributed Biometric Data Sharing Platform** that enables LEAs and Forensic Institutes to exchange biometric data and intelligence with integrity and accountability, leveraging state-of-the-art distributed (including energy efficient blockchain [Monrat et al., 2019]) and interoperable (Gaia-X and EOSC compliant) biometric data sharing mechanisms. External data sources are connected through the Gaia-X gateway while IDS Connectors are utilised to interconnect with distributed data storage such as Solid, ensuring data and system interoperability while allowing each Member State to keep the national biometric database following the existing paradigm (Prüm System). The European Biometric Data Space will ensure that all the Member States leverage a common standard in biometric data sharing, while allowing researchers to build upon existing

standards and speed up the path to commercialisation. To strengthen the security and privacy, the biometric templates will be stored and encrypted [A. Acar et al. 2018] through the Biometric Data Protection and Privacy module, which will enable the biometric templates to become revocable in case of a breach. The Large-scale Biometric Data Indexing provides efficient biometric data storage combined with intelligent searching mechanism [V. Talreja et al, 2021] to allow security practitioners perform fast identification and identity verification based on a biometric template [D. Zhong et al. 2019]. Security practitioners will have the ability to extract several types of biometrics as well as other more or less distinctive features that will assist in the identification, identity verification, intelligence derivation and investigation process. Various Physiological Biometrics will be collected, extracted, analysed and cross-correlated including Face and Person, Voice and Fingerprint Biometrics. Furthermore, Behavioural Biometrics will be inferred from video and IoT devices in order to understand the Gait, movement, device usage, app usage and transactional patterns. Additional less and more distinctive features will be extracted from each of the biometrics such as height, weight, age, gender, mark wearing etc. Investigation of explainable and reasonable AI methods that will be evaluated at hand of physiological and behavioural biometrics, will be fused through the Decision Support System to compensate the error of each individual biometric mechanism and create a multi-modal fusion of intelligence. Last, the security practitioners will have the ability to derive information from the Mobile Device Forensics tools including (a) the unlocking of mobile devices that are protected by biometrics or other means of authentication, the extraction of the data of the device, (b) in depth analysis of the content of the device with a single click of a button, (c) in some cases extract the biometric from the secure device storage.

4. CONCLUSION

This paper presents a high-level overview for a holistic solution that will assist LEAs and Forensic Institutes in extracting, sharing and storing biometric evidence in a technically robust and privacy preserving manner. Its innovation lies in the combination of the core components of the platform, exploiting the potential of behavioural and physiological biometrics and enabling the derivation of concrete and robust contextual evidence.

5. ACKNOWLEDGMENT

6. REFERENCES

A. A. Monrat, O. Schelén and K. Andersson, (2019). A Survey of Blockchain from the Perspectives of Applications, Challenges, and Opportunities, in IEEE Access, vol. 7, pp. 117134-117151, doi: 10.1109/ACCESS.2019.2936094.

Abbas Acar, Hidayet Aksu, A. Selcuk Uluagac, and Mauro Conti, (2018). A Survey on Homomorphic Encryption Schemes: Theory and Implementation. ACM Computing Surveys, 51, 4, Article 79, doi: 10.1145/3214303.

V. Talreja, M. C. Valenti and N. M. Nasrabadi, (2021). Deep Hashing for Secure Multimodal Biometrics," in IEEE Transactions on Information Forensics and Security, vol. 16, pp. 1306-1321, doi: 10.1109/TIFS.2020.3033189.

D. Zhong, H. Shao and X. Du, (2019). A Hand-Based Multi-Biometrics via Deep Hashing Network and Biometric Graph Matching, in IEEE Transactions on Information Forensics and Security, vol. 14, no. 12, pp. 3140-3150, Dec. 2019, doi: 10.1109/TIFS.2019.2912552.

ASSESSING THE POTENTIAL OF CONDUCTIVE TEXTILE MATERIALS FOR ELECTRONIC APPLICATIONS

Stavrakis, Adrian K.[1], Simić, Mitar[1], and Stojanović, Goran M.[1]

[1]Faculty of Technical Sciences, University of Novi Sad, Trg. Dositeja Obradovica 6, 21000, Novi Sad, Serbia
E-mail: sadrian@uns.ac.rs

1. INTRODUCTION

Flexible electronic devices have seen an interest rise in recent years, primarily owing to the popularity of wearables, and enabled by technologies and ecosystems such as the Internet of Things. However, the conventional lithographic processes are often incompatible with their fabrication process, for reasons such as rigidity, use of cytotoxic substances, user discomfort, or intolerance to frictions and tensions present in a wearable device. Therefore, the industry shifts to either printed electronics, such as through screen printing or jetting (Kadara *et al.*, 2008),(Kim *et al.*, 2015), or textile electronics to accommodate power transmission and element interconnects, which is primarily achieved through conductive textiles and yarns, or thin metallic microwires.

To date, there is a plethora of applications relying on conductive yarns and threads already showcased by various research groups, ranging from sensing (Wang *et al.*, 2021), and energy generation (Fan, Tian and Lin Wang, 2012) to antennas (Chauraya *et al.*, 2012), (Kapetanakis *et al.*, 2021).

Even though one of the most cost-effective processes for textile electronics is the utilization of conductive threads and computerized embroidery, the performance of off-the-shelf solutions still remains unverifiable to some extent, as the datasets provided by the manufacturers give a range of values per property, such as resistance of less than 200 Ohms/meter. Hence, this work aims to fill this void by subjecting conductive threads under electrical, thermal, and mechanical loading, both in terms of embroidery tensions, as well as during washing.

Our findings demonstrate that even though some performance degradation occurs, this is primarily translated as a resistance increase, which should be considered when designing a device that relies on detecting resistance changes and is caused by delamination of the plating outside the polymer core of the threads.

2. MATERIALS AND METHODS

For the planned experiments in this study, readily available silver-plated polyamide and polyamide/polyester hybrid threads were procured by AMANN Group (SilverTech 30, 50, 120 and SilverTech+ 100, 150) and Madeira (HC 12, HC 40)(AMANN Group, 2019) (MADEIRA Garnfabrik, 2019b) (MADEIRA Garnfabrik, 2019a). The studied items correspond to 80 % and 100 % of the respective conductive thread product catalog of the two manufacturers.

For both the electrical and thermal characterization steps, a custom holder was designed in order to accommodate the suspension of a 1 cm specimen, connected to the onward system via crocodile clips and copper wiring. The rest of the circuit comprises of a voltage divider topology, where the specimen acts as one of the two parts, and monitoring instruments; namely an ammeter connected in series between the two resistors of the divider and a voltmeter connected in parallel to the specimen. Lastly, a programmable DC source was utilized. The reason for selecting this topology is that given the fact that the absolute maxima in terms of voltage and power are under investigation, it provides a reliable approach to measure both of them continuously, until the total breakdown.

Twenty-five specimens were examined per thread, under two conditions: firstly, a constant

increase in voltage at a rate of 0.1 V/s was applied until total breakdown, and secondly the same increase rate was used, but the voltage was sustained for 60 s at every step, until total breakdown. The aim was to infer whether an instantaneous increase in voltage, which translates at a higher power, can be tolerated at a higher value rather than a constant high voltage, which is an effective simulation of an electrical fault.

Consequently, for five specimens per thread, and for a voltage set at the average maximum value observed at the continuous step, the amount of time elapsed before failure was measured, while simultaneously the specimens were targeted by a thermal camera to observe their temperature profile.

In the tensile characterization step, fifty specimens of 25 cm were inserted into a tension testing system (34SC-2, Instron, Norwood, USA) which was programmed to elongate them until break at a constant displacement rate, in line with the provisions of the ISO 2062 standard. After the mean force and elongation at break were established, ten more specimens of each thread were subjected to a cyclic loading test, which elongated them to the point of 90 % of the mean break force and then released them to the point of zero displacement for 100 cycles. Moreover, more specimens were loosely embroidered on a piece of cotton fabric, in order to undergo a repeated washability test for 10 rounds. The embroidery was facilitated by digitizing stitches from a .dxf file created in AutoCAD 2023, utilizing a proprietary software by ZSK. A jump stitch was selected, in order to cause the least possible damage to the threads at the embroidery step, and at the same time to allow for their release from the fabric post-wash. The stitch machine code was then transferred on an industrial embroidery machine (JCZA 0109-550, ZSK, Krefeld, Germany).

For further characterization, samples of all stages were then examined under a Scanning Electron Microscope (TM3030, Hitachi, Tokyo, Japan).

3. RESULTS AND DISCUSSION

After the electrical loading of the studied threads, in terms of the thread resistance, it can be seen that the manufacturer values are significantly lower than the measured ones (Fig. 1). That, in conjunction with the visual inspection of the threads, can be attributed to partial delamination (shedding) of the silver conductive threads (Fig, 2a). In addition to that, as expected, the instantaneous voltage increase allowed for a slightly higher power before failure, which is also in line with common wire conductors. Lastly, from the transient analysis it can be seen that the HC 12 is remarkably stable compared to the rest of the group, with only slight variation, while the HC 40 is exhibiting a significantly different behavior. As it is the thickest of the tested threads, this can potentially be attributed to a combination of gradual failure of the material and increased catenary gravitational forces pulling it towards the ground due to its increased weight. A general thread constriction before failure was observed by the thermal camera across all specimens, which unilaterally caused them to shrink lengthwise before their failure, to different extents.
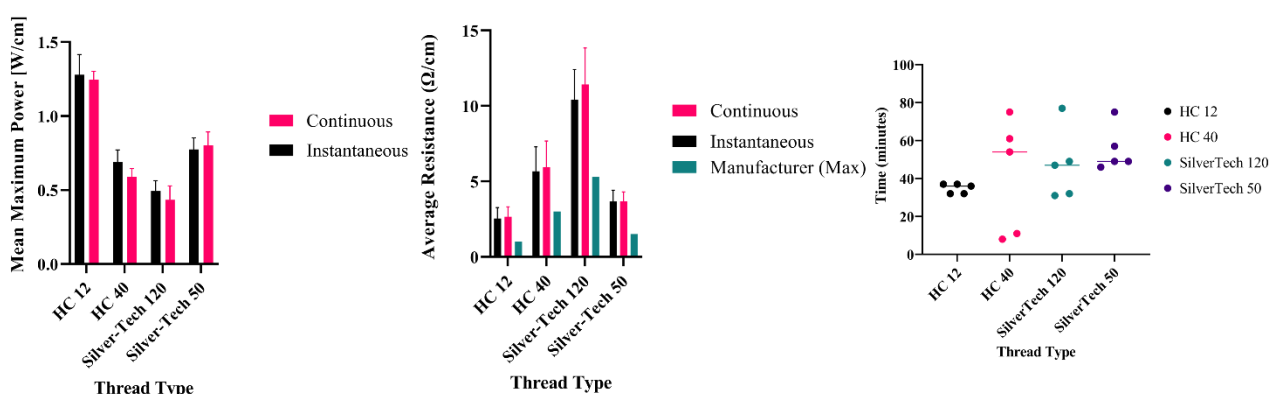

Fig. 1: Average Power, Resistance, and Time Before Failure per thread

It can also be observed from the SEM analysis (Fig. 2), that the breakdown between the two cases is different. In the first case, a distinct failure point can be seen, while in the second we observe black spots coming out of the spun fibers, which seem to have joined together. As it is a SEM image, the black material is in reality molten plastic from the fiber cores. This observation concurs with the thermal camera observations of a shortening of the material before failure, as the sample in Fig. 2c is significantly narrower and straighter than the other two cases, denoting that the material started to escape from the molten core until the silver could not be further supported and the conductivity stopped because the continuity was severed.
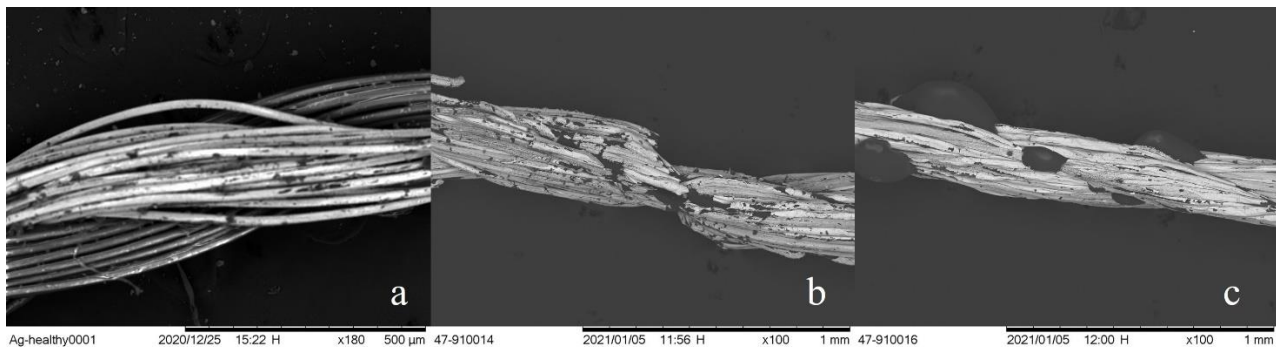
Fig. 2: SEM images of a healthy specimen (a), a failed specimen under instantaneous load increase (b) and under sustained increased voltage levels (c)

From the tension testing and washability testing, there are three main observations that can be deduced. Firstly, the threads observed a significant delamination after the break test (Fig. 3a). Even though that can be justified by the tensioning effects which cause a radial shortening and lengthwise elongation of the thread, this is present to a lesser extent even in healthy (untested) specimens (Fig. 2a). However, in the case of the cyclic load test, there is another structural defect that starts to manifest, and that is the presence of microfractures, as seen in Fig. 3b. Even though the first effect did not generally impact the continuity of the conductive material as it is highly localized, in this case it can be observed that the ripples reach the inner polymer cores, denoted by the change in color in the SEM images throughout the specimen. Moreover, most of the conductive material thickness is lost, with only minuscule pieces retaining the full plating, as seen inside the highlighted oval area.
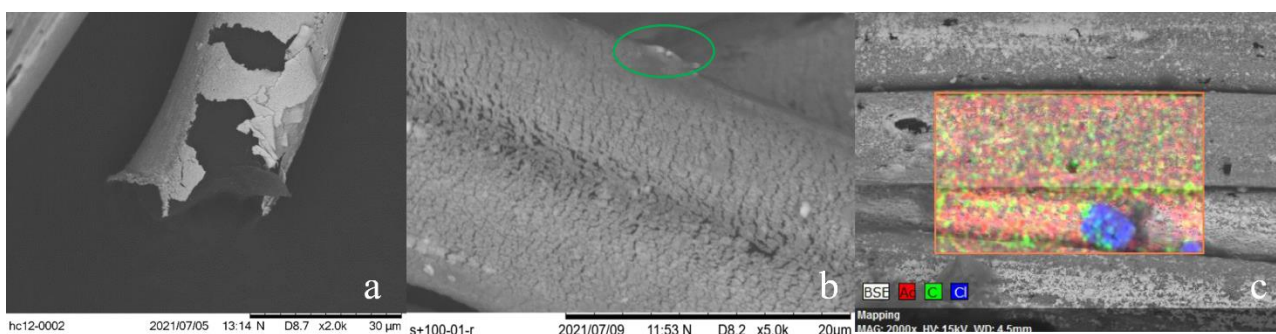
Fig. 3: SEM images of threads after breaking test (a), cyclic test (b) and washing, with an overlay of EDS (c)

Lastly, washability of the material seems to be guaranteed by the fact that there are no significant deposits of foreign elements either from the water or the cleaning products, with the exception of traces of chlorine, as verified by Energy Dispersive Spectroscopy (Fig. 3c). The conductive material can be seen scuffed albeit the thread resistance only marginally changed across the ten cycles (Fig. 4), which leads to the conclusion that this is mostly a surface effect and does not penetrate deep to the fiber cores.

Resistance Change vs Washing Cycles
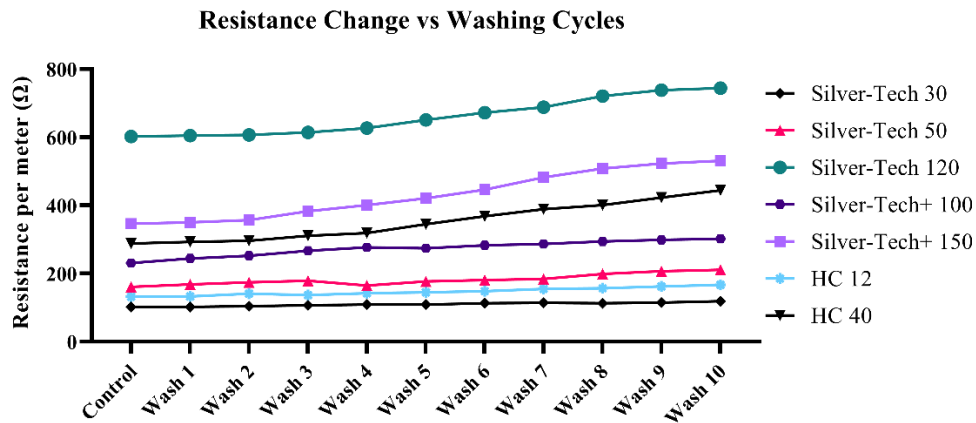
Fig. 4: Average change in resistance per thread type and per wash cycle

4. CONCLUSION

Conductive threads are a relatively cost-effective material that allows for the substitution of traditional wires for wearable applications with a satisfactory performance stability. Even though our findings demonstrate that after being subject to mechanical stresses a portion of the metal coating of the fibres tends to shed and detach, the overall performance degradation stabilizes.

Another observation was the fact that due to the nature of the material, namely multiple strings of fibres spun together, a current flow leads to a significantly increased temperature on the internal part of the thread due to ohmic heating, owing to lack of exposure to ambient air and convective heat transfer. This should be accounted for in the design stage, as it might lead to material failure, and adverse effects for the wearer, ranging from discomfort to skin burns.

Lastly, even though repeated washing does not significantly affect the metal plating of the threads, it leads them to become slightly stiffer, potentially due to intrinsic stresses modification during the wash cycles. Therefore, contrary to conventional electronics design which relies heavily on topological optimizations, textile electronics design should consider the wearer experience and modify the design to accommodate that, rather than being driven by the geometry.

5. ACKNOWLEDGMENT

6. REFERENCES

AMANN Group (2019) *AMANN TechX Brochure*. Available at: https://www.amann.com/fileadmin/user_upload/AMANN_TechX_Brochure_EN.pdf (Accessed: 9 September 2022).

Chauraya, A. *et al.* (2012) 'Addressing the challenges of fabricating microwave antennas using conductive threads', in *2012 6th European Conference on Antennas and Propagation (EUCAP)*. *2012 6th European Conference on Antennas and Propagation (EuCAP)*, Prague, Czech Republic: IEEE, pp. 1365–1367. Available at: https://doi.org/10.1109/EuCAP.2012.6205910.

Fan, F.-R., Tian, Z.-Q. and Lin Wang, Z. (2012) 'Flexible triboelectric generator', *Nano Energy*, 1(2), pp. 328–334. Available at: https://doi.org/10.1016/j.nanoen.2012.01.004.

Kadara, R.O. *et al.* (2008) 'Manufacturing electrochemical platforms: Direct-write dispensing versus screen printing', *Electrochemistry Communications*, 10(10), pp. 1517–1519. Available at: https://doi.org/10.1016/j.elecom.2008.08.002.

Kapetanakis, T.N. *et al.* (2021) 'Embroidered Bow-Tie Wearable Antenna for the 868 and 915 MHz ISM Bands', *Electronics*, 10(16), p. 1983. Available at: https://doi.org/10.3390/electronics10161983.

Kim, J. *et al.* (2015) 'Wearable temporary tattoo sensor for real-time trace metal monitoring in human sweat', *Electrochemistry Communications*, 51, pp. 41–45. Available at: https://doi.org/10.1016/j.elecom.2014.11.024.

MADEIRA Garnfabrik (2019a) *Technical Datasheet HC 12*. Available at: https://www.madeira.com/embroidery-solutions/embroidery-supplies/industrial-embroidery-threads/technical-threads/high-conductive-threads (Accessed: 9 September 2022).

MADEIRA Garnfabrik (2019b) *Technical Datasheet HC 40*. Available at: https://www.madeira.com/embroidery-solutions/embroidery-supplies/industrial-embroidery-threads/technical-threads/high-conductive-threads (Accessed: 9 September 2022).

Wang, R. *et al.* (2021) 'Stretchable gold fiber-based wearable textile electrochemical biosensor for lactate monitoring in sweat', *Talanta*, 222, p. 121484. Available at: https://doi.org/10.1016/j.talanta.2020.121484.

MAGNETIZATION STUDY OF A FCC COBALT BASED MATERIAL UNDER THE EXISTENCE OF THE EARTH MAGNETIC FIELD

Barmpatza, A.*, Baklezos, A., Vardiambasis, I., and Nikolopoulos, C.*

Laboratory of Telecommunications and Electromagnetic Applications,
Department of Electronic Engineering, School of Engineering,
Hellenic Mediterranean University
* abarmpatza@hmu.gr; cnikolo@hmu.gr

1. INTRODUCTION

Magnetic nanoparticle are very important materials that can be used in many industrial and scientific fields like the drug delivery and anticancer (Racca & Cauda, 2021), the molecular imaging (Yao & Xu, 2014), the catalysis (Govan & Gun'ko, 2014; Zhang et al., 2019), the food industry (Singh et al., 2017), the agriculture (Neme et al., 2021) etc. Due to the fact that magnetic nanoparticles are useful in many applications, the scientific community needs to know their properties and to obtain simple, economical and robust tools for their characterization.

In this work, the authors try to identify various parameters that affect the ferromagnetic nanoparticles' magnetization in order to provide the chemical engineers with the necessary information for catalytic sample structure and thus its production process. Consequently, this work is a preliminary step of nanoparticle material characterization procedure.

2. MATERIALS AND METHODS

The under-investigation nanoparticle material is a sample with 20% wt cobalt content and a Face Centered Cubic (FCC) formation. The material has a weight of 11.19 gr, is embedded on wax, while its saturation magnetization (M_S) equals to 168 emu/gr. The study was achieved with the Magpar tool, which is a software that enables micromagnetic simulation and analysis. However, before the FEM analysis every under analysis case was designed and meshed with the Gid software, because the Magpar software gives the opportunity to design only predetermined geometries. The specific material properties are introduced in the program using .log files and namely the magneto-crystalline anisotropy constant (K), was determined to be equal to 2.7×10^5 J/m^3, while the exchange constant (A) was determined to be equal to $A = 1.3 \times 10^{-11}$ J/m.

3. RESULTS AND DISCUSSION

As aforesaid, in this article a nanoparticle sample based on cobalt is studied. More specifically, the magnetization behavior of this sample is investigated when the terrestrial magnetic field is applied. For the investigation the hysteresis loops of the nanoparticle sample are exported and compared for two different cases. In both cases the total volume of the material is retained constant and two phenomenon are studied. The first phenomenon concerns the influence of the nanoparticles number, provided the total sample mass will be retained invariable. The sample is simulated with different number of spheres and the corresponding hysteresis loops are compared. The second phenomenon concerns the impact of the distance among the nanoparticles. The total sample was depicted as two spheres and different distance between these two spheres are taken into account. For the study the Finite Element Method (FEM) is utilized and the hysteresis loops in every investigated case are exported.

From the analysis it is revealed that when the changes the number of simulated nanoparticles the magnetization of the sample, in the region of terrestrial magnetic field, remains approximately constant, as seen also in Table 1. Contrary, when changes the distance between the spheres the magnetization under the existence of the terrestrial magnetic field changes. Observing Table 2, it can be concluded that as higher is the distance among the particles, as lower is the magnetization of the sample.

Table 1. Magnetization of nanoparticle sample when the number of simulated spheres is changing.

NUMBER OF SPHERES	VALUE OF MAGNETIZATION
Two	4.44 emu/gr
Six	4.99 emu/gr
One Hundred	4.91 emu/gr

Table 2. Magnetization of nanoparticle sample when the distance among the spheres is changing.

DISTANCE AMONG THE SPHERES	VALUE OF MAGNETIZATION
10 mm	0.34 emu/gr
100 nm	2.79 emu/gr
10 nm	4.91 emu/gr

4. CONCLUSION

In summary, the study examines the magnetization of FCC nanoparticle material which contains cobalt, when the magnetic field of the earth is applied. The FEM is used for the analysis, while the hysteresis loops are studied and more specifically the part of the hysteresis loop that is close to the terrestrial magnetic field. It can be assumed that the magnetization under this magnetic field does not change due to the number of simulated spheres, but changes due to the distance among the spheres. These assumptions are important for chemical engineers in order to obtain information about the properties of the catalytic nanoparticle materials.

5. ACKNOWLEDGMENTS

6. REFERENCES

Govan, J., and Gun'ko, Y.K. (2014). Recent advances in the application of magnetic nanoparticles as a support for homogeneous catalysts. *Nanomaterials 4*(2): 222–241. doi: 10.3390/nano4020222

Neme, K., Nafady, A., Uddin, S., & Tola, Y. B. (2021). Application of nanotechnology in agriculture, postharvest loss reduction and food processing: food security implication and challenges. *Heliyon*, *7*(12), e08539. doi: 10.1016/j.heliyon.2021.e08539

Racca, L., and Cauda V. (2021). Remotely activated nanoparticles for anticancer therapy. *Nano-Micro Letters* 13(1). doi.org/10.1007/s40820-020-00537-8

Singh, T., Shukla S., Kumar P., Wahla V., and Bajpai V.K. (2017). Application of nanotechnology in food science: Perception and overview. *Frontiers in Microbiology 8*: 1–7. doi: 10.3389/fmicb.2017.01501

Yao, L., and Xu S. (2014). Detection of magnetic nanomaterials in molecular imaging and diagnosis applications. *Nanotechnology Reviews*, *3*(3): 247–268. doi: 10.1515/ntrev-2013-0044

Zhang, Q., Yang X., and Guan J. (2019). Applications of magnetic nanomaterials in heterogeneous catalysis. *ACS Applied Nano Materials 2*(8): 4681–4697. doi: 10.1021/acsanm.9b00976

POLY (3-HEXYLTHIOPHENE)-BASED TRANSISTORS USING IONIC LIQUID DROPLETS AS THE GATE DIELECTRIC

I. Marinakis*, E. Kapetanakis

Department of Electronic Engineering, Hellenic Mediterranean University, 73133, Chania, Greece.
E-mail: ddk71@edu.hmu.gr

1. INTRODUCTION

Liquid-gated organic transistors (LGTs) have attracted considerable attention due to their reduced fabrication time, low cost, low operating voltage and potential use in several applications, such as ultrasensitive sensors for in loco diagnosis (e.g., for the detection of biomarkers, ions, and molecular analytes as well as for the transduction of bioelectrical signals). The gate dielectric in these devices is immersed in a liquid phase, typically an aqueous electrolytic solution; application of a gate potential (V_{GS}) results in the buildup of two electrical double layers (EDLs), at the gate/electrolyte and electrolyte/active material interfaces, which are responsible of charge modulation in the semiconductive organic layer and of the subsequent change of the source–drain current (I_{DS}). Amongst a variety of aqueous dielectric layers used as LGTs, ionic liquids (ILs) is a promising materials for this application because of their excellent electrochemical properties such as wide electrochemical window and good electrical conductivity along with high thermal stability.

In the current presentation the electrical performance of IL-gate poly (3-hexylthiophene) (P3HT) organic thin-film transistors (OTFTs) are studied using 1-butyl-3-methylimidazolium tricyanomethanide [BMIM][TCM] droplets as the gate dielectric and tungsten (W) probe as gate electrode. Device operation is examined as a function of the following two processing parameters: (1) the introduction or not of a thin PMMA film at the P3HT/IL-droplet interface and (2) the thickness of the P3HT layer. The first parameter relates to P3HT/IL-droplet and P3HT/PMMA/IL-droplet stacks where for the latter, the P3HT/PMMA films are annealed in a single step after their successive deposition. Here, motivation in using an additional PMMA film is threefold: (a) to protect P3HT against oxidation, especially during the post-deposition annealing step which favors such a reaction, (b) to prevent IL-droplet/P3HT interface mixing that could cause interfacial electrochemical doping and, (c) to avoid anion penetration into the P3HT during transistor operation and thereby, possible bulk electrochemical doping. Modulation of the channel current is examined as a function of the applied V_{GS} sweep rate, introduction or not of a thin PMMA barrier and P3HT thickness for getting more insight into device operation and the issue of whether electrochemical doping occurs in the bulk of the P3HT (Figure 2). Also, the hysteresis in the transfer characteristics, the effect of charging (under constant negative V_{GS}) and discharging ($V_{GS}=0V$) of the EDL layer on the channel current (and the gate leakage current) and the response of IL-gate P3HT transistors to square voltage waveform at the gate terminal are studied. Our measurements show that On current (I_{ON}) in [BMIM][TCM]-gated P3HT transistors, with constant active layer thickness, increases with introduction of a thin PMMA film at the P3HT/IL-droplet interface. This increase of I_{ON} may relates in hole mobility enhancement in these transistors.

2. MATERIALS AND METHODS

Materials: Regio regular poly (3-hexylthiophene-2,5-diyl) (P3HT) with regioregularity = 97.6% and Mn = 60000-110000 (Ossila Ltd) were used as bought without further purification or treatment. Poly(methyl methacrylate) (PMMA) with 996000 molecular weight was purchased from Sigma-Aldrich. The following solvents have been used for dielectric and semiconductor formulations: methyl isobutyl ketone (MIBK, Sigma-Aldrich), chloroform ($CHCl_3$, Merck). Hexamethyldisilazane (HMDS) and Hellmanex® III were purchased from Microchemicals and Ossila, respectively.

Device Fabrication: The source-drain (S-D) electrodes were made of ITO materials physical layouts. ITO (100nm-thick) S/D electrodes patterned on 1.5x2cm^2 glass samples with a 20nm-thick SiO$_2$ coating on top were obtained from Ossila Ltd. They consist of interdigitated fingers (see Fig. 1(a) with channel length L=50µm and channel width W=30mm. Cleaning of the samples was carried out by (a) successive sonication in acetone and isopropanol, rinsing in 25°C deionized (DI) water and nitrogen blow-drying and (b) sonication in hot (60°C) 10% NaOH for 5 min/rinsing in 25°C DI water / sonication in hot (60°C) 2% Hellmanex for 5 min / rinsing in 50°C DI water / sonication in 50°C IPA for 5 min/rinsing in 50°C DI water/nitrogen blow-drying. Next, HMDS was spin-coated on the substrates at 2000 rpm for 30s prior to deposition of the P3HT materials. Before HMDS treatment, the samples were exposed to an oxygen plasma to modify the Work Function of the S-D electrodes. Then, P3HT dissolved in chloroform at 5mg ml^{-1} concentration was spin-coated on the substrates. The resulting 20 nm (5 mg ml^{-1} concentration, 4000 rpm), 50 nm (5 mg ml^{-1}, 1000 rpm) thick P3HT layers were used for the devices examined in this study. A thermal treatment under ambient conditions for 5 min on a hotplate set to a temperature of 130°C was applied after P3HT deposition. Each sample contain five devices.

(a)   (b)

(c)   (d)
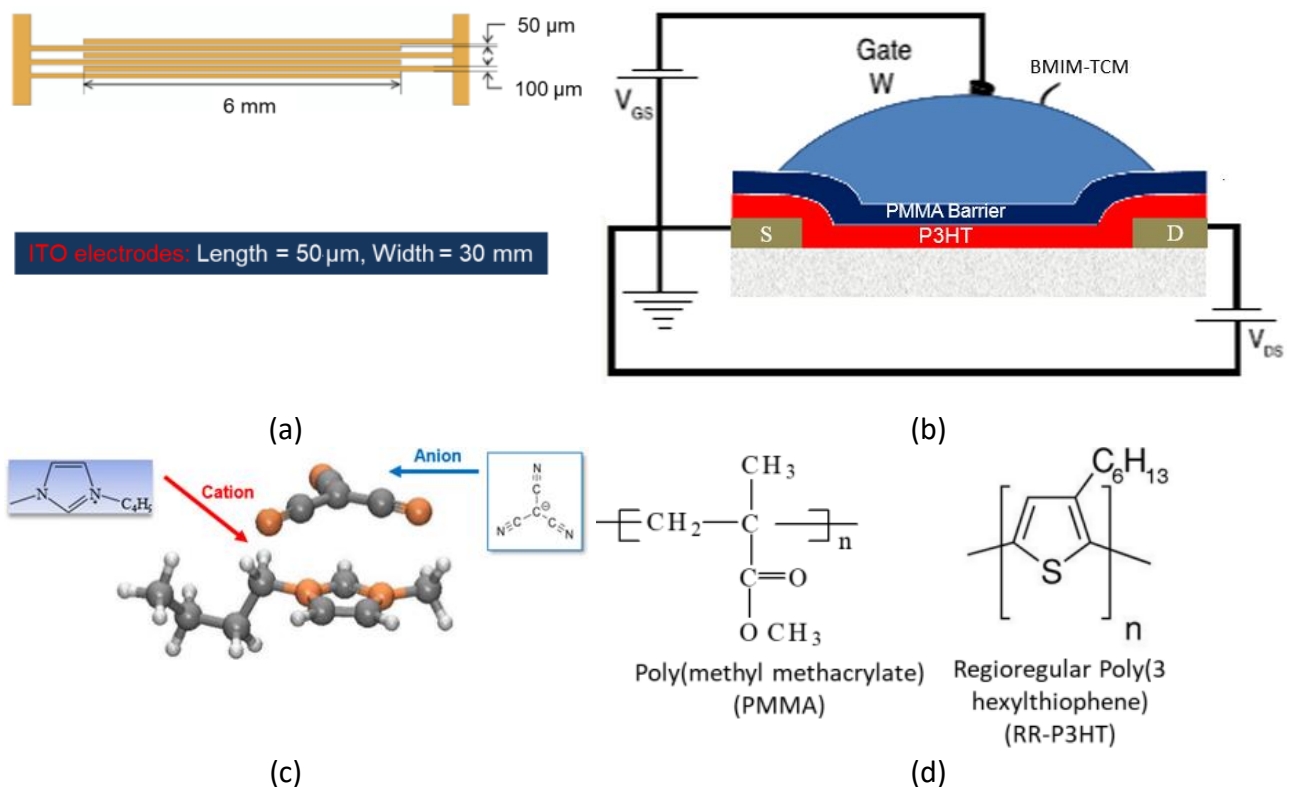
Figure 1: (a),(b) Schematic drawing of source (S) and drain (D) in top-bottom gate contact p-type OFETs considered in this study. The two conductive contacts are formed on a glass substrate (SiO$_2$). (a) Indium tin oxide (ITO, 100 nm thick) dipstick electrodes. (b) Schematic cross-section of top-bottom gate p-junction type OFETs. The S and D electrodes are composed of ITO materials. The thickness of the spin-coated semiconductor material (peripheral P3HT) is in the range of 15-110nm. Then, a 20 nm thick PMMA film was formed on top of the P3HT layer. The gate dielectric consists of a drop of Ionic liquid (electrolyte) [BMIM][TCM]. (c) Chemical structure of the cation–anion of [BMIM][TCM] [2]. (d) Chemical structure of PMMA and P3HT [1].

Electrical characterization: The electrical characterizations of the devices were performed with a probe station connected to a Keysight B2912A Source/Measure unit and the electrical contacts were ensured by three micromanipulators. The measurements were performed in the common source (see Fig. 1b) configuration and the transistors operated in the linear regime and saturation region.

All measurements were performed at room-temperature in dark conditions.

3. RESULTS AND DISCUSSION

In the figures below (Figure 2) the Transfer characteristics are compared in terms of the sweep rate of the V_{GS} voltage, for two different thicknesses of P3HT, in the linear operation of the transistors. Both in the case without the PMMA film and when the film is present.


(a)   (b)
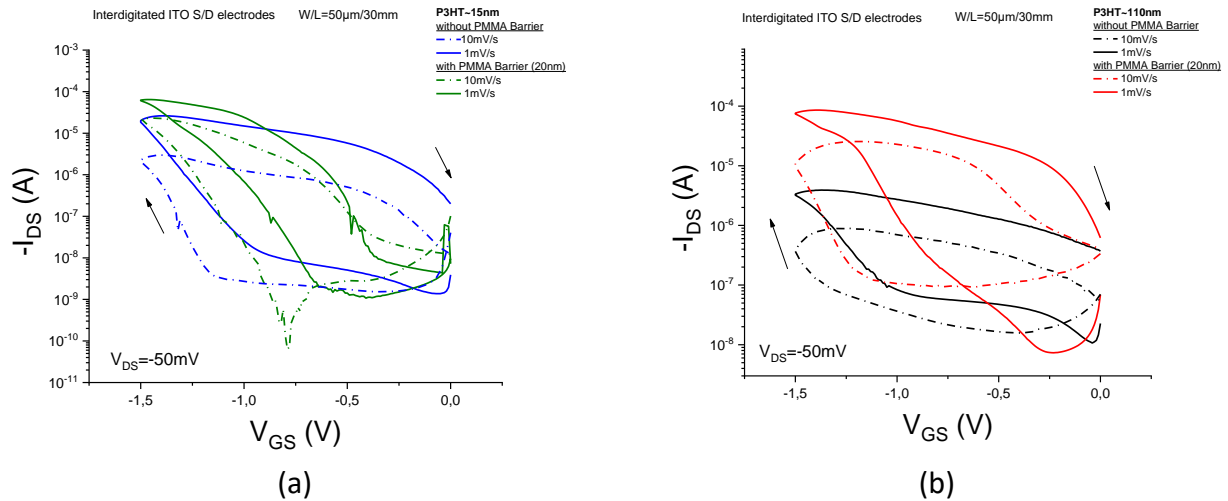
Figure 2: Characteristic transfer curves in linear mode and in saturation for two different sweep rates of the V_{GS} voltage. (a) Case, micro-thick P3HT~15nm with and without PMMA. (b) Large thickness P3HT~110nm. Due to the low ion mobility of the ionic liquid at the lowest scan rate (1 mV/s) a higher drain current (I_{DS}) occurs.

(a)   (b)
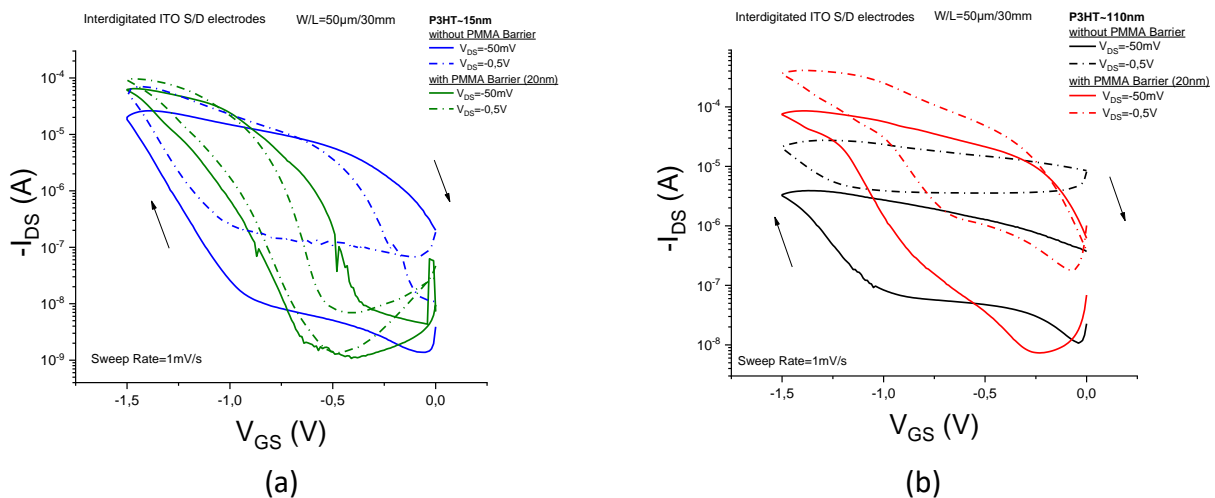
Figure 3: In both semiconductor thicknesses, in the case where there is a PMMA layer, a higher Drain current (I_{DS}) and a lower hysteresis occur. Sweep rate of voltage V_{GS}, 1mV/s.

In the previous figures (Fig.3) it can be seen that the transistors with the PMMA film show a higher drain current in the linear region and in the saturation region. Below, the difference of gate and drain currents is compared. The gate current is smaller by about three orders of magnitude compared to the drain current (I_{DS}). In the case where the PMMA film is present, the I_{GS} current increases slightly possibly due to fewer charge traps at the P3HT interface. (Fig. 4).

(a)

(b)
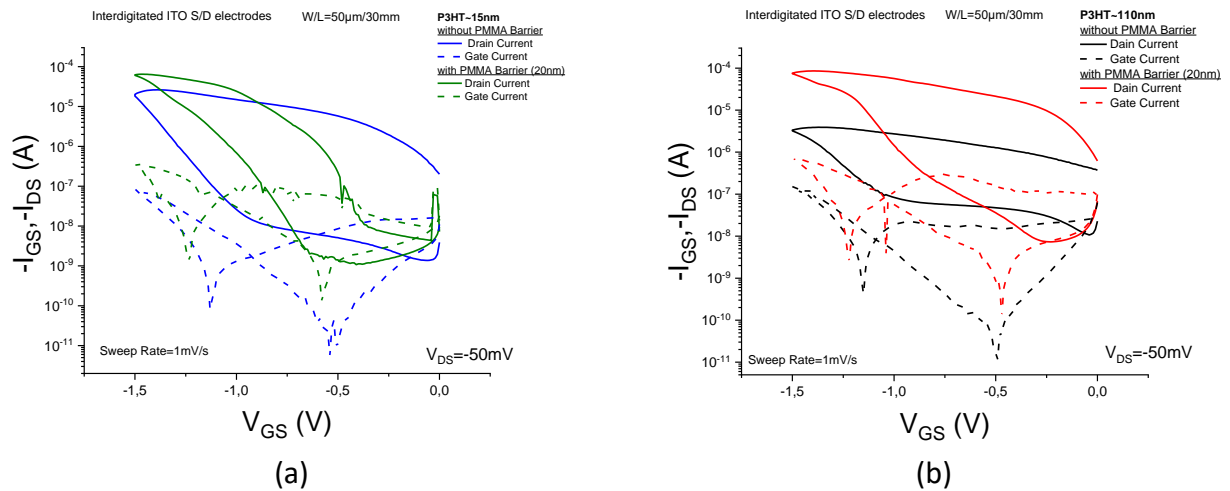
Figure 4: Comparison of the characteristic Transfer curves in the linear region. (a) for thicknesses of P3HT~15nm and (b) for corresponding thicknesses of 110nm. Sweep rate of voltage V_{GS}, 1mV/s.

The figures below show the response of the used transistors in terms of time (Fig. 5a,b) by applying to the gate terminal a square wave of amplitude 1.5V of period 700 seconds. A -1.5 V square pulse lasting 700 seconds is applied to the gate electrode while a constant -0.5V voltage is applied to the drain.

As it works, packets are repeated. In the case where the PMMA film is present, the current in the conductor is larger, while when the PMMA is not present, the I_{DS} current is smaller. Also, with PMMA the transistor responds faster. Finally, these figures show that the transistors used can be reused.


(a)

(b)
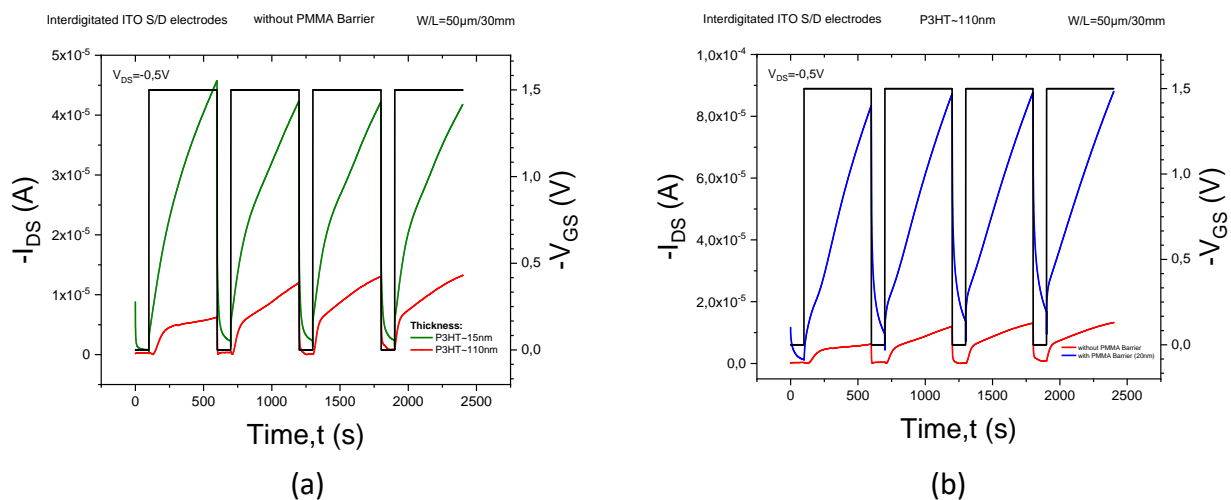
Figure 5: (a) Comparison of two different thicknesses of P3HT without PMMA. In the thicker layer the I_{DS} current is smaller due to the larger contact resistance (bulk resistor). (b) Comparison of I_{DS} currents for the same semiconductor thickness. When the PMMA is present, the current is greater.

Figure 6(a) shows the state of charge of the transistors used, applying a constant voltage of -1.5V to the gate terminal while a pulsed voltage of -50mV/0.2s is applied to the drain electrode, measuring the gate and drain current with time. In all semiconductor thicknesses the maximum I_{DS} currents reach approximately the same maximum value. While Figure 6(b) shows the discharge state of the transistors when no voltage is applied to the gate.

(a)   (b)
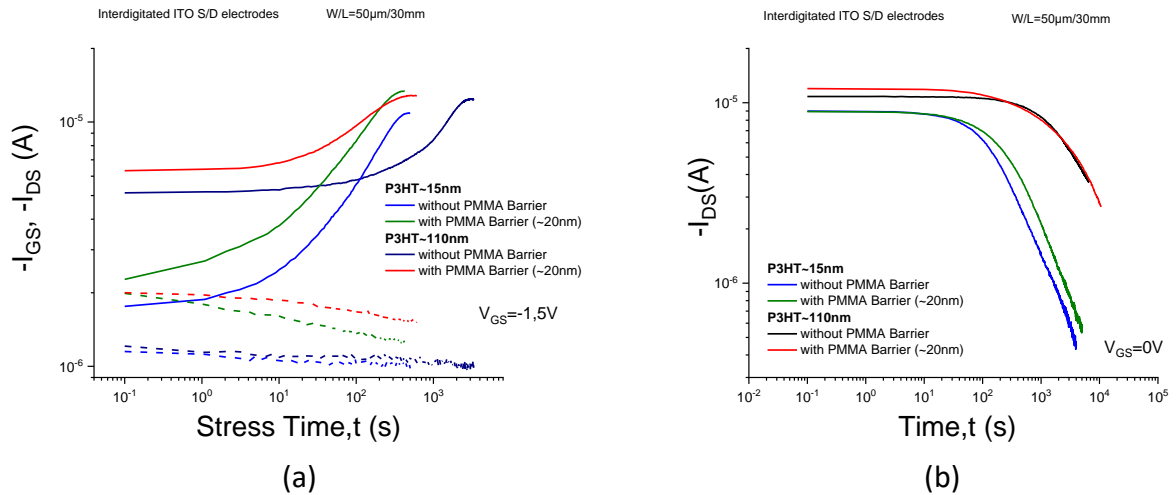
Figure 6: Logarithmic scale I_{DS}-t characteristics (a) When charging the devices used in the two thicknesses of P3HT with or without PMMA under constant gate voltage V_{GS}=- 1.5V. At greater thickness the charging time is longer due to the contact resistance (b) At discharge when there is no gate voltage.
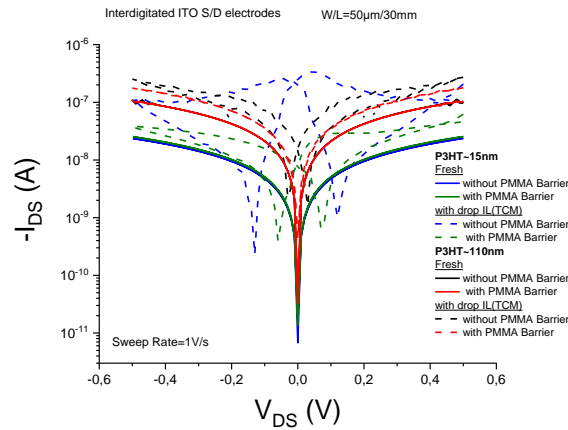

Figure 7: Characteristic I_{DS}–V_{DS} of two terminals before and after the addition of the ionic liquid [BMIM][TCM]. After the addition of ionic liquid, the conductivity of P3HT increases because the IL droplet can induce more electric carriers into the semiconductor. When the thin PMMA film is not present, a longer hysteresis is observed after the addition of the liquid due to more charge traps that are created during the exposure of P3HT to the environment.

View parameters of LGTs used

From the characteristic Transfer curves (Fig.3) the corresponding Transconductance characteristics (g_m) were calculated from the mathematical equation (Figure 8):

$$g_m = \frac{\partial(I_{DS})}{\partial(V_{GS})}$$

From the characteristic transfer curves of the linear region and saturation, the most basic parameters are calculated (Figure 9).

(a)

(b)
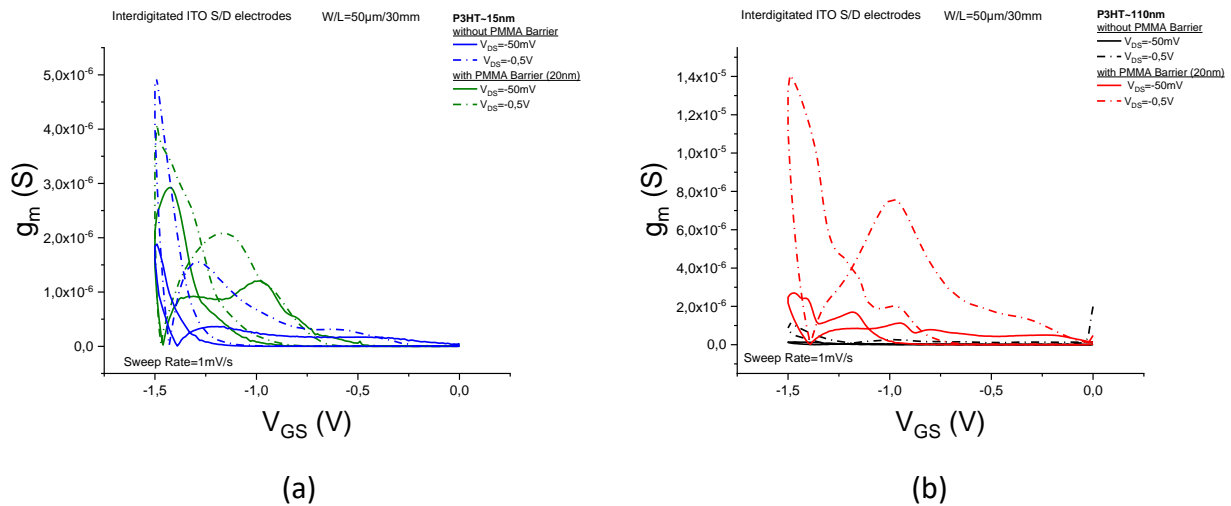
Figure 8: Transconductance characteristic curves in linear mode and in saturation with V_{GS} voltage sweep rate, 1mV/s. (a) Case, thin P3HT~15nm thickness with and without PMMA. (b) Large thickness P3HT~110nm with and without PMMA respectively.

(a)

(b)

(c)

(d)
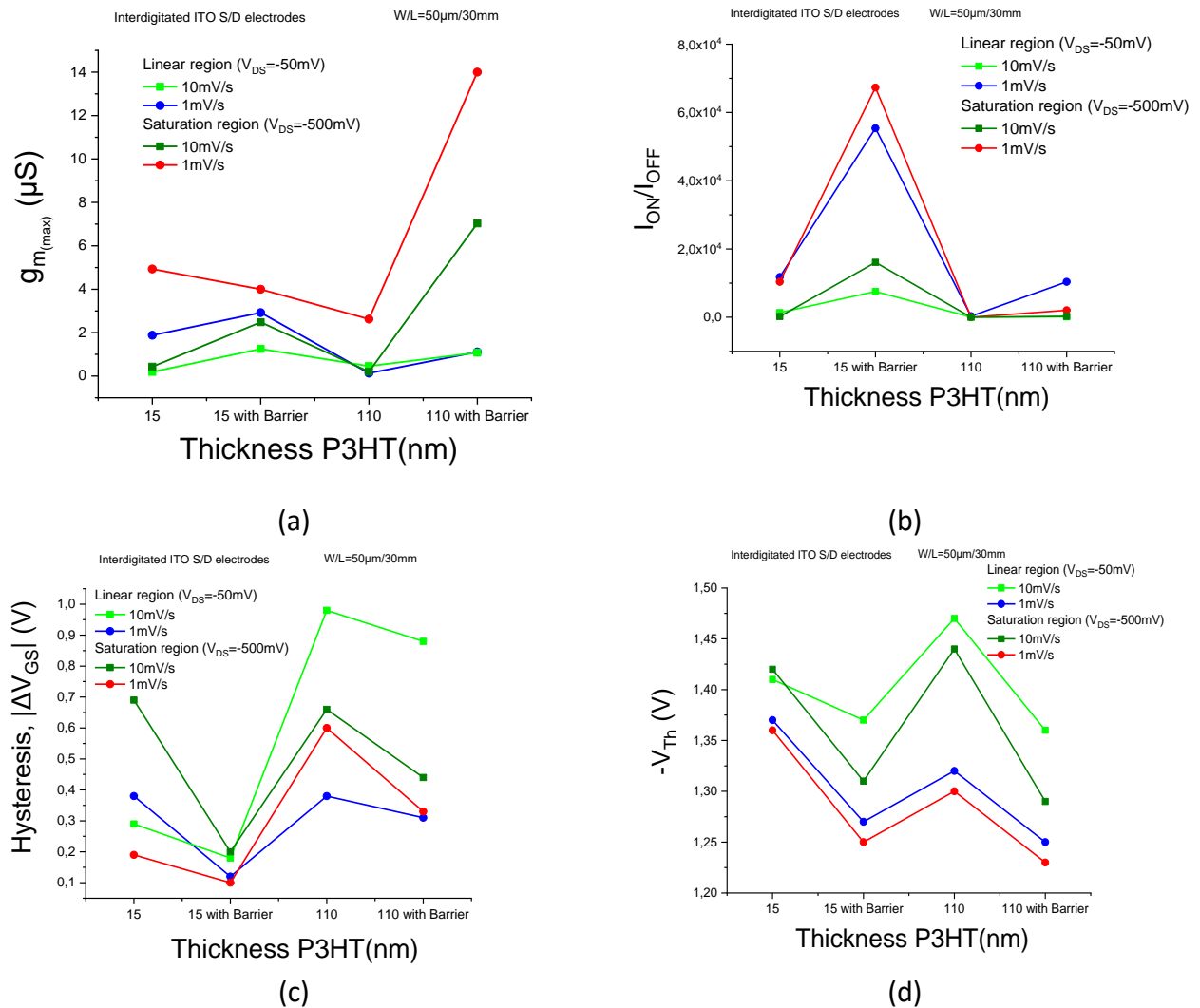
Figure 9: (a) Comparison of Transconductance curves of LGTs with and without PMMA film, in the Linear regime and in the saturation regime. (b) On/Off current ratio. Transistor performance is better with slow gate voltage sweep rate as well as when thin PMMA film is present. (c) Calculation of hysteresis. The hysteresis is mainly due to P3HT charge traps and gate liquid dielectric impurities. (d) At larger thicknesses, Threshold voltage (V_{Th}) increase where they decrease when PMMA film is present. The values of V_{Th} were calculated using the Constant Current method.

Observations

Applying a negative gate voltage causes the anions to move towards the P3HT interface, inducing polarons (holes) in the semiconductor. This results in the discoloration of the semiconductor (whitening) (Fig. 10).

(a)

(b)

(c)

(d)

(e)

(f)
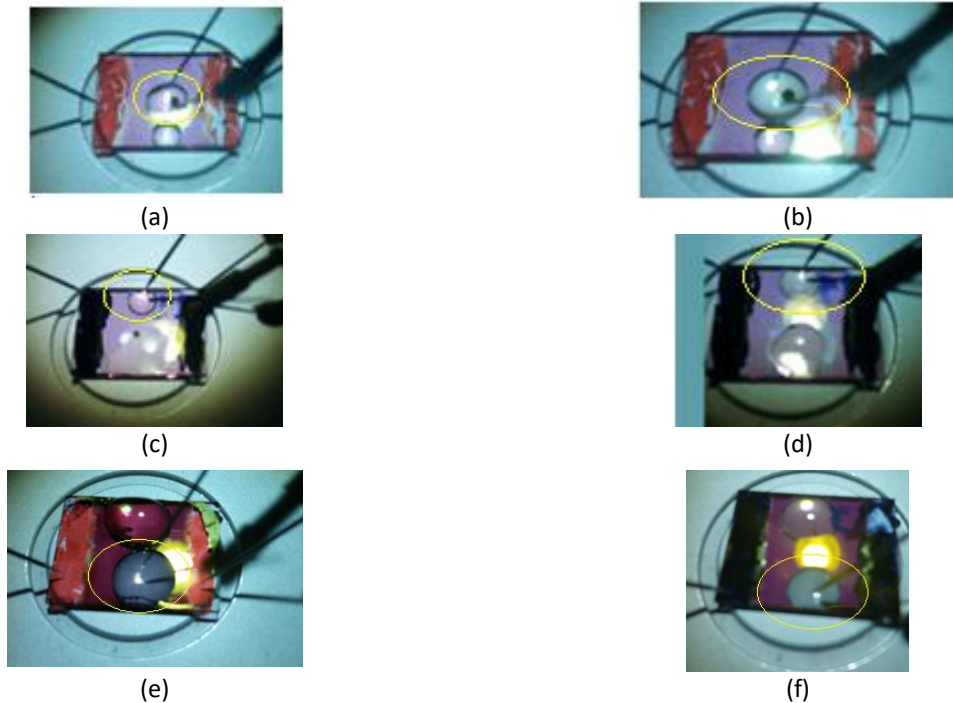
Figure 10: Discoloration of the P3HT surface enclosed by the Ionic Liquid droplet, after -1.5V gate voltage stress. (a) P3HT~15nm without PMMA, before stress. (b) After stress -1.5V. (c) P3HT~15nm with PMMA barrier before stress. (d) after stress voltage -1.5V. (e) P3HT~110nm without PMMA after gate biasing -1.5V. (f) P3HT~110nm with PMMA after -1.5V stress voltage.

4. CONCLUSION

Our measurements show that the (I_{ON}) current in [BMIM][TCM] gate P3HT transistors, with constant active layer thickness, is increased by introducing a PMMA thin film at the P3HT/IL droplet interface. This increase in I_{ON} may be related to the improvement of hole mobility in these transistors due to the better interface between the PMMA and the semiconductor. Because the absence of the thin film leaves the P3HT exposed to environmental conditions creating additional charge traps that limit hole mobility. This is also the reason why there is less lag with PMMA. [4]

Also, the presence of the PMMA film reduces the equivalent capacitance (dielectric constant) IL-PMMA increasing the mobility of the ions and therefore the response time of the transistor.[3]

Of course, the significant lag that is observed whether we have PMMA or not, can come from the impurities of the IL or even from the atmospheric humidity. Also, perhaps the contact of the ionic liquid with the P3HT creates some reaction causing reduced performance of the transistors without PMMA.

Our results suggest that the devices under examination operate in the field-effect regime and do not exhibit bulk electrochemical doping. We cannot exclude the possibility that some degree of ion migration into the semiconductor layer due to the electrical bias stress also lead to a partial oxidation of P3HT most superficial layer. This interfacial region seems to be the same region involved in the field-effect accumulation of charge carriers.

5. ACKNOWLEDGMENT

6. REFERENCES

[1] Eleftherios Kapetanakis; Charalampos Katsogridakis; Dimitra Dimotikali; Panagiotis Argitis; and Pascal Normand (2020). Ion-Activated Greatly Enhanced Conductivity of Thin Organic Semiconducting Films in Two-Terminal Devices (https://doi.org/10.1002/aelm.202000238). Mater. 6, 2000238.

[2] LYDIA GKOURA (2019). DIFFUSION STUDIES OF FLUIDS IN MESOPOROUS AND NANOPOROUS MATERIALS USING NUCLEAR MAGNETIC RESONANCE (NMR) METHODS. DOCTORAL DISSERTATION.

[3] S. Ono; K. Miwa; S. Seki; J. Takeya (2009). A comparative study of organic single-crystal transistors gated with various ionic-liquid electrolytes (https://doi.org/10.1063/1.3079401). Appl. Phys. Lett. 94, 063301.

[4] S. Ono; S. Seki; R. Hirahara; Y. Tominari; J. Takeya (2008). High-mobility, low-power, and fast-switching organic field-effect transistors with ionic liquids (https://doi.org/10.1063/1.2898203). Appl. Phys. Lett. 92, 103313.

UNEXPECTED OBSERVATION OF A DRAMATIC INCREASE IN THE ELECTRICAL CONDUCTIVITY OF P3HT FILMS WHEN THEY ARE DEPOSITED ON COPLANAR ELECTRODES AND COVERED WITH AN ELECTROLYTE POLYMER LAYER.

Eleftherios Kapetanakis,[1, 2] *Pascal Normand*[2]

[1]*Department of Electronic Engineering, Hellenic Mediterranean University, 73133, Chania, Greece.*

[2]*Institute of Nanoscience and Nanotechnology, National Centre for Scientific Research "Demokritos", PO Box 60228, 15310 Athens, Greece.*

Metal (M) / organic semiconductor (OSC)/electrolyte (E) systems are a critical component of a variety of 'traditional' (opto-)electronic and emerging bioelectronic devices. M/OSC interface typically serving to either inject or extract charges from an OSC film. The movement of ions in the electrolyte is accompanied by the formation of an electric double layer at the OSC/E interface (if the interface is ion-permeable) or doping/dedoping of OSC (if the OSC bulk is accessible to the ions). Understanding the very fundamentals of the electrostatics of these interfaces and the physico-chemical properties of OSC/E interface under equilibrium conditions lie at the heart of developing efficient strategies to overcome present-day limitations and to further push the boundaries in the science and technology of organic electronics.

As detailed in the current presentation, an increase of up to three orders of magnitude in the conductivity of thin OSC films is observed in gate-less coplanar-electrode devices using p-type organic semiconductor (poly 3-hexyl thiophene, P3HT) / electrolyte bilayer stacks. Our investigations revealed that this unusual phenomenon arises from synergistic effects between the energetics of the metal/P3HT interface, charge carrier transport and electrolyte ionic conductivity. It results of the spontaneous evolution of the metal/P3HT/electrolyte system towards thermodynamic equilibrium.

Our experiments make evident the existence of a thickness-dependent electrostatic potential at the upper edge of P3HT films formed on metal surfaces. For a metal/P3HT/electrolyte system, such a potential leads to ion-assisted hole accumulation at the P3HT surface and thereby, to the enhanced conductivity phenomenon mentioned above. Unlike most published research in surface/interface characterization of metal/P3HT systems (mostly conducted by photoelectron spectroscopy and Kelvin probe techniques), we show that the metal-work-function-dependent space-charge may extend far into the bulk of P3HT with an effective depletion layer thickness of about 60 nm as extracted in the case of O_2 plasma/HMDS modified ITO electrodes.

Most of our experiments were conducted with the aim of (1) introducing minimal changes in device materials when a polymer layer with or without mobile ions is deposited on a metal/P3HT system and (2) elucidating the kinetics associated to the evolution of a metal/P3HT/electrolyte system towards equilibrium. To this end, polymer materials made of PMMA with embedded photo-acid generators (PAGs) have been primarily employed. When unexposed they behave as dielectrics whereas upon irradiation they provide mobile ions allowing a straightforward comparison of the two cases and enable the elucidation of the observed phenomenon. Furthermore, electrolytes with low anionic mobility can be produced depending on the PAG used thus allowing unique observations of the aforementioned kinetics through time-dependent experiments.

While the present study focuses on P3HT and specific electrode/electrolyte materials, we strongly believe that it:

i) Offers original information on the energetics of metal / organic semiconductor / electrolyte interfaces and the way they can impact the operation of relevant electronic devices.

ii) Can serve as a generic approach for the extraction of parameters like the space-charge width of metal/organic semiconductor junctions.

iii) Provides insights for new routes towards the development of advanced performance organic devices, especially of polymer electrolyte-gated OFETs.

iv) Greatly enhances the potential of the examined two-terminal devices for a range of applications in the area of sensing devices including radiation detection and characterization of ionic chemical species behavior in various environments.
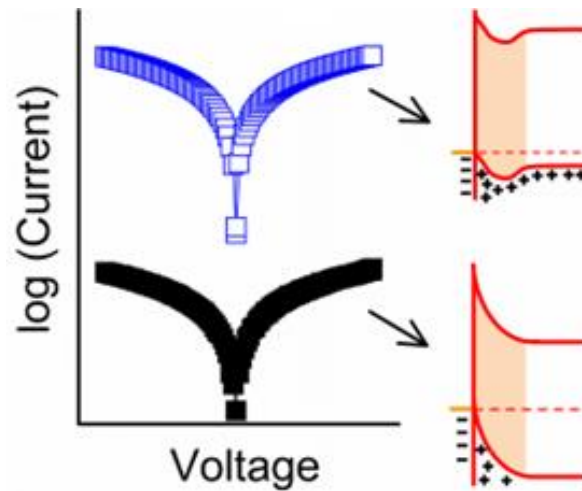
Figure 1. The presence of an electrostatic potential at the surface of thin organic semiconductor (OSC) films significantly reduces the resistance of planar two-terminal OSC/electrolyte devices. The examined devices not only provide information about the space-charge layer thickness and design of electrolyte-gated transistors but can also be used for a variety of sensing applications.

RESEARCH METHODOLOGY OF ELECTRONIC CIRCUITS LABORATORY LEARNING

Tokatlidis C.G.[1], Tselegkaridis S.A.[1], Sapounidis T.P.[2], Hatzopoulos A.T.[1] and Papakostas D.K.[1]

[1]Department of Information and Electronic Engineering, International Hellenic University, Alexander Campus, Sindos – Thessaloniki, 57400, Thessaloniki, Greece

[2]School of Philosophy and Education, Aristotle University of Thessaloniki (AUTh), 54124 Thessaloniki, Greece
xrstok@gmail.com

1. INTRODUCTION

Conducting experiments in physical laboratories helps to understand significantly basic concepts and acquire skills in sciences learning process (Hofstein & Lunetta, 2004), (Bybee, 2000). In the field of electronic circuits, physical laboratories play a key role in the deeper understanding of the subject. In the years of covid19 pandemic, most universities used distance learning. The basic tool used for this purpose was virtual laboratories; hence, the question of whether virtual laboratories are equal or better than the physical ones, has naturally arisen. In order to compare these two laboratory types, a method that could evaluate the effectiveness of both, had to be found. In addition, the combination of two types' laboratories could be evaluated in order to obtain a more comprehensive approach to the teaching of electronic circuits. This paper presents the methodology of a research that aims to investigate all of the above comparisons. In order to develop this methodology, existing tools were used in their original form or modified to fit the needs of the specific object and tools were created from scratch.

The research started in October 2022 at the International Hellenic University - Department of Information and Electronic Engineering and it has been carried out in the framework of a PhD prepared by the author.

Research design, implementation and analysis stages will be presented as well as key points, materials and difficulties encountered during the research. Results and discussion are based on early findings since data collection will be completed in the 2023-2024 academic year.

2. MATERIALS AND METHODS

Research started in October 2022 and will take place over two academic years (2022-2023 & 2023-2024). It will be conducted in three stages: design, implementation and analysis.

The first stage involved research design in which a sample of students was divided into four groups. Students of all groups performed six exercises-experiments involving basic electronic amplifier layouts. In order to quantify potential benefits, pre-post tests were used. Each student individually performed six experiments and answered the relevant questionnaires (tests) before and after each experiment. Students of the first group performed all six experiments in physical laboratories and with physical means. The materials used were basic electronic components such as resistors, capacitors, transistors and operational amplifiers. Circuits were implemented on breadboards and measurements were taken with oscilloscopes and digital multimeters.

Students of the second group performed all six experiments as well, but in virtual laboratories. The tool used for the virtual labs was Texas Instrument's circuit design and simulation tool, Tina Ti. On this environment, electronic parts breadboards and instruments were available in digital form. Measurements were taken with virtual oscilloscope and multimeter.

Third group's students performed the first three experiments in physical laboratories and the
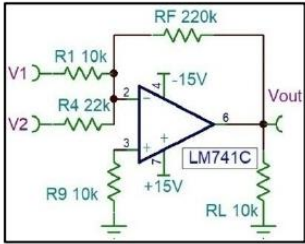
remaining three in virtual ones while students of the fourth group performed experiments in the reverse order.

Virtual laboratories took place in the same area as the physical ones, using computers. All groups conducted the experimental exercises locally and not remotely, on facilities of the physical laboratories and were provided with the same guidance from experienced instructors before conducting each experiment.

The duration of each experimental exercise was 115 minutes. In the beginning, students answered a 15 minutes test (pre test). For the next 10 minutes instructors provided students with short guidance related to subject basics, tools, and implementation of the circuit. Next, students conducted the experiment for 75 minutes and afterwards answered the same 15 minutes test (post test). Pre and post tests were identical and consisted of a questionnaire.

Due to the fact that research in the field of electronic circuits was limited, no existing questionnaires were available. Thus, at that stage a questionnaire had to be developed in order to be used as pre-post test which would quantify learning gain for each student. Its content was reviewed and approved by two experienced university professors who have been teaching the subject of electronic circuits for over twenty years. Each questionnaire included 21 questions which were divided into three sections. Each section consisted of 7 questions. In the first section, questions measured the learning gain resulting from each intervention. Second section questions measured the development of critical skills for each experimental method while the questions of the third section involved the development of measurement skills. The questions were of multiple choice type and each question had four possible answers and one "I don't know" answer. To further increase the attention and motivation of the students, evaluation of the answers included a positive and negative score. Therefore, the structure of the possible answers had to be scalar. Only one possible answer was correct and scored 4, one close to correct scored 1, one slightly improbable scored -1, and one was completely improbable scored -2. The answer "I don't know", was neutral and evaluated with 0. The duration of all six experiments for every group was six academic weeks. A short example of a sixth experiment question is given below (figure 1):

Figure 1.Scores, [A]: 4, [B]: -1, [C]: 1 and [D]: -2.

Second stage involved the implementation of the research: the timetable, the instructors who would guide the students and the instructions they would follow.

The timetable of the survey was a critical point and it was given special attention. Research was conducted within the course "Electronic Devices". The course is held in the winter semester of the second year of studies and is attended by approximately 150 students. So, to ensure a sufficient sample of participants, which could give a safe result, research should be completed in two academic years (300 students estimated sample).

The first cycle of data collection took place in the winter semester of the current academic year. The students attended the course in 20 classes which were divided into four groups as described above. Thus, each group contained five classes of seven to eight students.

Due to the rather large number of classes, the guidance of the intervention was done by four

teachers. In order to eliminate as much as possible the influence of different teaching personalities on the intervention (bias), each teacher guided classes from every group. The teachers were given specific instructions and topics to be discussed before performing each exercise so that all participants had the same guidance.

The third stage included analysis of pre-post test scores. Division of students into classes and groups was done randomly since they chose the class they wished to attend by themselves. Therefore, it should have been examined whether the students had approximately the same cognitive starting point for each exercise or large deviations. For this purpose the independent samples t-test analysis, for all groups' pre-tests scores were used.

The second parameter that should have been examined was whether or not there was a learning gain from intervention for all types of laboratories. To achieve this goal, a paired-samples t-test analysis was performed on the pre-post tests of each student for all groups.

Finally, in order to extract and compare the learning gain offered by each laboratory type or a combination of both, an ANCOVA analysis was performed on the post-test scores taking into account the pre-test scores as a covariance.

3. RESULTS AND DISCUSSION

Results are indicative since they were based on early findings. They can also be used as an example to highlight the analysis method used in this research. For the following analysis types, scores of the pre and post tests of the sixth exercise were used. They involved only students of the first and second group (physical and virtual laboratories respectively).

Initially, in order to examine whether the 2 groups started from the same level, an independent sample t-test was performed in the pre-tests.

Table 1.Independent Samples t-Test.

	F	Sig.	t	df	Sig. (2-tailed)	Mean Difference	Std. Error Difference	95% Confidence Interval of the Difference	
								Lower	Upper
Pre-test (Group 1 vs Group2)	2,177	0,142	0,135	144	0,892	0,393	2,905	-5,348	6,134

According to the table 1, there are no statistically significant differences between the two groups, therefore they can be considered equivalent.

Afterwards, a paired-samples t-test analysis was performed, between the pre-post tests for each student of both groups, in order to find out whether the intervention (regardless of the type of laboratory) led to statistically significant findings.

Table 2. Paired Samples t-Test.

	Mean	Std. Deviation	Std. Error Mean	95% Confidence Interval of the Difference		t	df	Sig. (2-tailed)
				Lower	Upper			
Pre-test physical – Post-test physical	-9,629	12,677	1,515	-12,651	-6,606	-6,355	69	,000
Pre-test Virtual – Post-test Virtual	-6,724	9,833	1,128	-8,971	-4,477	-5,961	75	,000

According to the table 2, there are statistically significant differences for both types of laboratories between the post test and the pre test. Therefore, the educational intervention led to a learning gain.

Last but not least, in order to compare the learning gain of the two types of physical and virtual laboratory, an Ancova analysis was performed for the post tests, taking into account pre tests as a covariance.

According to the results, the two types of laboratories helped the students equally as there are no statistically significant differences between them, $F(1,2)=2.873$, $p=0.092$. This result is in line with several studies that compare the effectiveness of physical and virtual laboratories in the learning of various scientific fields. It is a common conclusion that there is no significant difference in efficiency between physical and virtual laboratories (Kapici et al., 2019), (Evangelou & Kotsis, 2019), (Chen at al., 2014), (Wong at al., 2020), (Chien at al., 2015), (Kollöffel & De Jong, 2013), (Zacharia, 2007). However, although in the above surveys, a slight advantage in favor of virtual laboratories is observed, in this survey there is a clear trend in favor of the physical laboratories (figure 2).
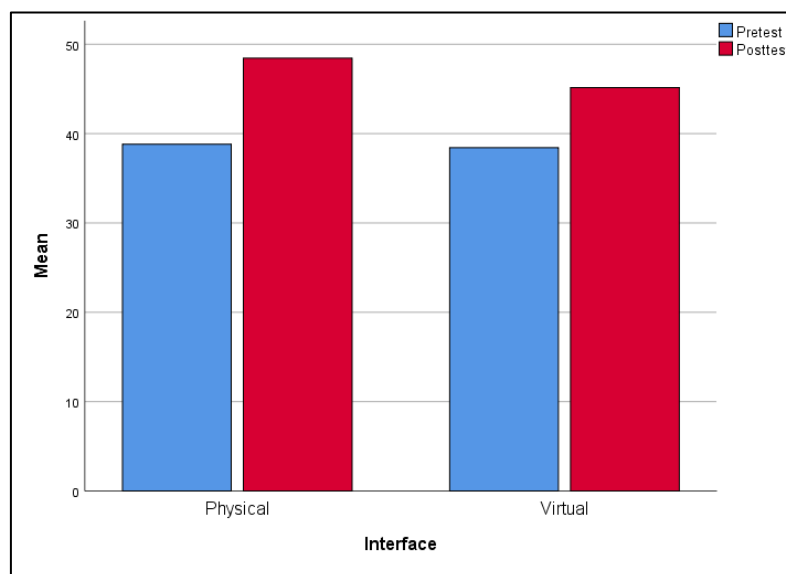

Figure 2.Mean of pre, post test scores for physical and virtual labs.

The overall results remain to be seen from the total sample after the data collection is complete. In addition, the participation of all four groups is likely to differentiate the results. In the literature on similar subjects, the combination of the two types of laboratories appears to be the most beneficial (Kapici et al., 2019), (Tsihouridis at al., 2015).

4. CONCLUSION

This paper presented the methodology of a research which compares the effectiveness of physical and virtual laboratories and their combination for the subject of electronic circuits. Specifically, its three stages were presented: design, implementation and analysis. The results were based on early findings as the research is in progress and data collection has not yet been completed.

All in all, it was observed that intervention through both physical and virtual laboratories had a positive effect on students' learning gain. However, the two types of workshops appeared equivalent in terms of learning gain. The above conclusion emerged from a small sample of research that concerns one out of six exercises and thus constitutes an encouraging indication for the effectiveness of the methodology used to conduct the research.

In addition to positive indications from the research so far, several difficulties have emerged. The most important was the following:

- Separation of students into classes and groups was a particularly demanding process. Each group needed approximately the same number of participants, but at the same time the

choice of class should have been made by students in order to serve their overall timetable.

- The questionnaires for the pre-post tests had to be very carefully designed. In fact, they had to correspond to both types of laboratory, have a sufficient number of questions and at the same time require the least possible time to fill in so enough time for conducting the experiment could be left.

5. REFERENCES

Bybee R. (2000). Teaching science as inquiry. Inquiring Into Inquiry Learning and Teaching in Science. American Association for the Advancement of Science (AAAS), pp: 20-46.

Chen S., Chang W.H., Lai C.H. and Tsai C. Y. (2014). A Comparison of Students' Approaches to Inquiry, Conceptual Learning, and Attitudes in Simulation-Based and Microcomputer-Based Laboratories. Sci. Educ., 98: 905-935.

Chien K.P., Tsai C.Y., Chen H.L., Chang W.H. and Chen S. (2015). Learning differences and eye fixation patterns in virtual and physical science laboratories. Comput. Educ., 82: 191- 201.

Evangelou F. and Kotsis K. (2019). Real vs virtual physics experiments: comparison of learning outcomes among fifth grade primary school students. A case on the concept of frictional force. Int. J. Sci. Educ., 41: 330-348.

Hofstein N. and Lunetta V. (2004). The laboratory in science education foundations for the twenty-first century. Science Education, 88: 28-54.

Kapici H.O., Akcay H. and De Jong T. (2019). Using Hands-On and Virtual Laboratories Alone or Together - Which Works Better for Acquiring Knowledge and Skills?. Journal of Science Education and Technology, 28: 231-250.

Kollöffel B. and De Jong T. (2013). Conceptual understanding of electrical circuits in secondary vocational engineering education: Combining traditional instruction with inquiry learning in a virtual lab. J. Eng. Educ., 102: 375-393.

Tsihouridis C., Vavougios D., Ioannidis G.S., Alexias A., Argyropoulos C. and Poulios S. (2015). The effect of teaching electric circuits switching from real to virtual lab or vice versa - A case study with junior high-school learners. Proc. 2015 Int. Conf. Interact. Collab. Learn. (ICL 2015), pp: 643-649.

Wong W.K., Chen K.P. and Chang H.M. (2020). A comparison of a virtual lab and a microcomputer-based lab for scientific modeling by college students. J. Balt. Sci. Educ., 19: 157-173.

Zacharia Z.C. (2007). Comparing and combining real and virtual experimentation: An effort to enhance students' conceptual understanding of electric circuits. J. Comput. Assist. Learn., 23: 120-132.

LEARNING ENGINEERING THROUGH APPLIED RESEARCH

Reyes Tolosa, M.D.[1], E-Martín Y.[2], Sánchez Diana L.D. [1]

[1]Florida Universitària (Engineering Unit)
[2] Florida Universitària (ICT Unit)
{mdreyes,yescudero,lsanchez}@florida-uni.es

1. INTRODUCTION

Industry demands fully trained professionals; that is, the graduated engineers must have achieved the general, basic, specific, and transversal competencies of their university training in engineering (Hirudayaraj et al., 2021). The subjects addressed in the courses guarantee a satisfactory scope of general, basic, and specific skills. However, it is not the same with the transversal ones being these competencies fundamental in the selection of personnel for a team in industries. This is because they encompass characteristics such as teamwork, problem solving, leadership, critical thinking, decision making, among others (Ananiadoui & Claro, 2009).

This is why in this work we propose an applied research team to train students from different courses and degrees in engineering and other disciplines such as business administration and management. They all participate along with junior and senior researchers working on solving challenges in the field of renewable energies and energy efficiency. We decided to work in this field since is one of the most promising and the most necessary in society (Gkonis et al., 2020).

While they belong to the research team, students receive specific training in the field of renewable energies and energy efficiency from professionals in the sector. In addition, they face challenges in this area such as design of wind turbines integrated into nature, microturbines that can be incorporated into irrigation ditches, rehabilitation of hydraulic mills, sensorization, and monitoring of generated energy, social awareness, among others.

In this way, it is guaranteed that students from the second year to final degree project obtain the transversal competencies that industry demands (Strnadová et al., 2014). Their team participation guarantees the address of different tasks such as analysis of situations, organization of work, critical thinking, research, design and manufacture of prototypes, study, commissioning, analysis, and improvement of prototypes.

All the challenges are worked through different projects, where the professors involved in the team perform the evaluation of them. Without doubt, this methodology is a commitment to active learning, based on research, which provides students with extra skills to their professional profiles (Caeiro-Rodríguez et al., 2021).

This extended abstract is structured as follows. Section 2 introduces the organization of this applied research team. Section 3 describes the work plan designed to go through this project. Section 4 shows the preliminary results of this implementation. Last, Section 5 summarizes the obtained conclusions.

2. ORGANIZATION

The applied research team, namely Energy Student, was created with the aim of providing students with the necessary transversal competencies for their futures jobs. Most of the qualified jobs require professionals from different fields to work in their multidisciplinary teams. For this reason, the main condition of our new team was that it consisted of students and professors from different degrees taught at Florida Universitària, which are within the following areas of knowledge:

- Technical: Degree in Mechanical Engineering, Degree in Industrial and Automatic Electronic Engineering, and Degree in Design and Development of Video Games and Interactive Experiences.
- Business: Degree in Business Administration and Management, and Degree in Transport and Logistics Management.
- Teaching: Degree in Early Childhood Education, and Degree in Teacher in Primary Education.

We decided that the group should consist of students from different degrees and, moreover, from different courses from second to fourth year, including the final year project dissertation. In addition to that, we had to choose the research topic, which we knew had to be topic of current interest that was also feasible to be developed by the group (students and senior researchers). These reasons led us to choose renewable energies and energy efficiency.

The formation of the group was performed on a voluntary basis by both faculty and students. We obtained a high participation from students and professors from engineering and business administration and management degrees. Although the participation was voluntary, we considered the development and knowledge acquired by students, which was part of the 25% of the grade of each of the subjects addressed during the corresponding degree. For this reason, we developed different rubrics that testified the evolution of students during their participation in the group.

3.   WORK PLAN

The team's work plan followed the next steps:

- 1st stage: foundation of the team
- 2nd stage: obtaining specific training
- 3rd stage: start-up
- 4th stage: analysis of the obtained results

3.1 Building of the team

Figure 1 shows the planning we followed during the creation of the team, which consisted of these four stages: Registration, Selection, Training, and Start-up, although we will deal with the last two stages independently.
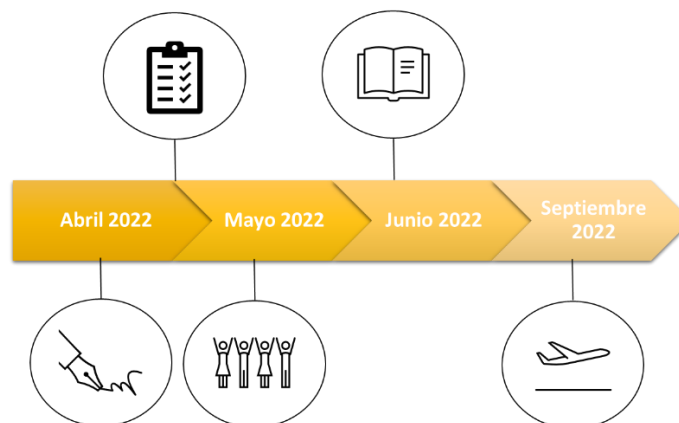

Figure 1. Planning followed during the team building stage.

As we mentioned above, during the creation of the team we wanted to guarantee that the team

consisted of students and professors from different areas of knowledge. For this reason, we gave several presentation sessions of the team to all faculty and students. Figure 2 shows the board we displayed during the presentation sessions.
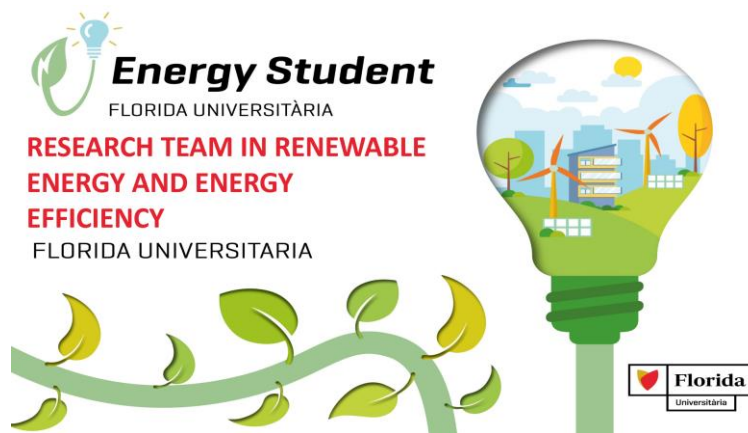

Figure 2. Energy Student logo.

During the presentation sessions, we exposed the theme of the work to develop and highlighted the importance of research as a tool for the development of transversal competencies in students. During these talks, we brought the opportunity to students and professors to join through an online registration form.

The registration process was an exist. There was a high number of students interested in joining the team so that we had to perform a selection process, which we based on their academic records and a personality test.

3.2 Obtaining specific training

Once the team was created, we offered specific training to all members. It is worth mentioning that such training was open to all faculty members and students interested in it.

The training consisted of different sessions in different areas:

- Legal and juridical framework in renewable energy systems in the European Union, Spain, and specifically Valencia Community
- Energetically self-sufficient towns
- New energy communities
- Hydro, wind, solar, and biomass energy

3.3 Start-up

The team was set up with the aim of developing new small-scale technologies that could be applied in the rural environment of the Caudiel. Caudiel is a town in the Valencian community (Spain) that has a many natural resources such as water, wind, sun, and biomass, since it is located between two mountains.

Before starting to work, all participants of the Energy Student group went to visit Caudiel to know its orography, resources, and possibilities. Figure 3 shows a picture of the visit.

Figure 3. Enery Student participants visiting Caudiel.

Given the different field of study to be applied, we divided the group into the working groups shown in Figure 4.

Figure 4: Working groups of Energy Student.

4.   RESULTS

In this section, we present the results obtained in the Energy Student applied research group in its first year of operation, which are the following:

- Students found the participation in the research team riveting, especially to those belonging to technical areas of knowledge such as engineering
- Students from different degrees and different courses have worked together
- Students have developed the following tasks: design, manufacture, and start-up of prototypes in the field of wind and hydraulic energy as well as preparation of technical reports and their presentation in public

Given that, we can confirm that participation in this type of teams allows students to develop transversal competencies such as:

- Social and environmental commitment
- Innovation and creativity
- Teamwork and leadership
- Effective communication
- Responsability and decisión making

5. CONCLUSION

This work shows how the participation of students from different degrees and different courses in a research applied group encourage the development of their transversal competencies. We need to consider two important things. On one hand, this type of participation makes sense to adapt it throughout students' entire period of study. On the other hand, not all the students have the skills and the autonomy required to perform research.

6. ACKNOWLEDGMENT

7. REFERENCES

Ananiadoui, K., & Claro, M. (2009). 21st century skills and competences for new millennium learners in OECD countries.

Caeiro-Rodríguez, M., Manso-Vázquez, M., Mikic-Fonte, F. A., Llamas-Nistal, M., Fernández-Iglesias, M. J., Tsalapatas, H., ... & Sørensen, L. T. (2021). Teaching soft skills in engineering education: An European perspective. *IEEE Access*, *9*, 29222-29242.

Gkonis, N., Arsenopoulos, A., Stamatiou, A., & Doukas, H. (2020). Multi-perspective design of energy efficiency policies under the framework of national energy and climate action plans. *Energy Policy*, *140*, 111401.

Hirudayaraj, M., Baker, R., Baker, F., & Eastman, M. (2021). Soft skills for entry-level engineers: What employers want. *Education Sciences*, *11*(10), 641.

Strnadová, I., Cumming, T. M., Knox, M., Parmenter, T., & Welcome to Our Class Research Group. (2014). Building an inclusive research team: The importance of team building and skills training. *Journal of Applied Research in Intellectual Disabilities*, *27*(1), 13-22.

ENGAGING ICT FOR RELIGIOUS EDUCATION IN PRIMARY SCHOOLS

Dalaka Kanellia Ioanna[1]

[1]Author at Stamoulis Publications, Averof 2, Athens, GR10433, Greece
dalakalia@hotmail.com (corresponding author)

1. INTRODUCTION

The use of ICT in religious education in primary shools can make the subject more engaging and interesting for students (Konstantaras, Dalaka et al., 2022), allowing them to absorb even the most complex concepts through interactive learning. Students become active participants in the learning process, researching and analyzing on their own, and developing critical thinking skills. Traditional religious education is enriched by modern electronic media, which helps to present the timeless truths of Orthodoxy in a more contemporary and relevant way. ICT tools such as PowerPoint, videos, animation, digital cameras, and virtual tours can be used to make learning more dynamic and interactive.

Using ICT in Religious Education makes the subject more attractive and interesting for students (Karakostantaki and Stavrianos, 2021), as they can easily assimilate and internalize even the most complex concepts in the form of games. In this way, students participate in the learning process, researching, seeking and analyzing themselves, which turns them from passive recipients and secondary characters to participants in teaching and protagonists. They move away from sterile memorization and learn in a creative and experiential way, cultivating their critical thinking. They can even communicate with students from other schools, either from the inside or from abroad, and exchange views on Orthodox Faith.

The traditional subject of Religious Education, as enriched by modern electronic means, becomes more current by projecting the timeless truths of Orthodoxy. PowerPoint can be used as tools to display tables, maps, diagrams and presentations, video projections, documentaries, animation films with various themes, such as the life of Christ, video cameras for videotaping educational activities, radio CDs with Christian hymns and songs for learning, digital camera and virtual tours to visit Orthodox Churches and Monasteries. Moreover, the use of online resources, such as interactive educational platforms and e-books, can provide students with the opportunity to expand their knowledge on various religious topics (Broadbent, 2004) and also allow them to access information and resources in a more convenient and efficient way.

In conclusion, the integration of ICT in Religious Education can have a positive impact on students' learning outcomes, as it enhances their motivation, participation, and critical thinking skills. Additionally, it allows them to gain a deeper understanding of religious concepts and ideas, which can help them develop a more meaningful relationship with their faith and their community.

2. ACKNOWLEDGMENT

3. REFERENCES

Broadbent, L. (2004). The contribution of religious education to whole school initiatives. Issues in religious education, pp. 157-168.

Karakostantaki, E., & Stavrianos, K. (2021). The use of ICT in teaching religious education in primary school. Education and Information Technologies, 26(3), 3231-3250.

Konstantaras, A., Dalaka, K. I., Kourasi, M. and Maravelakis E. (2022). K-12 Agile Learning with Educational Software and Robotics Technology. International Journal of Advanced Research in Science, Engineering and Technology, 9 (9): 1-7.

3D PRINTING USING PLASTIC PELLET MELT EXTRUSION

Bolanakis, N[1], Kalderis, D[1], Vidakis, N[2], Petousis, M[2], and Maravelakis, E[1]

[1]Hellenic Mediterranean University – Dept. of Electrical Engineering
[2] Hellenic Mediterranean University – Dept. of Mechanical Engineering
bolanakis@hmu.gr

1. INTRODUCTION

Three-dimensional (3D) printing, which is one ofthe most famous AM technologies, has recently attracted interest on both academia, as well as various industrial sectors for objects' manufacturing and/or prototyping purposes(Vidakis, N., et al 2020). Several types of plastics are commonly used in 3D printing, such as Acrylonitrile Butadiene Styrene (ABS), Polylactic Acid (PLA), and Polyethylene Terephthalate Glycol (PETG).

Acrylonitrile butadiene styrene (ABS) is a triblock copolymer from a group of styrene terpolymers and exhibits good mechanical properties such as strength and toughness combined with high impact and resistance to heat and scratching (Vidakis, N., et al, 2023). It is commonly used in applications that require impact resistance and toughness, such as automotive parts and toys (Biron, 2007). ABS can be difficult to print with due to its tendency to warp, but modifications to the printing process, such as using a heated build platform, can help mitigate this issue. **Polylactic acid (PLA)** is a biodegradable thermoplastic material that is made from renewable resources such as cornstarch or sugarcane (Cerneels, J, et al., 2013). Is a commonly used bio-based polymer at a wide range of applications (Vidakis, N., et al 2021) that require a low melting point, such as food packaging and disposable cups. PLA is also popular in the 3D printing community due to its ease of use and low warping. **Polyethylene terephthalate glycol (PETG)** is a tough and durable thermoplastic material that is commonly used in applications that require chemical resistance and transparency, such as water bottles and food packaging (Arunprasath, K., et al, 2022).

FDM is the most commonly used technique for printing with plastics. It works by melting the plastic filament and extruding it through a nozzle layer by layer. FDM allows for the creation of large and structurally sound parts. However, it may result in visible layer lines and reduced surface quality (Gao et al., 2015). Various additives and processing techniques have been explored to improve the printing quality and performance of plastic materials. The addition of nucleating agents has been shown to enhance the crystallization kinetics of PLA, resulting in improved mechanical properties (Zhang et al., 2019). Other studies have focused on optimizing printing parameters to minimize defects and achieve higher resolution prints (Salonitis et al., 2010).

Biocarbon, also known as biochar, is a carbon-rich material that is produced from the pyrolysis of organic matter. Biocarbon has a wide range of potential applications, including soil amendment, water treatment, and energy storage. Biocarbon is a highly porous material with a large surface area, which makes it an effective adsorbent for a variety of pollutants. Biocarbon is also stable under a wide range of environmental conditions, and it can remain in soil for hundreds or even thousands of years. Biocarbon can be produced from a variety of organic feedstocks, including agricultural waste, forestry residues, and municipal solid waste.

The work of Idrees et al. (Idrees et al. 2018) was among the first to demonstrate the effects of adding biochar to develop a sustainable and cost-effective composite with an upgraded thermomechanical response. The authors melt-mixed biochar with recycled PET and produced 1.75 mm feedstocks using a filament extruder. The results also depicted that a 0.5% wt. loading of biochar in PET induced a 32% raise of the tensile strength, whereas a 5% wt. induction led to a 60% raise in

tensile modulus compared to the raw PET matrix (Idrees et al. 2018). In a similar approach, Strongone et al. (Dugmore, T, et al. 2018) dispersed biochar from coffee waste in bisphenol-A-ethoxylate-diacrylate at various loadings in the range from 0.01 to 1.0% wt. and attempted to depict correlations between the thermal, optical and rheological properties of the composites and the corresponding properties of the reference materials.

2. MATERIALS AND METHODS

Biocarbon that was created from local olive trees was mixed with PLA filament. The melt extrusion used to create the admixture (biochar - PLA) is shown in the picture below (Picture 1)



Picture 1: Diagram of melt extrusion

At the beginning, the extruder was used to create pure PLA filament for the 3D printer (about 20gr) and then for various concentrations of (biocarbon - PLA), corresponding materials were created using the extruder. The mixing the plastic grain with the carbon was first using mixing machine and after that was placed in to the extruder to create the filament. Finally, for each mix made, a material with a diameter between 1.63 - 1.76mm was created (Picture 2).
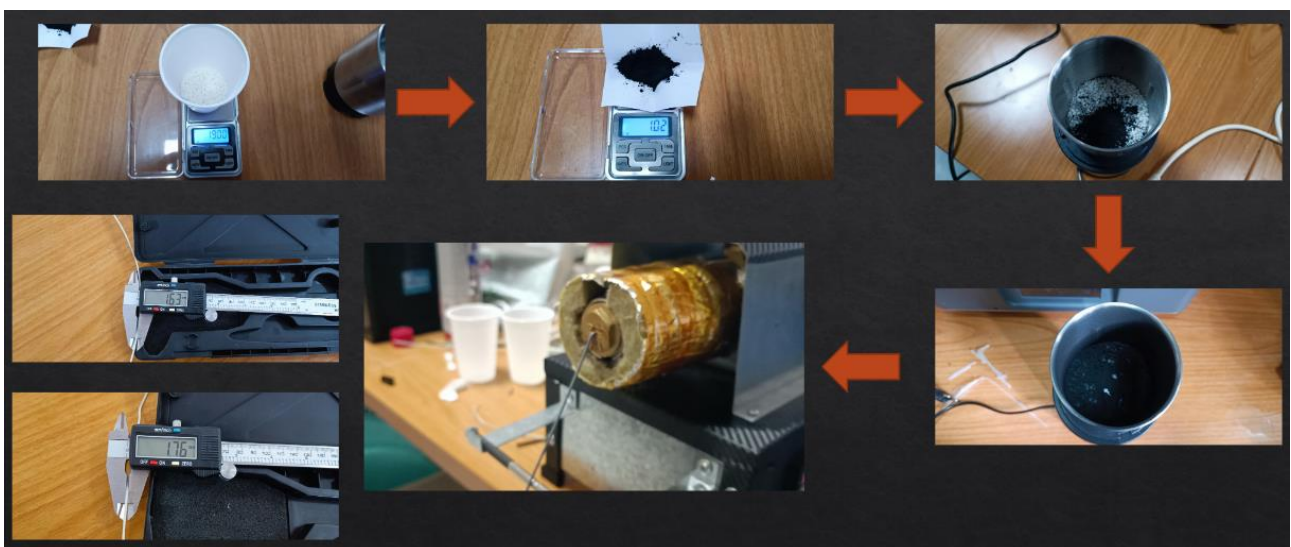
Picture 2: The creation process of filament

3. RESULTS AND DISCUSSION

Comparisons between samples of pure pla and pla - biochar, indicated significant improvements in the properties of the produced material (Figure 1).
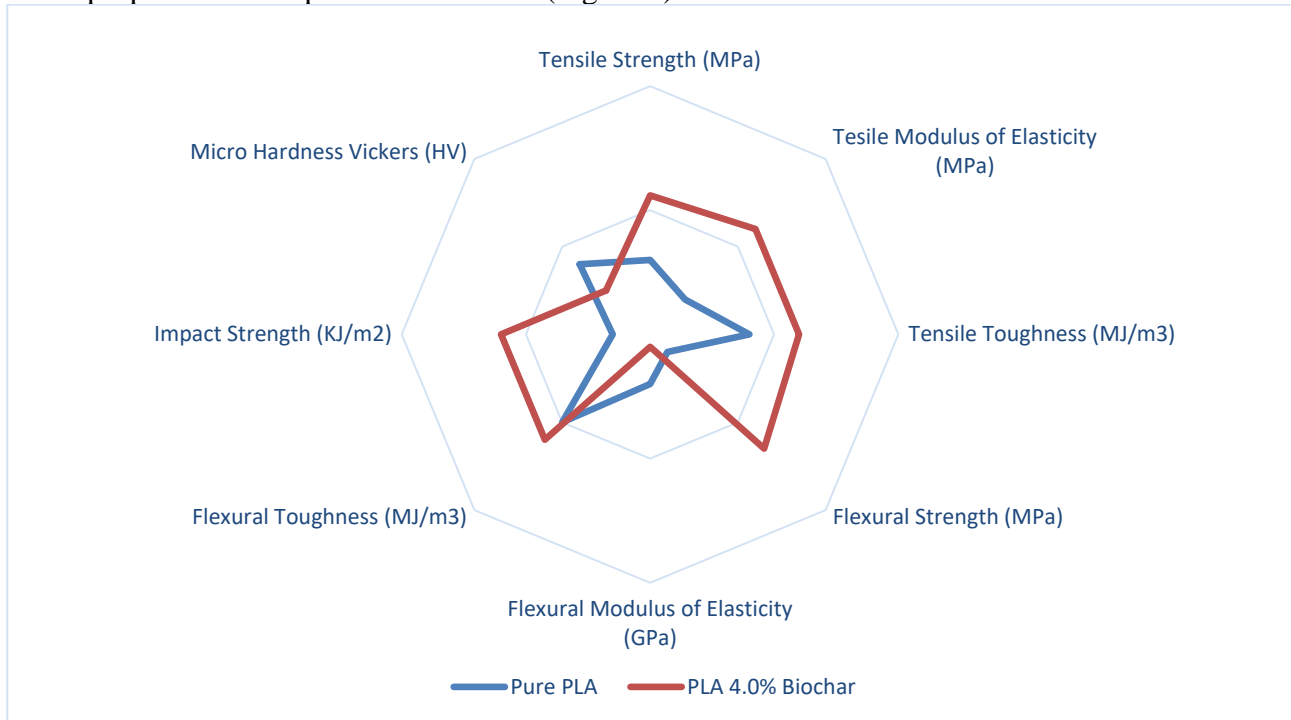
Figure 7: Comparison chart between samples of Pure PLA & PLA – Biochar

As shown in the figure above, with the addition of 4% biochar to the PLA, there was a significant improvement in most of the measurements performed on the as-made samples compared to the pure PLA. The only ones where the pure PLA was superior are in the measurement of microhardness and in the measurement of the flexural modulus.

4. REFERENCES

Arunprasath, K., Vijayakumar, M., Ramarao, M., Arul, T. G., Pauldoss, S. P., Selwin, M., ... & Manikandan, V. (2022). Dynamic mechanical analysis performance of pure 3D printed polylactic acid (PLA) and acrylonitrile butadiene styrene (ABS). Materials Today: Proceedings, 50, 1559-1562.

Biron, M. (2007). Thermoplastics and thermoplastic composites: technical information for plastics users. Elsevier.

Cerneels, J., Voet, A., Ivens, J., & Kruth, J. P. (2013). Additive manufacturing of thermoplastic composites. Composites Week@ Leuven, 1-7.

Dugmore, T. I., Clark, J. H., Bustamante, J., Houghton, J. A., & Matharu, A. S. (2018). Valorisation of biowastes for the production of green materials using chemical methods. Chemistry and Chemical Technologies in Waste Valorization, 73-121.

Gao, W., Zhang, Y., Ramanujan, D., Ramani, K., Chen, Y., Williams, C. B., ... & Zavattieri, P. D. (2015). The status, challenges, and future of additive manufacturing in engineering. Computer-Aided Design, 69, 65-89.

Idrees, M., Jeelani, S., & Rangari, V. (2018). Three-dimensional-printed sustainable biochar-recycled PET composites. ACS Sustainable Chemistry & Engineering, 6(11), 13940-13948.

Salonitis, K., Pandremenos, J., Paralikas, J., & Chryssolouris, G. (2010). Multifunctional materials: engineering applications and processing challenges. The International Journal of Advanced Manufacturing Technology, 49, 803-826.

Vidakis, N., Mangelis, P., Petousis, M., Mountakis, N., Papadakis, V., Moutsopoulou, A., & Tsikritzis, D. (2023). Mechanical Reinforcement of ABS with Optimized Nano Titanium Nitride Content for Material Extrusion 3D Printing. Nanomaterials, 13(4), 669.

Vidakis, N., Petousis, M., Velidakis, E., Mountakis, N., Fischer-Griffiths, P. E., Grammatikos, S., & Tzounis, L. (2021). Fused filament fabrication three-dimensional printing Multi-Functional of polylactic acid/carbon black nanocomposites. C, 7(3), 52.

Vidakis, N., Petousis, M., Velidakis, E., Mountakis, N., Tzounis, L., Liebscher, M., & Grammatikos, S. A. (2021). Enhanced mechanical, thermal and antimicrobial properties of additively manufactured polylactic acid with optimized nano silica content. Nanomaterials, 11(4), 1012.

Zhao, X., Yu, J., Liang, X., Huang, Z., Li, J., & Peng, S. (2023). Crystallization behaviors regulations and mechanical performances enhancement approaches of polylactic acid (PLA) biodegradable materials modified by organic nucleating agents. International Journal of Biological Macromolecules, 123581.

DESIGN PRINCIPLES, PROPULSION AND MANEUVERABILITY OF A FLEXIBLE AUTONOMOUS UNDERWATER VEHICLE

George G. Volanis[1], Emmanuel Maravelakis[1], Konstantinos-Alketas Oungrinis[2], George Fouskitakis[1] and Georgios E. Stavroulakis[3]

[1]Department of Electronic Engineering, Hellenic Mediterranean University
[2]School of Architecture, Technical University of Crete,
[3]School of Production Engineering and Management, Technical University of Crete,
E-mail: gevolanis@gmail.com

1. INTRODUCTION

Underwater exploration in the last decades focuses in marine environments which are too deep and hazardous for human divers or long-term marine research. Also, the consumption of huge amount of funds, especially while involving a research ship, lead to the rapid development of the AUVs (Autonomous Underwater Vehicles) [2,3,12]. Most research activities in recent years have emphasized the standardization and implementation of a variety of conventional types of underwater mechanisms and vehicles [1,10,13]. Our goal is, to determine the functional and morphological characteristics of a conceptual underwater AUV, which are interdependent with the marine environment they operate, in order to define the resulting constraints on the geometry, the shell structure and the motion actuation mechanism.

The type of AUV on which this paper will focus, belongs to the category of underwater gliders [6,7,10]. Underwater Gliders (UGs) are specialized vehicle that belong to the category of Autonomous Underwater Vehicles (AUVs) and travel through water by constant changes of buoyancy. Utilizing wings, the vertical motion generates horizontal straight forward propulsion, creating a saw-tooth profile. The resulting saw-tooth motion is slow but highly efficient, making gliders an effective tool for several oceanographic uses such as water quality measurement, ocean mapping, search missions and ocean exploration. By 2004 gliders were successfully deployed for ocean data sampling missions [6,7,14]. The combination of the particular functional characteristics of gliders, allows us to have self-propelled underwater vehicles without relying on traditional means of propulsion, such as electric motors or internal combustion engines. Thus, we can achieve silent operation, high-strength shell, uninterrupted long-term operation, and vital space for the installation of electronic subsystems to control the sensory instruments.

A typical underwater glider design, consists of a cylindrical or ellipsoidal hull with fixed wings and caudal tail. The buoyancy-driven underwater gliders, utilizes a variable ballast system, in order to control attitude, by reducing or expanding the displaced volume and thus control the descent rate and glide path. Combined with the utilization of long span wings, they can glide forward in the water. As a result, thrust is generated, able to propel the glider without the use of conventional propulsion system. Our current work focuses to the adaptation of the internal actuation mechanism, by replacing the ballast pumps with a conceptual parameterized flexible shell, working as a deformable bladder under pressure. Finally, the dynamic and kinematic models are presented. These are necessary steps, needed to be accurately described in order to create an appropriate pre-simulation environment.
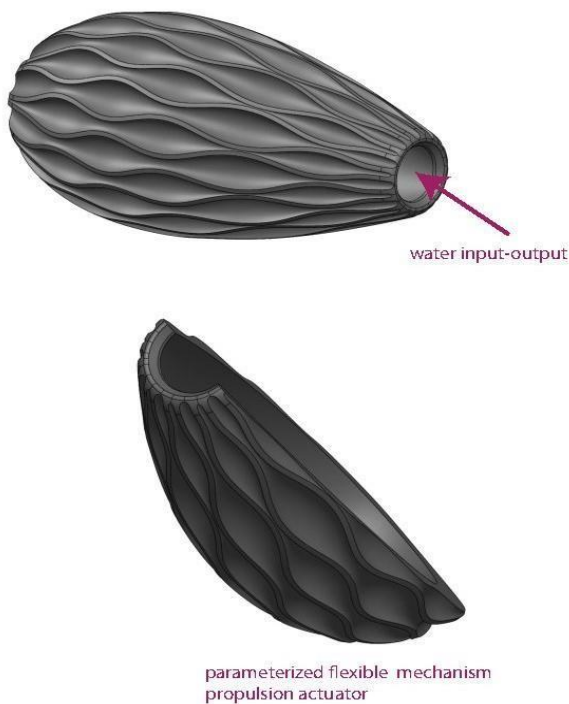
2. CONCEPTUAL PAPRAMETERIZED FLEXIBLE ACTUATION MECHANISM

In this chapter is essential to mention the differences of the motion actuation principles, between the typical glider, as explained above, and the AUV glider we propose. First of all, when the AUV glider gets close to the bottom of the sea level, it does not land as a typical glider would. Instead, because of the parameterized flexible enclosure [Figure 1], that is installed as a mechanism to activate the motion, it starts a steady ascent path. More specifically, the traditional way of activating the

motion (electric ballast pump), is replaced by a bladder shaped parameterized shell, consisting of both rigid and flexible elements. The aim is to create a compression/decompression cycle of the deformable enclosure, which is determined by the pressure difference resulting from an increase or decrease in depth. Last but not least, a defined volume of water enters the flexible casing, sufficient enough to change the weight of the AUV and thus create a negative buoyancy force, resulting to a steady and constant horizontal sliding towards the bottom of the sea. When it reaches the depth necessary to deform the flexible membrane, due to pressure, quantity of water will begin to leave the AUV glider at a constant rate proportional to the depth, so that when it reaches the necessary weight it will be able to ascend due to the positive buoyancy force. Essentially, we create a repetitive compression-decompression cycle of the flexible membrane, taking advantage of the pressure difference due to a difference in depth. This creates a slow but steady path of ascent to the surface. This process is repeated, and thus creating a controlled pattern of propulsion due to the reciprocating horizontal movement.

The proposed geometry for the AUV hull, which will house the flexible actuation mechanism, is an ellipsoidal shaped geometry, similar to that of a penguin body [9,15,16]. Due to low cruising speed and low Reynolds numbers ($Re = 5 \times 10^6$), according to Th. Lutz and S. Wagner (1997), this geometry becomes ideal for numbers close to ($Re = 5 \times 10^6$). That means, that it reaches the lowest drag coefficient possible in this region. For rather "low" Reynolds numbers of (5×10^6), the evolution strategically attained optimal form corresponds to a laminar spindle.

water input-output

parameterized flexible mechanism
propulsion actuator

Figure 1. Conceptual design of the parameterized flexible mechanism

2.1 Kinematic Model

The dynamics and kinematics of the motion of underwater gliders and AUVs in general, is a topic already being discussed by the following references [8,9,11,15,16] and our research is based on common ground, as expected. First of all, we have to define crucial parameters such as, the center of gravity (CG), the center of buoyancy (CB), the rotational matrix R and the velocity V. the CG is slightly offset from the CB, in order to create a constant gravitational torque. The mentioned parameters are defined as:

$$CG = [x_g, y_g, z_g]^T \qquad\qquad [1]$$

$$CB = [x_b, y_b, z_b]^T \qquad [2]$$

$$V = [v, \omega] \qquad [3]$$

$$R = \begin{bmatrix} \cos\psi\cos\theta & -\sin\psi\cos\varphi + \cos\psi\sin\theta\sin\varphi & \sin\psi\sin\varphi + \cos\psi\cos\varphi\sin\theta \\ \sin\psi\cos\theta & \cos\psi\cos\varphi + \sin\varphi\sin\theta\sin\psi & -\cos\psi\sin\varphi + \sin\theta\sin\psi\cos\varphi \\ -\sin\theta & \cos\theta\sin\psi & \cos\theta\cos\varphi \end{bmatrix} \qquad [4]$$

where,

$$v = [u, \quad v, \quad w]^T \qquad [5]$$

$$\omega = [p, \qquad q, \qquad r]^T \qquad [6]$$

2.2 Dynamic Model

In the conceptual AUV glider, there are three masses that need to be defined for the proposed dynamic model. The largest of them is the AUV glider's body mass, m_h, which is composed from the hull, nose, tail, wings, and rudder. Then, the variable mass of the flexible actuation mechanism, m_b, is located near the nose of the glider's body. It has fixed position, and is considered as a non-stationary mass, because as mentioned above, it can be deformed in a controlled way, through the pressure difference accordingly to the depth deference, $\dot{m}_b$. Finally, the last mass is, m_p, which is a stationary mass but with variable position and is correlated with the center of buoyancy and located in the middle section of the glider's hull. The motion of this mass, creates a gravitational moment, on the AUV's body, based on the amount of the distance it cover during change of the center of buoyancy, due to mass loss from the flexible actuation mechanism, as mentioned above. In order to control the pitch angle of the glider, the sliding mass moves along the x-z plane and thus the velocity is defined, $\dot{r}_p = [\dot{r}_{px}, \quad 0, \quad \dot{r}_{py}]$ The pressure applied to the mass, is denoted as:

$$P_p = [p_{px}, \quad 0, \quad p_{pz}] \qquad [7]$$

As a result, the net buoyancy of the glider is defined as:

$$m_0 = m_{rb} - m = (m_h + m_b + m_p) - p\nabla \qquad [8]$$

where, p is the water density and ∇ is the volume of the AUV glider's body.

Continuing with the dynamic analysis, the presence of water currents, V_c, must be included in the calculation of forces and moments, τ. Thus, a 6 degree of freedom (DOF) nonlinear dynamic equation is applied:

$$MV + \tau_c + \tau_d + \tau_r = \tau \qquad [9]$$

where M is the system inertia matrix, τ_c is the Coriolis force and moment, which in our case is equal to zero, τ_d is the damping force and moment, and τ_r is the restoring force and moment. The system inertia, M, is composed of, the inertia matrix of the rigid body or hull, M_{rb} and inertia matrix of added mass, M_a. The system inertia matrix, M, is defined as:

$$M = M_{rb} + M_a \qquad\qquad [10]$$

At this point we have to mention the fact that, the damping forces and moments, τ_d, take place at the center of dissipative force. The dissipative force is equal to the product of pressure and area, which depends on the cross-sectional areas in the x, y, and z direction. In addition, the presence of water currents, V_c, are included in the damping force equations. As a result, the dumping force and moment is defined as:

$$\tau_d = D(V - V_c)(V - V_c) \qquad\qquad [11]$$

where, D, is the damping matrix which composed of linear and nonlinear damping matrix.

The restoring forces and moments, which are also correlated to the gravitational and buoyancy forces and moments, are occurred due to weight, W, and buoyancy, B. The underwater AUV glider is designed so we can achieve positive buoyancy $(B > W)$, so that the glider will surface automatically in the case of an emergency situation, such as a collision with an obstacle. Finally, the restoring force and moment is defined as:

$$\tau_r = \begin{bmatrix} (W - B)\sin\Theta \\ -(W - B)\cos\Theta\sin\Phi \\ -(W - B)\cos\Theta\cos\Phi \\ -(y_g W - y_b B)\cos\Theta\cos\Phi + (z_g W - z_b B)\cos\theta\sin\Phi \\ (z_g W - z_b B)\sin\theta + (x_g W - x_b B)\cos\theta\cos\Phi \\ -(x_g W - x_b B)\cos\theta\sin\Phi - (y_g W - y_b B)\sin\theta \end{bmatrix} \qquad [12]$$

where, $W = m_{rb} \times g, B = pg\nabla$ and g is the gravitational constant value.

3. CONCLUSION

In this paper, a novel design approach is proposed for synthesizing the internal structural layout of a morphing wing. By adopting bioinspired morphing long span wings and tail [17], we try concentrate our efforts on how to achieve good directional stability, maneuverability, and minimal adverse response to turbulent flow, properties that are highly desirable for glider AUVs, but are presently difficult to achieve. The characterization of the internal structure and mechanical deformation of a solid is a difficult task, often requiring solutions to inverse problems with unknown topology, geometry and material properties combined with nonlinear deformation and invoke the mandatory use of topology optimization methods. However, the modelling of underwater AUV vehicles in terms of dynamic analysis and control, is extremely difficult due to the complexity of the distribution of the forces exerted on it in terms of depth ratio [5]. In most scientific applications, physical conservation laws (such as those for momentum and energy) are framed by very general, mathematical formulations [e.g. those invoking partial differential equations (PDEs) in fields such as solids mechanics, fluid mechanics and diffusion of materials], together with experimental validation by recourse to laboratory testing. The problem becomes even more challenging when large deformations (i.e., geometric nonlinearity) and nonlinear mechanical properties (i.e., highly nonlinear constitutive behavior of the solid material) are involved. Our current research is focused on extending the proposed methodology to capture a wider design space including further effects on the performance coefficients. Applications regarding oceanic research, are constantly evolving towards the design of more advanced and complex systems due to technological progress and increasing requirements. However, the design and analysis of these systems are highly depend on classical numerical simulations that require a huge amount of computing power and processing time.

At this point, artificial intelligence based surrogate models offer a new alternative in subjects such as design, design optimization, and mathematical modeling via a low cost and time. Thus for future work we focus on combination of different simulation methods, such as classical finite elements method with neural networks, specifically the PINNs method, in order to analyze the mechanical deformation of the glider AUV surfaces from external forces due to their interaction with the surrounding fluid.

4. REFERENCES

[1] Anugrah Adiwilaga, Imam Taufikurrahman, Egi Hidayat, Bambang Riyanto (2017). Design of a Modular, Compact, Long Endurance Autonomous Underwater Vehicle with Gliding Capabilities for Research Purpose Operations. Trilaksono School of Electrical Engineering and Informatics Bandung Institute of Technology Bandung, Indonesia.

[2] C. Eriksen, T. Osse, R. Light, T. Wen, T. Lehman, P. Sabin, J. Ballard, and A. Chiodi (Oct 2001). Seaglider: a long-range autonomous underwater vehicle for oceanographic research. IEEE Journal of Oceanic Engineering, vol. 26, no. 4, pp. 424–436.

[3] D. R. Blidberg (2001). The development of autonomous underwater vehicles (auv); a brief summary. in IEEE International Conference on Robotics and Automation (ICRA), vol. 4.

[4] Hasan Karali, Mustafa Umut Demirezen, M. Adil Yukselen, Gokhan Inalhan (2021). A Novel Physics Informed Deep Learning Method for Simulation-Based Modelling, Istanbul, Technical University, Istanbul, Cranfield University, Bedford, ITU Aerospace Research Center, Istanbul.

[5] Hasan Karali, Gokhan Inalhan, M Umut Demirezen and M Adil Yukselen (22 April 2021). A new nonlinear lifting line method for aerodynamic analysis and deep learning modeling of small unmanned aerial vehicles, International Journal of Micro Air Vehicles.

[6] IOOS (2014), Toward a U.S. IOOS underwater glider network plan: Part of a comprehensive subsurface observing system.

[7] J. Sherman, R. E. Davis, W. Owens, and J. Valdes (2001). The autonomous underwater glider spray, IEEE Journal of Oceanic Engineering, vol. 26, no. 4, pp. 437–446.

[8] Khalid Isa, Mohd Rizal Arshad (2011). Dynamic Modeling and Characteristics Estimation for USM Underwater Glider. Underwater Robotics Research Group (URRG), School of Electrical and Electronic Engineering, Universiti Sains Malaysia, Nibong Tebal, Pulau Penang, Malaysia Department of Computer Engineering, Faculty of Electrical and Electronic Engineering, Universiti Tun Hussein Onn Malaysia, Batu Pahat, Johor, Malaysia, IEEE Control and System Graduate Research Colloquium.

[9] Leland H. Jorgensen (April 1973). A method for estimating static aerodynamic characteristics for slender bodies of circular and noncircular cross section alone and with lifting surfaces at angles of attack from 0 to 90. Tech. Rep. NASA TN D-7228, Ames Research Center, Moffett Field, Calif. 94035.

[10] Naomi Ehrich Leonard and Joshua G. Graver (October 2001). Model-Based Feedback Control of Autonomous Underwater Gliders, IEEE Journal of Oceanic Engineering.

[11] R.V. Shashank Shankar and R. Vijayakumar (March 2020). Numerical Study of the Effect of Wing Position on Autonomous Underwater Glider, Department of Applied Mechanics, Indian Institute of Technology Delhi, Department of Ocean Engineering, Indian Institute of Technology Madras.

[12] R. V. Shashank Shankar and R. Vijayakumar (2019). Effect of Rudder and Roll Control Mechanism on Path Prediction of Autonomous Underwater Gliders, IEEE OCEANS 2022.

[13] Saeedeh Ziaeefard (2018). Extending Maneuverability of Internally Actuated Underwater Gliders, An Attempt to Develop an Open Platform For Research and Education, Michigan Technological University.

[14] Teledyne (2011). Teledyne webb research reaches second milestone with u.s. navy lbs-glider program. http://www.webbresearch.com/newscenter/Reaches Second Milestone.aspx

[15] Th. Lutz and S. Wagner (1997). Drag reduction and shape optimization of airship bodies. Institute for Aerodynamics and Gas Dynamics University of Stuttgart, Germany.

[16] W. E. Pinebrook, Charles Dalton (1983). The evolution strategy applied to drag minimization on a body of revolution, University of Houston.

[17] Werner Nachtigall and Alfred Wisser (2015). Bionics by Examples. Department Natural Sciences and Technology, Saarland University Saarbrücken Germany, pp 224-225.

STONE BY STONE SEGMENTATION FROM THE ORTHOPHOTO TO THE 3D CAD MODEL OF A MASONRY FAÇADE

Demitrios Galanakis[1*], Koubouratou Idjaton[2], Sylvie Treuillet[2], Xavier.Brunetaud[2], Nectarios Vidakis[3], Markos Petousis[3], Marilena Tsakoumaki[4] and Emmanuel Maravelakis[1]

[1]Department of Electronic Engineering, Hellenic Mediterranean University, Chania, Greece
[2]University d' Orleans, INSA CVL, PRISME EA 4229, F45072, Orleans, France
[3]Department of Mechanical Engineering, Hellenic Mediterranean University, Iraklion, Greece
[4]Ephorate of Antiquities of Phocis Ministry of Culture and Sports of Greece

*Corresponding Author: galanakisdemitris@gmail.com

1. INTRODUCTION

The unprecedented growth of LIDAR technology along with the advances in image-based 3D modelling (Pepe et al., 2020) offer now new perspectives in digital acquisition media and allow for almost instant data gathering with high accuracy and resolution (Maravelakis et al., 2013; Matrone & Martini, 2021; Pepe et al., 2020) and with no restrictions usually associated with site's accessibility, location or scaling (Maravelakis et al., 2015). Some of the most versatile reality-capturing methods deploy unmanned aerial vehicles (UAVs) (Costantino et al., 2021) with high-resolution cameras on board that utilize Structure-from-Motion (SfM) and Multi-View Stereo algorithms (MVS) for 3D scene restitution (Pepe et al., 2020).

Nevertheless, this new innovative 3D capturing technology, such as the Terrestrial Laser Scanners (TLS), that reshaped traditional ways of surveying cultural heritage assets (Maravelakis et al., 2014, 2015), involves too many parties (engineers, architects, archeologists, civil engineers, etc.…), with sometimes conflicting interests (Nieto-Julián et al., 2022; Pocobelli et al., 2018), working in parallel on a rather complicated workflow, with multiple data formats, data attributes, on different platforms, with loosely defined specifications or requirements (Maravelakis et al., 2013). Maravelakis et al., (2013) highlighted the problem in 2013 in his work trying to set the foundations for a meticulous 3D metadata network able to cope with this inherent complexity in a multidisciplinary and holistic approach. In this regard, the Architecture, Engineering and Construction (AEC) industry has shifted its main interest toward Building Information Modelling (BIM) (Macher et al., 2017; Nieto-Julián et al., 2022; Pocobelli et al., 2018; Ursini et al., 2022).

BIM was initially conceived as an improvement to the traditional 2D Computer Aided Design CAD-based representation but rapidly evolved as a complete process for accommodating heterogeneous historical architectural and engineering data in a consistent and reliable pipeline throughout the lifecycle of an asset (Dore & Murphy, 2013; Pocobelli et al., 2018). Unfortunately, BIM, especially within the context of Cultural Heritage (CH) or Heritage/Historic-BIM (HBIM) (Ursini et al., 2022), and despite its many advances in the last decade, remains a challenging issue due to the inherent complexity of digitizing already as-is buildings structures (Scan-to-BIM) that by-design tend to defy uniformity and standardization rules (Pocobelli et al., 2018).

Robust research findings highlight the importance of automation endeavors in segmentation (Macher et al., 2017; Matrone & Martini, 2021). Maravelakis et al., (2015) almost a decade before proposed a framework for automated identification of the building's layout to facilitate smart cities concept. In his image-processing scheme, 2D ortho-projections were used as input for creating a detailed 3D map of the surveyed area (Maravelakis et al., 2015). Bassier et al., (2017) validate a

feature extraction Support-Vector-Machine-based (SVM) algorithm that builds knowledge upon strict architectural constraints. Pierdicca et al., (2020) introduced a benchmark under the name of Architectural Cultural Heritage Dataset (ArCH) that comprises of 11 annotated scenes for testing and training Deep Learning (DL) frameworks. Matrone & Martini, (2021) invoked external classifiers and explores the possibilities of Transfer Learning (TL) and Dynamic Graph Convolutional Neural Network (DGCNN) in CH domain. Teruggi et al., (2020) proposed and validated a Multi-Level-Multi-Resolution (MLMR) Machine-Learning (ML) driven architecture for automatic point cloud segmentation that iterates down to instance segmentation, i.e., instances of the same class.

Moving on, Poux et al., (2017) established the term "smart" point cloud and utilized ontology-driven classification algorithms that can distinguish each tesserae in CH artifacts, Idjaton et al., (2021) demonstrates the validity of new algorithm for Stone-by-Stone segmentation of a planar masonry wall through DeepLabv3+ modified architecture, Liu et al., (2022) utilizes SfM and Deeplabv3, as well, for mesh segmentation and Valero et al., (2018) dismantles individual building blocks in masonry arrangements with Continuous Wavelet Transform (CWT). In the same research, stone-by-stone segmentation algorithm performs a binary classification between bricks and mortar/joint which according to authors can be generalized to non-planar wall objects (Valero et al., 2018). Shen et al., (2018) working on brick extraction, publish an algorithm that considers point cloud data, captured by TLS, as input and produces the exact coordinates of the vertices of each brick in the scene with an accuracy of 75% per brick. Finally, Galanakis et al., (2023) trace the radii profile of an ancient Doric Order column and decompose it to its constituent elements.t.

2. MATERIALS AND METHODS

As previously stated, mesh segmentation keeps attracting a lot of research interest (Alfio et al., 2022; Galanakis et al., 2023; Idjaton et al., 2021; Shaqfa & Beyer, 2022) and the entailed complexity increases when the model is to be tested against its structural stability. Traditionally, converting tangible cultural heritage assets to 3D FEM-intelligible objects varied on the exhibited complexity. Simple and easy-to-model geometries are usually translated to simple geometric primitives whereas in more organic entities, external packages and third-party software manages the external geometry using NURBS and then convert it to solid through some king of Boolean logic (Fabbrocino et al., 2006; Panagouli & Christodoulou, 2022; Papadopoulos et al., 2019; Ursini et al., 2022).

The proposed system consists of a multi-stage algorithm that takes a 3D high-resolution model created for visualization and rendering purposes and returns N water-tight meshes each representing a different building block in the scene. The main objective is to develop an end-to-end application that will be able to decimate 3D models down to stone-level accuracies. The procedure is as follows:

- Step 1. 3D model, in .obj format, is imported and analyzed following Principal Component Analysis PCA (Shen et al., 2018) for estimating rotation angles. This information will allow for the automatic ortho-projection of the scene on the XZ plane (Figure 1).
- Step 2. Stone-by-stone segmentation algorithm, developed and validated by (Idjaton et al., 2021), labels each pixel in the orthomosaic map.
- Step 3. Segmentation layout, created in step three, is streamed to free and open-source BIM-friendly platform, FreeCAD, which then utilizes .SVG to.BIM wall object conversion.
- Step 4. Steps are repeated along the remaining facades of the building

3. RESULTS AND DISCUSSION

Advances in Computer Vision (CV) (Jardim et al., 2022; Shen et al., 2018) , mesh segmentation (Barsanti et al., 2017; Ibrahim et al., 2020; Idjaton et al., 2021; Morbidoni et al., 2020; Murtiyoso et al., 2021; Teruggi et al., 2020; Valero et al., 2018) and BIM (Croce et al., 2021; Pocobelli et al., 2018; Xiong et al., 2013) now push scientists towards more sophisticated Digital Cultural Heritage (DCH)

application such as Finite Element Analysis (FEA) which seek to explore static and dynamic structural behavior of the building (Ursini et al., 2022). Nonetheless, high resolution heavy models, with refined geometry, usually provided by the 3D modelling phase, are not appropriate for numerical analysis and might result in significant computational time and resources (Pitilakis et al., 2017). In this sense, this aim of this research is a) to identify new intelligent mesh conversion alternatives within the concept of Scan-to-FEM that will further facilitate CH management rehabilitation and documentation.

4. ACKNOWLEDGMENT

5. REFERENCES

Alfio, V. S., Costantino, D., Pepe, M., & Garofalo, A. R. (2022). A Geomatics Approach in Scan to FEM Process Applied to Cultural Heritage Structure: The Case Study of the "Colossus of Barletta." Remote Sensing, 14(3). https://doi.org/10.3390/rs14030664

Barsanti, S. G., Guidi, G., & Luca, L. De. (2017). SEGMENTATION OF 3D MODELS FOR CULTURAL HERITAGE STRUCTURAL ANALYSIS – SOME CRITICAL ISSUES. IV(September), 115–122. https://doi.org/10.5194/isprs-annals-IV-2-W2-115-2017

Bassier, M., Vergauwen, M., & Van Genechten, B. (2017). AUTOMATED CLASSIFICATION of HERITAGE BUILDINGS for AS-BUILT BIM USING MACHINE LEARNING TECHNIQUES. ISPRS Annals of the Photogrammetry, Remote Sensing and Spatial Information Sciences, 4(2W2), 25–30. https://doi.org/10.5194/isprs-annals-IV-2-W2-25-2017

Costantino, D., Pepe, M., & Restuccia, A. G. (2021). Scan-to-HBIM for conservation and preservation of Cultural Heritage building: the case study of San Nicola in Montedoro church (Italy). Applied Geomatics, 2019. https://doi.org/10.1007/s12518-021-00359-2

Croce, V., Caroti, G., Piemonte, A., & Bevilacqua, M. G. (2021). From survey to semantic representation for cultural heritage: The 3D modelling of recurring architectural elements. Acta IMEKO, 10(1), 98–108. https://doi.org/10.21014/ACTA_IMEKO.V10I1.842

Dore, C., & Murphy, M. (2013). Semi-automatic techniques for as-built BIM façade modeling of historic buildings. Proceedings of the DigitalHeritage 2013 - Federating the 19th Int'l VSMM, 10th Eurographics GCH, and 2nd UNESCO Memory of the World Conferences, Plus Special Sessions FromCAA, Arqueologica 2.0 et Al., 1, 473–480. https://doi.org/10.1109/DigitalHeritage.2013.6743786

Fabbrocino, G., Iervolino, I., & Manfredi, G. (2006). Damage mitigation by innovative materials for Temple C at Selinunte. Construction and Building Materials, 20(10), 1040–1048. https://doi.org/10.1016/j.conbuildmat.2005.04.003

Galanakis, D., Maravelakis, E., Phaedra, D., Vidakis, N., Petousis, M., Konstantaras, A., & Tsakoumaki, M. (2023). SVD-based point cloud 3D stone by stone segmentation for cultural heritage structural analysis – The case of the Apollo Temple at Delphi. Journal of Cultural Heritage, 61, 177–187. https://doi.org/10.1016/j.culher.2023.04.005

Ibrahim, Y., Nagy, B., & Benedek, C. (2020). Deep learning-based masonry wall image analysis. Remote Sensing, 12(23), 1–28. https://doi.org/10.3390/rs12233918

Idjaton, K., Desquesnes, X., Treuillet, S., & Brunetaud, X. (2021). Stone-by-Stone Segmentation for Monitoring Large Historical Monuments Using Deep Neural Networks. Lecture Notes in Computer Science (Including Subseries Lecture Notes in Artificial Intelligence and Lecture Notes in Bioinformatics), 12667 LNCS, 235–248. https://doi.org/10.1007/978-3-030-68787-8_17

Jardim, S., António, J., & Mora, C. (2022). Graphical Image Region Extraction with K-Means Clustering and Watershed. Journal of Imaging, 8(6), 1–27. https://doi.org/10.3390/jimaging8060163

Liu, Z., Brigham, R., Long, E. R., Wilson, L., Frost, A., Orr, S. A., & Grau-Bové, J. (2022). Semantic segmentation and photogrammetry of crowdsourced images to monitor historic facades. Heritage Science, 10(1), 1–17. https://doi.org/10.1186/s40494-022-00664-y

Macher, H., Landes, T., & Grussenmeyer, P. (2017). From point clouds to building information models: 3D semi-automatic reconstruction of indoors of existing buildings. Applied Sciences (Switzerland), 7(10), 1–30. https://doi.org/10.3390/app7101030

Maravelakis, E., Konstantaras, A., Kabassi, K., Chrysakis, I., Georgis, C., & Axaridou, A. (2014). 3DSYSTEK web-based point cloud viewer. IISA 2014 - 5th International Conference on Information, Intelligence, Systems and Applications, July, 262–266. https://doi.org/10.1109/IISA.2014.6878726

Maravelakis, E., Konstantaras, A., Kilty, J., Karapidakis, E., & Katsifarakis, E. (2015). Automatic building identification and features extraction from aerial images: Application on the historic 1866 square of Chania Greece. 2014 International Symposium on Fundamentals of Electrical Engineering, ISFEE 2014, 7–12. https://doi.org/10.1109/ISFEE.2014.7050594

Maravelakis, E., Konstantaras, A., Kritsotaki, A., Angelakis, D., & Xinogalos, M. (2013). Analysing user needs for a unified 3D metadata recording and exploitation of cultural heritage monuments system. Lecture Notes in Computer Science (Including Subseries Lecture Notes in Artificial Intelligence and Lecture Notes in Bioinformatics), 8034 LNCS(PART 2), 138–147. https://doi.org/10.1007/978-3-642-41939-3_14

Matrone, F., & Martini, M. (2021). Transfer Learning and Performance Enhancement Techniques for Deep Semantic Segmentation of Built Heritage Point Clouds. Virtual Archaeology Review, 12(25), 73–84. https://doi.org/10.4995/var.2021.15318

Morbidoni, C., Pierdicca, R., Quattrini, R., & Frontoni, E. (2020). GRAPH CNN with RADIUS DISTANCE for SEMANTIC SEGMENTATION of HISTORICAL BUILDINGS TLS POINT CLOUDS. International Archives of the Photogrammetry, Remote Sensing and Spatial Information Sciences - ISPRS Archives, 44(4/W1), 95–102. https://doi.org/10.5194/isprs-archives-XLIV-4-W1-2020-95-2020

Murtiyoso, A., Lhenry, C., Landes, T., Grussenmeyer, P., & Alby, E. (2021). Semantic segmentation for building façade 3D point cloud from 2D orthophoto images using transfer learning. International Archives of the Photogrammetry, Remote Sensing and Spatial Information Sciences - ISPRS Archives, 43(B2-2021), 201–206. https://doi.org/10.5194/isprs-archives-XLIII-B2-2021-201-2021

Nieto-Julián, J. E., Farratell, J., Bouzas Cavada, M., & Moyano, J. (2022). Collaborative Workflow in an HBIM Project for the Restoration and Conservation of Cultural Heritage. International Journal of Architectural Heritage, 00(00), 1–20. https://doi.org/10.1080/15583058.2022.2073294

Panagouli, O. K., & Christodoulou, A. (2022). Numerical investigation of the contribution of metallic dowels to the stability of multi-drum columns. Developments in the Built Environment, 11(February), 100082. https://doi.org/10.1016/j.dibe.2022.100082

Papadopoulos, K., Vintzileou, E., & Psycharis, I. N. (2019). Finite element analysis of the seismic response of ancient columns. Earthquake Engineering and Structural Dynamics, 48(13), 1432–1450. https://doi.org/10.1002/eqe.3207

Pepe, M., Costantino, D., & Garofalo, A. R. (2020). An efficient pipeline to obtain 3D model for HBIM and structural analysis purposes from 3D point clouds. Applied Sciences (Switzerland), 10(4). https://doi.org/10.3390/app10041235

Pierdicca, R., Paolanti, M., Matrone, F., Martini, M., Morbidoni, C., Malinverni, E. S., Frontoni, E.,

& Lingua, A. M. (2020). Point cloud semantic segmentation using a deep learning framework for cultural heritage. Remote Sensing, 12(6), 1–23. https://doi.org/10.3390/rs12061005

Pitilakis, K., Tsinidis, G., & Karafagka, S. (2017). Analysis of the seismic behavior of classical multi-drum and monolithic columns. Bulletin of Earthquake Engineering, 15(12), 5281–5307. https://doi.org/10.1007/s10518-017-0160-4

Pocobelli, D. P., Boehm, J., Bryan, P., Still, J., & Grau-Bové, J. (2018). BIM for heritage science: a review. Heritage Science, 6(1), 23–26. https://doi.org/10.1186/s40494-018-0191-4

Poux, F., Neuville, R., & Billen, R. (2017). POINT CLOUD CLASSIFICATION of TESSERAE from TERRESTRIAL LASER DATA COMBINED with DENSE IMAGE MATCHING for ARCHAEOLOGICAL INFORMATION EXTRACTION. ISPRS Annals of the Photogrammetry, Remote Sensing and Spatial Information Sciences, 4(2W2), 203–211. https://doi.org/10.5194/isprs-annals-IV-2-W2-203-2017

Shaqfa, M., & Beyer, K. (2022). A virtual microstructure generator for 3D stone masonry walls. European Journal of Mechanics, A/Solids, 96, 104656. https://doi.org/10.1016/j.euromechsol.2022.104656

Shen, Y., Lindenbergh, R., Wang, J., & Ferreira, V. G. (2018). Extracting individual bricks from a laser scan point cloud of an unorganized pile of bricks. Remote Sensing, 10(11). https://doi.org/10.3390/rs10111709

Teruggi, S., Grilli, E., Russo, M., Fassi, F., & Remondino, F. (2020). A hierarchical machine learning approach for multi-level and multi-resolution 3d point cloud classification. Remote Sensing, 12(16). https://doi.org/10.3390/RS12162598

Ursini, A., Grazzini, A., Matrone, F., & Zerbinatti, M. (2022). From scan-to-BIM to a structural finite elements model of built heritage for dynamic simulation. Automation in Construction, 142(January 2021), 104518. https://doi.org/10.1016/j.autcon.2022.104518

Valero, E., Bosché, F., & Forster, A. (2018). Automatic segmentation of 3D point clouds of rubble masonry walls, and its application to building surveying, repair and maintenance. Automation in Construction, 96(May), 29–39. https://doi.org/10.1016/j.autcon.2018.08.018

Xiong, X., Adan, A., Akinci, B., & Huber, D. (2013). Automatic creation of semantically rich 3D building models from laser scanner data. Automation in Construction, 31, 325–337. https://doi.org/10.1016/j.autcon.2012.10.006

MEASURING DISPLACEMENT OF IPMC ACTUATOR

Tsiakmakis K., Delimaras V., Papadopoulou S.M., Hatzopoulos A.T.

Department of Information and Electronic Engineering
International Hellenic University, Sindos, Thessaloniki, Greece
ktsiak@ihu.gr

1. INTRODUCTION

Micromechanical actuators are commonly utilized in biomedical engineering, robotics, and microelectromechanical systems (MEMS). To effectively define the electromechanical properties of these devices, a comprehensive knowledge of their motion parameters, especially the actuator position, is required (Shahinpoor & Kim, 2001). Due to its unique properties, the Ionic Polymer Metal Composite (IPMC) is a potential actuator in this area. IPMCs are ionic polymer-based materials having platinum metal membranes on both sides. When an electric field is applied across their thickness, they bend and generate a detectable voltage when mechanically deformed.

Various monitoring systems have been developed to characterize the motion of micromechanical actuators with high resolution (Chen & Shahinpoor, 2005). The laser measurement system stands out among them due to its fast motion tracking capability and high precision (Bhat & Kim, 2004). This approach, however, has considerable limitations. First, it cannot measure materials with a highly reflecting surface, like some IPMC materials have. Additionally, when the actuator strip is long, the laser is unable to precisely measure its position since the material bends significantly and moves outside the field. In underwater conditions, measurement results may deviate significantly due to changes in the reflection index.

For effective use in a range of applications, micromechanical actuators' electromechanical properties must be precisely characterized. This research emphasizes the importance of a comprehensive understanding of an actuator's motion parameters. Although the laser measurement system has many advantages in terms of accuracy and speed, it has significant limitations, including difficulty measuring highly reflective IPMC materials accurately, inaccurate measurements of long actuator strips, and significant measurement deviations in underwater environments.

To resolve these issues, this paper employs a camera-based measuring system. This method has its own limitations, such as slow motion monitoring and a high computing power need. In addition, its resolution is poor and is normally determined by the resolution of the image sensor as well as the distance between the camera and the target. To gather all of the data required for the IPMC position analysis, appropriate imaging methods are used. Fast image processing algorithms for the actuator's interest point tracking are required to develop a real-time measuring system.

The proposed method is based on a low-cost camera sensor used to measure large and slow movements of the IPMC strips for underwater micro-robotic applications. This method was implemented using an ESP32 microcontroller with an integrated video camera. The microprocessor implements image processing for the displacement measurement and actuation of the IPMC via an adjustable voltage power circuit. The camera and laser- based methods are compared.

In previous work, fast techniques to locate the free edge with high accuracy using well-characterized cameras were presented [Tsiakmakis et al, 2007]. In this work, a very low-cost camera embedded in a microcontroller was used to track the position of the material when it is moving at a very low speed.

2.   SET-UP OF THE MEASUREMENT SYSTEM

Figure 1 depicts the experimental configuration used to detect the displacement of the IPMC strip. A low-cost camera was utilized, which exhibits no malfunctioning at low frame rates. The camera produces grayscale data with a resolution of 320x240 or 640x480 pixels per frame and a frame rate of 10 fps.

Under appropriate lighting conditions and against a well-contrasted background, the camera is oriented vertically and mounted onto the moving material. A separate esp32 microcontroller is used to produce a sinusoidal or step signal.
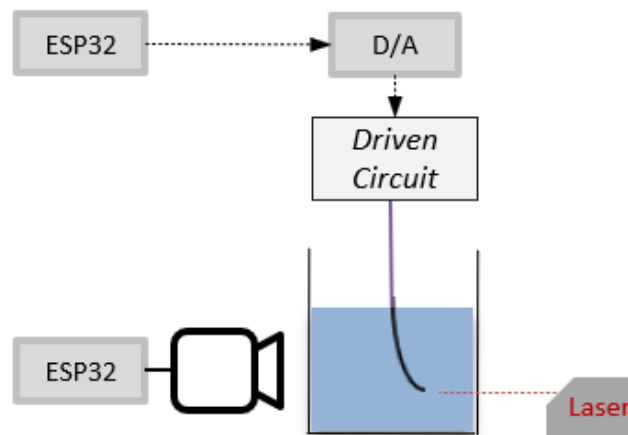
Figure 1. The experimental setup

Figure 2 depicts the circuit that was used in the experiment. The power-follower is driven by the MCP4822 digital-to-analog converter. Resistor R3 has been set to 1 in order to measure the current flowing through the actuator.
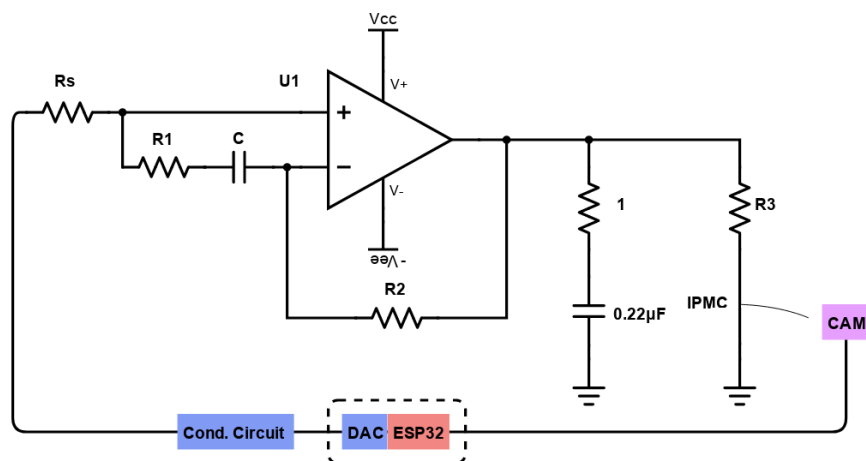
Figure 2. The circuit of the experimental setup

The power amplifier LM675 operates as a voltage follower to generate the IPMC driving voltage, which can deliver current up to 1A. Its primary function is to supply the necessary output current.

3.   TRACKING METHOD

The algorithm analyzes the entire frame, trying to locate the free end of the strip. This technique only makes advantage of the power of an esp32.

The algorithm detects the bottom of the IPMC shape, followed by the rightmost point-of-interest

at the bottom of the strip. Figure 3 describes the different approach to measuring distance for the camera and the laser.
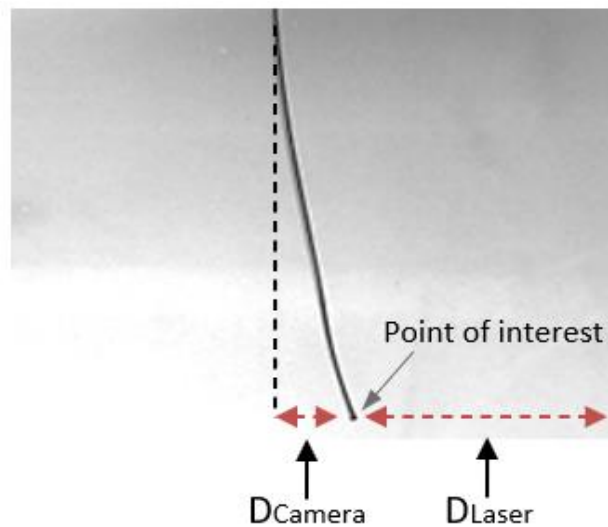
Figure 3. Different methods for calculating the displacement of an IPMC strip

The end point tracking method is thoroughly analyzed in a prior work by the same author [Tsiakmakis et al , 2009].

4.   EXPERIMENTAL RESULTS

The precise relationship between pixels and meters relies on the image resolution and the distance from the subject that the camera is pointing at. The field of view is modified according to the subject's dimensions for each trial.

The IPMC actuator is able to operate at frequencies higher than 80Hz, the camera can measure displacement clearly and satisfactorily at lower frequencies. Less than half of the value can be measured when the camera works at a frame rate of 10 frames per second. The findings demonstrate that this device was capable of measuring at 1Hz even when the camera was operating at a 10fps frame rate. In contrast to laser measurement systems, that exhibit differences in performance when used underwater due to glass reflection, performance is the same in both air and underwater applications.

The error between the measured and actual corner (point of interest) is used to establish position accuracy. It should be noticed that the corner point can only be defined by one pixel. If the corner is indicated on the actual point (pixel), the corner detection is successful. As a result, the resolution has a direct impact on the accuracy. The results of the experiment show a one-pixel difference between the marked and actual corner, which for an image resolution of 640x480 pixels corresponds to a position error of about 0.2mm, as shown in Table 1.

Table 1. Resolution for specific image size

Image Size (pixels)	Resolution (mm)	Error (mm)
640×480	0.2	0.01

The working distance must be adjusted to obtain a resolution of about 0.2mm. The resolution varies with image size, working distance and field of view in millimeters. This resolution is not the best but it is optimal for the specific setup and camera in order to provide a more efficient measurement with the lowest processing time. The lower edge of the material may come out of the

field if the distance and field of view are sufficiently decreased. The quality of the camera is very poor and introduces significant distortion to the image. To avoid additional distortion after calibration (Zhang, 2000), the working field of view is reduced and focused on the center of the image.

The detection accuracy here refers to how many corners are correctly detected. This is different for various camera quality and when IPMC presents high bending. Due to image quality, the experimental results show a low detection rate of 72%.

Camera is calibrated before each specific experiment and setup has an accuracy of 0.2 mm per pixel. For data transmission reliability, with fewer dropped frames, we have chosen the value of 10 fps. Figure 4 shows the comparison of measurements of displacements versus frequency in water using the laser and camera systems up to 1.8 Hz.
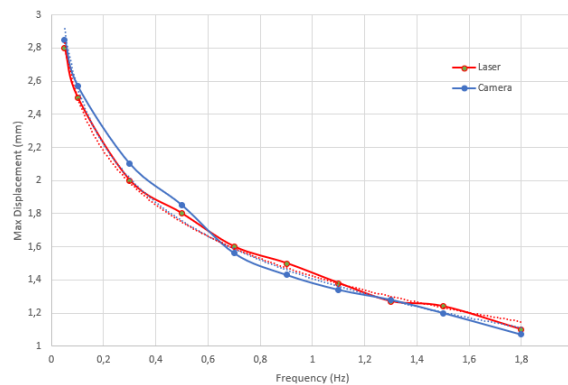
Figure 4. Comparison of measurements of displacements versus frequency in water using the laser and camera systems up to 1.8 Hz

Figure 5 depicts the camera and laser measurements for a sinusoidal input voltage signal of 100mHz.
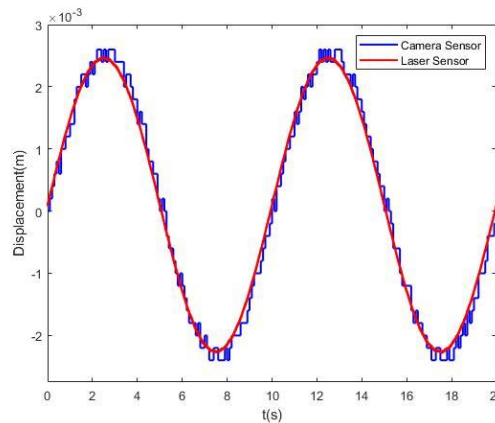
Figure 5. Measurements with camera and laser for a 100mHz sinusoidal input voltage signal

The image-processing algorithm can handle big bending conditions but the execution time for finding the endpoint is increased, as shown in Table 2.

Table 2. Execution time for camera approach

Frame Size (pixels)	Small Bending (ms)	Big Bending (ms)
640x480	43	56

These conclusions are achieved after 500 successive images that were processed by the camera during a 30-second period results in the average calculation time.

5. CONCLUSION

The proposed system utilizes an ESP32 microcontroller and a low-cost camera sensor to measure displacement and a circuit to activate the IPMC strips. The algorithm analyses the entire frame and finds the IPMC shape's bottom and rightmost point of interest.

The research compares the laser measurement system and a camera-based measuring system to characterize the motion of micromechanical actuators. The laser measurement system is known for its high precision and fast motion tracking capability, but it has limits when dealing with highly reflective IPMC materials, long actuator strips, and underwater conditions. The research proposes a camera-based measuring system to solve these restrictions, however it acknowledges its own drawbacks, such as slow-motion monitoring, a high computational power demand, poor resolution, and the need for fast image processing algorithms.

The experimental results reveal that the camera can measure displacement clearly and sufficiently at low frequencies, with a resolution of about 0.2mm per pixel. The frame rate of the camera influences its performance, and at 10 frames per second, the measurement performance is decreased. The camera's low-quality image and distortion present additional challenges, requiring calibration and focusing on the image's centre. Due to the image quality, the camera system has a reduced detection rate for corners, and the execution time for detecting the endpoint increases under large bending situations. The experimental results show that employing a low-cost camera for displacement measurement is feasible, but further enhancements are needed to improve detection rates and minimize execution time.

6. REFERENCES

Bhat, N., & Kim, W. J. (2004). Precision force and position control of an ionic polymer metal composite. Proceedings of the Institution of Mechanical Engineers, Part I: Journal of Systems and Control Engineering, 218(6), 421-432.

Chen, Z., Tan, X., & Shahinpoor, M. (2005). Quasi-static positioning of ionic polymer-metal composite (IPMC) actuators. In Proceedings of the IEEE/ASME International Conference on Advanced Intelligent Mechatronics (pp. 60-65).

Shahinpoor, M., & Kim, K. J. (2001). Ionic polymer-metal composites: I. Fundamentals. Smart materials and structures, 10(4), 819.

Tsiakmakis, K., Brufau, J., Puig-Vidal, M., & Laopoulos, T. (2007). Measuring motion parameters of ionic polymer-metal composite (IPMC) actuators with a CCD camera. In Proc. IEEE IMTC (pp. 1-6).

Tsiakmakis, K., Brufau-Penella, J., Puig-Vidal, M., & Laopoulos, T. (2009). A camera based method for the measurement of motion parameters of IPMC actuators. IEEE Transactions on Instrumentation and Measurement, 58(8), 2626-2633.

Zhang, Z. (2000). A flexible new technique for camera calibration. IEEE Transactions on pattern analysis and machine intelligence, 22(11), 1330-1334.

COMPARISON OF TRIGGER UNIT TOPOLOGIES FOR PSEUDOSPARK SWITCHES USED AT THE INSTITUTE OF PLASMA PHYSICS AND LASERS OF THE HELLENIC MEDITERRANEAN UNIVERSITY RESEARCH CENTRE

J. Chatzakis[1,2], G. Chatzipetrakis[1], A. Petridi[1], A. Skoulakis[2], I. Fitilis[1,2] and M. Tatarakis[1,2]

[1] Department of Electronic Engineering, School of Engineering, Hellenic Mediterranean University, Chania, Crete, GR 73133, Greece
[2] Institute of Plasma Physics and Lasers, University Research and Innovation Center, Hellenic Mediterranean University, Rethymno, Crete, GR 74100, Greece
E-mail: jchatzakis@hmu.gr

Abstract

The basic topologies that have been used at the Institute of Plasma Physics and Lasers of the Hellenic Mediterranean University Research Centre to trigger a pseudospark switch are reviewed and compared in this paper. Factors that affect their performance, life and construction difficulty and cost are examined.

1. INTRODUCTION

A dense plasma focus (DPF) exists at the Institute of Plasma Physics and Lasers of the Hellenic Mediterranean University Research Centre based its operation on a pseudospark switch [1]. Jitter is a critical factor for the whole system reliable operation. To lower the jitter a number of trigger units were developed, constructed and tested in the laboratory, decreasing the trigger unit jitter to less of 1nsec. To achieve this several topologies used and in this paper a comparison of these topologies related to their other characteristics is presented.

2. TRIGGER UNIT TOPOLOGIES COMPARISON

The first topology that was used at the Institute of Plasma Physics and Lasers of the Hellenic Mediterranean University Research Centre is the Forward Converter [2]. The basic diagram of this topology is shown in Fig1.
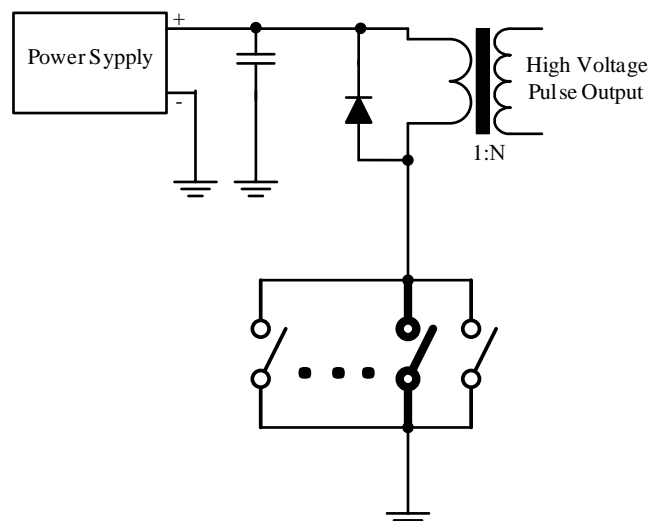

Fig. 1. The Forward Converter topology

In this topology a low supply voltage can be used and a lot of parallel semiconductor switches can handle the high current that is needed. A step-up transformer provides the required isolation and increases the output pulse voltage to meet the requirements od the pseudospark switch. Two are the main disadvantages of this topology: i)The transformer power must cover the peak pulse power and this makes the transformer bulky and decreases the power density, ii) the parasitic inductances of the transformer that decrease the slew-rate of the output pulse and thus increase jitter. The output pulse of this topology trigger generator is shown in Fig. 2.
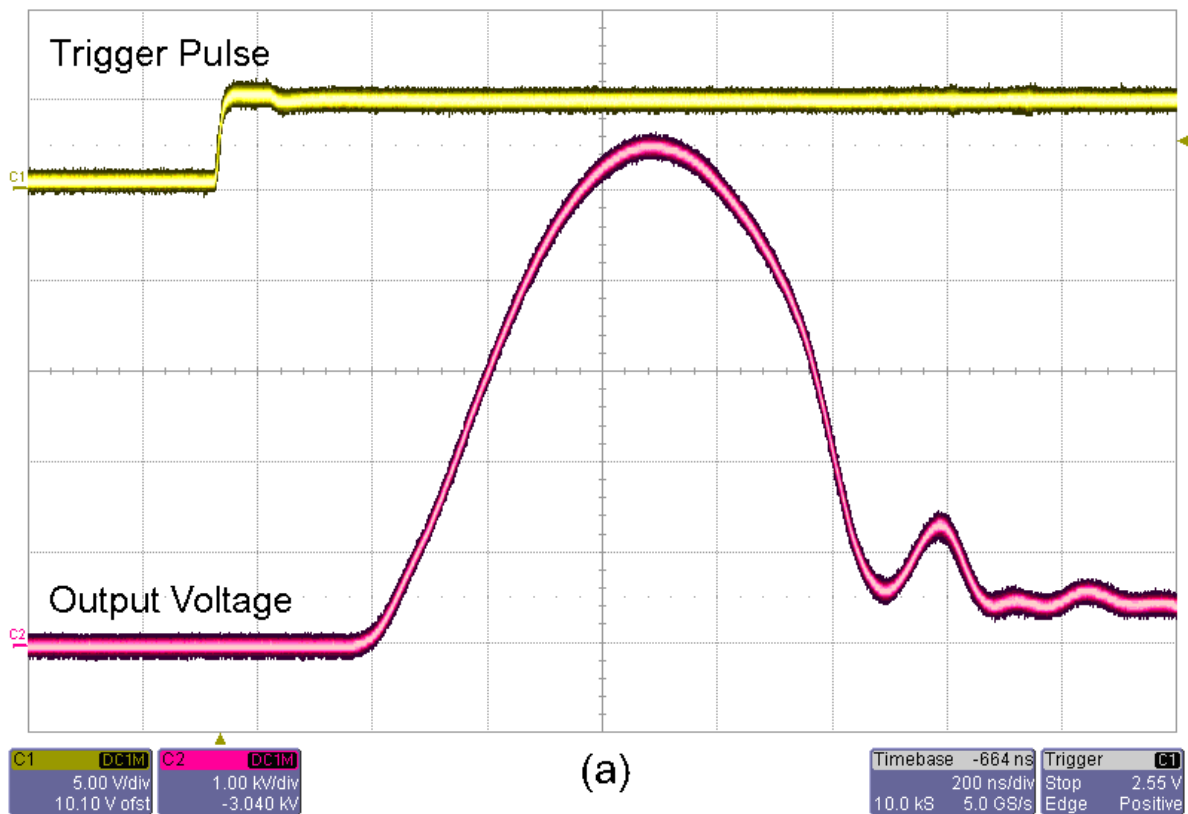
Fig 2. Output pulse of the Forward Converter topology.

Another topology that was used is the Series Connected semiconductor switches [3]. In this topology a number of lower voltage switches are connected in series in order to handle directly the high-voltage of the output pulse and can directly provide this pulse to the pseudospark switch. Any required isolation is provided from an isolated power supply. The basic diagram of this topology is shown in Fig3.
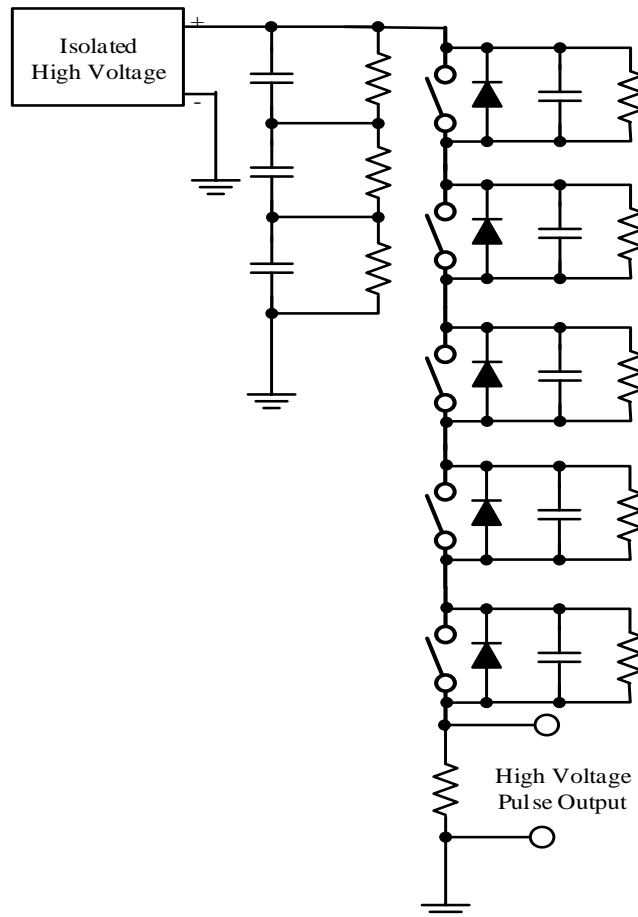
Fig. 3. The Series Connected semiconductor switches topology.

The Series Connected semiconductor switches topology increases the slew-rate of the output pulse and the power density. In the other hand any ununiformity (components tolerace included) will require higher sum voltge of the switches. Thus a high number of switches is required. The output pulse of the Series Connected semiconductor switches topology trigger generator is shown in Fig. 4.
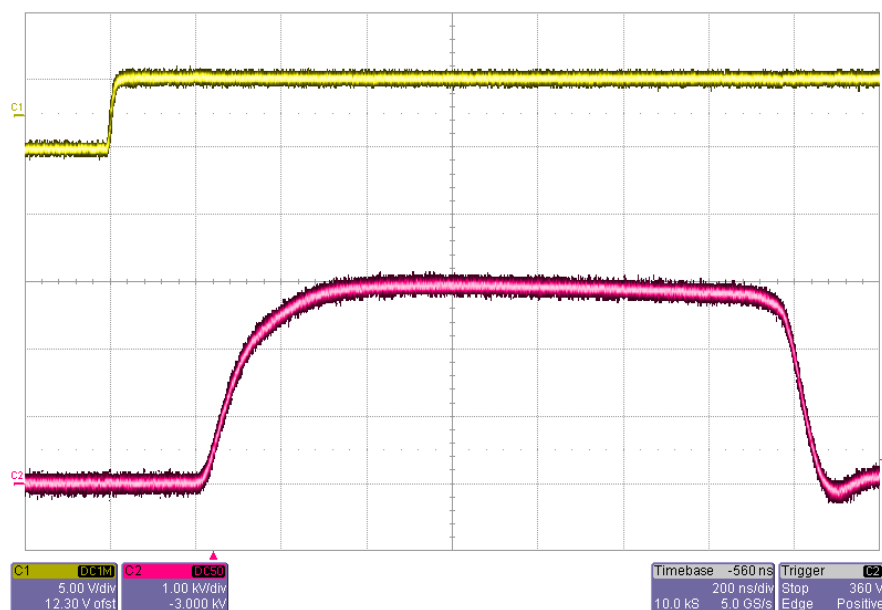

Fig 4. Output pulse of the Series Connected semiconductor switches topology.

The last topology that was used and will be compared int this paper is the Modular Multilevel Converter (mmc) topology [4]. This topology is a very advangeous topology for high voltage operation. The basic diagram of this topology is shown in Fig5.
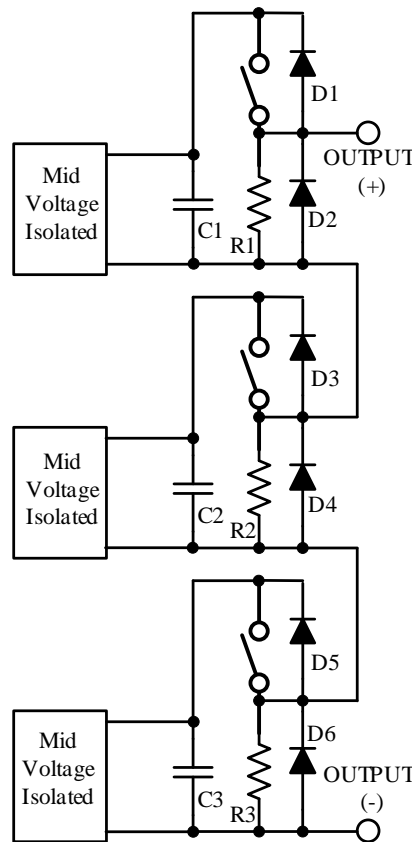
Fig. 5. The Modular Multilevel Converter topology.

The Modular Multilevel Converter topology produces the high-voltage that is neede for the output pulse by summing more lower voltages and directly provides this pulse to the pseudospark switch. The power circuity is simpler and performs better than tis of the Series Connected semiconductor switches topology. Switches is not needed to be identical, so no matching components are needed. The power switches voltage sum has to be just equal to the amplitude of the high voltage pulse. The output pulse of the Modular Multilevel Converter topology trigger generator is shown in Fig. 6.
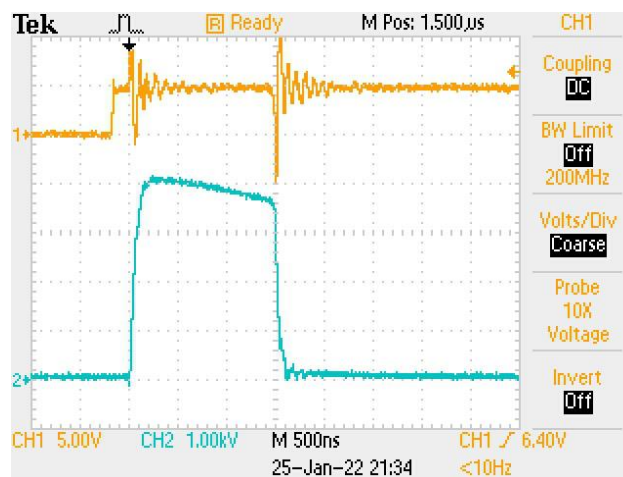
Fig 6. Output pulse of the Modular Multilevel Converter topology.

3.   RESULTS AND DISCUSSION

As the more interasting charachteristic that the Forward Converter topology performs can be assumed the constant low voltage inside the trigger generator. The supply voltage of this topology can be lower than the supply voltage of the other topologies that are presented, without to have a significant affect in the complication of the realization. Other charchteristics can be assumed the low slew-rate of the output pulse, the low Mean Time Between Failure (MTBF) due to the parallel switches connection, the easy construction as there is not required any special component and the high cost as the power switches must additionally handle the transformer losses power.

The Series Connected topology uses a high-voltage power supply. Consequently, the insulations are stressed continuously inside the trigger generator. The improove of the slew-rate of the output pulse is significant, but the matching components and the high number of high voltage switches decrease the MTBF and increase construction difficulty and cost.

The Modular Multilevel Converter topology seems to be the most advangeous. There is medium voltages constantly inside the trigger generator. the slew-rate of the output pulse is improoved, the MTBF is high and the construction difficulty and the cost are kept low.

4.   CONCLUSION

Each one of the topologies that have been used at the Institute of Plasma Physics and Lasers of the Hellenic Mediterranean University Research Centre to trigger a pseudospark switch seems to have its own advantages, but The Modular Multilevel Converter topology seems to be the one with the most advantages.

5.   REFERENCES

1 J. Chatzakis, S. M. Hassan, E. Clark, A. Talebitaher, P. Lee "Improved Detection of Fast Neutrons with Solid-State Electronics" International Conference on Applications of Nuclear Techniques, International Journal of Modern Physics: Conference Series, Vol. 1, No. 1 (2013) 1–5.
2 J. Chatzakis, S. M. Hassan, E. L. Clark, C. Petridis, P. Lee, and M. Tatarakis, Rev. Sci. Instrum. 79 (8), 086103 (2008).
3 J. Chatzakis, S. M. Hassan, E. L. Clark, P. Lee, and M. Tatarakis, Rev. Sci. Instrum. 86 (1), 016108 (2015).
4 A. Petridi, G. Chatzipetrakis, A. Skoulakis, I. Fitilis, M. Tatarakis, J. Chatzakis, Rev. Sci. Instrum. 93 (6), 064711 (2022).

MODULAR MULTILEVEL CONVERTER (MMC) AS HIGH AUDIO AMPLIFIER

Chatzipetrakis G.[1], Papastergiou K.[2], Chatzakis J.[1]

[1] Department of Electronic Engineering, Hellenic Mediterranean University, 73133 Chalepa, Chania, Greece
[2] Geneva, Switzerland

E-mail (chatzipet@hmu.gr)

1. INTRODUCTION

The Modular Multilevel Converters they started as idea from Alesina and Venturini almost from 1981[1][2].They become realistic the 2003 with the creation a family of modular converters with multilevel output that established with the acronym MMC or M2C, from the Marquardt[3], Lesnicar[4], and Glinka[5]. In compare with the other multilevel converter topologies the MMC topology is modular and based on identical submodules, that each one operates only to a cluster of the supply voltage[6]. This is the major advance of the MMC topology, as the converter design is simple and the implementation more cost effective[7]. In our days MMC is the major topology for the converters of high voltage, STATCOMs, electric trains and in large electrical machines[8]. In this paper the way to use the MMC topology to create a high power audio amplifier is described.

2. MMC TOPOLOGY ANALYSIS

In the figure 1 the main structure of a three-phase modular multilevel converter is shown. The DC supply voltage Vdc supplies the three legs of the three-phase converter, One leg for each phase[9]. Each leg is consisted of two arms and each arm is consisted of a number of identical submodules[10]. The legs are Leg α, Leg b, Leg c. The arms separate to the upper arms with letter u and lower arms with letter l[11]. Each arm has a group of submodules and an inductor L. The inductor L is used to limit the surge currents[12]. The submodules can be categorized in one of five different types that can be:
  i.   Half bridge (HB) submodule.
 ii.   Full bridge (FB) submodule.
iii.   Flying capacitor (FC) submodule.
iv.   Cascade half-bridge (CH) submodule.
 v.   Double clamp (CD) submodule.

The proposed analysis uses the half bridge (HB) submodule that is the simplest in design and operation[13]. The half bridge submodule is referred to as a chopper cell [14]. The circuit in figure 2 uses two IGBTs, the S_1 and $\overline{S_1}$ with antiparallel diodes and one capacitor. The two IGBTs devices are operated in a complementary manner to regulate the DC capacitor voltage at a value of u_c. The dc capacitor voltage is given by the follow equation:

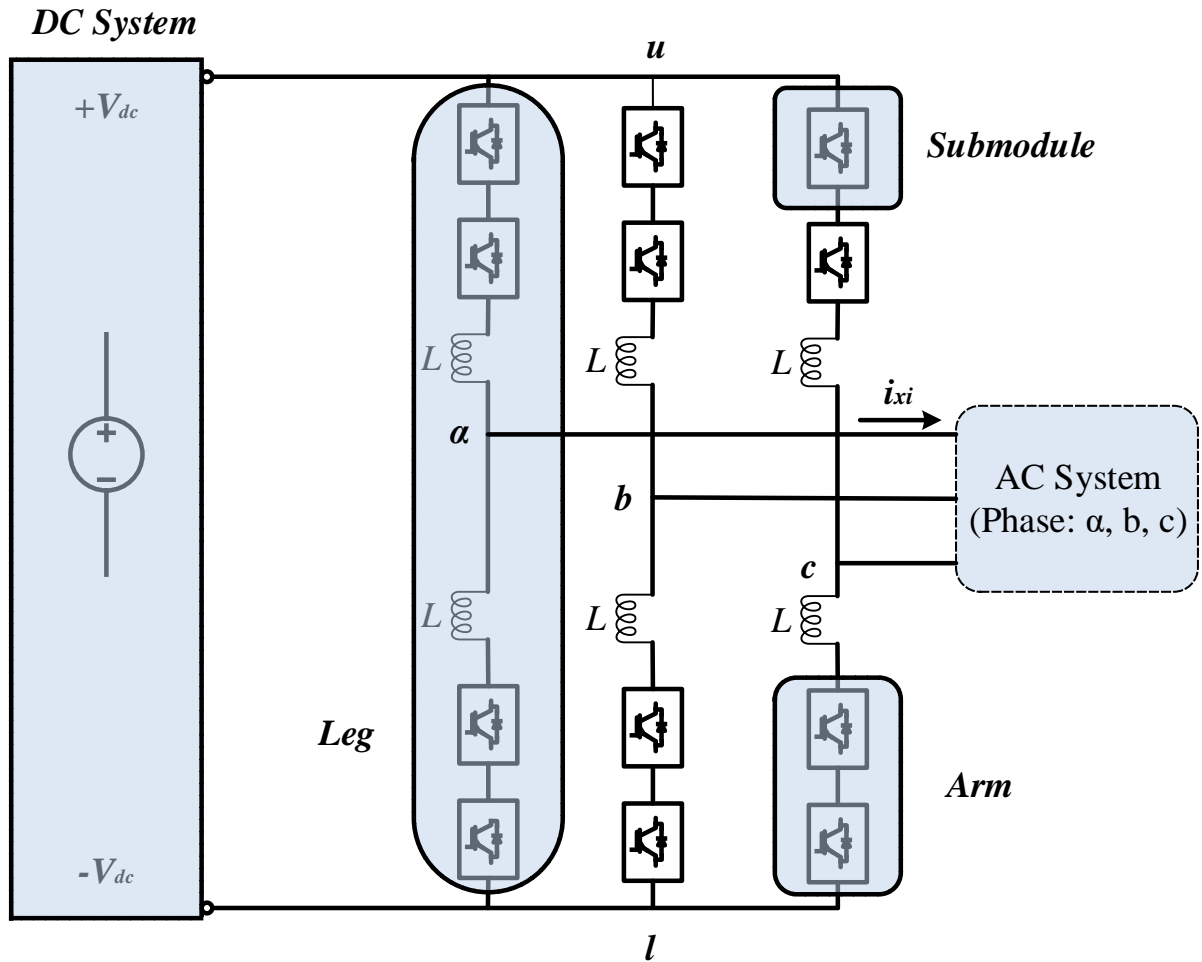$$u_c = \frac{1}{C} \int_{0^+}^{t} i_c(\tau)d\tau \qquad [1]$$

Figure 1.The topology of MMC with IGBTs submodules.

The DC capacitor current in terms of AC current (i_{xy}) and the switching state of top-device $\overline{S_1}$ is given by

$$i_c = S_1 i_{xy} \qquad [2]$$

The states the switch is in the *table 1* that in state 1 $u_H = 0$ and state 2 that $u_H = u_c$.

Table 1.The states of the half bridge submodules.

STATE	S_1	u_H	$i_{xy} > 0$	$i_{xy} \leq 0$
1	0	0	$u_c \approx$	$u_c \approx$
2	1	u_c	$u_c \uparrow$	$u_c \downarrow$

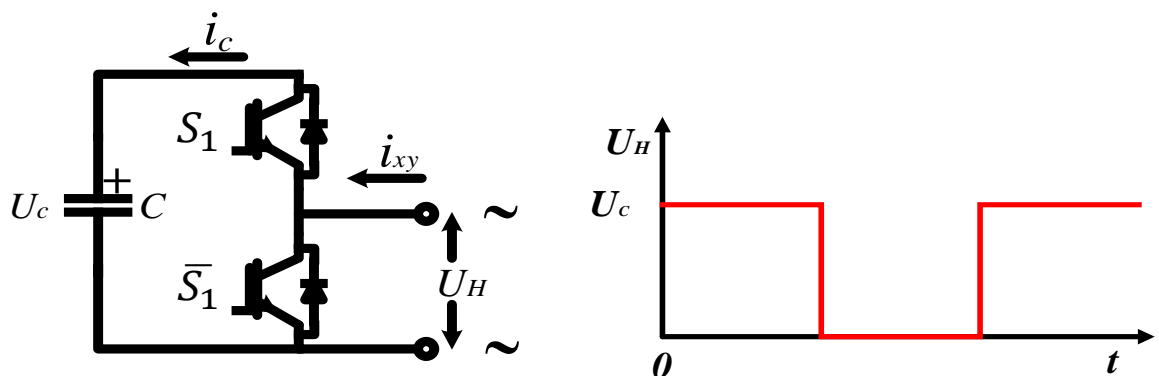$\approx$ = No change, $\uparrow$ = Increasing, $\downarrow$= Decreasing

Figure 2.The half bridge submodules.

3. MMC SIMULATION RESULTS AS HIGHT POWER AMPLIFIER

The circuit topology utilizes a half bridge multilevel converter (chopper cell) based on two legs of twenty (N=20) submodules per arm[15]. This configuration found from the simulations to be the smaller number of submodules that keeps the Total Harmonic Distortion THD less than 6% in a plain (without feedback) system[16]. The submodules use as switches MOSFETs and simulation results are presented in Figure 3. For the simulation setup the reference signal is sinusoidal with f_r=25khz (that is the scale of the acoustic band of the human 15Hz-25kHz), switches frequency is f_{sw}=40kHz and PSC-PWM (Phase Shift Carry Pulse Width Modulation) is used. For the lowest signal distortion modulation factor is m_α=1. The multilevel output has 81 levels and is demodulated using an LC filter before led to an ohmic load. Simulation results using Psim simulator show a THD at the fundamental frequency of 25kHz THD=5,44% at output load power of $P_{rms(LOAD)}$=8396.57Watt. In figure 3 we observe the time domein analisis of $V_{speaker}$ and $I_{speaker}$.

Table 2. **Modular multilevel variables values fort the simulation.**

VARIABLES	VALUES
u_{in}	380Volt
m_a	1
f_r	25kKertz
f_{sw}	40kHertz
$u_{a_{phase\ angle}}$	0°
$u_{b_{phase\ angle}}$	-180°
$R_{speaker}$	8ohms
L_m	5µH
$C_{submodule}$	30mF
L_f	10µH
C_f	15nF

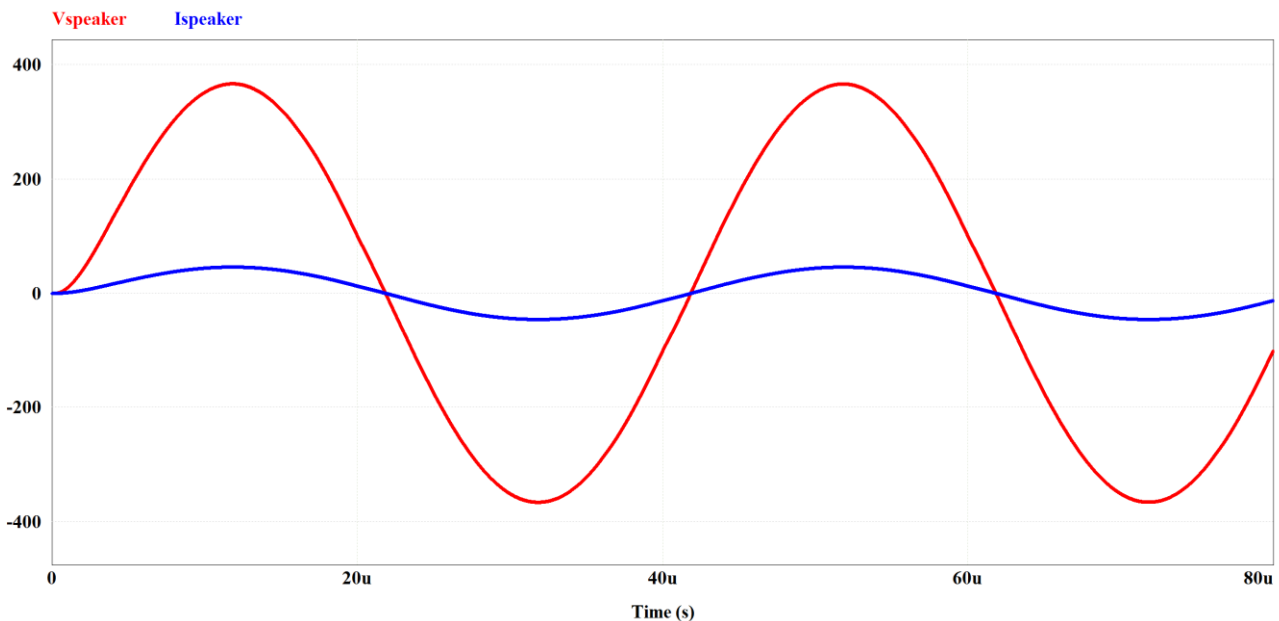**Figure 3.**Time domain analysis of $V_{speaker}$ and $I_{speaker}$.

4. CONCLUSION

In conclusion the next step of our research is to create a simulation thermal analysis model that it will provide more realistic results for the MMC audio amplifier[17]. The target it will be to improve the $THD_{(\%)}$ lesser than 0.1% that it can be possible with more submodules per arm[18], negative feedback[19] and an advance control system for the submodules[20].

5. REFERENCES

[1]   A. Alesina and M. G. B. Venturini, "Solid-State Power Conversion: A Fourier Analysis Approach to Generalized Transformer Synthesis," *IEEE Trans. Circuits Syst.*, vol. 28, no. 4, pp. 319–330, 1981, doi: 10.1109/TCS.1981.1084993.

[2]   R. José *et al.*, "Multilevel Converters: an Enabling Technology for High Power Applications," *Proc. IEEE*, vol. 97, no. 11, pp. 1786–1817, 2009, doi: 10.1109/JPROC.2009.2030235.

[3]   R. Marquardt, "Modular Multilevel Converter: An universal concept for HVDC-Networks and extended DC-bus-applications," *2010 Int. Power Electron. Conf. - ECCE Asia -, IPEC 2010*, pp. 502–507, 2010, doi: 10.1109/IPEC.2010.5544594.

[4]   A. Lesnicar and R. Marquardt, "An innovative modular multilevel converter topology suitable for a wide power range," *2003 IEEE Bol. PowerTech - Conf. Proc.*, vol. 3, pp. 6–11, 2003, doi: 10.1109/PTC.2003.1304403.

[5]   M. Glinka and R. Marquardt, "A new AC/AC multilevel converter family," *IEEE Trans. Ind. Electron.*, vol. 52, no. 3, pp. 662–669, 2005, doi: 10.1109/TIE.2005.843973.

[6]   L. G. Franquelo, J. Rodriguez, J. I. Leon, S. Kouro, R. Portillo, and M. A. M. Prats, "The age of multilevel converters arrives," *IEEE Ind. Electron. Mag.*, vol. 2, no. 2, pp. 28–39, 2008, doi: 10.1109/MIE.2008.923519.

[7]   J. Rodriguez, L. Jih-Sheng, and P. Fangzheng, "Multilevel inverters: A survey of topologies, controls, and applications," *IEEE Trans. Ind. Electron.*, vol. 49, no. 2, pp. 724–738, 2002, doi: 10.1109/TIE.2002.801052.

[8]   J. Rodríguez, S. Bernet, B. Wu, J. O. Pontt, and S. Kouro, "Multilevel voltage-source-converter topologies for industrial medium-voltage drives," *IEEE Trans. Ind. Electron.*, vol. 54, no. 6, pp. 2930–2945, 2007, doi: 10.1109/TIE.2007.907044.

[9]   S. Du, Apparao Dekka;, W. Bin, and N. Zargari, *Modular Multilevel Converters Analysis,Control,and Applications*. Wiley, 2018.

[10]   M. A. Perez, S. Bernet, Jose Rodriguez, S. Kouro, and R. Lizana, "Circuit Topologies, Modeling, Control Schemes, and Applications of Modular Multilevel Converters," *IEEE Trans. Power Electron.*, vol. 30, no. 1, pp. 4–17, 2015, doi: 10.1109/JESTPE.2017.2742938.

[11]   H. Akagi, "Classification, Terminology, and Application of the Modular Multilevel Cascade Converter (MMCC)," *IEEE Trans. Power Electron.*, vol. 26, no. 11, pp. 3119–3130, 2011, doi: 10.1109/TPEL.2011.2143431.

[12]   S. Rohner, S. Bernet, M. Hiller, and R. Sommer, "Modulation, losses, and semiconductor requirements of modular multilevel converters," *IEEE Trans. Ind. Electron.*, vol. 57, no. 8, pp. 2633–2642, 2010, doi: 10.1109/TIE.2009.2031187.

[13]   M. Saeedifard and R. Iravani, "Dynamic performance of a modular multilevel back-to-back HVDC system," *IEEE Trans. Power Deliv.*, vol. 25, no. 4, pp. 2903–2912, 2010, doi: 10.1109/TPWRD.2010.2050787.

[14]   P. Münch, D. Görges, M. Izák, and S. Liu, "Integrated Current Control, Energy Control and Energy Balancing of Modular Multilevel Converters," *IECON 2010 - 36th Annu. Conf. IEEE Ind. Electron. Soc.*, pp. 150–155, 2010, doi: 10.1109/PECON.2016.7951604.

[15]   G. S. Konstantinou and V. G. Agelidis, "Performance evaluation of half-bridge cascaded multilevel converters operated with multicarrier sinusoidal PWM techniques," *2009 4th IEEE Conf. Ind. Electron. Appl. ICIEA 2009*, pp. 3399–3404, 2009, doi:

10.1109/ICIEA.2009.5138833.

[16] M. Hagiwara and H. Akagi, "PWM control and experiment of modular multilevel converters," in *2008 IEEE Power Electronics Specialists Conference*, 2008, pp. 154–161.

[17] M. Hagiwara and H. Akagi, "Control and Experiment of Pulsewidth-Modulated Modular Multilevel Converters," *IEEE Trans. Power Electron.*, vol. 24, no. 7, pp. 1737–1746, 2009, doi: 10.1109/TPEL.2009.2014236.

[18] T. Brückner, S. Bernet, and H. Güldner, "The Active NPC Converter and Its Loss-Balancing Control," *IEEE Trans. Ind. Electron.*, vol. 52, no. 3, pp. 855–868, 2005, doi: 10.1109/TIE.2005.847586.

[19] A. Antonopoulos, L. Ängquist, and H. P. Nee, "On dynamics and voltage control of the modular multilevel converter," *2009 13th Eur. Conf. Power Electron. Appl. EPE '09*, 2009.

[20] D. Siemaszko, A. Antonopoulos, K. Ilves, M. Vasiladiotis, L. Ängquist, and H. P. Nee, "Evaluation of control and modulation methods for modular multilevel converters," *2010 Int. Power Electron. Conf. - ECCE Asia -, IPEC 2010*, pp. 746–753, 2010, doi: 10.1109/IPEC.2010.5544609.

CHARACTERIZATION OF OPTICALLY SHAPED GAS TARGET PROFILES FOR PROTON ACCELERATION EXPERIMENTS IN THE NEAR CRITICAL DENSITY PLASMA REGIME

I. Tazes[1,2], G. Andrianaki[1,3], A. Grigoriadis[1,4], S. Passalidis[5], A. Skoulakis[1], E. Kaselouris[1], J. Chatzakis[1,2], I. Fitilis[1,2], M. Bakarezos[1], E. Vrouvaki[1,2], V. Dimitriou[1], N.A. Papadogiannis[1] and M. Tatarakis[1,2]

[1] *Institute of Plasma Physics and Lasers - IPPL, University Research and Innovation Center, Hellenic Mediterranean University, Rethymno, Crete, Greece*
[2] *Department of Electronic Engineering, Hellenic Mediterranean University, Chania, Greece*
[3] *School of Production Engineering and Management, Technical University of Crete, Chania, Greece*
[4] *Department of Physics, University of Ioannina, 45110, Ioannina, Greece*
[5] CEA, DAM, DIF, 91296 Arpajon, France
tazes@hmu.gr

1. INTRODUCTION

Laser-induced proton acceleration has attracted increasing attention due to its potential applications in Inertial Fusion Energy (IFE), associated with the proton driven fast ignition and proton-boron schemes, in biomedical applications (hadron therapy) and as laboratory plasma diagnostic (Proton radiography). Laser-plasma ion accelerators typically rely on the interaction of an intense laser pulse with a solid target in the over-dense plasma regime. However, these targets are destroyed upon irradiation and cannot be used as high repetition rate (HRR) proton sources. To address this limitation, extreme-pressure gas-jet targets that can reach the near-critical (NCR) density plasma regime are being explored as HRR, debris-free proton sources. State-of-the-art simulations predict that Magnetic Vortex Acceleration (MVA) can generate hundreds of MeV protons. However, MVA remains experimentally challenging for super-intense, short-wavelength, femtosecond laser pulses due to the extremely steep density gradient plasma profiles required.

In this study, we present the optical shaping of a long density scale length, high-pressure, gas-jet density profiles via multiple, laser-induced, hydrodynamic, Sedov-type blast waves (BWs) to generate near-critical, steep density gradient, gas target profiles. The counterpropagating BWs compress the gas-jet targets, achieving NCR slabs of a few microns thickness upon their shock fronts' collision. These profiles are considered suitable candidates for laser-induced proton acceleration experiments using ZEUS 45TW laser system, hosted at the Institute of Plasma Physics and Lasers (IPPL).

2. METHODS

We perform Magnetohydrodynamic (MHD) simulation results, using the modular, parallel, multiphysics code FLASH (Fryxell et al., 2000), demonstrating the capability of multiple laser pulses interacting with high-density gas-jet profiles to optically shape plasma targets. Specifically, we report on multiple laser-generated, colliding Blastwave (BW) (Passalidis et al., 2020), (Marquès et al, 2021), (Tazes et al., 2022) schemes that can compress the gas target into NCR steep density gradient plasmas of a few microns thickness. We also present simulation results of the interaction between the compressed target and the super-intense accelerating, femtosecond laser pulse of the ZEUS 45TW laser system (Clark et al., 2021) using the fully relativistic, 3D Particle-In-Cell (PIC) code EPOCH (Arber et al., 2015).

Finally, we provide an experimental characterization of high-pressure, supersonic gas-jet density profiles using Mach-Zehnder interferometry. The interferograms are analyzed using an in-house developed code for Abel inversion following the Freeman and Katz approach (Mosburg 1968). The density profiles are generated using 3D printed de Laval, cylindrical, and conical nozzles with diameters of a few hundred microns. Preliminary results on the optical shaping of the gas-jet profiles using am 840mJ, Nd:YAG, nanosecond laser are presented.

3. RESULTS AND DISCUSSION

Figure 1 presents MHD simulation initial conditions and temporal evolution of quadruple perpendicularly intersecting laser pulses, generating four counterpropagating BWs. The peak initial density of the gas profile is $n = 0.06 n_{cr}$, where n_{cr} is the plasma critical density. For a laser pulse of wavelength $\lambda = 800 nm$, $n_{cr} = 1.7\ 10^{21} electrons/cm^3$.
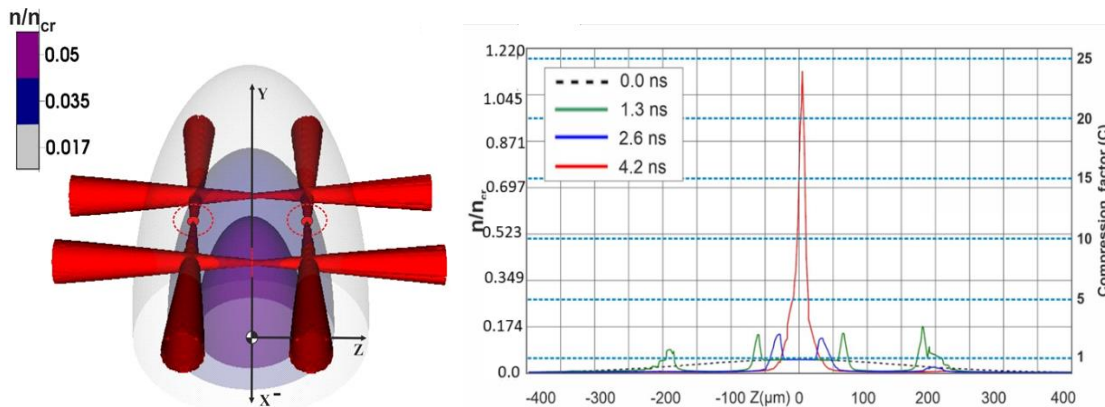
Figure 1. (left) Initial conditions of the MHD simulation of the quadruple perpendicularly intersecting laser pulse generated BWs (right) Temporal evolution of the density profile

The BWs are colliding at the peak density region of the gas target profile, resulting in an extremely high compression of ~25 times its initial density, exceeding critical density of the accelerating laser wavelength $n = 1.15 n_{cr}$. The optical shaped target profile is extremely steep, with scale length $l_s = 14 \mu m$ at 1/e of its maximum density.

Figure 2 presents 3D PIC results of the interaction of the main accelerating pulse of ZEUS laser system with the compressed NCR density profile.
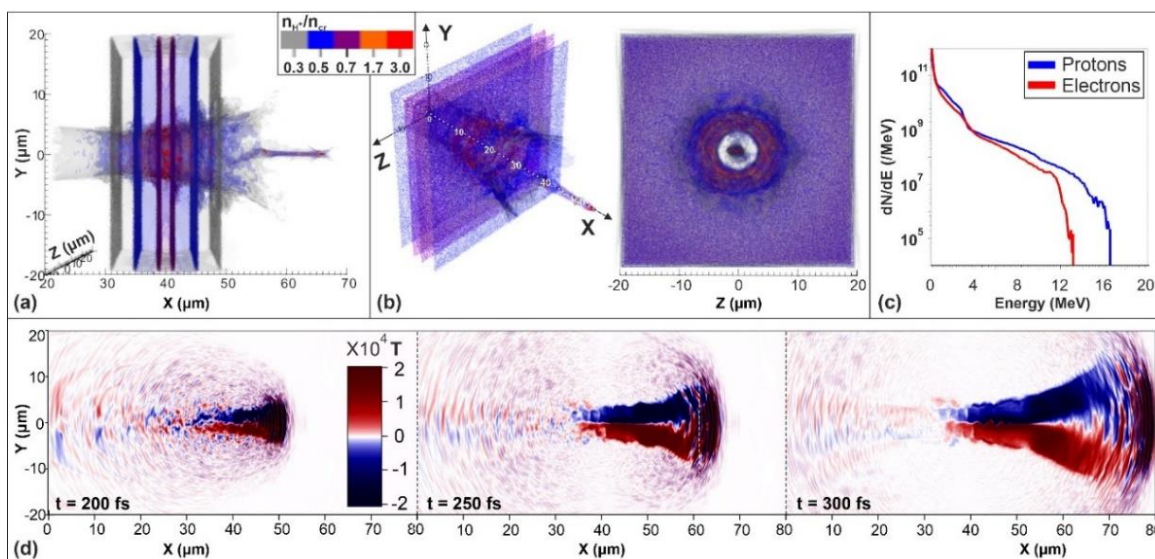
Figure 2. accelerate proton results of the MVA. (a) left view at t = 600 fs; (b) isometric and front view (c) proton and electron energy spectra. (d) Temporal evolution of the azimuthal magnetic field Bz of the vortex.

Simulation results show that the protons acquire their maximum energy before 500 fs of the PIC simulation, resulting in cut-off kinetic energies above 15 MeV. MVA (Willingale et al., 2006) (Bulanov et al., 2007) (Nakamura et al., 2010) is the dominant particle acceleration mechanism, demonstrated by the evolution of the azimuthal magnetic field.

These density profiles compression lifetime is limited to ~200 picoseconds, making experimental synchronization with the main accelerating pulse unfeasible, due to the inherent laser system jitter. Here, we propose an optical shaping set-up able to generate compressed target profiles sustaining their density structure for several nanoseconds. These profiles are characterized by a long and controllable lifetime able to provide NCR densities allowing for efficient synchronisation of the femtosecond laser pulse with the compressed target. Figure 3 present 3D MHD simulation results of the double, intersecting in a 60° angle, ns laser pulses generated BWs, optical shaping set-up.
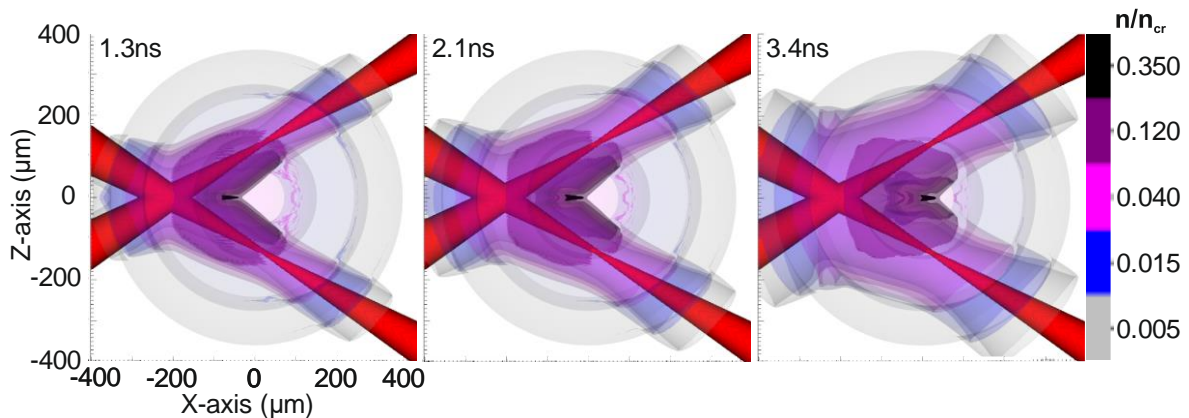

Figure 3. MHD simulation results of the density temporal evolution for 1.0, 2.1 and 3.4 ns.

The set-up delivered a sufficient compression of $n = 0.55 n_{nr}$, with peak compression density sustained for longer than 2.5 ns. This finding secures the experimental synchronization with the main accelerating fs laser pulse and provides the ground for an achievable experimental implementation.
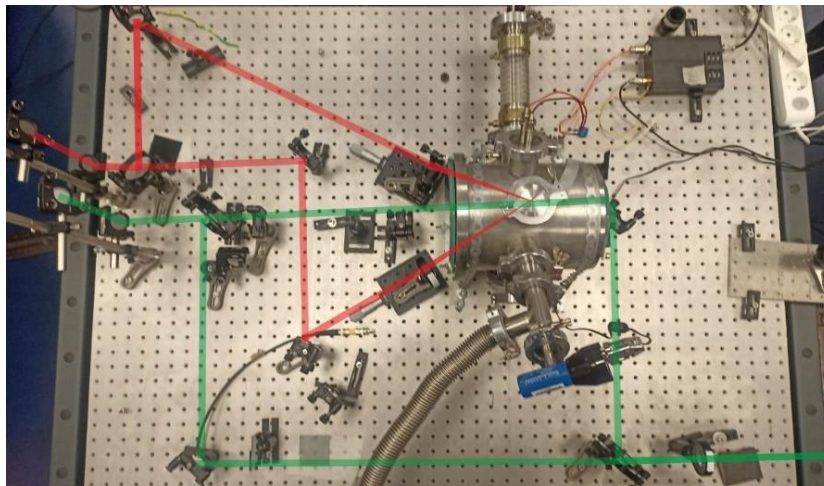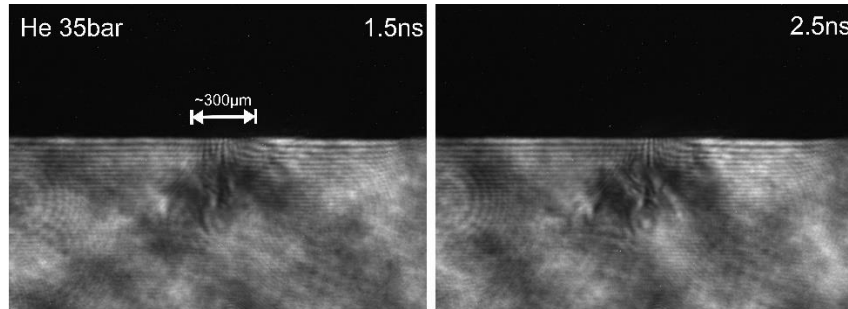

Figure 4. Double intersecting laser pulses experimental set up

Figure 4 presents the experimental set-up for the characterization of the optical shaping of high-pressure gas jet profiles by double intersecting laser pulses. The high-pressure gas-jet targets are delivered by a Haskel air-driven hydrogen gas booster, able to support 1000 bar of backing pressure, along with a Clark Cooper Solenoid valve. A Q-smart 850 Nd:YAG laser is used for the generation of the BWs in a vacuum chamber of 28cm diameter. The 2ω of the Nd:YAG laser, with $\lambda = 532nm$

is used for optical probing characterization of the interaction, using shadowgraphy and Mach-Zhender interferometry.

Figure 5. Preliminary experimental results using shadowgraphs for double intersecting pulses generated BW

Figure 5 presents preliminary shadowgraphy results of the double intersecting laser pulses optical shaping in 35bar He. The centered dark region corresponds to the NCR compressed target maintenance its compression after 2.5 ns of the interaction.
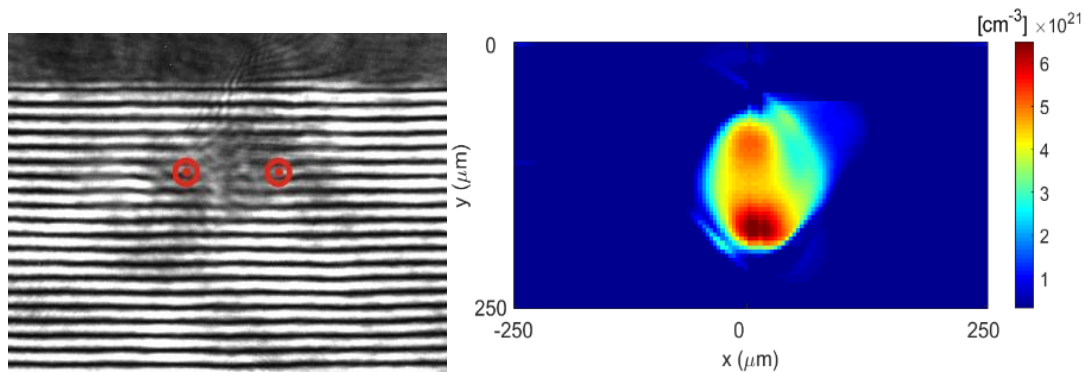
Figure 6.   Preliminary interferometry analysis of experimentally obtained results

Figure 6 present preliminary interferometric results of the compressed profile. Cylindrical symmetry can not be considered to perform Abel inversion. To retrieve the cubic plasma density, tomography is necessary. Here we use an in-house developed code for Abel inversion numerical solution that takes into account asymmetries of the measured phase shift, by assuming cylindrical symmetry in a small region around the plasma we acquire an indicative cubic density value.

4.   CONCLUSION

In this work, we investigate the feasibility of proton acceleration by TW laser pulses interacting with high pressure, optically shaped gas-jet profiles. The study of optical shaping of the gas-jet profiles via the generation of multiple BWs was performed by MHD simulations. The gas-jet profiles were compressed upon the BWs shock front collision, into near critical density target profiles. An intersecting ns laser double pulse geometrical set-up is identified to be an optimal candidate for the generation of compressed target profiles, able to sustain their density distribution for several nanoseconds. These profiles are characterized by a controllable compression time window, able to provide plasma density profiles for effective laser induced ion acceleration experiments. The proposed laser set-up eliminates the experimental laser-target synchronization restrictions between the interaction fs laser with the optically shaped target. Preliminary experimental measurements using optical probing methods, indicates feasibility of the optical shaping method for proton acceleration experiments.

5. ACKNOWLEDGMENT

6. REFERENCES

Fryxell, B., et al., (2000). "FLASH: An adaptive mesh hydrodynamics code for modeling astrophysical thermonuclear flashes." The Astrophysical Journal Supplement Series 131.1: 273.

Passalidis, S., et al. (2020). Hydrodynamic computational modelling and simulations of collisional shock waves in gas jet targets. High Power Laser Sci. Eng., 8, e7.

Marquès, J-R., et al. (2021). Over-critical sharp-gradient plasma slab produced by the collision of laser-induced blast-waves in a gas jet: Application to high-energy proton acceleration. Phys. Plasmas, 28, 023103.

Tazes, I. et al., (2022). A computational study on the optical shaping of gas targets via blast wave collisions for magnetic vortex acceleration High Power Laser Sci. Eng., 10, e31.

Clark, E. L., et al. (2021). High Intensity Laser Driven Secondary Radiation Sources Using the ZEUS 45 TW Laser System at the Institute of Plasma Physics and Lasers of the Hellenic Mediterranean University Research Centre. High Power Laser Sci. Eng., 9, e53.

Arber, T. D., et al. (2015). Contemporary particle-in-cell approach to laser-plasma modelling. Plasma Phys. Control. Fusion, 57.11: 113001.

Mosburg, Earl R. (1968). Solution of the Abel integral transform for a cylindrical luminous region with optical distortions at its boundary. Vol. 368.

Willingale, L., et al. (2006). Collimated Multi-MeV Ion Beams from High-Intensity Laser Interactions with Underdense Plasma. *Phys. Rev. Lett., 96.24: 245002.*

Bulanov, S. V., & Esirkepov, T. Z. (2007). Comment on "collimated multi-MeV ion beams from high-intensity laser interactions with underdense plasma". Phys. Rev. Lett., 98, 049503.

Nakamura, T., et al., (2010). High-energy ions from near-critical density plasmas via magnetic vortex acceleration. Phys. Rev. Lett., 105.13: 135002

CHARACTERIZATION OF A MINIATURE MATHER-TYPE PLASMA FOCUS MACHINE AS NEUTRON SOURCE

C. Karvounis[1,2], A. Skoulakis[1,2], I. Tazes[1,2], D. Mancelli[1,2], J. Chatzakis[1,2], V. Dimitriou[1], N.A. Papadogiannis[1], M. Tatarakis[1,2] & I. Fitilis[1,2]

1 Institute of Plasma Physics and Lasers, University Research and Innovation Center, Hellenic Mediterranean University, Rethymno, Crete, GR-74100, Greece
2 Department of Electronic Engineering, School of Engineering, Hellenic Mediterranean University, Chania, Crete, GR-73133, Greece

1. INTRODUCTION

The Mather-type plasma focus machine represents a significant advancement in the field of plasma physics, offering versatile and efficient means of generating plasma discharges. This extended abstract aims to provide a concise yet comprehensive overview of the theoretical description and the electrical circuit and the optical and electrical diagnostics of a Mather-type plasma focus machine. Additionally, it highlights the machine's exceptional capabilities as a neutron source, supported by the utilization of a two-frame shadowgraphy for visualizing plasma dynamics, a photomultiplier system (PMT) for measuring neutron energy and a BD-PND bubble detector for neutron yield calculation.

2. THEORETICAL DESCRIPTION

The Mather-type plasma focus machine operates on the principles of the Z-pinch effect, where an intense magnetic field is generated by a rapidly collapsing current sheath. This process results in the compression and heating of the plasma to extreme temperatures and densities, facilitating the creation of a highly energetic plasma environment. A typical Dense Plasma Focus (DPF) device consists of two coaxial cylindrical electrodes closed at one end and open at the other one. The central electrode is called anode and the outer one is called cathode. A part of the anode is covered by an insulator
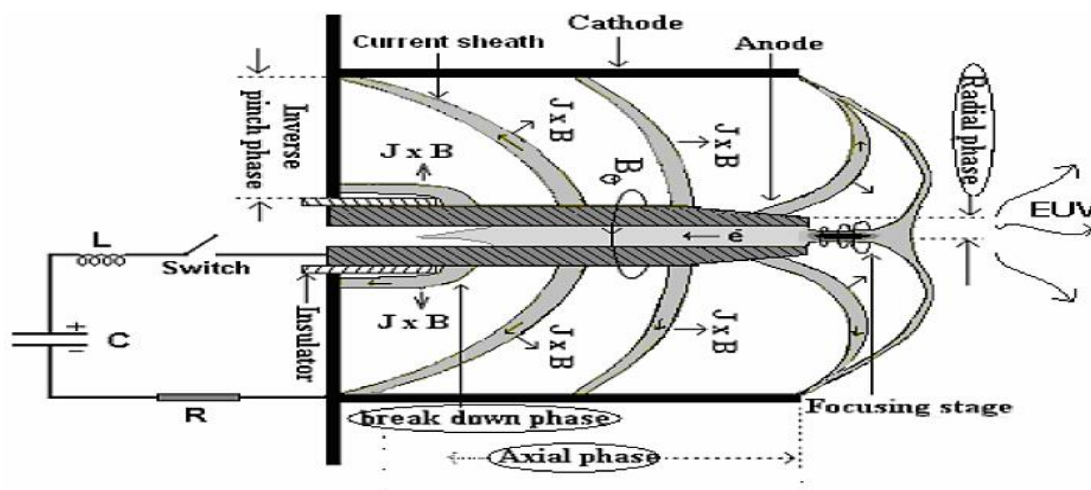

Figure 1: Plasma dynamics in a Mather-type device [1].

sleeve which separates it from the cathode. The anode is connected to the high potential of a capacitor while the cathode is normally grounded. The plasma dynamics in a Mather-type plasma focus machine can be divided into three main phases: the breakdown phase, the axial acceleration phase and the radial phase as shown in Fig1.

When high voltage is applied between the anode and the cathode, an electric field is developed across the insulator and due to the free electrons of the working gas a sliding discharge appears along the surface of the insulator. When this discharge reaches the bottom of the insulator, current filaments are generated through which the discharge current flows and due to the Lorentz force these current filaments move towards the inner wall of the cathode while a uniform current sheath is formed. This is the end of the breakdown phase and the current sheath that just created enters the axial acceleration phase. Then, the current sheath starts to accelerate towards the open end of the electrodes along the z-axis by its own $\vec{J} \times \vec{B}$ force. Studies have shown that the current sheath acquires a parabolic shape while maintaining its axisymmetric character [2]. The end of the axial phase comes when the current sheath reaches the end of the anode and enters the next phase, the radial phase. The radial phase is the last phase of plasma compression and plays the most important role due to its extremely high energy density, its transient character and being a source of intense radiation, high energy particles as well as nuclear fusion products when deuterium or D-T mixture are used as working gas. The start of the radial phase comes when the current sheath reaches the open end of the anode and the $\vec{J} \times \vec{B}$ force drags part of the current sheath radially inward. This inward radial force compresses the snowplowed plasma carried by the current sheath on the top of the anode. This hollow column is squeezed inwards with azimuthal symmetry. The compressed plasma is also squeezed adiabatically to a high density and high temperature plasma column. Some studies have shown that during radial compression, plasma resistance as well as system inductance increases and as a result magnetic field diffuses into the plasma column [3]. This phase leads to the creation of the pinching, which is the compression of the plasma using magnetic forces. During this phase there is emission of Soft X-Rays (SXR) and Hard X-Rays (HXR). If Deuterium gas is used neutrons and protons are also produced.

3. THE PLASMA FOCUS MACHINE

The plasma focus machine that was used comprises the energy bank, the pseudo spark switch with a heating module, the pulse shaping transmission lines and the vacuum chamber with the Mather-type plasma focus configuration. The energy bank includes a high voltage power supply and 6 capacitors with the following specifications: C = 0.56μF, L = 30nH, V_{max} = 30kV. The power supply charges the capacitors and the machine obtains 600J of energy when the capacitors are charged at 19kV. To initiate the discharge, a trigger unit is employed, generating a 2.5kV of 1μs impulse that is transmitted to the pseudo spark switch through the pulse shaping circuit consisting of 2 coaxial lines and an intermediate self-brake spark gap [4,5]. The energy of the capacitors through 4 planar copper transmission lines is transferred to the anode rod inside the vacuum chamber whose wall forms the cylindrical cathode of the plasma focus.
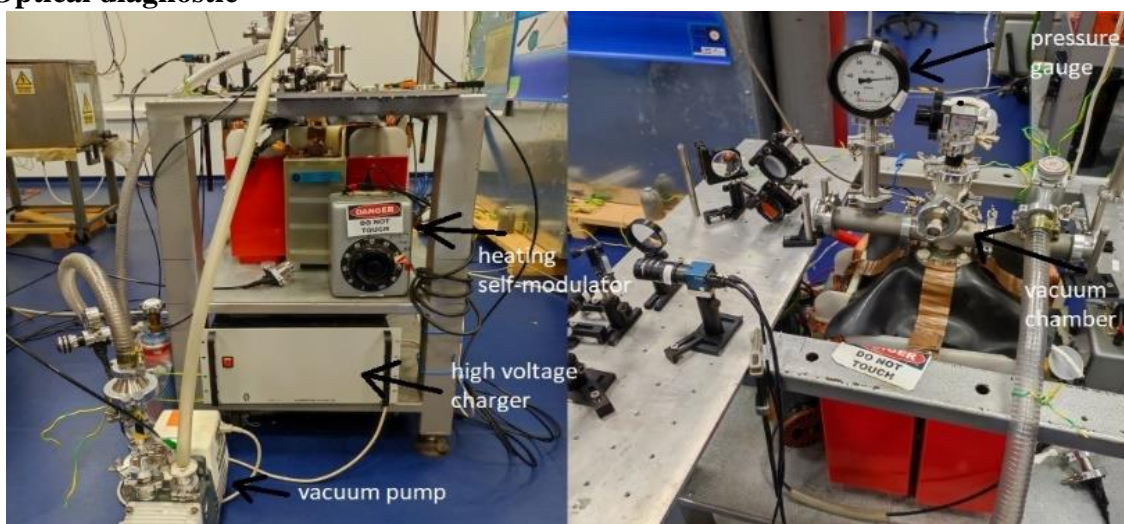
4. Optical diagnostic

Figure 2: The plasma focus machine

gs

A two-frame shadowgraphy, as can be seen in Figure 3, was used in order to record the plasma dynamics. The main laser beam was separated into different beams, using a beam splitter, which travel different distance to make a time difference of 9ns between them. The two beams passed through the vacuum chamber with a slight angle difference and recorded in two CCD cameras that image the anode region. The experiments were performed many times in order to record the dynamic of the plasma from the

Figure 3: Two-frame shadowgraphy setup

beginning of the axial phase till the end of the whole process. In Figure 4 are presented all the phases of the plasma focus machine (axial, radial and breakdown). The first image is shown the end of the axial phase as the sheath reaches the top of the anode. In the next figure plasm is in radial phase and is compressed by magnetic fields. In c and d figures are shown a few nanoseconds before and a few nanoseconds after pinching and in the last two figures there is after the breakdown of pinching and the bubble-like plasma that is observed at the end of the whole phenomenon. The time in each picture refers to the time of the pinching which corresponds to the dip that there is in the time derivative of the current. Also, Figure 4 shows that the plasma sheath has a very good symmetry, something that is very important for successful pinching
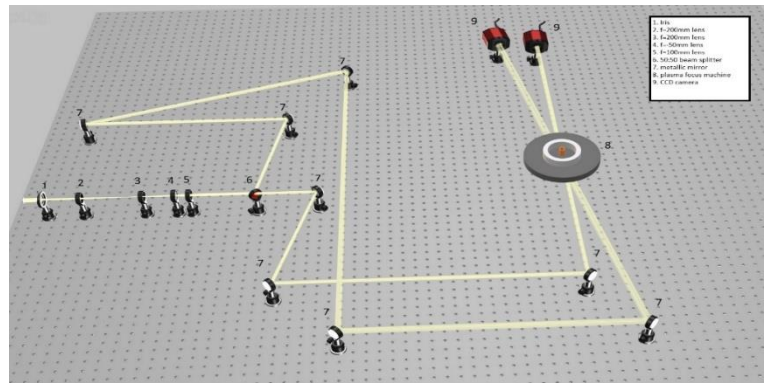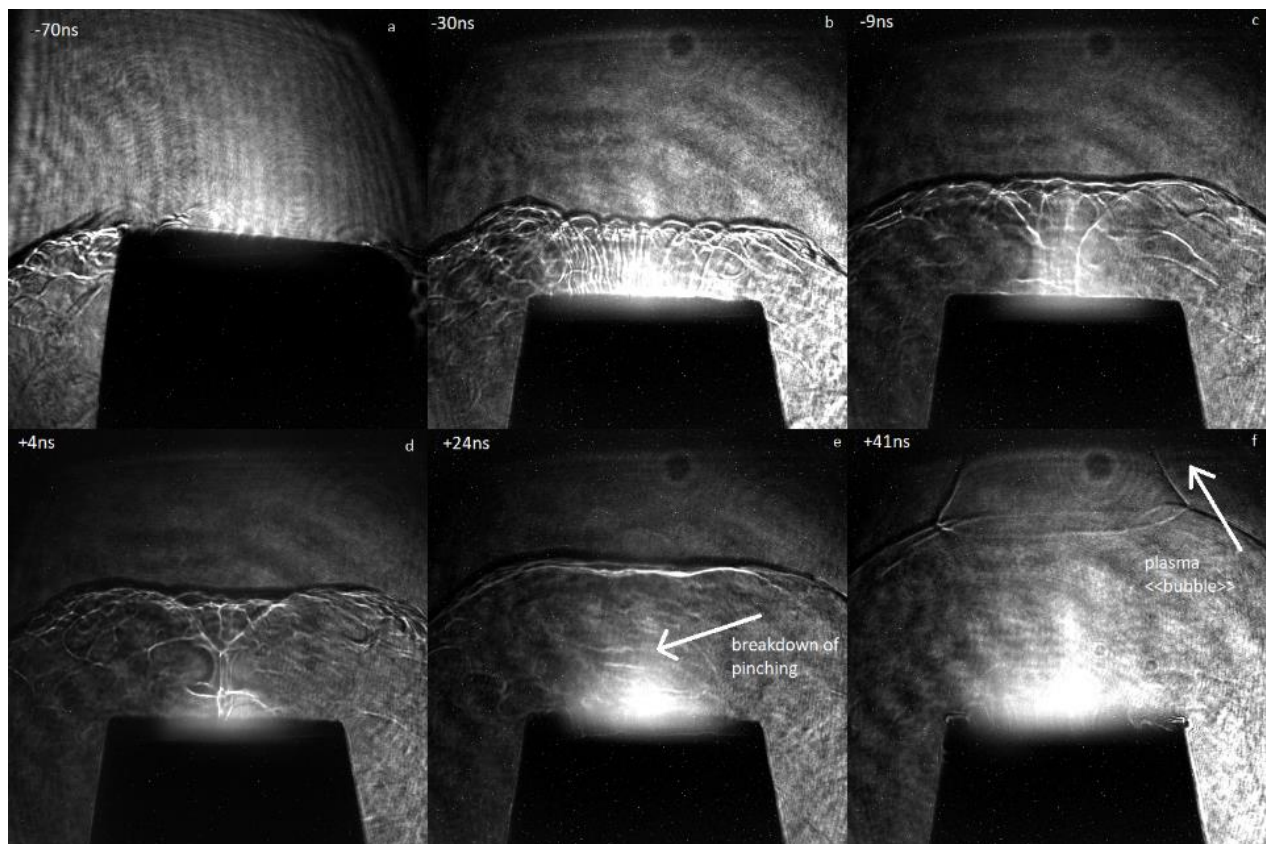

Figure 4: Shadowgraphy photo sequence showing the plasma dynamics

5.   NEUTRON DETECTION

In order to measure the energy of the emitted neutron a simple time of flight (TOF) technique is used by a detector in a well-known distance L from the source to record the signals that are produced from Hard X Rays (HXRs) and neutrons. The detector was a photomultiplier system which consists of plastic scintillator and a photomultiplier system which multiplies the signal a million times. Neutrons are travelling with slower speed compared to the speed of light and this fact gives different time of flights and different outputs in the oscillator. The signals from the detector which recorded in the oscilloscope were synchronized by the subtraction of the time delay that comes from the cables (4.68 ns/m) and the photomultiplier (28 ns). Especially for the photomultiplier signal the time of flight of the HXR was also subtracted so that the time that the first pulse appears to be the same with the time that is emitted. The time of flight of the Soft X rays, recorded near the pinch, is <1 ns and so is negligible. Figure 5 show a typical signal recordings and nd an histogram of the measured neutron energy where in the majority of the shots was measured to have value close to 2.45 MeV, in agreement with theory.
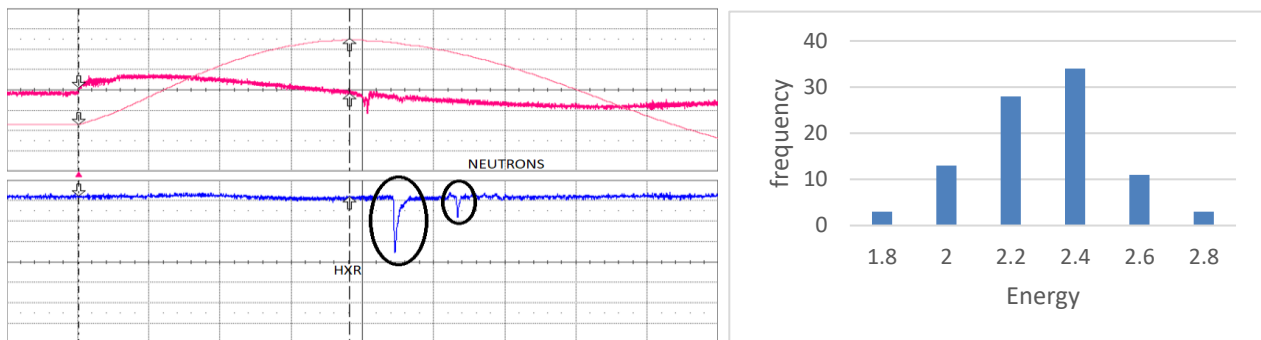
Figure 5: (Right) The oscilloscope signals that shows the two peaks for HXRs and neutrons (Left) histogram of the neutron energy.

The neutron yield was calculated, using the bubble detector, in a pressure range from 16 to 24mbar and it was found that the maximum neutron yield was 0.8×10^6 neutrons/shot for 19mbar pressure. Bubble detectors are sensitive and accurate neutron dosimeters and provide visible detection and measurement of neutron dose. Inside the detector there are tiny droplets of superheated liquid that dispersed throughout a clear polymer. When a neutron strikes a droplet, the droplet immediately vaporizes, forming a visible gas bubble trapped in the gel. The number of bubbles provide a direct measurement of the tissue-equivalent neutron dose. This neutron detector has an isotropic angular response and also has zero sensitivity to gamma radiation.

Figure 6: BD-PND bubble detector

6.   CONCLUSIONS

In conclusion, this extended abstract has presented an overview of the theoretical description, the electric circuit and the diagnostics employed in the Mather-type plasma focus machine. Through the integration of two-frame shadowgraphy, a photomultiplier system and a bubble detector, researchers gain valuable insights into the plasma dynamics, neutron energy and yield characteristics. This comprehensive understanding and diagnostic capability pave the way for further advancements in plasma physics research and the diverse applications enabled by the Mather-type plasma focus machine.

7. REFERENCES

[1] Murtaza Hassan (2010): Development and Studies of Plasma EUV Sources for Lithography. Phd Thesis

[2] Chow, S. P., Lee, S., & Tan, B. C. (1972). Current sheath studies in a co-axial plasma focus gun. Journal of Plasma Physics, 8(1), 21-31.

[3] G. Decker, W. Kies & G. Pross (1983). The first and the final fifty nanoseconds of a fast focus discharge. The Physics of Fluids, 26(2), 571-578.

[4] J. Chatzakis, S. M. Hassan, E. L. Clark, C. Petridis, P. Lee, M. Tatarakis (2008). High repetition rate preudospark trigger generator, Rev. Sci. Instrum., 79(8)

[5] A. Petridi, G. Chatzipetrakis, A. Skoulakis, I. Fitilis, M. Tatarakis, & J. Chatzakis (2022). A modified modular multilevel converter topology trigger generator for a pseudospark switch. Rev. Sci. Instrum., 93(6).

VARIATIONS OF PHYSICOCHEMICAL PARAMETERS AND PHOTOSYNTHETIC PIGMENTS IN A SMALL-SIZED WETLAND IN PREFECTURE OF CHANIA, GREECE

Giannoudakis N[1], Zacharioudaki D-E[1], and Kotti M[1]

[1]Department of Electronic Engineering, Hellenic Mediterrranean University
E-mail (kotti@hmu.gr)

1. INTRODUCTION

In Greece, there are many island wetlands that are protected by conventions. Most of them consist of a large area. The studied wetland is located at Municipality of Chania, Crete. It is known as Kalathorema estuary. It is a coastal wetland next to the famous Kalathas beach and its area is only 0,56 Ha. Human activities are very intense and have a great impact on its quality. To our knowledge, this wetland has not been studied in the past. This work aimed: (a) to understand the geochemistry, (b) to assess the pollution and the trophic status and (c) to evaluate the productivity of the biotope. The future perspective is to make people aware of the threatened wetlands.

2. MATERIALS AND METHODS

All the examined quality parameters were measured according to the standard methods of analysis (APHA 2005). The chemical reagents were of analytical grade. pH, electrical conductivity (EC) and salinity (S) were measured by a multiparameter probe. Total hardness and chloride were measured by titration with EDTA and $AgNO_3$, respectively. The analysis of nutrients was performed spectrophotometrically. The photosynthetic pigments chlorophyll-a (chl a), chlorophyll-b (chl b), chlorophyll-c (chl c) and carotenoids were determined by the spectrophotometric trichromatic method.

Samples from six stations were collected from November 2019 to October 2020 and analyzed immediately. Two months March and April were not included as there was a traffic ban due to COVID-19 pandemic.

3. RESULTS AND DISCUSSION

The physicochemical parameters are depicted in Fig. 1 (a-d). From figure 1a it is clear that pH values of S1-6 followed the same behaviour till June and in S2-5 during all months. Higher pH values were detected in May and June while lower in January, February and July. All values were above 7,3 units.

No fluctuations in electrical conductivity were observed for S1- 5 (Fig. 1b). Higher EC values were appeared in July and August, while lower values in January, February, May and October. On the contrary, point 6 showed high values during October and December (both rainy months). The same profiles with EC were observed for chloride and total hardness (Fig.1c and d). These parameters have already shown strong positive correlations among them in other wetland systems (Kotti, 2018).

The minimum, maximum and mean values of the photosynthetic pigments and nutrients are summarized in Table 1. All values are expressed in mg/L. Zero values indicate that they were below limit of the detection of method.
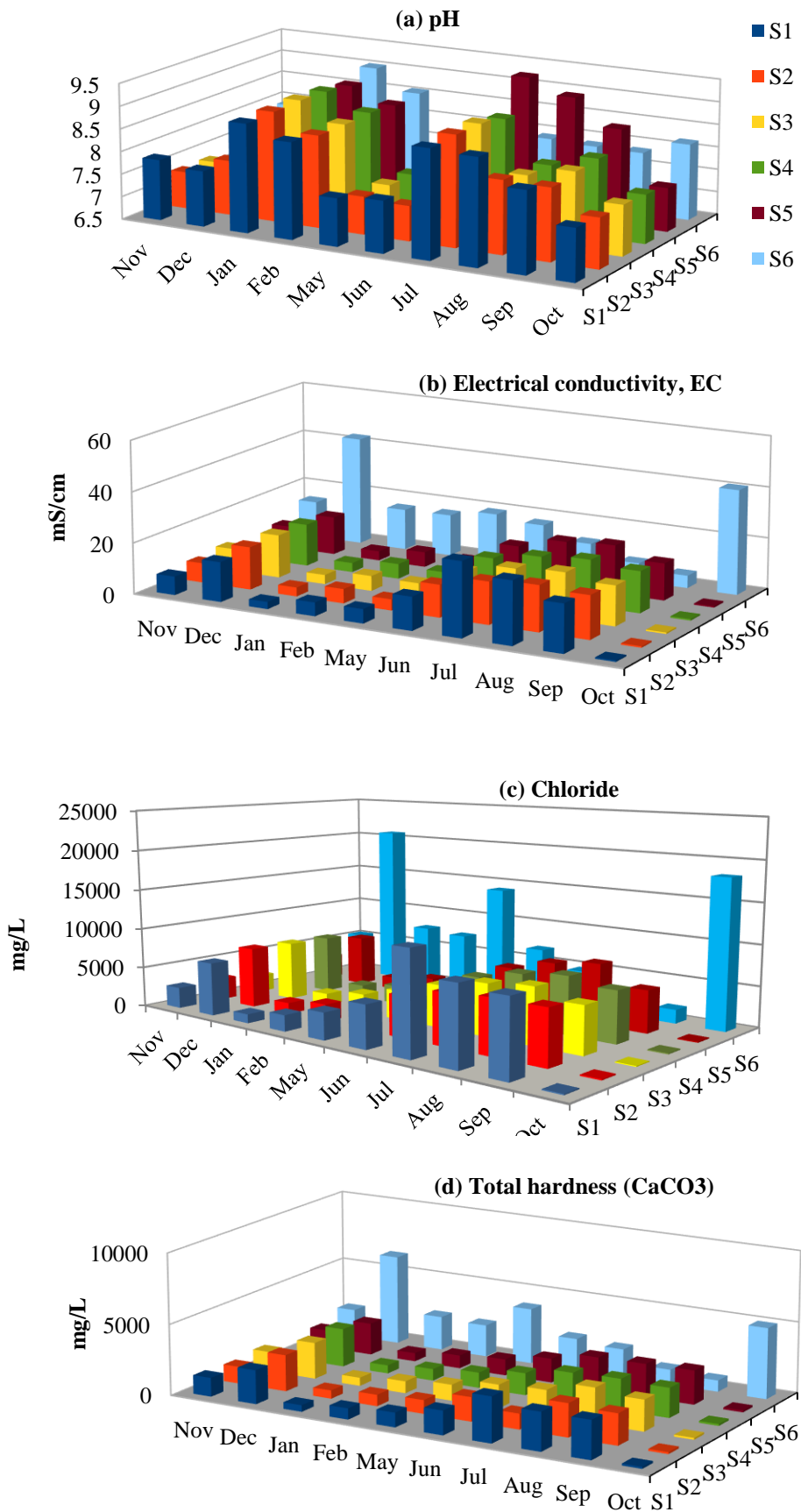
Figure 1. The spatiotemporal variations of physicochemical parameters: (a) pH, (b) EC, (c) chloride and (d) total hardness for the six sampling stations in Kalathas estuary.

Table 1. Minimum, maximum and mean values of the quality parameters for the six sampling stations in Kalathas estuary.

	S1	S2	S3	S4	S5	S6
Chl a						
min	6,5E-05	0,00082	0,00041	0,00163	0,00082	0,00034
max	0,13924	0,11513	0,06044	0,04032	0,06813	0,03395
mean	0,02088	0,03618	0,02348	0,02854	0,02762	0,01066
Chl b						
min	0	0	0,00052	0,00036	4,8E-06	0
max	0,00221	0,00022	0,01194	0,00912	0,0122	0,00776
mean	0,0009	0,00675	0,00538	0,00721	0,00466	0,00246
Chl c						
min	0	0,00086	0,00061	0,00045	0,00079	0
max	0,01211	0,01477	0,01021	0,01075	0,0036	0,00487
mean	0,00324	0,00739	0,00329	0,00427	0,00326	0,00344
Total carotenoids						
min	0	0,00092	0	0	0	0,00031
max	0,06548	0,03833	0,02631	0,04864	0,02761	0,01808
mean	0,02232	0,02266	0,01448	0,01263	0,01503	0,00789
Si						
min	0,989	0,663	0	0,378	0,582	0,213
max	9,92	13,7	6,24	14,2	6,72	12,1
mean	2,92	4,27	2,20	4,67	2,33	4,86
P						
min	0	0	0	0	0	0
max	0,626	0,668	0,472	0,506	0,583	0,353
mean	0,141	0,175	0,1304	0,0881	0,112	0,163
N						
min	0,233	0,033	0,191	0,014	0,029	0,014
max	1,70	1,02	15,5	0,916	1,90	3,30
mean	0,647	0,492	2,00	0,448	0,594	0,717

Among the chlorophyll forms a, b and c, chla was the dominant form. Chl a and carotenoids showed high values in S2 and lower in S6. Chl b and c showed high values in S2,4 and lower in S1. Chl a is constituent of all photosynthetic organisms, chl b is in green algae, while chl c is in marine algae (diatoms). Carotenoids are found also in diatoms and dinoflagellates.

PO_4-P concentrations fluctuated monthly and less spatially. Specifically, months November, January and February the values were high in all points. During next months, P concentrations were below LOD with few exceptions. The maximum and mean values of P indicate that the water body of Kalathas estuary is eutrophic according to classification systems (OECD, 1982). Ammomium as N varied spatially and monthly with high values in most points during February and lower from June until the end of the sampling period. High values of ammonium are usually attributed to pollution either from agricultural and farm activities or from sewage runoff (Maksimovic, 2020). Si concentrations fluctuated strongly both spatially and monthly. S2,4 and 6 showed higher mean values Si compared with S1,3,5.

4. CONCLUSION

The present study has monitored the variations of the physicochemical parameters and the photosynthetic pigments in the small wetland of Kalathas, Chania, Greece. The wetland has not been studied in the past although it is protected by national legislation. The only description of the wetland known as KRI 187, has been recorded by WWF Greece (http://www.oikoskopio.gr/ygrotopio/general/report.php?id=381&param=themeleiwdn&lang=en_US). It is obvious that the wetland is threatened as it receives many anthropogenic pressures. The results from the present study are: (1) the water body is alkaline, the parameters EC, chloride and total hardness varied in the same way, being high during hot months and low during wet season, (2) The last point 6 is an exception as it varied differently, (3) it receives N and P loads probably from agricultural activities and sewage runoff and its trophic status is eutrophic (5) the silica varies spatiotemporarily probably because of the diatoms presence, (6) all chlorophylls varied spatiotemporarily and among them, chla is the abudant form and (7) the part of the wetland that is situated from the other side of the street (S6) has different physicochemical properties.\

5. REFERENCES

APHA (2005). Standard methods for the examination of water and wastewater. Washington: American Public Health Association, and Water Environment Federation

Kotti E., Zaxarioudaki D. E., Kokinou E., & Stavroulakis G. (2018). Characterisation of water quality of Almiros river (Northeastern Crete, Greece): Physicochemical parameters, polycyclic aromatic hydrocarbons and anionic detergents. Modeling Earth Systems and Environment, 4 (4): 1285–1296. https://doi.org/10.1007/s40808-018-0504-3

Maksimović T., Lolić, S., & Kukavica, B. (2020). Seasonal Changes in the Content of Photosynthetic Pigments of Dominant Macrophytes in the Bardača Fishpond Area. *Ekológia (Bratislava)*, 39: 201-213. 10.2478/eko-2020-0015

OECD (1982). Eutrophication of waters: monitoring, assessment, and control. Final Report. OECD Cooperative Program on Monitoring of Inland Waters (Eutrophication Control, Environment Directorate). Paris, France: OECD.

ΦΕΚ 229/ΑΑΠ/2012, in Greek

ΦΕΚ 1242/Β/1973, in Greek

APPLICATION OF LASER INDUCED FLUORESCENCE FOR CHARACTERIZATION OF WATER QUALITY IN TWO WETLANDS

Zacharioudaki D-E[1], Filtilis I[1] and Kotti M[1]

[1] Department of Electronic Engineering, Hellenic Mediterranean University
E-mail (despoinazax@gmail.com)

1. INTRODUCTION

Water quality was monitored in two coastal wetlands, one located at Heraklion (Almyros Stream) and the other at Chania (Kalathorema estuary), Greece. From January to December 2022, water samples for chemical analyses were collected monthly from ten stations of Almyros and from six stations of Kalathas. The fluorescence constituents of all samples were measured by laser induced fluorescence (LIF). The excitation was achieved by a solid laser source and the signal was recorded for each sample. Physicochemical parameters, nutrients and photosynthetic pigments were measured according to the standard methods of analysis. The fluorescence signals as well as the other parameters revealed extensive information for the water quality of the studied wetlands.

2. MATERIALS AND METHODS

Ten samples from Almyros and six samples from Kalathas were collected during year 2022. The physicochemical parameters, nutrients and photosynthetic pigments were measured. Electrical conductivity, pH, and salinity were measured with a multiparameter probe (Sension 156 Hach). Total hardness and chloride were analyzed by titration with EDTA and $AgNO_3$ (Mohr method), respectively, according to standard methods of analysis (APHA 2005). Analysis of nitrate, ammonium, orthophosphate and silicate was performed spectrophotometrically (APHA 2005). The photosynthetic pigments chlorophyll-a (chl a), chlorophyll-b (chl b), chlorophyll-c (chl c), and carotenoids were determined by using the spectrophotometric trichromatic method (APHA 2005). Moreover, the fluorescence was measured by laser induced fluorescence method (LIF) with a laser source. The samples were excited by laser light with an excitation at 266 nm, while the pulse energy was 77 mJ and the pulse duration was 6 ns. The intensity of the laser sheet is diminished as it passes through and is absorbed by molecules, so cylindrical lens (f = 50 cm) was used to produce a light sheet. The light that coming out of the laser, reflected to a mirror and as it passed through a lens, was directed to the cuvette that was contained the samples. The distance from the cylindrical lens to the cuvette was 16 cm. An optical fiber, that was used to measure the reflection, was connected to another lens, which passes though the spectrophotometer, in order to record the signal of fluorescence on a computer for each sample.

3. RESULTS AND DISCUSSION

PHYSICOCHEMICAL PARAMETERS, NUTRIENTS AND PHOTOSYNTHETIC PIGMENTS

In Almyros stream pH values, have almost the same fluctuations, with the lowest values in February. The salinity values haven't shown any spatial variations, except at station 3 (fig.1). Chloride concentrations were low, except at station 3, that higher concentrations were observed especially during August (fig.1). Total hardness followed the same tendency as chloride (fig 1), with the highest values at station 3. Conductivity values at Almyros stream were low from January to May, while the highest values were at station 3. Figure 1 shows that at all stations the values of conductivity were increased from July until September.
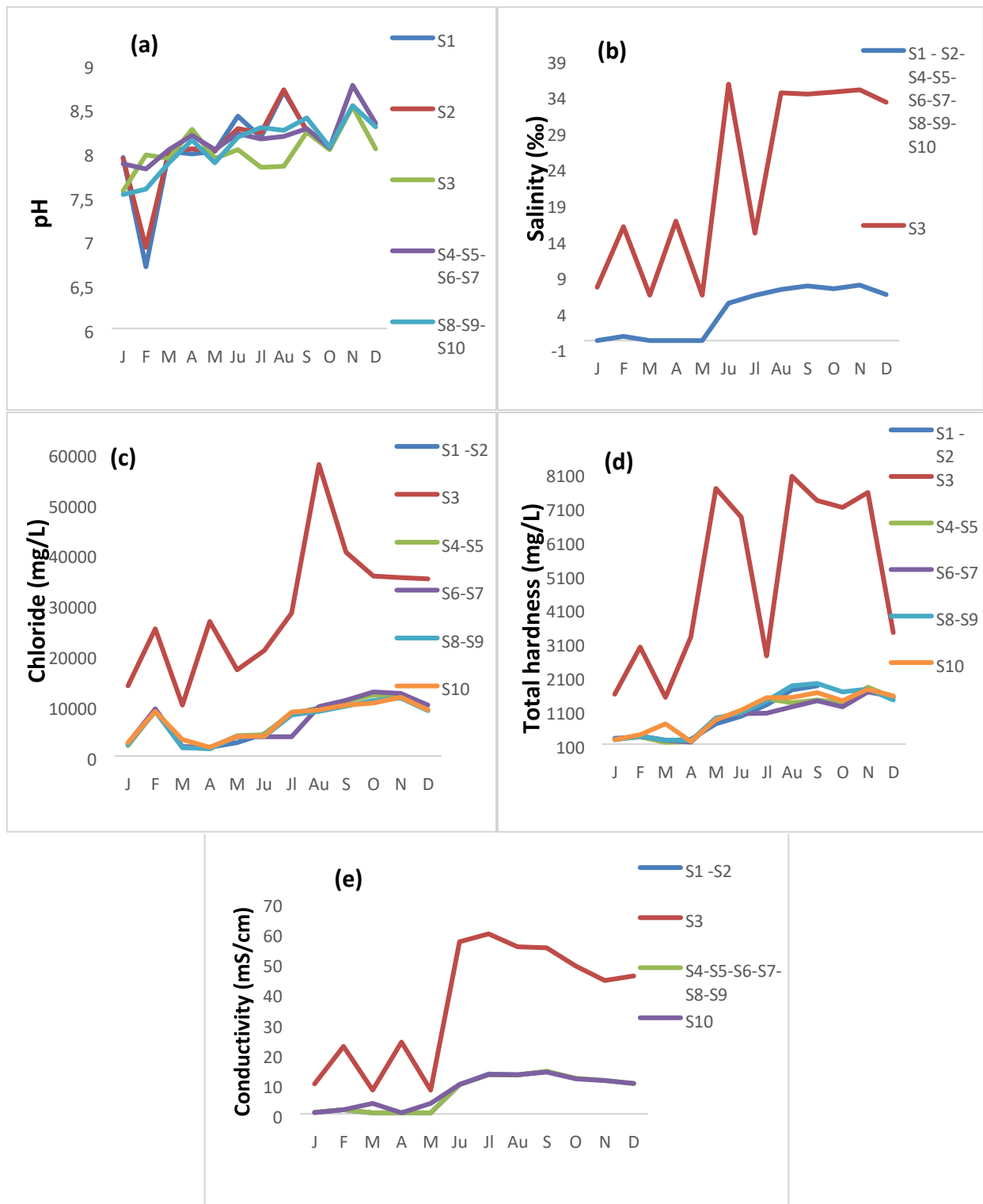
Figure 1: Monthly measurements of physicochemical parameters from January to December 2022 at the ten sampling stations at Almyros Stream: (a) pH, (b) salinity, with values of salinity at stations 1, 2 and stations from 5 to 10 almost matching for all months, (c) chloride, with values almost matching for all months except July, and (d) total hardness of water samples, with values matching for January, February, April, May, June, November and December, except for station 3 (e) conductivity, with values at stations 1 and 2, and from station 4 till station 9 almost matching .

In Kalathas estuary, the pH values haven't shown spatial fluctuations, with the lowest values in January and an increase of pH in February (fig. 2). Salinity had the highest value at station 6 in April and the lowest in March. Chloride concentrations have shown the same fluctuations at all stations, except at station 6 (fig. 2), where was the highest measurement. Also, the highest value of total hardness was observed at station 6 and an increased was shown on February at the other stations. Conductivity values at Kalathas estuary were found high at all stations except station 6 on February, while the lowest was on May at the same stations (fig. 2).
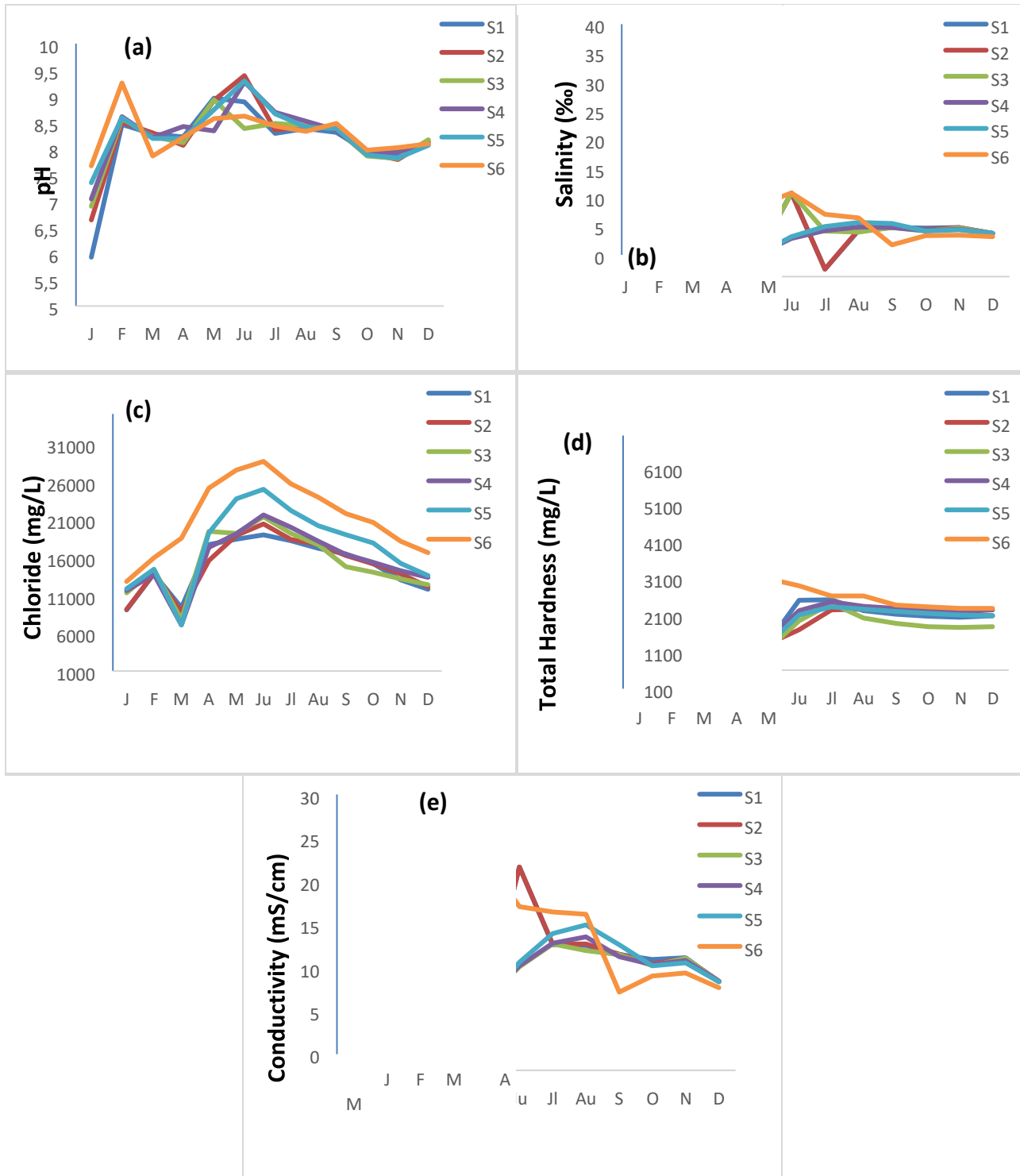
Figure 2: Monthly measurements of physicochemical parameters from January to December 2022 at the six sampling stations at Kalathas estuary: (a) pH, (b) salinity, (c) chloride and (d) total hardness of water samples (e) conductivity.

Table 1: Minimum, maximum and mean values of nutrients and pigments of ten sampling stations of Almyros stream. The name of the station is in parentheses.

Almyros Stream			
Nutrients	**minimum**	**maximum**	**mean**
N-NH$_4$ (mg/L)	0.00 (all)	1.97 (S3)	0.22
N-NO$_3$ (mg/L)	0.01 (S3)	1.68 (S7)	0.30
P-PO$_4$ (mg/L)	0.00 (all)	0.13 (all)	0.04
Si-silicate (mg/L)	0.00	41.30 (S1)	7.50
Pigments	**minimum**	**maximum**	**mean**
Chl a (µg/L)	0.0	94.3 (S5)	11.5
Chl b (µg/L)	0.0	137.2 (S5)	20.4
Chl c (µg/L)	0.0	307.1 (S10)	20.3
Carotenoids (µg/L)	0.0	65.5 (S5)	8.3

Table 2: Minimum, maximum and mean values of nutrients and pigments of six sampling stations of Kalathas estuary. The name of the station is in parentheses.

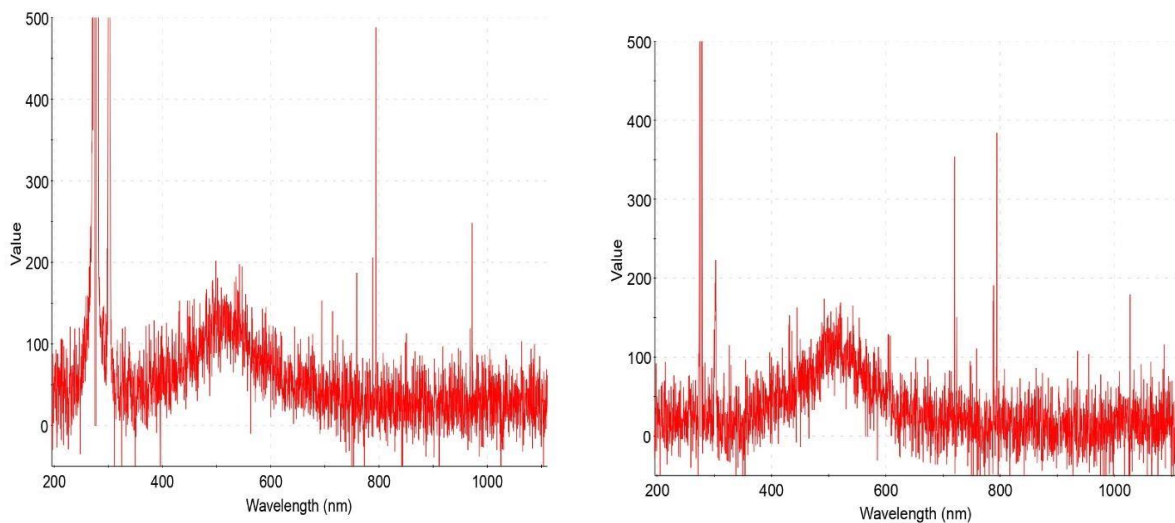| Kalathas estuary			
Nutrients	**minimum**	**maximum**	**mean**
N-NH$_4$ (mg/L)	0.00 (all)	2.61 (S5)	0.25
N-NO$_3$ (mg/L)	0.00 (all)	1.16 (S4)	0.37
P-PO$_4$ (mg/L)	0.00 (all)	0.13 (all)	0.04
Si-silicate (mg/L)	0.00 (all)	9 (S1)	1.98
Pigments			
Chl a (µg/L)	0.00	40.42 (S3)	14.6
Chl b (µg/L)	0.00	29.5 (S4)	7.15
Chl c (µg/L)	0.00	37.3 (S3)	14.7
Carotenoids (µg/L)	0.00	35.1 (S2)	2.05

Ammonium concentrations at Almyros showed monthly variations, with the highest value at station 3. Phosphate, nitrate, and silicate showed also monthly fluctuations, with high values at station 7 (NNO$_3$) and at station 1 (Si) (table 1). Phosphate concentrations did not vary spatially neither in Almyros nor in Kalathas (table 2). In Kalathas, ammonium concentrations fluctuated, with the

highest value at station 5, while nitrate was higher at station 4 and silicate was higher at station 1. Moreover, from table 2, it is obvious that maximum values of chl a and chl c were at station 3, while chl b has the maximum value at station 4. The maximum value of total carotenoids was detected at station 2. From table 1 is clear that maximum concentrations of chl a and chl b were at station 5 at Almyros Stream, while chl c had the maximum concentration at station 10.

LASER-INDUCED FLUORESCENCE (LIF)

The use of laser source for excitation at 266 nm, revealed the absence of fluorescent compounds at Almyros Stream, and presence of fluorescent compounds at Kalathas estuary. Examples of emission spectra recorded at Kalathas estuary are depicted in figure 3. Specifically, at stations 1-5 the emission spectra were similar showing a maximum in the UV-Visible region (450 – 600 nm). Station 6 lacked fluorescent compounds.

Figure 3: Emission spectra recorded at station 5 in January (at the left side) and in August (at the right side) at Kalathas estuary, by using the LIF method.

The Raman line appears at emission wavelengths from 280 to 400 nm (fig. 3). Raman scatter happens because the light is absorbed and re-emitted with loss in photon energy. The fluorescence near 450 nm is due to dissolved organic compounds (DOCs) in the water (Killinger, 2006). Humic substances, derived from decaying plant, emit from 310 to 500 nm when excited from 220 to 390 nm and proteins emit from 290-350 nm when excited at 220 and 275nm (table3) (Zacharioudaki, 2022). Moreover, certain types of algae and cyanobacteria, such as those containing chlorophyll, can emit fluorescence in the 450-650 nm range when excited at 266 nm.

Table 3: Main fluorophores in waters at emission and excitation wavelengths.

Name	Excitation(nm)	Emission(nm)
Humic-like	340-360	420-480
Fulvic-like	240-260	380-460
Tyrosine-like	265-285	290-310
Tryptophan-like	265-285	290-310
Marine-like	310-330	390-410
Humic-like	370-390	480-500

4.   CONCLUSION

The water body is slightly alkaline at both study areas. Ammonium concentrations were measured higher that 0.1 mg/L and is possibly due to the leaching of N from farm manure and/or pollution from sewage (Maksimović et al. 2020) and silicate concentrations were lower during the summer period, at Almyros and Kalathas, which is maybe due to algal growth. Water with fertilizers or sewage may contain high concentrations of chl a and excess amounts of algae (Filazzola, 2020). At both study areas, the high values of chlorophylls and carotenoids showed high algal productivity (Tani et al. 2009) characterizing their status as eutrophic. The LIF measurements revealed the presence of fluorophores at stations 1-5 of Kalathas and the absence of fluorophores in Almyros stream and at station 6 of Kalathas. The fluorophores are humic-type substances as they emit from 450 to 600 nm when radiated at 266 nm.

5.   5. REFERENCES

APHA (2005). Standard methods for the examination of water and wastewater. Washington: American Public Health Association, and Water Environment Federation.

Filazzola A, Mahdiyan O, Shuvo A, Ewins C, Moslenko L, Sadid T, Blagrave K, Imrit MA, Gray DK, Quinlan R, O'Reilly CM, Sharma S. A database of chlorophyll and water chemistry in freshwater lakes. Sci Data. 2020 Sep 22;7(1):310. doi: 10.1038/s41597-020-00648-2. PMID: 32963248; PMCID: PMC7508946. Killinger, D. and Sivaprakasam, V. (2006) "Water Monitoring with Laser Fluorescence," Optics and Photonics News 17, 1.

Maksimović T., Lolić, S., & Kukavica, B. (2020). Seasonal Changes in the Content of Photosynthetic Pigments of Dominant Macrophytes in the Bardača Fishpond Area. Ekológia (Bratislava), 39, 201213. 10.2478/eko-2020-0015.

Tani, Y., Matsumoto, G. I., Soma, M., Soma, Y., Hashimoto, S., & Kawai, T. (2009). Photosynthetic pigments in sediment core HDP-04 from Lake Hovsgol, Mongolia, and their implication for changes in algal productivity and lake environment for the last 1 Ma. Quaternary International, 205(1-2), 74– 83. 10.1016/j.quaint.2009.02.007.

Zacharioudaki, D-E., Fitilis, I., Kotti, M. (2022). Review of Fluorescence Spectroscopy in Environmental Quality Applications. Molecules, 27 (15) p. 4801

4th International Conference in Electronic Engineering, Information Technology & Education
EEITE – 2023